

## Regime shifts in sediment concentrations in tide-dominated estuaries

Dijkstra, Yoeri

**DOI**

[10.4233/uuid:28e12122-9c63-4260-aa87-b9e8f7de35fe](https://doi.org/10.4233/uuid:28e12122-9c63-4260-aa87-b9e8f7de35fe)

**Publication date**

2019

**Document Version**

Final published version

**Citation (APA)**

Dijkstra, Y. (2019). *Regime shifts in sediment concentrations in tide-dominated estuaries*. [Dissertation (TU Delft), Delft University of Technology]. <https://doi.org/10.4233/uuid:28e12122-9c63-4260-aa87-b9e8f7de35fe>

**Important note**

To cite this publication, please use the final published version (if applicable).  
Please check the document version above.

**Copyright**

Other than for strictly personal use, it is not permitted to download, forward or distribute the text or part of it, without the consent of the author(s) and/or copyright holder(s), unless the work is under an open content license such as Creative Commons.

**Takedown policy**

Please contact us and provide details if you believe this document breaches copyrights.  
We will remove access to the work immediately and investigate your claim.



Yoeri Dijkstra

Regime shifts  
in sediment  
concentrations  
in tide-dominated  
estuaries





# **REGIME SHIFTS IN SEDIMENT CONCENTRATIONS IN TIDE-DOMINATED ESTUARIES**





# **REGIME SHIFTS IN SEDIMENT CONCENTRATIONS IN TIDE-DOMINATED ESTUARIES**

## **Proefschrift**

ter verkrijging van de graad van doctor  
aan de Technische Universiteit Delft,  
op gezag van de Rector Magnificus prof. dr. ir. T.H.J.J. van der Hagen  
voorzitter van het College voor Promoties,  
in het openbaar te verdedigen op dinsdag 30 april 2019 om 15:00 uur

door

**Yoeri Matthijs DIJKSTRA**

Ingenieur in de Technische Wiskunde, Technische Universiteit Delft, Nederland  
Ingenieur in de Civiele Techniek, Technische Universiteit Delft, Nederland  
geboren te Sneek, Nederland



Dit proefschrift is goedgekeurd door de promotoren.

Samenstelling van de promotiecommissie:

Rector Magnificus,	voorzitter
dr. H.M. Schuttelaars,	Technische Universiteit Delft, promotor
prof. dr. ir. Z.B. Wang,	Technische Universiteit Delft, promotor

*Onafhankelijke leden:*

prof. dr. C.T. Friedrichs,	Virginia Institute of Marine Science, Verenigde Staten
prof. dr. H. Burchard,	Leibniz-Institut für Ostseeforschung Warnemünde, Duitsland
prof. dr. H.E. de Swart,	Universiteit Utrecht
prof. dr. ir. A.W. Heemink,	Technische Universiteit Delft
prof. dr. ir. C. Vuik,	Technische Universiteit Delft, reservelid

*Overige leden:*

prof. dr. ir. J.C. Winterwerp,	Technische Universiteit Delft
--------------------------------	-------------------------------



*Cover and illustrations:* Aron Dijkstra

*Printed by:* ProefschriftMaken || [www.proefschriftmaken.nl](http://www.proefschriftmaken.nl)

Copyright © 2019 by Y.M. Dijkstra

ISBN 978-94-6380-311-3

An electronic version of this dissertation is available at  
<http://repository.tudelft.nl/>.

# Contents

Summary	vii
Samenvatting	xi
<b>Part I</b>	<b>Development of a theoretical framework</b>
Chapter 1	Introduction 1
Chapter 2	The iFlow Modelling Framework v2.5 31
Chapter 3	The hyperturbid state of the water column 61
<b>Part II</b>	<b>Application to the Ems and Scheldt</b>
Chapter 4	Modelling the transition to high sediment concentrations as a response to channel deepening in the Ems River Estuary 85
Chapter 5	A regime shift from low to high sediment concentrations in a tide-dominated estuary 111
Chapter 6	Can the Scheldt River Estuary become hyperturbid? 125
<b>Part III</b>	<b>Discussion and outlook</b>
Chapter 7	Important processes and challenges in modelling the transition to a hyperturbid state 153
Chapter 8	Conclusions 181
Model availability and acknowledgement for data	193
Acknowledgements	195
Curriculum Vitæ	199
List of Publications	201





## Summary

Within estuaries one can often observe areas where the concentration of fine suspended sediments is higher than in the surrounding waters, called estuarine turbidity maxima (ETM). ETM play an important role in the natural and socio-economic value of estuaries. The suspended sediments can for example greatly diminish the value of the estuarine ecosystem by negatively affecting the light climate and oxygen level, as well as the economic value by leading to increased dredging costs for maintaining the depth of shipping channels. In at least two tide-dominated estuaries, the Ems River (Netherlands, Germany) and Loire River (France), the suspended sediment concentration has increased dramatically over the course of several decades. This has resulted in a great decline of the ecosystem and increase in dredging costs. As it is not well understood why these so called *regime shifts in suspended sediment concentrations* occurred, it remains unclear whether similar regime shifts can occur in other tide-dominated estuaries. The current leading hypothesis states that the regime shifts in the Ems and Loire are a result of man-made deepening of the estuary in the preceding decades. In addition, the hypothesis states that a similar regime shift can also occur in other tide-dominated estuaries that are subject to deepening. In this thesis, this hypothesis is systematically investigated by investigating the main physical processes that drive the sediment dynamics in tide-dominated estuaries and their response to channel deepening. This is illustrated by taking examples of two estuaries: the Ems (Netherlands, Germany) and Scheldt (Netherlands, Belgium).

To this end, we developed the iFlow model: an idealised computational model that solves for the width-averaged equations governing the water motion and sediment dynamics in estuaries. In this model it is assumed that the tidal water level elevation is small compared to the average depth and that the essential estuary-scale processes can be reproduced by only accounting for estuary-scale bathymetric features. Furthermore, the forcing of the water motion is simplified to only include an  $M_2$  and  $M_4$  tide and constant river discharge. These assumptions allow for the use of mathematical scaling and perturbation methods and harmonic analysis, which result in a fast model in which the effect of individual physical processes can be identified and analysed. The model is used to compute a dynamic equilibrium, i.e. a state in which the water motion and sediment concentration change on a tidal timescale but not on a subtidal timescale, representing a state that will be attained after a long time of constant tide and river discharge forcing.

The first application of the model was directed towards the better understanding of the regime shift in the Ems River. The observed regime shift occurred some time between the 1970s and early 2000s and consists of an increase of the maximum near-bed sediment concentrations from values of the order of 1 g/l to 10-100 g/l and an upstream movement and widening of the ETM. In the model, the water motion was first calibrated for conditions representative for the Ems in 1965. The resulting sediment concentrations are moderate with values near the bed of the order of 0.1-1 g/l. Next, the channel depth in

the model was increased to conditions representative for 2005, keeping all other parameters the same. For a river discharge below  $70 \text{ m}^3/\text{s}$  (occurring ca. 60% of the time), the observations are qualitatively reproduced by the model by finding sediment concentrations up to  $30 \text{ g/l}$  near the bed in two ETM that form a wide zone of highly turbid water in the most upstream part of the estuary. The model does not reproduce the regime shift for higher river discharges. It is not yet understood why the observed sediment concentrations remain high during periods of high discharge.

Assuming that the channel depth changed gradually between 1965 and 2005 we identified a river discharge-dependent critical depth profile. If the estuary is deeper than the critical depth profile and assuming a constant river discharge, the dynamic equilibrium sediment concentration can suddenly jump to much higher values, thus constituting the regime shift. By comparing the model results to long-term observations, it is estimated that the regime shift in the Ems started in approximately 1989 and it took approximately 6 years to evolve towards the new dynamic equilibrium with high sediment concentrations.

The physical processes driving the regime shift in the Ems were analysed according to two aspects: along-channel sediment transport and vertical resuspension of sediment from the bed. Regarding sediment transport, we identified that deepening leads to a higher sediment import due to several contributions related to the  $M_2$ - $M_4$  tidal velocity asymmetry. The resulting increased sediment concentrations lead to sediment-induced stratification and therefore a reduction of turbulence. In turn, this causes amplification of the tide in a way that further increases the sediment import due to  $M_2$ - $M_4$  tidal velocity asymmetry and forms a positive feedback mechanism. This mechanism has been especially strong in the Ems, because the  $M_4$  tide evolved to a state close to resonance and is thus strongly amplified. Regarding vertical resuspension, it is found that the tidal motion is able to keep all the imported sediment in suspension, assuming that the parameter governing erosion in the model has a sufficiently large value.

The second application of the model was directed to the question if the Scheldt River can become hyperturbid due to deepening, as a result of similar processes as in the Ems. To investigate this, the model was set up for a configuration representing depth conditions in 2010. The water motion and overall magnitude of the sediment concentration, which is of the order of  $0.1 \text{ g/l}$ , were calibrated to observations. The modelled distribution of sediment along the estuary corresponds well to observations, showing three ETM. Deepening of the estuary in the model led to lower sediment concentrations in all ETM when using the estimated best parameter settings. A small increase of the sediment concentration after deepening may be found for some other parameter choices. However, a regime shift to high sediment concentrations is not found. Nevertheless, high sediment concentration were found in the Scheldt model representing 2010 conditions when the parameter governing erosion was increased by more than one order of magnitude. Further research is needed to investigate if such large increase in this erosion parameter could occur in reality.

On a process level, the Scheldt differs from the Ems on two main aspects in our model. Firstly, for low to average discharge conditions the sediment concentration in the Scheldt

is not restricted by the amount of sediment imported into the estuary (i.e. sediment transport) but by the ability of the tide to keep this sediment in suspension (i.e. vertical resuspension). Deepening leads to a decrease in the bed shear stress at the locations of the ETM, which results in less resuspension and lower sediment concentrations. Secondly, the sediment transport in the Scheldt is dominated by  $M_2$ - $M_4$  tidal asymmetry as in the Ems, but only a few contributions to this asymmetry lead to sediment import, while other contributions lead to sediment export. As a result of deepening, some of these contributions become more importing and others become more exporting. Hence, the effect of deepening on the total sediment import is relatively small and depends strongly on the exact parameter settings and forcing conditions. Therefore, a positive feedback mechanism as in the Ems is therefore absent in the Scheldt.

To investigate if the results obtained using iFlow can be extended to more realistic models, the application to the Ems was repeated using a Delft3D model; a state-of-the-art complex model. The model was configured in a similar way as the iFlow model, so that results of both model could be compared in detail. The results of the Delft3D and iFlow models correspond closely when applied to 1965 conditions. However, when applied to 2005 conditions, the regime shift to high sediment concentrations was not reproduced using the Delft3D model. Three main differences were identified to explain these results. Firstly, when increasing the parameter governing erosion beyond some value in Delft3D, sediment import decreases. Hence high sediment concentrations are only reproduced in a model when this erosion parameter is sufficiently large not to limit the sediment concentration too much but also not too large. Secondly, sediment-induced damping of turbulence leads to a reduction of the bed shear stress in Delft3D, more than in iFlow. As a result, the amount of vertical resuspension of sediment is reduced more than in iFlow. Finally, the Delft3D model displayed convergence problems and spurious oscillations for several cases where high sediment concentrations occurred, so that these results could not be trusted. The origin of these convergence problems and oscillations is not yet understood.

Concluding, the results of this study support the hypothesis that deepening led to the regime shift that occurred in the Ems River and can be used to identify the main physical processes governing this regime shift. These processes however do not generically lead to a regime shift to high sediment concentrations, as illustrated by the Scheldt River case. Therefore, in order to understand the effects of deepening on the sediment concentration in other estuaries, it is important to understand the essential physical processes that govern sediment dynamics in each of these estuaries. It has been demonstrated that the iFlow model is a good tool to investigate this. Furthermore, we have identified several processes that need to be better understood in order to model the high sediment concentrations, like in the Ems, more realistically.



# Samenvatting

In estuaria kan men vaak gebieden identificeren waarin de concentratie fijn gesuspenseerd sediment hoger is dan in de aangrenzende wateren: zogeheten estuariene troebelheidsmaximum (ETM). ETM spelen een belangrijke rol in de natuurlijke en sociaal-economische waarde van estuaria. Gesuspenseerd sediment kan bijvoorbeeld de ecologische waarde van estuaria sterk verminderen door zijn negatieve invloed op het lichtklimaat en het zuurstofgehalte. Daarnaast kan door gesuspenseerd sediment de economische waarde van estuaria sterk verminderen, doordat het leidt tot een verhoging van de baggerkosten die gepaard gaan met het op diepte houden van de vaargeul. In tenminste twee getij-gedomineerde estuaria, de Eems (Nederland, Duitsland) en Loire (Frankrijk), is de concentratie gesuspenseerd sediment sterk gestegen in de loop van de decennia. Dit heeft geleid tot een verslechtering van het ecosysteem en verhoging van de baggerkosten. Omdat deze zogeheten systeemomslagen in de gesuspenseerde sedimentconcentratie nog niet goed begrepen worden, is het onduidelijk of soortgelijke systeemomslagen ook kunnen plaatsvinden in andere getij-gedomineerde estuaria. De voornaamste hypothese op dit moment zegt dat de systeemomslagen in de Eems en de Loire het gevolg zijn van de verdieping van de estuaria door de mens in de afgelopen decennia. De hypothese suggereert ook dat een soortgelijke systeemomslag kan plaatsvinden in andere estuaria die verdiept worden. In dit proefschrift wordt deze hypothese systematisch onderzocht, door onderzoek te doen naar de belangrijkste fysische processen achter de sedimentdynamica in getij-gedomineerde estuaria en hun reactie op verdieping van de vaargeul. Dit wordt geïllustreerd aan de hand van twee voorbeelden: de Eems (Nederland, Duitsland) en de Schelde (Nederland, België).

Om de hypothese te kunnen toetsen, werd het iFlow model ontwikkeld: een geïdealiseerd rekenmodel dat de breedte-gemiddelde wiskundige vergelijkingen voor de waterbeweging en sedimentdynamica in estuaria oplost. In het model wordt aangenomen dat de getijslag klein is ten opzichte van de gemiddelde diepte en dat de belangrijkste processen op de schaal van het gehele estuarium beschreven kunnen worden door alleen rekening te houden met de breedte- en dieptevariëaties op de schaal van het gehele estuarium. Daarnaast is de modelforcering vereenvoudigd. Deze bevat alleen het  $M_2$  en  $M_4$  getij en een constante rivierafvoer. Door deze aannames is het mogelijk om wiskundige schalings- en storingstechnieken te gebruiken en harmonische analyse toe te passen. Dit zorgt voor een model dat snel is en waarin het mogelijk is om het effect van verscheidene fysische processen afzonderlijk te identificeren en onderzoeken. Het model berekent een dynamisch evenwicht; een toestand waarin de waterbeweging en sedimentconcentratie variëren gedurende de periode van een getij, maar niet gemiddeld over een getijperiode. Dit vertegenwoordigt de toestand die bereikt zal worden na langere tijd met constante getijforcering en rivierafvoer.

De eerste toepassing van het model was gericht op het ontwikkelen van een beter begrip van de systeemomslag in de Eems. De waargenomen systeemomslag gebeurde ergens

tussen de jaren 1970 en 2000 en bestond uit een toename van de maximale sedimentconcentratie nabij de bodem van waarden in de orde van 1 g/l tot waarden van 10-100 g/l, een bovenstroomse verschuiving van het ETM en een verbreding van het ETM. In het model is ten eerste de waterbeweging gekalibreerd voor een toestand die representatief is voor het jaar 1965. De resulterende sedimentconcentratie is matig met waarden nabij de bodem in de orde van 0,1 tot 1 g/l. Vervolgens is de diepte van het estuarium in het model vergroot naar waarden die representatief zijn voor het jaar 2005, waarbij verder alle modelparameters gelijk werden gehouden. Als de rivierafvoer lager is dan  $70 \text{ m}^3/\text{s}$  (dit gebeurt ca. 60% van de tijd), dan worden de waargenomen fenomenen in het model kwalitatief gereproduceerd. Dat wil zeggen, de sedimentconcentratie neemt waarden aan tot 30 g/l nabij de bodem in twee ETM, welke samen een brede zone van hoge sedimentconcentraties vormen in het meest bovenstroomse deel van het estuarium. De systeemomslag wordt niet gereproduceerd met het model als de rivierafvoer hoger is dan  $70 \text{ m}^3/\text{s}$ . De reden waarom waargenomen sedimentconcentraties hoog blijven gedurende periodes van hoge rivierafvoeren is nog onbekend.

Als wordt aangenomen dat de diepte geleidelijk is veranderd tussen 1965 en 2005, is het mogelijk om, afhankelijk van de rivierafvoer, een kritiek diepteprofiel te definiëren. Als het estuarium dieper is dan dit kritieke diepteprofiel en als wordt aangenomen dat de rivierafvoer constant is, dan kan het dynamisch evenwicht van de sedimentconcentratie plotseling springen naar veel hogere waarden: de systeemomslag. Door de modelresultaten te vergelijken met lange-termijn waarnemingen, wordt geschat dat de systeemomslag in de Eems in ca. 1989 is begonnen en het ongeveer zes jaar heeft geduurd voordat de sedimentconcentraties passend bij het nieuwe dynamisch evenwicht werden bereikt.

De fysische processen die gezorgd hebben voor de systeemomslag in de Eems zijn geanalyseerd op basis van twee aspecten: sedimenttransport in de lengterichting van het estuarium en verticale opwerveling van sediment van de bodem. Met betrekking tot het sedimenttransport, is gevonden dat verdieping van de vaargeul leidt tot een toename van de import van sediment. Dit komt doordat verdieping leidt tot een toename van het sedimentimport door verscheidene bijdragen aan de  $M_2$ - $M_4$  snelheidsasymmetrie. De resulterende verhoging van de sedimentconcentratie leidt tot stratificatie, wat zorgt voor demping van turbulentie. Deze turbulentiedemping zorgt vervolgens voor een toename de getijamplitude op zodanige wijze dat sedimentimport door de  $M_2$ - $M_4$  asymmetrie in de getijsnelheid toeneemt. Dit leidt tot een terugkoppelingsmechanisme. Dit mechanisme is in de Eems vooral sterk, doordat het  $M_4$  getij veranderd is naar een toestand dichtbij resonantie en dus sterk geamplificeerd is. Met betrekking tot de verticale opwerveling van sediment is gevonden dat de getijstroming al het geïmporteerde sediment in suspensie kan houden als wordt aangenomen dat de modelparameter voor erosie een voldoende hoge waarde heeft.

De tweede toepassing van het model was gericht op de vraag of de Schelde hypertroebel kan worden ten gevolge van verdieping door soortgelijke processen die de systeemomslag in de Eems hebben veroorzaakt. Om dit te onderzoeken is het model toegepast op een situatie die representatief is voor condities in het jaar 2010. De waterbeweging en de orde-grootte van de sedimentconcentratie, ca. 0,1 g/l, zijn hiervoor gekalibreerd aan de hand van metingen. De gemodelleerde verdeling van sediment in het estuarium komt



goed overeen met de waarnemingen en laat drie ETM zien. Verdieping van het estuarium in het model leidde tot lagere sedimentconcentraties in alle drie ETM wanneer de geschatte optimale parameterwaarden worden gebruikt. Een kleine toename van de sedimentconcentratie bij verdieping kan worden waargenomen voor enkele andere parameterinstellingen, maar een systeemomslag naar een hypertroebele situatie wordt niet gevonden. Wel kunnen hoge sedimentconcentraties worden gevonden in de 2010 situatie als de waarde van de modelparameter voor erosie met meer dan een orde-grootte wordt verhoogd. Verder onderzoek is nodig om te onderzoeken of een zodanige toename van de waarde van deze erosieparameter realistisch kan zijn.

Op procesniveau verschilt de Schelde op voornamelijk twee aspecten van de Eems in het iFlow model. Ten eerste wordt bij lage tot gemiddelde rivierafvoer de sedimentconcentratie in de Schelde niet beperkt door de mate van sedimentimport (nl. sedimenttransport), maar door het vermogen van de stroming om het geïmporteerde sediment in suspensie te houden (nl. verticale opwerveling). Verdieping van het estuarium leidt tot een lagere bodemschuifspanning op de locaties van de ETM, wat leidt tot minder opwerveling en daardoor een lagere sedimentconcentratie. Ten tweede wordt het sedimenttransport in de Schelde gedomineerd door processen die gerelateerd zijn aan de  $M_2$ - $M_4$  getijasymmetrie, net als in de Eems, maar slechts enkele van deze processen veroorzaken import van sediment, terwijl de andere processen zorgen voor een export van sediment. Door verdieping worden enkele van deze processen sterker importerend, terwijl andere sterker exporterend worden. Het totale effect van verdieping op het sedimenttransport is daarom zwak en hangt nog sterk af van de exact gekozen parameterinstellingen en forceringscondities. Een terugkoppelingsmechanisme zoals in de Eems wordt in de Schelde niet waargenomen.

Om te onderzoeken of de iFlow resultaten uitgebreid kunnen worden naar meer realistische modellen, is het modelexperiment voor de Eems herhaald met een Delft3D model; een state-of-the-art complex model. Het model is zodanig opgezet dat het zo veel mogelijk lijkt op het iFlow model, zodat de resultaten uit beide modellen tot in detail vergeleken kunnen worden. De Delft3D en iFlow resultaten komen goed overeen voor de 1965 condities. Echter, bij toepassing van het Delft3D model voor 2005 condities kon de systeemomslag naar hoge sedimentconcentraties niet gereproduceerd worden. Drie verschillen tussen de modellen zijn aangewezen als belangrijkste verklaring voor deze resultaten. Ten eerste neemt de sedimentconcentratie in Delft3D af als de parameter voor erosie hoger is dan een bepaalde waarde. Daardoor kunnen hoge sedimentconcentraties alleen worden gevonden als deze erosieparameter voldoende hoog is om niet de sedimentconcentratie sterk te beperken, maar ook niet te hoog. Ten tweede leidt de demping van turbulentie ten gevolge van sediment in Delft3D, meer dan in iFlow, tot een verlaging van de bodemschuifspanning. Dit heeft tot gevolg dat de opwerveling van sediment lager is dan in iFlow. Tenslotte treden er convergentieproblemen en onechte oscillaties op in Delft3D in een aantal gevallen waar hoge sedimentconcentraties voorkwamen, zodat deze resultaten niet vertrouwd kunnen worden. De oorzaak van deze problemen en oscillaties is nog niet bekend.

In conclusie: de resultaten van dit onderzoek ondersteunen de hypothese dat verdieping heeft geleid tot de systeemomslag die is waargenomen in de Eems en kunnen gebruikt

worden om de belangrijkste fysische processen achter deze systeemomslag aan te wijzen. Deze processen leiden echter niet generiek tot een systeemomslag naar hoge sedimentconcentraties, zoals is geïllustreerd met behulp van de toepassing op de Schelde. Om de effecten van verdieping op de sedimentconcentratie in andere estuaria te begrijpen is het daarom noodzakelijk om de belangrijkste fysische processen voor sedimenttransport te begrijpen voor elk van deze estuaria. Dit onderzoek laat zien dat het iFlow model een nuttig model is om dit te doen. Daarnaast zijn verscheidene processen geïdentificeerd die beter begrepen moeten worden om hoge sedimentconcentraties, zoals deze voorkomen in de Eems, meer realistisch te modelleren.

# CHAPTER 1

Introduction



### 1.1. WHY STUDY ESTUARINE SEDIMENT DYNAMICS?

An estuary, from a physical perspective, is defined as a semi-enclosed coastal body of water, which has a free connection with the open sea and within which saline sea water is measurably diluted with fresh water from land drainage, often in the form of a river (Pritchard, 1967). Most estuaries are characterised by tides propagating into the estuary from the open sea. This lends them their name from the Latin *aestuarium*, with *aestus* meaning ‘tide’. In some definitions and in general use, the term estuary is extended to include the tidal river (Fairbridge, 1980): the part of the river where tides are observed but where the water is entirely fresh. This is also the definition that is adopted in this thesis, see Fig. 1.1. This thesis focusses specifically on tide-dominated estuaries. This means that flow velocities and stresses exerted by the motion of the tides dominate over those exerted by the fresh-water run-off or wind waves.

Sediment in the estuary originates either from the sea or from the watershed, transported into the estuary by the river flow. It comes in various sizes from gravel ( $> 2 \text{ mm}$ ) and coarse sand to clay ( $< 2 \text{ }\mu\text{m}$ ) and organic particles. The finer sand, silt and mud fractions can be suspended and transported over considerable distances by the water motion in the estuary. These sediments are periodically deposited on the bed of the estuary or inter-tidal area and resuspended into the water column. In most estuaries, the complex interplay of sediment transport, deposition and resuspension leads to the formation of regions where the concentration of suspended sediment in the water is higher than in its direct surroundings, called *estuarine turbidity maxima (ETM)*. In a recent review, ETM are formally defined as local maxima of the cross-sectionally averaged and tidally averaged suspended sediment concentration (Burchard et al., 2018), but the term is also used to indicate maxima of the suspended sediment concentration in single locations of a cross-section or at single moments in time. ETM are typically large-scale phenomena with along-channel length scales of the order of 10 km and sediment concentrations ranging from 10 mg/l to more than 100 g/l (e.g. Uncles et al., 2002), see Fig. 1.2.

The motivation for studying sediment and ETM dynamics in estuaries is two-fold. Firstly, suspended sediments are an important factor affecting the natural and economic value of estuaries and secondly, sediment dynamics is changing in many estuaries. This leads to potential changes in this natural and economic value, which we want to understand and forecast. This will be elaborated below.

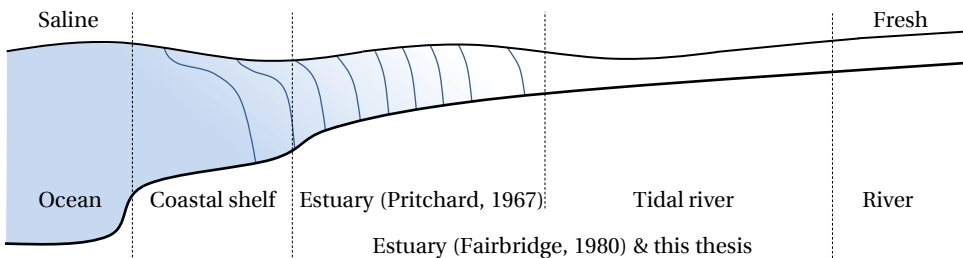


**Figure 1.1:** Sketch defining the estuary and tidal river. The blue lines indicate lines of equal salinity. In this thesis an estuary is defined as the brackish estuarine zone and the tidal river.

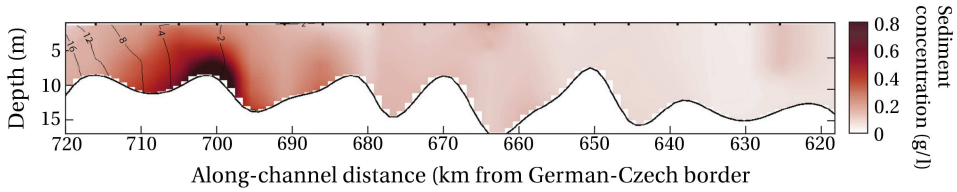


**Figure 1.2:** Example of an along-channel section of the Elbe River Estuary (Germany) with the observed salinity (black isolines, in PSU) and sediment concentration (colours, in g/l) on March 29, 1990. Figure adapted from Burchard et al. (2018).

Estuaries have a great natural value, which is largely related to their potential to support a large primary production (Boynton et al., 1982; Underwood and Kromkamp, 1999), i.e. the conversion of  $\text{CO}_2$  to amino acids and other organic carbon compounds, which provides the basis of the food web. Primary production is mainly realised through photosynthesis by phytoplankton (i.e. algae in the water), benthic micro-algae (i.e. organisms living on the bed) and vascular plants. These species have a high potential to grow in estuaries, because the (tidally averaged) flow is calm compared to rivers and the supply of nutrients is high compared to seas. However, primary production by photosynthesis requires sunlight, which is blocked by suspended sediments starting from concentrations of 10–100 mg/l (e.g. Wofsy, 1983). In many estuaries, the suspended sediment concentration is the dominant limitation on the primary production (Colijn, 1982; Cloern, 1987; Kromkamp and Peene, 1995) and therefore plays an essential role as a stress factor in the estuarine food web. Furthermore, bacteria living in suspended organic sediments consume oxygen, so that high sediment concentrations are often associated with hypoxia, greatly degrading the living conditions for estuarine fauna (see Talke et al. (2009a) and references therein). Finally, due to these effects of suspended sediment dynamics on photosynthesis, biomass and oxygen levels, it plays an important role in the total  $\text{CO}_2$  emission or absorption of estuaries (Cloern et al., 2014).

Many estuaries are also of great economic value, supporting some of the world's biggest ports. Deposition of sediments in ports and navigation channels can strongly reduce the navigability and needs to be countered by expensive maintenance dredging. Furthermore, suspended sediment dynamics plays an important role many other economic ecosystem services including fishing, shell-fish farming and tourism.

The natural and economic value of estuaries is subject to change when suspended sediment dynamics change, either due to changes in natural conditions (e.g. sea level rise or climate change) or anthropogenic changes to the estuary. Focussing on anthropogenic changes, in many estuaries banks have been restricted and reinforced to control flooding, floodplains and intertidal areas have been removed to accommodate growing cities and shipping channels have been deepened or relocated to accommodate larger ships. In the Ems River (Netherlands, Germany) and Loire River (France) these changes are likely the cause of a dramatic increase, or *regime shift* in suspended sediment concentrations to what is called a *hyperturbid state* (Winterwerp and Wang, 2013). Winterwerp et al. (2013) observed that many other European estuaries have similar geometric and

tidal characteristics as the Ems and Loire and are also heavily engineered. Based on this, they raised the suggestion that other estuaries, including the Weser, Elbe (Germany) and Scheldt (Netherlands, Belgium), are at risk of evolving to a hyperturbid state if they are further engineered.

As no modelling study has yet been able to dynamically model the regime shift in the Ems or Loire, one cannot be confident that a possible regime shift in the Weser, Elbe or Scheldt can be correctly predicted using existing models. Also, as high sediment concentrations remain a challenge in modelling (Dyer, 1989; Burchard et al., 2018), it is still impossible to confidently test scenarios for mitigation of the high concentrations in the Ems and Loire. In order to forecast, prevent or mitigate changing sediment concentrations in estuaries, it is therefore important to increase the understanding of the underlying sediment dynamics. These dynamics are highly complex due to its dependence on multiple aspects of the water motion (e.g. tides, river flow, wind-driven flow, waves and turbulence) and sediment properties. Therefore it is required to focus on a smaller set of processes that are thought to be important based on observations. In line with this thought, the goals of this thesis are as follows:

1. to identify and better understand the essential processes driving a shift of the regime to hyperturbid conditions, by studying observed characteristics exemplified by the Ems River, and
2. to determine whether these processes are generically able to drive a regime shift to hyperturbidity in other estuaries, demonstrated by taking the Scheldt River as an example.

In view of these goals, this thesis presents the construction and analysis of a model that is as simple as possible in order to understand the mechanisms underlying sediment dynamics and test the robustness of the results within the large range of uncertainty, thereby gaining confidence in the model results (Schuttelaars et al., 2013). The model is applied to the Ems and Scheldt River Estuaries, focussing on reproducing the main features of the observed regime shift in the Ems and investigating the possibility that the Scheldt becomes hyperturbid due to similar processes as in the Ems.

The remainder of this chapter further introduces the terminology, existing knowledge, analysis methods related to the research goals and the approach of this research. Section 1.2 discusses observed characteristics and features of ETM and sediment suspensions that are important to understand this thesis and its implications. Next, Section 1.3 presents the general definition of a regime shift and the meaning of regime shifts in the context of this thesis. Having defined the necessary concepts, Sections 1.4-1.6 focus on the analysis of sediment dynamics. Section 1.4 gives a review of existing knowledge of sediment transport processes. Section 1.5 introduces the two estuaries that feature in this thesis, the Ems and Scheldt, briefly discussing some of the main results of past studies on sediment dynamics. Finally, Section 1.6 presents the modelling approach used in this thesis, followed by the research questions and an outline of this thesis.



## 1.2. CHARACTERISTICS OF ETM, SEDIMENT SUSPENSIONS AND HYPERTURBIDITY

The characteristics of ETM and sediment suspensions have been extensively described in literature, yielding a vast amount of literature describing different characteristics on scale levels ranging from less than a millimetre to more than 10 km. This section gives a short introduction to a few concepts important for understanding this thesis, separated in concepts related to ETM (Section 1.2.1) and sediment suspensions (Section 1.2.2). Using these concepts, a definition of hyperturbidity is proposed in Section 1.2.3.

### 1.2.1. ETM AND TRAPPING LOCATIONS

ETM form due to the combination of sediment transport (i.e. mainly horizontal processes) and sediment deposition and resuspension from the bed (i.e. mainly vertical processes). Focussing on the tide-averaged transport of sediment, this transport may be directed upstream or downstream in different parts of the estuary. This often leads to the existence of one or more locations where the sediment transport convergences or gets trapped, called *trapping locations*. In nature, trapping locations may be observed as locations with relatively more fine sediments on the bed than elsewhere in the estuary. Such locations are often found on shallow areas, near dams or locks or inside harbour basins, where the velocities are low and sediments settle easily. Sediment trapping can however also occur in much more energetic areas in the channel of the estuary (see e.g. Sommerfield and Wong (2011) for an example). ETM are often directly associated with sediment trapping (e.g. Burchard et al., 2018), but this is clearly not generally true; ETM are for example hardly found near dams or locks. Apart from the high availability of sediment in trapping locations, the formation of an ETM requires that the sediment is resuspended from the bed and kept in suspension by the flow. Formation of an ETM thus requires sufficient energy from e.g. the tide or wind to mix the water column and prevent the sediments from settling to the bed. ETM are therefore often found close to but not at, trapping locations in sufficiently energetic environments.

In many estuaries, an ETM is found near the limit of the salinity intrusion (see e.g. Burchard et al. (2018) and references therein). However, ETM are also found well upstream from the salinity intrusion limit in e.g. the rivers Gironde, Aulne (Allen et al., 1980) and Ems (De Jonge et al., 2014). Additionally, ETM may be found near rapid changes in topography (see examples mentioned by Burchard et al. (2018)). These and other examples have shown the diversity of ETM observed in nature and of the physics that leads to their existence.

### 1.2.2. CHARACTERISTICS OF SEDIMENT SUSPENSIONS

The characteristics of the sediment and the behaviour of the sediment-fluid mixture can change considerably depending on the suspended sediment concentration. In this section, four partially overlapping categories of sediment concentrations with different characteristics are discussed. These categories are summarised in Fig. 1.3.

Firstly, for low or moderate sediment concentrations of the order of 10 mg/l - 1 g/l, fine sediment particles can form clusters containing multiple primary particles called *flocs*. The formation and break-up of sediment flocs, called flocculation, is a complex set of processes and the reader is referred to Winterwerp and Van Kesteren (2004) and Mehta

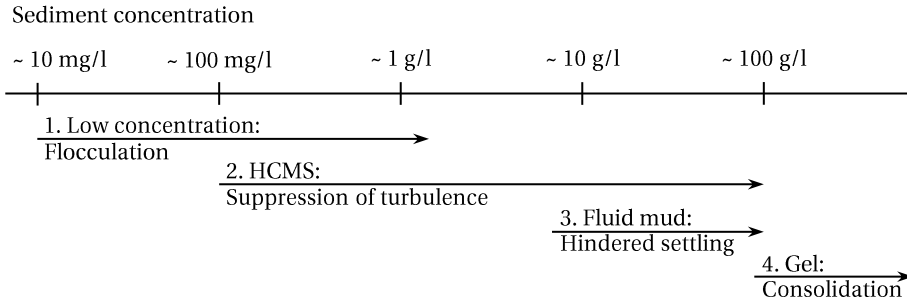


**Figure 1.3:** Range of sediment concentrations with names and characterising physical processes of four intervals.

(2014) for an introduction. Sediment flocs have a larger velocity with which they settle to the bed than primary particles, thus affecting the distribution of the sediment in the water column. This in turn is essential to the net transport of sediment by the flow.

Secondly, if sediment concentrations are of the order of 100 mg/l or higher, they significantly affect the density of the suspension. Such suspensions are sometimes called *high concentration mud suspensions* (HCMS) (Winterwerp and Van Kesteren, 2004). In a typical vertical sediment distribution, the concentration decreases as one moves further up in the water column, leading to a negative vertical density gradient. Such density gradients affect the water motion through the suppression of turbulent eddies, leading to less friction experienced by the flow and less mixing of the water column.

Thirdly, at even higher concentrations of the order of 10-100 g/l, sediment particles and flocs settle in each others wake, leading to a reduction in their effective settling velocity, called *hindered settling* (Richardson and Zaki, 1954). The water motion is also affected by the sediment, as the dense network of sediment particles increases the apparent friction. This results in an apparent viscosity of the suspension that is higher than that of clear-water. Also, pore-water pressure may build up and the response of the suspension to stresses depends on whether it was initially at rest or moving; i.e. non-Newtonian behaviour starts to play a role.

Finally, for concentrations of the order of 100 g/l, the sediments may start to form a space-filling network, called *gelling*. At and above the gelling concentration, the suspension starts to behave more like a solid. For example, sediment particles no longer settle in the suspension but consolidate, i.e. they press water out of the suspension, and build up shear strength. Nevertheless, when the stress exerted on the mud by the flow exceeds this shear strength, the suspension liquefies and behaves like a fluid.

A term that is often used to characterise sediment suspensions with high concentrations is *fluid mud*. Introduced by Inglis and Allen (1957) and Krone (1962), this term never got an unambiguous definition. Some authors include suspensions with concentration above the gelling concentration in their definition (e.g. Winterwerp and Van Kesteren,

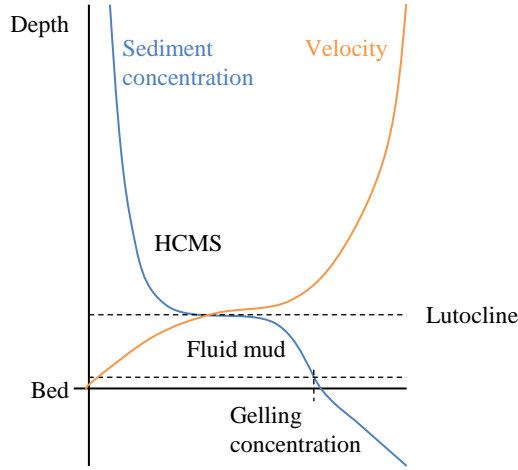


**Figure 1.4:** Sketch of a vertical sediment profile (blue) and vertical velocity profile (orange), marking the lutocline, fluid mud layer and bed.

2004), while others do not (e.g. Mehta, 2014). For practical purposes, the definition used in this thesis is that of Mehta (2014): a suspension with a concentration below the gelling point where hindered settling is important, thus categorised in the third category in Fig. 1.3.

All four categories may be identified in a single water column as illustrated in Fig. 1.4. In the top part of the water column, concentrations are typically in the first or second interval. Moving further down, a sharp interface, called a *lutocline*, marks the start of a distinct layer of fluid mud, which may have a thickness of decimetres to metres (Winterwerp and Van Kesteren, 2004). This layer is so clear, because the fluid mud settles only slowly due to hindered settling, while any sediment above it settles into the fluid mud more rapidly. Moreover, as the density difference between the fluid mud and the overlying water is large, turbulence on the interface between the fluid mud and overlying water is almost absent, resulting in a strongly reduced mixing between the layers. The bottom of the water column is marked by the *bed*. The bed is formally defined as the location where the flow velocity vanishes. This location varies in time and space based on the strength of the consolidating sediment and strength of the flow.

### 1.2.3. DEFINITION OF A HYPERTURBID ESTUARY

Estuaries where HCMS or fluid mud occurs are sometimes called *hyperturbid estuaries*. This term was introduced by Winterwerp (2011) and elaborated on by Winterwerp and Wang (2013) but is without a formal definition. Here, a qualitative definition is proposed.

**Definition 1.1.** *A hyperturbid estuary is an estuary where fluid mud occurs in such a large part of the estuary that it significantly affects the estuary-scale water motion (i.e. water level or tidal range) and is found during a significant portion of the year.*

It is at this point neither possible nor useful to set a stricter or more quantitative defini-

tion, given the variety of examples of hyperturbid estuaries. Examples of naturally hyperturbid estuaries exist due to a highly concentrated fluvial supply, e.g. in the Yangtze River (e.g. Wang et al., 2015) and Amazon River (Meade et al., 1985), or due to strong sediment trapping, e.g. in the Gironde (Castaing and Allen, 1981), Humber (Uncles et al., 2006) and Severn (Dyer, 1984). Furthermore, examples have been presented of the Ems and Loire River Estuaries, which have become hyperturbid over time (Winterwerp et al., 2013).

### 1.3. DEVELOPMENT OF HYPERTURBIDITY: REGIME SHIFT THEORY

#### 1.3.1. REGIME SHIFT THEORY

Unusually rapid, large and persisting changes in a dynamic system, such as the large increase in suspended sediment concentration observed in the Ems River, are called *regime shifts* (e.g. Biggs et al., 2012). Regime shift theory is a well-developed sub-field of dynamical systems theory in mathematics of which some terminology and phenomenology is presented in this section, omitting the underlying mathematical theory.

In regime shift theory, a *regime* denotes a dynamic equilibrium state of a system. The term *equilibrium* denotes a stationary state. The notion of equilibrium can be extended to that of a *dynamic equilibrium*, indicating a state that may vary depending on fluctuations in the forcing conditions of the system. In order to describe a regime, it is therefore necessary to describe the set of varying conditions that are counted as forcing and to describe the varying equilibrium state of the system given this forcing.

A regime shift (also *transition*) describes the change from one regime to another as a function of changing external conditions. These external conditions can be any change to the system that is different to the variations included in the set of varying forcing conditions. This definition means that a regime shift is not necessarily a big change in absolute sense. Instead, it represents a change in response to the same forcing conditions due to changed external conditions.

To provide more classification to this rather broad definition, a regime shift can be described as a smooth, abrupt or discontinuous function of these conditions (e.g. Scheffer et al., 2001). These three types are illustrated in Fig. 1.5. The smooth regime shift (Fig 1.5a) occurs gradually while external conditions are changing and can be reversed by reversing the conditions. An abrupt regime shift (Fig 1.5b) indicates a relatively large change in regime as a consequence of a small change in external conditions but can also be reversed by reversing the conditions. The distinction between a smooth and abrupt regime shift is largely subjective as it depends on how one defines a small or large change in the external conditions and regime. The discontinuous regime shift (Fig. 1.5c) also indicates a relatively large change in regime as a consequence of a small change in conditions and in addition cannot be reversed by reversing the conditions. The discontinuous regime shift can only be reversed by a much larger reverse change in the conditions. Such asymmetry in the transition between two regimes is called hysteresis.

The type of regime shift only gives information about the change of the regime as a function of the change in conditions, not as a function of time. The behaviour of the regime shift in time depends on the time it takes for the system to evolve from one dynamic

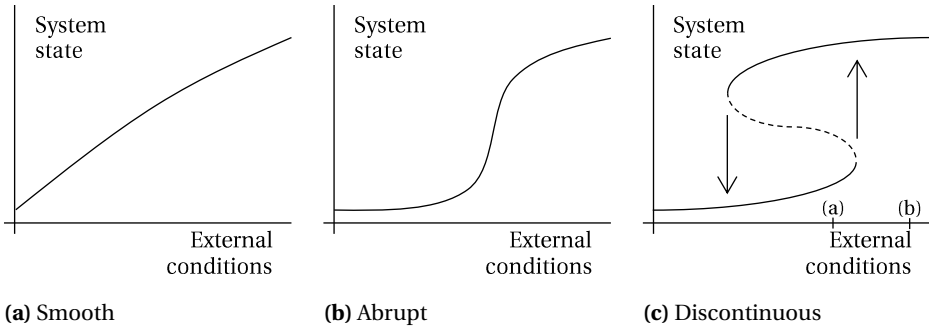


**Figure 1.5:** Three types of regime shifts sketched in general form as a system state (e.g. suspended sediment concentration) versus a condition (e.g. bottom depth), see also Scheffer et al. (2001).

equilibrium to another. Hence, when conditions change, e.g. from (a) to (b) in Fig. 1.5c, the dynamic equilibrium state changes suddenly, but the actual state of the system adapts gradually to this new dynamic equilibrium. The timescale of this adaptation process cannot be inferred from the figure. When the adaptation time is of the same order of magnitude as the time over which the conditions change, it may be impossible to infer the type of regime shift from observations. The regime shift type may then only be inferred from a mathematical model.

### 1.3.2. REGIME SHIFTS AND HYPERTURBIDITY

While the definition of a regime shift does not necessarily imply a big change, regime shifts in the context of estuarine sediment dynamics are associated with big changes (Winterwerp et al., 2013). In this thesis, it will be used to indicate a change in typical sediment concentrations between two regimes: hyperturbid and not hyperturbid, following the qualitative definition in Section 1.2.3. To further define these regimes, the forcing conditions are defined to include the forcing at the water surface and boundaries with adjacent waters, e.g. by the tides, wind, river discharge, salinity and sediment concentration with their typical variations on timescales of hours to seasons. The regime is thus defined as the typical sediment concentration and sediment distribution given these variable forcing conditions. In this thesis, the external conditions (i.e. horizontal axis in Fig. 1.5) are related to the geometry of the estuary, specifically the depth of the channel.

A regime shift as described above was first discussed by Winterwerp (2011) in context of the Ems River and elaborated on by Winterwerp and Wang (2013) and Winterwerp et al. (2013). Winterwerp and Wang (2013) formulate a hypothesis stating that a regime shift to hyperturbid conditions can occur due to the feedback mechanism illustrated in Fig. 1.6. According to the hypothesis, deepening leads to tidal amplification, or, more generally, tidal deformation (Van Maren et al., 2015). This could lead to more import of sediment, leading to higher sediment concentrations. The higher sediment concentrations lead to a reduction of turbulence or drag (cf. Section 1.2.2), which leads to a further deformation of the tide, hence forming a feedback loop. It is unknown what type of regime shift, i.e. smooth, abrupt or discontinuous, is described by this hypothesis. Moreover, various

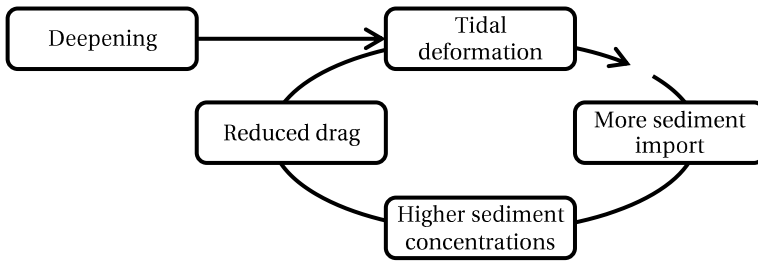


**Figure 1.6:** Sketch of the feedback processes hypothesised by Winterwerp and Wang (2013) to underlie a regime shift to hyperturbid conditions as a consequence of deepening. The figure combines the figures and text on this process by Winterwerp and Wang (2013) and Van Maren et al. (2015) to bring out the most important elements of the hypothesis.

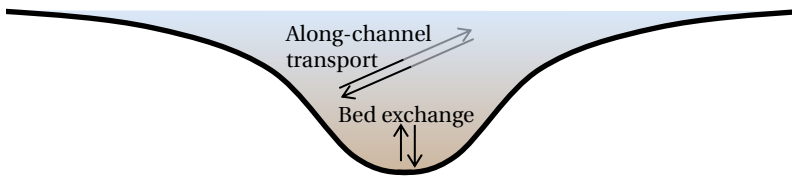


**Figure 1.7:** Sketch of an estuarine cross-section with sediment distributed non-uniformly. Cross-sectionally averaged, sediment can either be transported along the length of the estuary or deposit or resuspend from the bed.

processes that underlie this hypothesis have not been confirmed. Specifically, it has not been shown whether deepening and reduced drag generally lead to a deformation of the tide in such a way that more sediment is imported into the estuary, it has not been shown that increased sediment import generally leads to higher sediment concentrations, and it has not been shown that such feedback mechanism can be sufficiently strong to cause a big change in regime. A model study by Van Maren et al. (2015) shows that this hypothesis might hold for the Ems; they suggested that deepening and drag reduction indeed lead to more import of sediment and higher sediment concentrations but could not show whether this feedback mechanism is strong enough to cause a regime shift.

#### 1.4. ANALYSIS OF SEDIMENT DYNAMICS: AN OVERVIEW OF PRESENT KNOWLEDGE

In order to improve understanding of the sediment dynamics regime and changes to this regime for changing conditions in various estuaries, it is necessary to systematically analyse the processes contributing to the estuarine sediment dynamics. Averaged over an estuarine cross-section, sediment can either be transported along the estuary, or deposit on or resuspend from the bed, as illustrated in Fig. 1.7. As this thesis focusses on long-term dynamics, variations on the tidal timescale are filtered out, and focus is on the tidally averaged sediment transport and bed exchange processes. These processes are discussed in Sections 1.4.1 and 1.4.2, respectively.

#### 1.4.1. SUBTIDAL SEDIMENT TRANSPORT

The formation of trapping zones (see Section 1.2.1), i.e. the convergence of sediment transport, often involves a dominant downstream contribution due to the river flow balanced by a subtidal upstream transport. This subtidal upstream transport can be due to various physical processes. Below I give an overview of many of such processes that have been described in literature.

**CLASSICAL PROCESSES** As ETM were first found near the limit of the salinity intrusion, the different effects of salinity were explored as source of this subtidal upstream transport. These processes are known as *classical processes* and three main transport mechanisms can be identified. Firstly, along-estuary gradients in salinity generate gravitational circulation: a subtidal flow directed upstream near the bed and downstream near the surface. Postma and Kalle (1955) were the first to note that gravitational circulation on average transports sediment upstream, because the sediment concentration is usually largest near the bed. Following this observation, they suggested that ETM result from the balance between sediment transports by gravitational circulation and river discharge. This idea was systematically tested in a model for the first time by Festa and Hansen (1978).

Secondly, vertical stratification in salinity reduces turbulence. Including this subtidal damping of turbulent mixing further concentrates the sediment near the bed, hence leading to a stronger transport by gravitational circulation and a more intense ETM (Geyer, 1993).

Thirdly, tidal motion leads to variations in salinity stratification over the tidal cycle and therefore variations of turbulence, known as strain-induced periodic stratification or SIPS (Simpson et al., 1990). In estuaries this typically results in a more intensified subtidal flow upstream near the bed and more intensified subtidal flow downstream near the surface, amplifying the gravitational circulation (Jay and Musiak, 1994). Along similar lines, variations in salinity stratification may be caused by the wind, leading to either an amplification or weakening of the gravitational circulation, depending on the wind direction (Burchard and Hetland, 2010).

**NON-CLASSICAL SUBTIDAL PROCESSES** Many other processes, unrelated or weakly related to salinity, are able to generate subtidal flows and thereby transport sediment. These processes will be called *non-classical subtidal processes*. These include wind-driven flow (Scully et al., 2005), along-channel non-linear advective processes (i.e. asymmetry between accelerating and decelerating flow) (Li and O'Donnell, 2005), flow generated by channel curvature (Chant, 2002) and the flow generated by the Earth's rotation (i.e. due to Coriolis force) (Huijts et al., 2006). Furthermore, high sediment concentrations have a significant influence on the density of water (Section 1.2.2), thus generating gravitational circulation itself (e.g. Talke et al., 2009b). Additionally, variations of turbulence over the tidal cycle are not only generated by salinity as in the classical model (SIPS and wind straining, see above) but are generated by the tide, leading to additional contributions to the subtidal flow that have the same vertical structure as gravitational circulation. These flow contributions are called eddy viscosity-shear covariance (ESCO) circulation (Dijkstra et al., 2017). The effect of some of these ESCO circulation contribu-



tions on sediment transport was investigated by Burchard et al. (2013). Circulation in the lateral direction is furthermore found to affect along-channel flow (Fischer, 1972; Lerczak and Geyer, 2004; Huijts et al., 2009; Burchard and Schuttelaars, 2012; Schulz et al., 2015). Finally, along-channel differences in sediment properties, such as the settling velocity, affect all of the above transport contributions (Donker and De Swart, 2013).

**TIDAL PUMPING** Subtidal flows are not the only way of establishing subtidal sediment transport. Tidal covariance of the flow velocity and sediment concentration, known as *tidal pumping*, has been shown to be equally or more important in many estuaries (Allen et al., 1980; Uncles et al., 1985; Geyer et al., 2001; Scully and Friedrichs, 2007; Chernetsky et al., 2010). Tidal pumping can be subdivided into two main contributions. Firstly tidal pumping is related to temporal asymmetries (i.e. differences during ebb and flood) of the sediment concentration, flow velocity or water level. Secondly, tidal pumping is related to horizontal gradients in the flow velocity and sediment concentration, known as spatial settling lag. Both contributions are discussed elaborately below.

Temporal asymmetries in the sediment concentration, velocity and water level can be related to many interactions of physical processes. Here it is chosen to name individual interactions after the process that causes temporal asymmetry in the water motion, settling velocity, eddy diffusivity or sediment availability on the bed. Temporal asymmetries in the flow velocity and water level may be generated by non-linear tidal propagation (see e.g. Friedrichs (2010) for an introduction). The many different physical processes that generate temporally asymmetric flow include the flow due to asymmetric external tidal forcing, non-linear advection and tidal return flow. As the flow causes sediment to resuspend from the bed and advects sediment through the estuary, each of these contributions to the water motion contributes to an asymmetric sediment concentration. These contributions to the flow velocity and sediment concentration can only be distinguished using specifically designed models (Chernetsky et al., 2010; Kumar et al., 2017).

Additional temporal asymmetry in the vertical sediment distribution can be generated by tidal variations in the settling velocity (e.g. as a consequence of flocculation (Winterwerp, 2011)), turbulence or availability of sediment on the bed. A well known example related to tidal variations in turbulence is due to salinity-related turbulence variations (i.e. SIPS). SIPS not only generates a subtidal flow (see above) but also leads to more sediment mixed up into the water column during flood than during ebb. Therefore sediment is more easily transported during flood than during ebb, leading to a net upstream sediment transport (Burchard and Baumert, 1998; Scully and Friedrichs, 2003). Similarly, the effect of sediment on the density creates variations in turbulence (also called mud-induced periodic stratification, MIPS, Becker et al. (2018)), leading net upstream sediment transport following the same reasoning. Asymmetry in the availability of erodible sediment can occur if the bed shear stress exerted by the flow is smaller than the critical shear stress for erosion, known as scour lag (Dyer, 1997). This lag may be asymmetric as the flow is asymmetric.

In the absence of temporal asymmetries in the water motion, settling velocity, eddy diffusivity or sediment availability but with any spatial gradients in these quantities, tidal pumping can still occur due to spatial settling lag (see Postma, 1954; Van Straaten and

Kuenen, 1957). No further decomposition of the contributions to spatial settling lag will be made. In the presence of horizontal gradients of the flow velocity for example, spatial settling lag describes the transport towards areas where the tidal velocity amplitude or sediment concentration are lowest. Therefore it is an especially efficient trapping mechanisms at the landward limit of bays and estuaries, where the tidal velocity vanishes.

An additional process known as temporal settling lag (Groen, 1967), indicating the effect of inertia on the sediment concentration, is often mentioned as a contribution to tidal pumping. Temporal settling lag plays a role in all the contributions to tidal pumping identified above and is therefore not distinguished as a separate process causing tidal pumping in this thesis. Theoretically, it is possible to explicitly distinguish the effect of temporal settling lag on each contribution to tidal pumping, but this distinction is not made in this thesis.

#### 1.4.2. SUBTIDAL EXCHANGE WITH THE BED

As introduced in Section 1.2.1, sediment trapping may cause accumulation of sediment, but this only leads to formation of an ETM if the sediment can be resuspended from the bed by the flow. The amount of resuspension is related to three aspects: the flow, the strength and erosive properties of the bed and the amount of easily erodible sediment available on the bed. The strength and erosive properties of the bed depend on many factors including the amount of coarse material (sand, gravel) on the bed, degree of consolidation, the type of clay minerals in the sediment and biological activity on the bed (see e.g. Winterwerp and Van Kesteren (2004) and Mehta (2014) for introductions into these subjects). The description of strength and erosive properties is largely based on empirical formulations derived from results of laboratory experiments. These formulations, such as Partheniades' formulation (Kandiah, 1974), usually include one or more uncertain model parameters, including the erosion parameter and critical shear stress for erosion. Although the value of these parameters can be estimated in the field using measurements (e.g. Widdows et al., 2007), little is known about the way these parameters change as a consequence of long-term changes in forcing conditions, bed composition and estuary geometry.

The amount of easily erodible sediment on the bed, sometimes described as the *bottom pool*, fluctuates over time following changes in the flow velocity and sediment transport with a time lag on timescales ranging from several hours to months (e.g. Sommerfield and Wong, 2011). This time lag highly complicates the analysis of ETM dynamics, because the ETM observed at some moment in time not only depends on the sediment trapping and resuspension at that moment but also on the trapping and resuspension in the past. Therefore, some studies consider a state of *morphodynamic equilibrium*, defined as a state in which the sediment concentration and bed level do not change when averaged over a chosen timescale (e.g. see Friedrichs et al. (1998), Chernetsky et al. (2010) or see Zhou et al. (2017) for an in-depth review). Time lags longer than the chosen averaging timescale are not taken into account in morphodynamic equilibrium, thereby highly simplifying the analysis. The assumption of morphodynamic equilibrium is not valid in engineered estuaries where the bed level is artificially maintained at non-equilibrium levels by dredging. The same effect of eliminating time lags from the analysis can then be achieved by assuming a *concentration equilibrium* (this thesis), which

is defined as a state in which the sediment concentration does not change. The bottom pool is allowed to grow naturally in this state, but it is assumed that this growing bottom pool is continuously maintained by dredging. Hence, the bed level neither changes because of the formation of a bottom pool nor due to dredging.

## 1.5. INTRODUCTION TO THE EMS AND SCHELDT RIVER ESTUARIES

In this thesis, the response of the sediment concentration to deepening is discussed for two estuaries in particular: the Ems River and Scheldt River Estuaries. This section provides a short introduction to both rivers, focussing on past large-scale changes in the depth, water motion and sediment dynamics and discussing past research into the sediment dynamics of these estuaries.

### 1.5.1. THE EMS RIVER ESTUARY



(a) Location of the Ems in northwest Europe (b) The Ems-Dollard Estuary

**Figure 1.8:** Map of the Ems-Dollard Estuary (Netherlands/Germany) and its location in northwest Europe. Some places are marked by circles and their names. Additionally, the semi-permeable dam (Geisedamm) and shallow Dollard Bay are marked in italics.

The Ems River Estuary is located in Northern Germany and Netherlands and stretches from the tidal inlet near the island Borkum in the Wadden Sea to a tidal weir at Herbrum, approximately 110 km upstream, see Fig. 1.8b. The part between the sea and Knock is called the outer Ems Estuary, a wide multi-channel estuary with a large area of shallows. Near Knock, the Ems connects to the shallow Dollard Bay. Between Knock and Emden is the Emden Fahrwasser, where the Ems and Dollard are separated by a semi-permeable dam (the Geisedamm). Upstream from Emden in the lower Ems River, where the Ems is a narrow estuary (see e.g. Krebs and Weilbeer (2008) for an elaborate description).

Engineering works in the Ems have taken place for centuries. Starting in the 11th century, dikes were built and land has been reclaimed from the Ems floodplain (van Maren et al., 2016). Between 1897 and 1899, the tidal weir at Herbrum was constructed. Around

the same time, dredging of the inner Ems estuary and Emden waterway began, with the Emden waterway attaining its current depth in 1964 (Krebs and Weilbeer, 2008). The lower Ems River was deepened substantially between 1984 and 1995 to accommodate for large cruise ships built in Papenburg (see Fig. 1.8). Most of the major deepening operations are named after the cruise ships that were built at that time and are:

- 1984/1985: Homeric deepening to 5.7 m below mean high water (MHW),
- 1991: Zenith deepening to 6.3 m below MHW,
- 1993: unnamed deepening to 6.8 m below MHW,
- 1994/1995: Oriana deepening to 7.3 m below MHW.

Besides these deepening operations, a comparison of measured depths obtained between 1965 and 2005 shows that the lower Ems River was already much deeper in 1981 compared to 1965 (De Jonge et al., 2014), likely as a result of combined natural and anthropogenic movement of sand at the bed.

The tidal range has increased considerably since the 1950s, with over 1.5 m of amplification in the most upstream part of the estuary, see Fig. 1.9. Sediment concentrations in the lower Ems River have also changed strongly over time, see Fig. 1.10. Observations from 1949 show tidally averaged sediment concentrations in the Emden waterway of 100 mg/l (surface) - 500 mg/l (bottom) and near Pogum of 200 mg/l (surface) - 1 g/l (bottom) (Dechend, 1950). De Jonge et al. (2014) presents measurements from 1954 showing concentrations up to 200 mg/l (surface) in the Emden waterway. These different sources give some idea of the natural variation in sediment concentration and suggest that the concentrations were moderate on average. Observations from 1975 indicate that concentrations in the Emden waterway have increased to 200-300 mg/l (surface) - 2 g/l (bed) (BAW, 1975), with concentrations in the ETM of at least 400 mg/l (surface) (De Jonge et al., 2014). Average concentrations in the mid-upper water column between 1988 and 1995 increased to 0.5-2 g/l (Spinget and Oumeraci, 2000). In 1992/1993 concentrations as high as 3 g/l (surface) were observed upstream from Emden (De Jonge et al., 2014), with year-averaged values up to 1 g/l (surface). Observations of the near-bed concentration in 2006 and later show levels of ten to several hundreds of g/l in the entire section between Emden and Papenburg (Talke et al., 2009b; Wang, 2010; Papenmeier et al., 2013; Winterwerp et al., 2017; Becker et al., 2018). Clearly, the estuary underwent a regime shift (see Section 1.3) from a non-hyperturbid to hyperturbid state (Winterwerp and Wang, 2013).

Several modelling studies were conducted to reproduce this regime shift. The current state-of-the art is the realistic modelling study by Van Maren et al. (2015), who used a Delft3D model of the lower Ems River representing several years between 1945 and 2005 using different prescribed depth profiles and calibrating the model for each year. They show that sediment concentrations in their model increase over time from less than 1 g/l to over 10 g/l at 1.5 m above the bed near Pogum. However, their study required recalibration of the model over time and cannot be used to simulate the transition dynamically over time.

In order to give more insight into the main processes resulting in the regime shift, several idealised models of the lower Ems River have been constructed. Talke et al. (2009a,b)

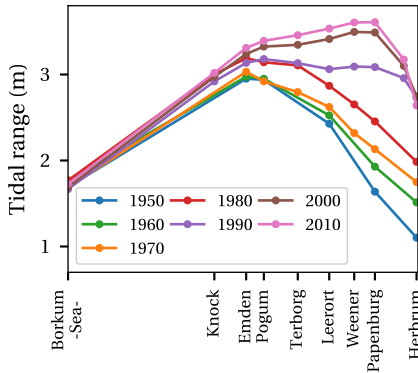


**Figure 1.9:** Tidal range at German stations. Data from WSA Emden.

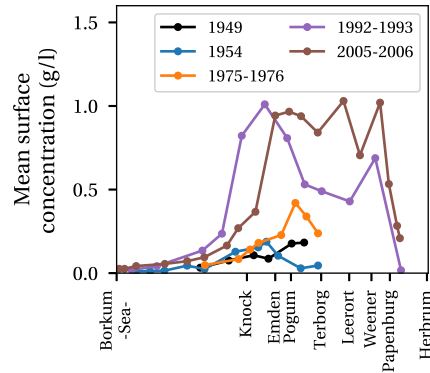


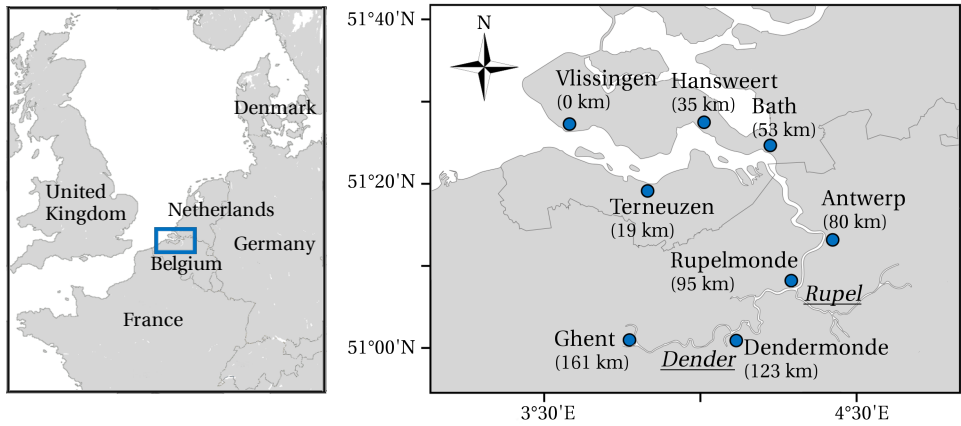
**Figure 1.10:** Surface sediment concentrations in the Ems reported by Dechend (1950) (year 1949) and De Jonge et al. (2014) (other years).

developed a highly idealised width-averaged classical subtidal (see Section 1.4.1) model, supplemented with sediment-related gravitational circulation. Assuming very little turbulent mixing, they reproduced the ETM and increase in maximum sediment concentration after deepening. Chernetsky et al. (2010) extended this model to a width-averaged model that resolves classical balance as well as several contributions to tidal pumping. They showed that the tidal pumping terms are dominant over the classical mechanisms when assuming more a more realistic amount of turbulence mixing. Comparing cases representing the Ems in 1980 and 2005, they reproduced the observed upstream movement of the ETM between 1980 and 2005. This shift was related to a decreased friction over time, possibly due to sediment-induced stratification. However, this was not dynamically resolved by their model. De Jonge et al. (2014) applied the same model to several years from 1965 to 2005, showing friction decreased over time but mostly between 1980 and 1992. The idealised model was extended to three dimensions by Kumar et al. (2017), showing that including a realistic three-dimensional bathymetry representing 2005 conditions yields the observed wide ETM between Leer and Papenburg and an additional ETM in the Emden Fahrwasser. However, all of these idealised studies require recalibration of friction parameters when applied to different years and cannot model the increase in sediment concentration.

From this it is concluded that no model study, has yet been able to describe the observed regime shift without adjusting model settings. As a consequence, it is unclear whether deepening is indeed the main cause of the observed regime shift, what processes have caused the regime shift and whether models describe these processes sufficiently well.

### 1.5.2. THE SCHELDT RIVER ESTUARY

The Scheldt River Estuary is located in the southwest of Netherlands and in Belgium and stretches from the mouth in the North Sea to sluices at Ghent, approximately 160 km upstream, see Fig. 1.11b. The Dutch Western Scheldt (< km 55) is a wide, multi-channel es-



(a) Location of the Scheldt in northwest Europe

(b) The Scheldt River Estuary

**Figure 1.11:** Map of the Scheldt River Estuary (Netherlands, Belgium) and its location in northwest Europe. Some places and their along-channel distance from the origin in Vlissingen are marked.

tuary, while the Belgian Sea Scheldt (> km 55) is a much narrower single channel system. Salt water typically intrudes up to Antwerp (km 80). Engineering works in the Scheldt have been going on since at least the 11th century in the form of land reclamation, stabilisation of the channels, building of dikes, removal of meanders and construction of ports and canals (Jeuken et al., 2007). Large amounts of sand are extracted yearly from both the Sea Scheldt and Western Scheldt since at least 1950 (IMDC et al., 2013). The effect of the sand extraction since 1950 on the depth of the river can be estimated by dividing the net mass of sand extracted (i.e. gross extraction minus re-location of extracted sand inside the estuary) by the total surface area. This is done for the Western Scheldt and Sea Scheldt separately resulting in the average deepening of both parts of the river since 1950, see Fig. 1.12. These estimates of the average depth development correspond closely to the development of the average depth computed using observed depth profiles from 1960, 2001 and 2010. Three official deepening campaigns were conducted in 1968-1973, 1997-1998 and 2008-2010 (red markings in the figure) and construction works in 1989-1990 led to further accelerated deepening. Apart from the sand extraction, maintenance dredging for the port of Antwerp takes place continuously since 1981 and all of the dredged material is deposited back into the estuary.

As a result of these engineering works and of sea level rise, the tidal range in the Scheldt has increased considerably, see Fig. 1.13. However, changes in the suspended sediment concentration in the estuary seem mild. This is illustrated in Fig. 1.14, which shows along-channel profiles of the surface sediment concentration between 1970 and 2015 according to different sources. These sources report ETM near Prosperpolder (km 60), Antwerp (km 80) and Rupelmonde-St. Amands (km 90-110) with sediment concentrations of 100-300 mg/l. The ETM at Prosperpolder is most pronounced during high dis-

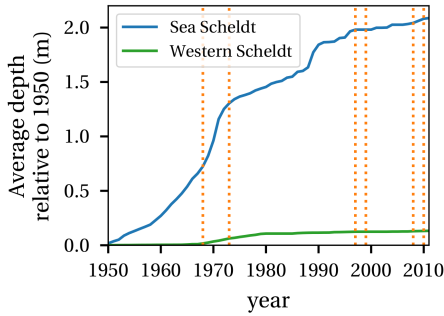


**Figure 1.12:** Estimated development of the average depth of the Western Scheldt and Sea Scheldt since 1950 based on yearly net sand extraction volumes. These estimates correspond closely to computations of the average depth development using observed depth profiles from 1960, 2001 and 2010. Red lines in the figure indicate the time of the official deepening campaigns executed additional to regular sand extraction.

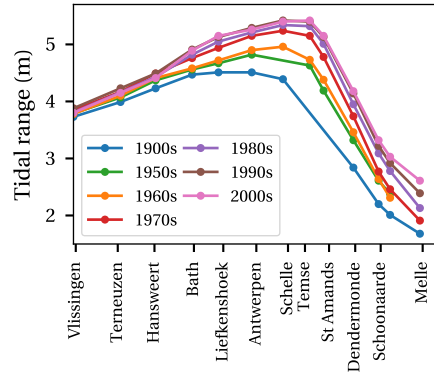


**Figure 1.13:** Tidal range along the Scheldt, corrected for the 18.6 year cycle. Figure redrawn from Winterwerp et al. (2013); see references in Kuijper and Lescinski (2012) and Plancke et al. (2012) for an overview of the original sources of the data.

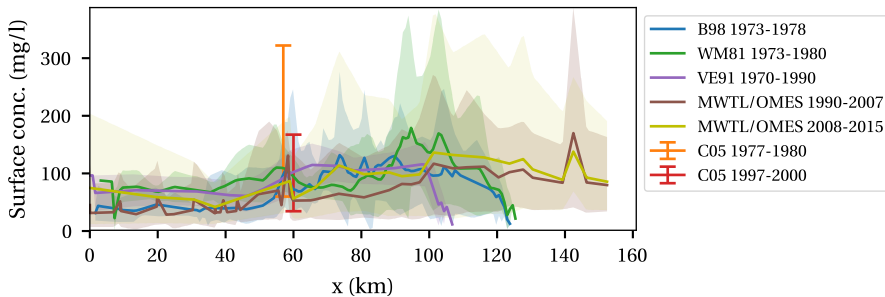


**Figure 1.14:** Observations of surface sediment concentrations in the Scheldt River Estuary between 1970 and 2015. Legend entries contain a reference to the source of the data and the years covered by the data. B98: Baeyens et al. (1998) from 11 along-channel profiles at low and high tide in several seasons (plot shows mean, maximum and minimum). WM81: Wollast and Marijns (1981) from measurements by Flanders Hydraulics Research in several seasons (plot shows mean and 5 and 95 percentile). VE91: Van Eck et al. (1991) based on their computation of minimum, maximum and high sediment concentrations. MWTL/OMES are tide-independent monthly-biweekly measurements (plot shows mean and 5 and 95 percentile). C05: Chen et al. (2005) from biweekly measurements at low tide during spring tide (plot shows 5 and 95 percentile).



charge periods, while the ETM at St. Amands is more pronounced during low discharge Wollast and Marijns (1981); Maris and Meire (2017). Additional to these surface concentrations, Wartel (1973, 1977) report concentrations of 1-5 g/l near the bed in the ETM in the summers of 1967-1969. In the years 1990-2015 average near-bed concentrations of 300-400 mg/l are observed in the ETM, with maximum values just over 1 g/l (Maris and Meire, 2017; Vanlierde et al., 2016).

Currently, several extensive long-term monitoring programmes called MWTL (Western Scheldt, since 1971), OMES (Sea Scheldt, since 1995) and Moneos (Sea Scheldt, since 2008) are maintained. Extensive analysis of data from these programmes by Vandenberghe et al. (2016) and Maris et al. (2017) show an increase of the extreme values of observed sediment concentrations in some parts of the Sea Scheldt during dry periods since 2008. These trends have not been explained, and Maris et al. (2017) point out that it is important to investigate this as it may be a warning sign indicating a possible regime shift.

Compared to the number of observations, few studies have concentrated on modelling and explaining the physical processes driving sediment transport in the Scheldt River Estuary. Peters and Sterling (1976) discuss transport mechanisms and point to the importance of spatial settling lag and tidal asymmetry in the Scheldt, yet conclude that the sediment dynamics is dominated by classical mechanisms and spatial differences in flocculation. Chen et al. (2005) also emphasise spatial differences in flocculation but suggest that tides may be important as well, though not specifying the exact mechanisms. Using a depth-averaged model and therefore not resolving classical processes, Gourgue et al. (2013) show good correspondence between model and observations, supporting the idea that tidal pumping is more important than the transport related to subtidal flows (see Section 1.4.1). Using an idealised width-averaged model, Brouwer et al. (2016) explicitly show that tidal pumping is more important than the transport related to subtidal flows. They further specify that spatial settling lag is one of the dominant contributions to tidal pumping in the Scheldt. Three-dimensional sediment modelling studies have been conducted by Salden (1997); Van Kessel et al. (2008); Vanlede et al. (2015) but have only been used for small-scale and short-timescale forecasting.

Concluding, despite large scale changes in the depth in the Scheldt since the 1950s and significant tidal amplification, it seems that the sediment concentration has remained of a similar order of magnitude over time. However, since 2008 it seems that extreme values of the sediment concentration are slowly and locally increasing. Due to the limited understanding of the sediment transport processes in the Scheldt and their changes due to a changing depth, it is unclear whether the observed changes are due to channel deepening and whether they are signalling a regime shift towards hyperturbid conditions.

## 1.6. APPROACH AND RESEARCH QUESTIONS

### 1.6.1. MODELLING APPROACH

Many approaches to modelling of estuarine sediment dynamics exist, ranging from *exploratory* (or *idealised*) to *complex* (Murray, 2003). Exploratory or idealised models are highly schematised, focussing on understanding the effect and importance of particular processes and the sensitivity of model results to changes in model parameters. Thereby

these models are a great tool to improve understanding of estuarine dynamics. However, this type of models also requires considerable simplification of the model description of natural processes and estuarine geometry. As a result of these simplifications, comparison with real-life estuaries needs to be qualitative and requires careful consideration of the model assumptions. On the other side of the spectrum, complex models aim at a quantitative comparison between model output and observations in estuaries. This requires the implementation of most known processes, state-of-the-art parameterisation and realistic geometry. The resulting models are often computationally expensive and less suitable for identifying the essential processes.

Following the goal of this thesis of improving understanding of processes that are responsible for a regime shift to a hyperturbidity regime (see Section 1.1), the model that is developed is on the idealised side of the spectrum. Central to the work in this thesis is the development and application of a width-averaged process-based model based on a perturbation method. Perturbation methods are a well-founded sub-field of mathematical physics and have been successfully applied to modelling estuarine hydrodynamics (e.g. Kreiss, 1957; Ianniello, 1977, 1979; Speer and Aubrey, 1985; Shetye and Gouveia, 1992; Lanzoni and Seminara, 1998; Li and O'Donnell, 2005; Kumar et al., 2016; Alebrektse and Swart, 2016), salinity dynamics (Jay and Smith, 1990a,b; McCarthy, 1993; Cheng et al., 2010; Wei et al., 2016) and sediment dynamics (Friedrichs et al., 1998; Chernetsky et al., 2010; Kumar et al., 2017; Brouwer et al., 2018; Wei et al., 2018). In particular, perturbation methods have proven an excellent way of distinguishing the effect of individual physical mechanisms, superior to any other available technique. However, the method only applies to weakly non-linear dynamics, an assumption that fails in high-concentration mud suspensions when sediment-water interactions dominate (see Section 1.2.2).

In this thesis the model is therefore extended based on the perturbation method but with the addition of several strongly non-linear processes, including sediment-induced damping of turbulence, hindered settling and the build-up of a sediment bottom pool. A sufficient ability to analyse the model output in detail is conserved by using an idealised large-scale geometry, idealised tidal and riverine forcing conditions and by solving for a concentration equilibrium (see Section 1.4.2), instead of transient conditions. The model complexity is gradually increased throughout this thesis, allowing for a systematic investigation of the effect and importance of various physical mechanisms. To support the development and analysis of this model development, other non-perturbative idealised models are also used. Firstly, a state-of-the-art water column model is used for investigating the mechanism of hindered settling (Chapter 3). Secondly, a fully non-linear numerical model is used with simplified geometry to verify and discuss the results of the perturbation approach (Chapter 7).

### 1.6.2. RESEARCH QUESTIONS

As stated in Section 1.1, the main goals of this thesis are:

1. to identify and better understand the essential processes driving a shift of the regime to hyperturbid conditions, by studying observed characteristics exemplified by the Ems River, and
2. to determine whether these processes are generically able to drive a regime shift to hyperturbidity in other estuaries, demonstrated by taking the Scheldt River as an example.

In pursue of these goals, this thesis attempts to provide an answer to the following questions.

- 21 What are the essential processes describing the sediment dynamics in the Ems River before reaching a hyperturbid state and in the Scheldt River in the current state?
- 22 What are the essential additional processes and changes to processes that explain the shift to a hyperturbid regime in the Ems?
- 23 What is the timescale of the regime shift in the Ems and what does this imply with respect to the essential processes responsible for this regime shift?
- 24 Can the Scheldt undergo a regime shift to hyperturbid conditions due to the same processes that are responsible for the regime shift in the Ems?
- 25 To what extent is the description of the regime shift using only a set of essential processes sufficiently representative of the physics described in state-of-the-art models?

### 1.6.3. OUTLINE OF THIS THESIS

This thesis consists of three parts after this introduction, divided into seven chapters:

#### Part I: Development of a theoretical framework

##### **Ch. 2: Development of the iFlow model**

Development of a modelling framework for sediment transport (Section 1.4.1) based on the perturbation method (Section 1.6.1). The focus of this chapter is on the model philosophy and assumptions.

##### **Ch. 3: Analysis of resuspension in a water column**

Analysis of state-of-the-art water column model, focussing on parameter sensitivity of resuspension and hindered settling (Sections 1.2.2 and 1.4.2). This results in a theoretical threshold for resuspension that is used for interpreting the results of later chapters.

#### Part II: Application to the Ems and Scheldt

##### **Ch. 4: Physical processes essential to the regime shift in the Ems**

The iFlow model from **Chapter 2** is extended by several non-linear processes (see Section 1.6.1). The analysis methods in iFlow and the resuspension threshold derived in **Chapter 3** are then used to analyse the dominant processes governing sediment transport and resuspension in the Ems before and after deepening.

##### **Ch. 5: Development of the regime shift in the Ems over time**

Building further upon **Chapter 4**, the results presented in this chapter focus on the regime shift type and timescale (Section 1.3) in the Ems, combining the iFlow model and observations between 1965 and 2005.

##### **Ch. 6: Can the Scheldt become hyperturbid?**

Using the same methodology as in **Chapter 4**, this chapter focusses on the Scheldt estuary in a recent condition and after potential further large scale deepening. To represent recent conditions, the iFlow model is extended with sources of water and sediment originating from tributaries and sediment dumping. This chapter discusses the possibility of the Scheldt becoming hyperturbid.

#### Part III: Discussion and outlook

##### **Ch. 7: Comparison between iFlow and Delft3D**

Using the Delft3D model in the same width-averaged geometry and with the same forcing as the iFlow model, several experiments from **Chapter 4** are repeated for verification of the results. The chapter focusses on understanding the differences between the models, providing an outlook to mechanisms that need to be better understood to improve understanding of hyperturbid conditions in the future.

##### **Ch. 8: Conclusions**

Presentation of the main results of this thesis in context of the research questions, and outlook to possibilities for further research.

## REFERENCES

- Alembregtse, N. C. and Swart, H. E. D. (2016). Effect of river discharge and geometry on tides and net water transport in an estuarine network, an idealized model applied to the Yangtze Estuary. *Continental Shelf Research*, 123:29–49.
- Allen, G., Salomon, J., Bassoullet, P., Penhoat, Y. D., and de Grandpré, C. (1980). Effects of tides on mixing and suspended sediment transport in macrotidal estuaries. *Sedimentary Geology*, 26:69–90.
- Baeyens, W., van Eck, B., Lambert, C., Wollast, R., and Goeyens, L. (1998). General description of the Scheldt estuary. *Hydrobiologia*, 366:1–14.
- BAW (1975). Messungen im Emden Fahrwasser am 28.11.1975. Unpublished measurements, In German.
- Becker, M., Maushake, C., and Winter, C. (2018). Observations of mud-induced periodic stratification in a hyperturbid estuary. *Geophysical Research Letters*, 45:5461–5469.
- Biggs, R., Blenckner, T., Folke, C., Gordon, L. J., Norström, A. V., Nyström, M., and Peterson, G. D. (2012). *Encyclopedia of Theoretical Ecology*, chapter Regime Shifts, pages 609–617. University of California Press.
- Boynton, W., Kemp, W., and Keefe, C. (1982). A comparative analysis of nutrients and other factors influencing estuarine phytoplankton production. In *Estuarine Comparisons*, pages 69–90. Elsevier.
- Brouwer, R. L., Schramkowski, G. P., Dijkstra, Y. M., and Schuttelaars, H. M. (2018). Time evolution of estuarine turbidity maxima in well-mixed, tidally dominated estuaries: the role of availability- and erosion-limited conditions. *Journal of Physical Oceanography*, 48:1629–1650.
- Brouwer, R. L., Schramkowski, G. P., Verwaest, T., and Mostaert, F. (2016). Geïdealiseerde processtudie van systeemovergangen naar hypertroebelheid. WP 1.4 Basismodel sediment. Technical Report WL2015R13\_103, Flanders Hydraulics Research, Antwerp, Belgium. In Dutch.
- Burchard, H. and Baumert, H. (1998). The formation of estuarine turbidity maxima due to density effects in the salt wedge. a hydrodynamic process study. *Journal of Physical Oceanography*, 28:309–321.
- Burchard, H. and Hetland, R. D. (2010). Quantifying the contributions of tidal straining and gravitational circulation to residual circulation in periodically stratified tidal estuaries. *Journal of Physical Oceanography*, 40:1243–1262.
- Burchard, H. and Schuttelaars, H. M. (2012). Analysis of tidal straining as driver for estuarine circulation in well-mixed estuaries. *Journal of Physical Oceanography*, 42:261–271.
- Burchard, H., Schuttelaars, H. M., and Geyer, W. R. (2013). Residual sediment fluxes in weakly-to-periodically stratified estuaries and tidal inlets. *Journal of Physical Oceanography*, 43:1841–1861.
- Burchard, H., Schuttelaars, H. M., and Ralston, D. K. (2018). Sediment trapping in estuaries. *Annual review of Marine Science*, 10:14.1–14.25.
- Castaing, P. and Allen, G. P. (1981). Mechanisms controlling seaward escape of suspended sediment from the Gironde: A macrotidal estuary in France. *Marine Geology*, 40:101–118.
- Chant, R. J. (2002). Secondary circulation in a region of flow curvature: relationship with tidal forcing and river discharge. *Journal of Geophysical Research: Oceans*, 107:3131.
- Chen, M. S., Wartel, S., Eck, B. V., and Maldegem, D. V. (2005). Suspended matter in the Scheldt estuary. *Hydrobiologia*, 540:79–104.
- Cheng, P., Valle-Levinson, A., and De Swart, H. E. (2010). Residual currents induced by asymmetric tidal mixing in weakly stratified narrow estuaries. *Journal of Physical Oceanography*, 40:2135–2147.
- Chernetsky, A. S., Schuttelaars, H. M., and Talke, S. A. (2010). The effect of tidal asymmetry and temporal settling lag on sediment trapping in tidal estuaries. *Ocean Dynamics*, 60:1219–1241.
- Cloern, J. E. (1987). Turbidity as a control on phytoplankton biomass and productivity in estuaries. *Continental Shelf Research*, 7:1367–1381.

- Cloern, J. E., Foster, S. Q., and Kleckner, A. E. (2014). Phytoplankton primary production in the world's estuarine-coastal ecosystems. *Biogeosciences*, 11:2477–2501.
- Colijn, F. (1982). Light absorption in the waters of the Ems-Dollard estuary and its consequences for the growth of phytoplankton and microphytobenthos. *Netherlands Journal of Sea Research*, 15:196–216.
- De Jonge, V. N., Schuttelaars, H. M., Van Beusekom, J. E. E., Talke, S. A., and De Swart, H. E. (2014). The influence of channel deepening on estuarine turbidity levels and dynamics, as exemplified by the Ems estuary. *Estuarine Coastal and Shelf Science*, 139:46–59.
- Dechend, W. (1950). Die geologischen Untersuchungen in der Ems. Technical report, WSA Emden. In German.
- Dijkstra, Y. M., Schuttelaars, H. M., and Burchard, H. (2017). Generation of exchange flows in estuaries by tidal and gravitational eddy viscosity - shear covariance (ESCO). *Journal of Geophysical Research: Oceans*, 122:4217–4237.
- Donker, J. J. A. and De Swart, H. E. (2013). Effects of bottom slope, flocculation and hindered settling on the coupled dynamics of currents and suspended sediment in highly turbid estuaries, a simple model. *Ocean Dynamics*, 63:311–327.
- Dyer, K. R. (1984). Sedimentation processes in the Bristol Channel/Severn Estuary. *Marine Pollution Bulletin*, 15:53–57.
- Dyer, K. R. (1989). Sediment processes in estuaries: Future research requirements. *Journal of Geophysical Research*, 94:14327–14339.
- Dyer, K. R. (1997). *Estuaries. A Physical Introduction*. Wiley & Sons, Chichester, UK.
- Fairbridge, R. W. (1980). *Chemistry and Geochemistry of Estuaries*, chapter The estuary: its definition and geochemical role, pages 1–35. Wiley, New York.
- Festa, J. F. and Hansen, D. V. (1978). Turbidity maxima in partially mixed estuaries: A two-dimensional numerical model. *Estuarine and Coastal Marine Science*, 7:347–359.
- Fischer, H. B. (1972). Mass-transport mechanisms in partially stratified estuaries. *Journal of Fluid Mechanics*, 53:671–687.
- Friedrichs, C. T. (2010). *Contemporary issues in estuarine physics*, chapter Barotropic tides in channelized estuaries, pages 27–61. Cambridge University Press, Cambridge, UK.
- Friedrichs, C. T., Armbrust, B. A., and de Swart, H. E. (1998). Hydrodynamic and equilibrium sediment dynamics of shallow, funnel-shaped tidal estuaries. In Dronkers, J. and Scheffers, M., editors, *Physics of Estuaries and Coastal Seas*, pages 315–328, Rotterdam. Balkema.
- Geyer, W. R. (1993). The importance of suppression of turbulence by stratification on the estuarine turbidity maximum. *Estuaries*, 16(1):113.
- Geyer, W. R., Woodruff, J. D., and Traykovski, P. (2001). Sediment transport and trapping in the Hudson River Estuary. *Estuaries*, 24(5):670.
- Gourgue, O., Baeyens, W., Chen, M., de Brauwere, A., de Brye, B., Deleersnijder, E., Elskens, M., and Legat, V. (2013). A depth-averaged two-dimensional sediment transport model for environmental studies in the Scheldt Estuary and tidal river network. *Journal of Marine Systems*, 128:27–39.
- Groen, P. (1967). On the residual transport of suspended matter by an alternating tidal current. *Netherlands Journal of Sea Research*, 3:564–574.
- Huijts, K. M. H., Schuttelaars, H. M., de Swart, H. E., and Friedrichs, C. T. (2009). Analytical study of the transverse distribution of along-channel and transverse residual flows in tidal estuaries. *Continental Shelf Research*, 29:89–100.
- Huijts, K. M. H., Schuttelaars, H. M., De Swart, H. E., and Valle-Levinson, A. (2006). Lateral entrainment of sediment in tidal estuaries: An idealized model study. *Journal of Geophysical Research: Oceans*, 111:C12016.
- Ianniello, J. P. (1977). Tidally induced residual currents in estuaries of constant breadth and depth. *Journal of Marine Research*, 35:755–786.
- Ianniello, J. P. (1979). Tidally induced residual currents in estuaries of variable breadth and depth.

- Journal of Physical Oceanography*, 9:962–974.
- IMDC, Deltares, Svasek Hydraulics, and Arcadis (2013). Instandhouding Vaarpassen Schelde Milieuvergunningen terugstorten baggerspecie. LTV - Veiligheid en Toegankelijkheid Bag-geren en storten. Achtergrondrapport A-31. Technical report. In Dutch. Available through <http://www.vnsc.eu>.
- Inglis, C. C. and Allen, F. H. (1957). Maritime paper no. 38: the regimen of the Thames Estuary as affected by currents, salinities and river flow. *Proceedings of the Institution of Civil Engineers*, 7:827–868.
- Jay, D. A. and Musiak, J. D. (1994). Particle trapping in estuarine tidal flows. *Journal of Geophysical Research: Oceans*, 99:20445–20461.
- Jay, D. A. and Smith, J. D. (1990a). Residual circulation in shallow estuaries 1. Highly stratified, narrow estuaries. *Journal of Geophysical Research: Oceans*, 95:711–731.
- Jay, D. A. and Smith, J. D. (1990b). Residual circulation in shallow estuaries 2. Weakly stratified and partially mixed, narrow estuaries. *Journal of Geophysical Research: Oceans*, 95:733–748.
- Jeuken, C., Hordijk, D., Ides, S., Kuijper, C., Peeters, P., De Sonnevile, B., and Vanlede, J. (2007). Koploperproject LTV-O&M - Thema Veiligheid – deelpject 1. Inventarisatie historische on-  
twikkeling van de hoogwaterstanden in het Schelde estuarium. Technical Report Z4384, WL |  
Delft Hydraulics. In Dutch.
- Kandiah, A. (1974). *Fundamental aspects of surface erosion of cohesive soils*. PhD thesis, University  
of California, Davis.
- Krebs, M. and Weilbeer, H. (2008). Ems-Dollart Estuary. *Die Küste*, (74):252–262.
- Kreiss, H. (1957). Some remarks about nonlinear oscillations in tidal channels. *Tellus*, 9:53–68.
- Kromkamp, J. and Peene, J. (1995). Possibility of net phytoplankton primary production in the  
turbid Schelde Estuary (SW Netherlands). *Marine Ecology Progress Series*, 121:249–259.
- Krone, R. B. (1962). Flume studies of the transport of sediment in estuarial shoaling processes; final  
report. Technical report, Berkeley : Hydraulic Engineering Laboratory and Sanitary Engineering  
Research Laboratory, University of California.
- Kuijper, C. and Lescinski, J. (2012). LTV Veiligheid en Toegankelijkheid. Sub project B. Data-  
analysis water levels, bathymetry Western Scheldt. Report 1204405. Technical report, Deltares.
- Kumar, M., Schuttelaars, H., Roos, P. C., and Möller, M. (2016). Three-dimensional semi-idealized  
model for tidal motion in tidal estuaries. *Ocean Dynamics*, 66:99–118.
- Kumar, M., Schuttelaars, H. M., and Roos, P. C. (2017). Three-dimensional semi-idealized model  
for estuarine turbidity maxima in tidally dominated estuaries. *Ocean Modelling*, 113:1–21.
- Lanzoni, S. and Seminara, G. (1998). On tide propagation in convergent estuaries. *Journal of  
Geophysical Research: Oceans*, 103:30793–30812.
- Lerczak, J. A. and Geyer, W. R. (2004). Modelling the lateral circulation in straight, stratified estuar-  
ies. *Journal of Physical Oceanography*, 34:1410–1428.
- Li, C. and O'Donnell, J. (2005). The effect of channel length on the residual circulation in tidally  
dominated estuaries. *Journal of Physical Oceanography*, 35:1826–1840.
- Maris, T., Cox, T., and Meire, P. (2017). Nota wijzigingen in oppervlakte SPM concentraties in de  
Boven-Zeeschelde. Technical Report 017-R205, University of Antwerp, Department of Ecosys-  
tem Management (ECOB), Antwerp, Belgium. In Dutch.
- Maris, T. and Meire, P. (2017). Onderzoek naar de gevolgen van het Sigmaplan, baggeractiviteiten  
en havenuitbreiding in de Zeeschelde op het milieu. geïntegreerd eindverslag van het onder-  
zoek verricht in 2016. Technical Report 017-R206, University of Antwerp, Department of Ecosys-  
tem Management (ECOB), Antwerp, Belgium. In Dutch.
- McCarthy, R. K. (1993). Residual currents in tidally dominated, well-mixed estuaries. *Tellus*,  
45A:325–340.
- Meade, R. H., Dunne, T., Richey, J. E., de M. Santos, U., and Salati, E. (1985). Storage and remo-  
bilization of suspended sediment in the Lower Amazon River of Brazil. *Science*, 228(4698):488–  
490.

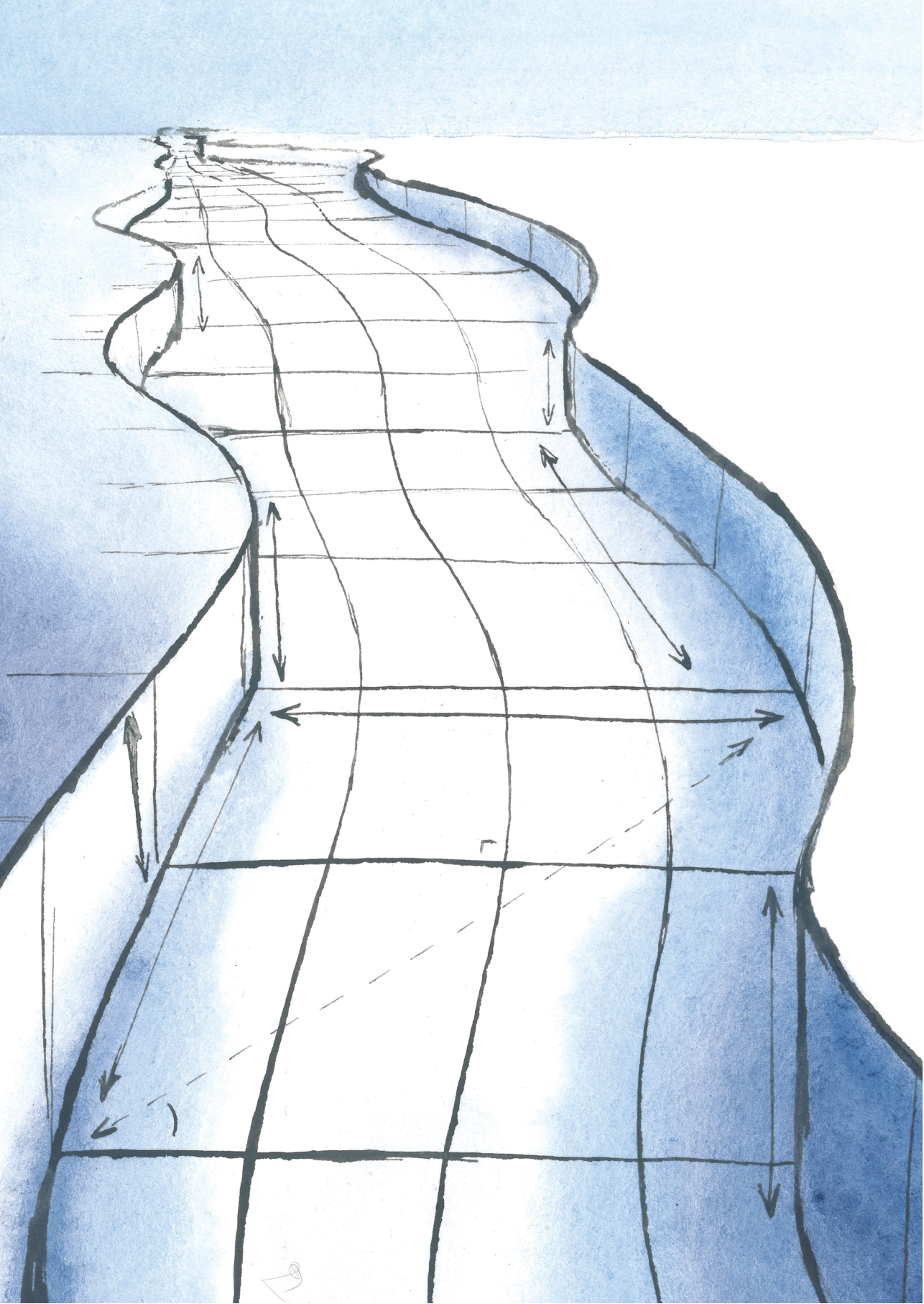


- Mehta, A. J. (2014). *An introduction to the hydraulics of fine sediment transport*. World Scientific.
- Murray, A. B. (2003). *Prediction in Geomorphology*, chapter Contrasting the Goals, Strategies, and Predictions Associated with Simplified Numerical Models and Detailed Simulations, pages 151–165. American Geophysical Union, Washington, D. C.
- Papenmeier, S., Schrottke, K., Bartholomä, A., and Flemming, B. W. (2013). Sedimentological and rheological properties of the water-solid bed interface in the Weser and Ems Estuaries, North Sea, Germany: Implications for fluid mud classification. *Journal of Coastal Research*, 29:797–808.
- Peters, J. J. and Sterling, A. (1976). Hydrodynamique et transport de sédiments dans l'estuaire de l'Escaut. In Nihoul, J. C. J. and Wollast, R., editors, *Project Sea, Final Report Part 10: The Scheldt Estuary*, pages 1–70. In French.
- Plancke, Y., Maximova, T., Ides, S., Peeters, P., Taveniers, E., and Mostaert, F. (2012). Werkgroep O&M - projectgroep veiligheid. Sub project 1: Data analysis and hypothesis - Lower Sea Scheldt. WL Rapporten, 756/05. Technical report, Flanders Hydraulics Research: Antwerp, Belgium.
- Postma, H. (1954). Hydrography of the Dutch Wadden Sea. *Archives Néerlandaises de Zoologie*, 10:405–511.
- Postma, H. and Kalle, K. (1955). Die Entstehung von Trübungszone im Unterlauf der Flüsse, speziell im Hinblick auf die Verhältnisse in der Unterelbe. *Deutsche Hydrographische Zeitung*, 8:138–144.
- Pritchard, D. W. (1967). What is an estuary: a physical viewpoint. *American Association for the Advancement of Science*, 83:3–5.
- Richardson, J. F. and Zaki, W. N. (1954). The sedimentation of a suspension of uniform spheres under conditions of viscous flow. *Chemical Engineering Science*, 8:65–78.
- Salden, R. M. (1997). Een slib-transportmodel van het Schelde estuarium ten behoeve van waterkwaliteitsmodellering. Technical Report RSKZ/OS-97.116X, RIKZ. In Dutch.
- Scheffer, M., Carpenter, S., Foley, J. A., Folke, C., and Walker, B. (2001). Catastrophic shifts in ecosystems. *Nature*, 413(6856):591–596.
- Schulz, E., Schuttelaars, H. M., Gräwe, U., and Burchard, H. (2015). Impact of the depth-to-width ratio of periodically stratified tidal channels on the estuarine circulation. *Journal of Physical Oceanography*, 45:2048–2069.
- Schuttelaars, H. M., de Jonge, V. N., and Chernetsky, A. S. (2013). Improving the predictive power when modelling physical effects of human interventions in estuarine systems. *Ocean and Coastal Management*, 79:70–82.
- Scully, M. E. and Friedrichs, C. T. (2003). The influence of asymmetries in overlying stratification on near-bed turbulence and sediment suspension in a partially mixed estuary. *Ocean Dynamics*, 53(3):208–219.
- Scully, M. E. and Friedrichs, C. T. (2007). The importance of tidal and lateral asymmetries in stratification to residual circulation in partially mixed estuaries. *Journal of Physical Oceanography*, 37:1496–1511.
- Scully, M. E., Friedrichs, C. T., and Brubaker, J. M. (2005). Control of estuarine stratification and mixing by wind-induced straining of the estuarine density field. *Estuaries*, 28:321–326.
- Shetye, S. and Gouveia, A. (1992). On the role of geometry of cross-section in generating flood-dominance in shallow estuaries. *Estuarine, Coastal and Shelf Science*, 35(2):113–126.
- Simpson, J. H., Brown, J., Matthews, J., and Allen, G. (1990). Tidal straining, density currents, and stirring in the control of estuarine stratification. *Estuaries*, 13:125–132.
- Sommerfield, C. K. and Wong, K.-C. (2011). Mechanisms of sediment flux and turbidity maintenance in the Delaware Estuary. *Journal of Geophysical Research*, 116(C1).
- Speer, P. and Aubrey, D. (1985). A study of non-linear tidal propagation in shallow inlet/estuarine systems part II: Theory. *Estuarine, Coastal and Shelf Science*, 21:207–224.
- Spingat, F. and Oumeraci, H. (2000). Schwebstoffdynamik in der Trübungszone des Ems Ästuars Anwendung eines Analysekonzeptes für hoch aufgelöste und dauerhaft betriebene



- Gewässergütemessungen. *Die Küste*, 62:159–219.
- Talke, S. A., De Swart, H. E., and De Jonge, V. N. (2009a). An idealized model and systematic process study of oxygen depletion in highly turbid estuaries. *Estuaries and Coasts*, 32:602–620.
- Talke, S. A., De Swart, H. E., and Schuttelaars, H. M. (2009b). Feedback between residual circulations and sediment distribution in highly turbid estuaries: an analytical model. *Continental Shelf Research*, 29:119–135.
- Uncles, R. J., Elliott, R. C. A., and Weston, S. A. (1985). Observed fluxes of water, salt and suspended sediment in a partly mixed estuary. *Estuarine, Coastal and Shelf Science*, 20(2):147–167.
- Uncles, R. J., Stephens, J. A., and Law, D. J. (2006). Turbidity maximum in the macrotidal, highly turbid Humber Estuary, UK: Floccs, fluid mud, stationary suspensions and tidal bores. *Estuarine, Coastal and Shelf Science*, 67:30–52.
- Uncles, R. J., Stephens, J. A., and Smith, R. E. (2002). The dependence of estuarine turbidity on tidal intrusion length, tidal range and residence time. *Continental Shelf Research*, 22:1835–1856.
- Underwood, G. J. C. and Kromkamp, J. C. (1999). *Advances in Ecological Research*, volume 29, chapter Primary production by phytoplankton and microphytobenthos in estuaries, pages 93–153. Academic press.
- Van Eck, G. T. M., De Pauw, N., Van den Langenbergh, M., and Verreet, G. (1991). Emissies, gehalten, gedrag en effecten van (micro)verontreinigingen in het stroomgebied van de Schelde en het Schelde-estuarium. *Water*, 60:84–99.
- Van Kessel, T., Vanlede, J., Eleveld, M., and Van der Wal, D. (2008). Mud transport model for the Scheldt estuary in the framework of LTV. Technical report, Deltares, Flanders Hydraulics, IVM, NIOO.
- van Maren, D., Oost, A., Wang, Z., and Vos, P. (2016). The effect of land reclamations and sediment extraction on the suspended sediment concentration in the Ems Estuary. *Marine Geology*, 376:147–157.
- Van Maren, D. S., Winterwerp, J. C., and Vroom, J. (2015). Fine sediment transport into the hyper-turbid lower Ems River: the role of channel deepening and sediment-induced drag reduction. *Ocean Dynamics*, 65:589–605.
- Van Straaten, L. M. J. U. and Kuenen, P. H. (1957). Accumulation of fine grained sediments in the Dutch Wadden Sea. *Netherlands Journal of Geosciences*, 19:329–354.
- Vandenbruwaene, W., Vanlede, J., Plancke, Y., Verwaest, T., and Mostaert, F. (2016). Slibbalans Zeeschelde: Deelrapport 4 - Historische evolutie SPM. Technical Report WL Rapporten 00\_029\_4, Flanders Hydraulics Research and Antea, Antwerp, Belgium. In Dutch.
- Vanlede, J., Smolders, S., Maximova, T., and Teles, M. J. (2015). The unstructured scaldis model: A new 3D high resolution model for hydrodynamics and sediment transport in the tidal Scheldt. In *Scheldt Estuary physics and integrated management, special session on the 36th IAHR world congress, Delft and The Hague, Netherlands*.
- Vanlierde, E., Ferket, B., Pauwaert, Z., Michielsen, S., Van De Moortel, I., Levy, Y., Plancke, Y., Meire, D., Deschamps, M., Verwaest, T., and Mostaert, F. (2016). MONEOS - jaarboek monitoring WL 2015. Factual data rapportage van monitoring hydrodynamiek en fysische parameters zoals gemeten door WL in het Zeescheldebekken in 2015. Versie 3.0. Technical Report 12\_070, Flanders Hydraulics Research. In Dutch.
- Wang, L. (2010). *Tide Driven Dynamics of Subaqueous Fluid Mud Layers in Turbidity Maximum Zones of German Estuaries*. PhD thesis, University of Bremen.
- Wang, Z., Maren, D. V., Ding, P., Yang, S., Prooijen, B. V., Vet, P. D., Winterwerp, J., Vriend, H. D., Stive, M., and He, Q. (2015). Human impacts on morphodynamic thresholds in estuarine systems. *Continental Shelf Research*, 111:174–183.
- Wartel, S. (1973). Variations in concentration of suspended matter in the Scheldt Estuary. *Bulletin Institut royal des Sciences naturelles de Belgique Sciences de la Terre*, 49:1–11.
- Wartel, S. (1977). Composition, transport and origin of sediments in the Schelde Estuary. *Geologie en Mijnbouw*, 56:219–233.

- Wei, X., Kumar, M., and Schuttelaars, H. M. (2018). Three-dimensional sediment dynamics in well-mixed estuaries: Importance of the internally generated overtide, spatial settling lag, and gravitational circulation. *Journal of Geophysical Research: Oceans*, 123:1062–1090.
- Wei, X., Schramkowski, G. P., and Schuttelaars, H. M. (2016). Salt dynamics in well-mixed estuaries: Importance of advection by tides. *Journal of Physical Oceanography*, 46:1457–1475.
- Widdows, J., Friend, P., Bale, A., Brinsley, M., Pope, N., and Thompson, C. (2007). Inter-comparison between five devices for determining erodability of intertidal sediments. *Continental Shelf Research*, 27(8):1174–1189.
- Winterwerp, J. C. (2011). Fine sediment transport by tidal asymmetry in the high-concentrated ems river: indications for a regime shift in response to channel deepening. *Ocean Dynamics*, 61:203–215.
- Winterwerp, J. C. and Van Kesteren, W. G. M. (2004). *Introduction to the Physics of Cohesive Sediment Dynamics in the Marine Environment*. Developments in sedimentology, 56. Elsevier.
- Winterwerp, J. C., Vroom, J., Wang, Z. B., Krebs, M., Hendriks, E. C. M., Van Maren, D. S., Schrottke, K., Borgsmüller, C., and Schöl, A. (2017). SPM response to tide and river flow in the hyper-turbid Ems River. *Ocean Dynamics*, 67:559.
- Winterwerp, J. C. and Wang, Z. B. (2013). Man-induced regime shifts in small estuaries - I: theory. *Ocean Dynamics*, 63:1279–1292.
- Winterwerp, J. C., Wang, Z. B., Van Brackel, A., Van Holland, G., and Kösters, F. (2013). Man-induced regime shifts in small estuaries - II: a comparison of rivers. *Ocean Dynamics*, 63:1293–1306.
- Wofsy, S. C. (1983). A simple model to predict extinction coefficients and phytoplankton biomass in eutrophic waters. *Limnology and Oceanography*, 28(6):1144–1155.
- Wollast, R. and Marijns, A. (1981). Evaluation des contributions de différentes sources de matières en suspension à l'envasement de l'Escaut. Technical report, Final report to the Ministry of Public Health and Environment. In French.
- Zhou, Z., Coco, G., Townend, I., Olabarrieta, M., van der Wegen, M., Gong, Z., D'Alpaos, A., Gao, S., Jaffe, B. E., Gelfenbaum, G., He, Q., Wang, Y., Lanzoni, S., Wang, Z., Winterwerp, H., and Zhang, C. (2017). Is “morphodynamic equilibrium” an oxymoron? *Earth-Science Reviews*, 165:257–267.





# CHAPTER 2

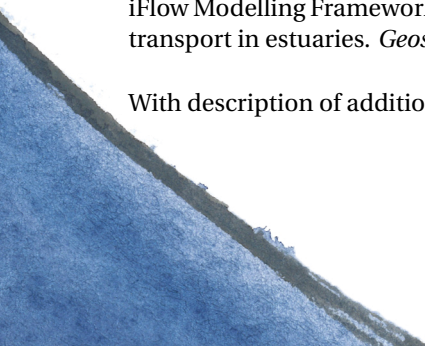
## The iFlow Modelling Framework v2.5

A modular idealised process-based model for flow and transport in estuaries

Based on section 1 to 5 of

Dijkstra, Y. M., Brouwer, R. L., Schuttelaars, H. M., and Schramkowski, G. P. (2017). The iFlow Modelling Framework v2.4. A modular idealized process-based model for flow and transport in estuaries. *Geoscientific Model Development*, 10:2691-2713.

With description of additions in iFlow version 2.5.



## **Abstract**

---

The iFlow modelling framework is a width-averaged model for the systematic analysis of the water motion and sediment transport processes in estuaries and tidal rivers. The distinctive solution method, a mathematical perturbation method, used in the model allows for identification of the effect of individual physical processes on the water motion and sediment transport and study of the sensitivity of these processes to model parameters. This distinction between processes provides a unique tool for interpreting and explaining hydrodynamic interactions and sediment trapping. iFlow also includes a large number of options to configure the model geometry and multiple choices of turbulence and salinity models. Additionally, the model contains auxiliary components, including one that facilitates easy and fast sensitivity studies.

iFlow has a modular structure, which makes it easy to include, exclude or change individual model components, called modules. Depending on the required functionality for the application at hand, modules can be selected to construct anything from very simple quasi-linear models to rather complex models involving multiple non-linear interactions. This way, the model complexity can be adjusted to the application. Once the modules containing the required functionality are selected, the underlying model structure automatically ensures modules are called in the correct order. The model inserts iteration loops over groups of modules that are mutually dependent. iFlow also ensures a smooth coupling of modules using analytical and numerical solution methods. This way the model combines the speed and accuracy of analytical solutions with the versatility of numerical solution methods.

---



## 2.1. INTRODUCTION

The dynamics of estuaries and tidal rivers are characterised by the complex interplay of mutually interacting processes related to the water motion (i.e. tidal propagation, river run-off), salinity and sediment dynamics, transport of nutrients and bathymetric changes. In many estuaries and tidal rivers these processes are subject to constant change due to human interventions, such as dredging and canalisation, or to natural changes, such as sea level rise or changing river discharge. These changes may lead to practical problems. Focussing on the hydrodynamics and sediment dynamics, examples are increasing risks of flooding related to tidal amplification or reflection (e.g. Friedrichs and Aubrey, 1994; Winterwerp et al., 2013; Schuttelaars et al., 2013) and deteriorating ecosystems due to a decreased light penetration caused by increasing suspended sediment concentrations (e.g. Colijn, 1982; Cloern, 1996; De Jonge et al., 2014). Many systems face several simultaneous natural and anthropogenic changes, which each affect multiple processes. Therefore the understanding of these processes and their interrelations through models, in combination with observational evidence, is of paramount importance in anticipating the effect of future natural and anthropogenic change.

A wide range of process-based models has contributed to the present-day understanding of flow and transport processes. These models range from linear one-dimensional along-channel models to non-linear three-dimensional numerical models. One way of classifying models is to describe their position in the spectrum ranging from *exploratory* to *complex* models (Murray, 2003). On one end of this spectrum, exploratory, or idealised, models typically include a limited number of processes that are thought to be important for the particular phenomenon that is studied. These models come in many forms, ranging from one-dimensional to three-dimensional and from analytic to numeric. The common property of these models is their excellent ability to quickly investigate the sensitivity to parameter variations and to systematically study individual physical processes. Since they are often custom-built, the applied solution techniques do not allow for an easy extension to more processes or complex model domains. Therefore the comparison between these models and real-life systems has to be qualitative, and one needs to consider carefully the effect of the underlying assumptions. On the other side of the spectrum, complex models aim at a quantitative comparison of the model results with observations in a wide range of real systems. This requires the implementation of most known processes and their mutual interactions through state-of-the-art parametrisations. As a result, such models are typically numerical and non-linear, and computation times are relatively long. This makes complex models less suitable for identifying the essential processes and conducting extensive sensitivity studies.

The aim of the iFlow modelling framework is to combine the strengths of both approaches identified above, that is, to represent some of the complex processes and interactions contained in complex models while retaining the ability to analyse these processes and study their sensitivity. iFlow is a width-averaged model for hydrodynamics and sediment transport processes in single-branch estuaries and tidal rivers, focussing on global estuarine processes. Within this context, the model is able to cover a wide range of complexity, reaching out to both the idealised and complex model types. This requires a structured and systematic approach. This approach starts from the exploratory model of Chernetsky et al. (2010), which solves for a specific subset of hydro- and sediment dy-

namical processes using a combination of analytical and semi-analytical solution methods. The power of iFlow lies in its ability to extend this basic model by adding more complex and realistic interactions, which can either be included in or excluded from the model depending on the application. These extensions can often only be resolved numerically and sometimes require iterative methods. The model thus naturally consists of a set of coupled and mutually interacting components that solve for different processes using different solution methods. These model components are called *modules* in iFlow. Modules form code-independent entities that can be developed independently and can be easily added to the model without requiring changes to other modules. The iFlow core takes care of the coupling of modules through a simple standardised input/output protocol, thus facilitating interactions between processes in different modules. This allows for a natural development of the model by implementing new processes or different implementations of already existing ones, motivated by the needs for the application at hand.

iFlow currently includes several modules that allow for the computation of the flow and suspended sediment transport. Most of these modules focus on identifying the effect of individual processes and to this end use a perturbation approach. This approach has been successfully applied before in the context of estuarine research by e.g. Ianniello (1977, 1979); Chernetsky et al. (2010); Cheng et al. (2010); Wei et al. (2016). The perturbation approach is used to identify processes that balance at different orders of magnitude. Under suitable assumptions of weakly non-linear flow, the leading-order flow and sediment balances reduce to linear equations describing the propagation of the tide and tidal re-suspension of sediment. These balances match classical exploratory model results (e.g. Prandle (1982); Hansen and Rattray (1965); Friedrichs and Aubrey (1994) and references therein). However, non-linear processes and other processes that are not of leading order are not neglected. Rather, linear estimates of the non-linear processes are taken into account at the first and higher orders. Because of the linearity, the effects of each process on the flow and sediment concentration can be evaluated separately. In this way, the fully non-linear solution can theoretically be approximated to any degree of accuracy, while the effects of individual processes and interactions can still be analysed. Practically, it turns out that the qualitative properties of the solution are often well described by only a limited set of orders and processes.

Summarising, the iFlow philosophy revolves around three central ideas:

1. The model is easily extendible by new processes.
2. The model allows for the combination of different solution methods for different processes, including analytical and numerical solution methods.
3. It is possible to identify the effects of individual physical forcing mechanisms and interactions.

This chapter is structured into two main parts. In the first part, in Section 2.2, the modular model structure is discussed in detail using a basic example involving four modules. This section ends with a list of the modules included in model version 2.5 in Section 2.2.3. This forms the introduction to the second part of this chapter, which discusses the specific modules that form iFlow's functionality in Sections 2.3-2.5. Section 2.3 presents the model domains and numerical grids currently allowed. Section 2.4 then provides

a discussion of the modules for hydrodynamics and sediment dynamics, focussing on the assumptions and options in these modules. A short outline of the other main modules, including the various turbulence closures, salinity models and sensitivity modules is provided in Section 2.5. While this chapter provides an overview of the model features and methods, an in-depth user manual and a full technical description of the model are provided online (see the Code Availability chapter at the end of this thesis).

## 2.2. MODULAR STRUCTURE

In order to satisfy the three criteria set in the introduction (extendibility, interchangeability and ease of analysis), the structure of iFlow has to be modular. Modules are separate model entities that implement certain physical processes or perform auxiliary tasks, such as plotting or initiating a sensitivity study. A module may use any approach to obtain the required variables, for example solving a set of equations, loading measured or modelled data from a file or even linking to another modelling suite. Modules are code-independent, meaning that the interaction between different modules is only on input and output level, not on code level. This allows an independent development of modules by different developers, while ensuring seamless interaction between different modules. It also allows easy interchangeability of modules that compute the same variables but that differ in the physical processes taken into account or the type of implementation used.

Depending on the problem at hand, users can select which variables to save, which physical processes to include and which auxiliary tasks to perform by selecting a set of modules. These modules are listed in an *input file*, together with the input parameters required by these modules. Upon the start of a simulation, iFlow will read the input file and start an automated two-step process: ordering the modules into a *call stack* and then calling the modules in this order. Below, these steps are explained and illustrated using the example displayed in Figure 2.1, which gives a simplified demonstration of the computation of the leading-order flow velocity (i.e. linear propagation of the tide) through a set of four interacting modules.

### 2.2.1. BUILDING THE CALL STACK

As a first step, iFlow reads the input file (Figure 2.1a) and compiles a list of the modules. In order to determine the order in which to call these modules, iFlow needs information on the input required and output returned by each module. This information is documented in a *registry file* (Figure 2.1b), which is provided with the modules and does not need to be given on input. The call stack is made by matching the output provided by each module to the input required by the other modules, such that the required input is available at the moment a module is called.

The input file lists four modules with a specific task each: *RegularGrid* for making a grid, *Geometry2DV* for setting the model geometry, *HydroLead* for computing the leading-order hydrodynamics and *KEFitted* as turbulence closure. At the end, the input file lists the variables that are required by the user, e.g. for saving or plotting, here these variables are the leading-order velocity  $u^0$  and eddy viscosity  $A_v$  (more information on these variables and the underlying equations will be provided in Sections 2.4 and 2.5). The registry file (Figure 2.1b) contains the same modules with their input and output variables. Us-



```
#####
## Input File ##
#####
## Grid ##

module numerical2DV.RegularGrid
xgrid equidistant 100
zgrid equidistant 50
fgrid integer 2

## Geometry ##
module analytical2DV.Geometry2DV
L 150000
B0 type functions.Polynomial
C -1.4e-6 7.5e-3 9.8e2
H0 type functions.Constant
C0 10

## Hydrodynamics ##
module numerical2DV.HydroLead
A0 0 1.5
phase0 0 0
Q0 100

## Turbulence ##
module analytical2DV.KEFitted
profile uniform
z0* 0.005
Avmin 1.e-6

Requirements u0 Av
```

```
#####
## Registry ##
#####
module RegularGrid
input xgrid zgrid fgrid H B L
output grid

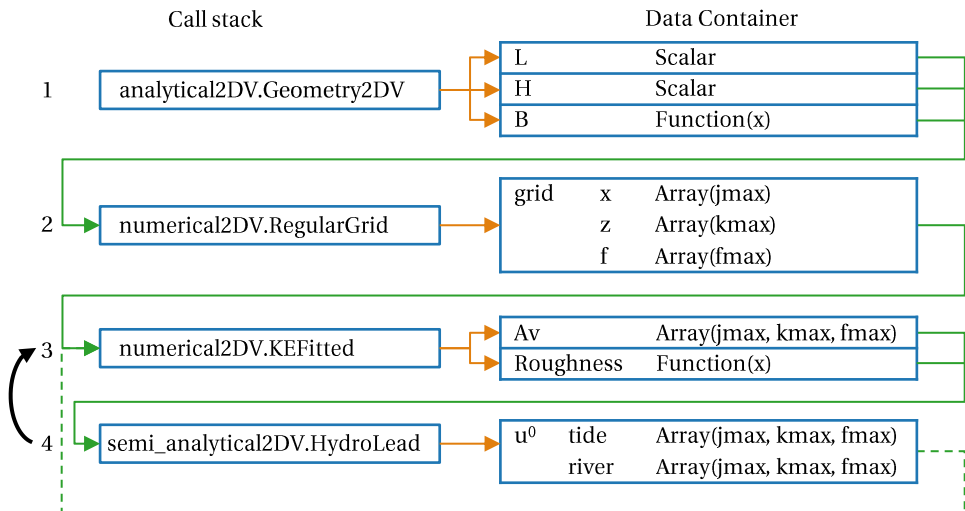
module Geometry2DV
input H0 B0 L
output H B L

module HydroLead
input A0 phase0 Q0 grid
output H B L Av Roughness
submodules u0
tide river

module KEFitted
inputInit profile z0* Avmin grid
Input profile z0* Avmin grid u0
output Av Roughness
Iterative True
```

(a) Input file

(b) Registry file

(c) Call stack and communication with the *DataContainer*

**Figure 2.1:** Basic example of input (a) and registry (b) files for a model with four modules. The core uses the input and registry files to make a call stack (c) with the correct order of the modules. The output of each module is stored in the data container to be used as input to other modules.

ing the registry file, iFlow assesses that the outputs of the *HydroLead* module,  $u^0$ , and of *KEFitted*,  $A_v$  are needed to obtain the required variables. iFlow then constructs the call stack, by determining the modules needed in order to run *HydroLead* and *KEFitted*. Focussing on *HydroLead*, it follows from the registry that this module requires nine input variables. These variables may be provided in the input file, by the output of other modules or in a configuration file (not shown here, see the manual for details). Three of these input variables,  $A^0$ ,  $\text{phase}^0$  and  $Q^0$  are provided in the input file, while the other six follow from the output of other modules. By matching all the input for and output of the four modules, iFlow constructs the call stack depicted in Figure 2.1c.

The call stack shows a loop between *HydroLead* and *KEFitted*, which is necessary as both require each other's output as input. This interdependency is resolved by defining *KEFitted* as an *iterative module*. Behind the keyword *inputInit* in the registry of *KEFitted* it can be seen that this module does not require the flow velocity  $u^0$ , computed by *HydroLead*, for its first run. In subsequent runs of the iteration,  $u^0$  is required. iFlow recognises the interdependency and constructs the smallest possible iteration loop, here involving the two interdependent modules only. The number of iterations follows dynamically from a convergence criterion that is implemented in the *KEFitted* iterative module.

As a consequence of the way that iFlow constructs the call stack, the model will not use modules that are not needed to compute the required variables. A notification of this is given when running a simulation. Similarly, a notification is given if the call stack cannot be completed, because certain input variables are missing.

The example discussed here can easily be extended, e.g. by adding modules for computing additional variables or by adding auxiliary modules for saving the output or plotting it. To allow for more flexibility, the input and output files allow for a number of additional options that are beyond the scope of this chapter, such as submodules and input-dependent output requirements. Details on this are provided in the iFlow manuals.

### 2.2.2. RUNNING AND DATA MANAGEMENT

After construction of the call stack, the modules are called sequentially in the determined order. As modules are required to be code-independent, they are not allowed to communicate directly with each other. Instead, the iFlow core regulates the distribution of the required input data and collection of the resulting output. The management of these data is facilitated by the *DataContainer* in the iFlow core. It collects the module's output upon completion and handles the input data requests by each module, see Figure 2.1c. To simplify the interchangeability of modules and the analysis of data, the *DataContainer* supports various data types and data decompositions as is discussed more elaborately below.

Different modules used within one simulation can have widely different degrees of complexity and are allowed to use different solution methods. Therefore the requested input and resulting output data can be of different types, including scalars, multi-dimensional arrays and analytical function descriptions. In our example, *Geometry2DV* sets a constant depth  $H$ , which is saved as a scalar value (see also Figure 2.1c). Other implementations of the depth allow for depths varying over the horizontal  $x$ -coordinate according to

prescribed analytical functions or data on a grid. This difference in the way the depth is prescribed should not influence the functioning of other modules. The *DataContainer* allows this by providing a uniform interface to all data types. This means that there is one command for a module to retrieve  $H$  (or any other variable) regardless of the underlying data type. The *DataContainer* handles this command based on the data type. For example, the *RegularGrid* module requests  $H$  on grid points. If  $H$  is stored as a scalar, the *DataContainer* automatically extends this scalar value to all requested points. If  $H$  is stored as an analytical function description, this function is evaluated at the grid points. Data stored on numerical grids may as well be used as input to analytical functions. If the numerical data are requested at other coordinates than the grid points, the *DataContainer* automatically interpolates these data to the requested coordinates. Similarly, a module can access the derivative of a variable. iFlow sees whether an analytical function or numerical data for this derivative is provided and, if not, will automatically perform numerical differentiation.

Since iFlow is designed to improve the understanding of physical processes, modules may offer decompositions of data into contributions resulting from different physical components. The method of decomposition is the responsibility of individual modules. An example of this using the perturbation method will be discussed in Section 2.4 for the hydrodynamics and sediment dynamics modules. Within iFlow's philosophy, it should be possible to interchange these modules with others that do not make decompositions or make decompositions in different components, without affecting other modules. The *DataContainer* supports this using sub-variables. This is illustrated in Figure 2.1c for the flow velocity variable  $u^0$ . This has contributions induced by the tide and by the river discharge, such that the sum of both yields the total flow velocity  $u^0$ . The *KEFitted* turbulence model does not require this decomposition and does not necessarily need to be aware that such a decomposition exists. It can therefore simply request  $u^0$  and iFlow will automatically sum the tide and river contributions. Alternatively a module may request a list of all the sub-variables of  $u^0$  and request each of these contributions separately.

### 2.2.3. iFlow STANDARD MODULES

The iFlow modelling framework includes a number of standard modules that may be used to simulate and analyse the water motion and sediment dynamics in estuaries and tidal rivers. Together, the standard modules provide a full model for hydrodynamics and sediment dynamics that may be used in different combinations to model various levels of complexity. Here we focus on the modules for computing the long-term equilibrium water motion and sediment dynamics. Functionalities that allow computation of the long-term dynamics are discussed by Brouwer et al. (2018). The modules are organised into four packages, *general*, *analytical2DV*, *numerical2DV* and *semi-analytical2DV*, containing auxiliary modules and modules using analytical, numerical or semi-analytical (i.e. largely analytical, with numerical components) solution methods respectively. All included standard modules for equilibrium computations and the location where they can be found are listed in Table 2.1. A short introduction to many of these modules is provided in the next sections.

Module	Description
<b>package general</b>	
Output	Save output variables for use within iFlow.
OutputMat	Save output variables to a .mat file for use in Matlab.
ReadSingle	Load a single iFlow output file.
ReadMultiple	Load multiple iFlow output files.
ReadIterative	Like ReadMultiple it reads multiple output iFlow output files but only loads one file at a time.
Sensitivity	Intelligently loop the simulation over any number of values of any number of variables.
Calibration	Automatic calibration of $M_2$ water level to observations using a specified cost function. Only for one-parameter calibration.
<b>package numerical2DV</b>	
RegularGrid	Create a 2DV standard grid and output grid.
HydroLead	Leading-order hydrodynamics using fully numerical methods.
HydroFirst	First-order hydrodynamics using fully numerical methods.
HydroHigher	Higher-order hydrodynamics up to any order using fully numerical methods.
HigherOrderIterator	Auxiliary module for higher-order computations (above first order).
ReferenceLevel	Computation of a subtidal reference level based on the river-induced set-up.
DiffusivityUndamped	Sets eddy diffusivity related to the eddy viscosity and a Prandtl-Schmidt number.
SedimentCapacity	Leading-, first- and part of the second-order sediment dynamics, computing the sediment capacity using fully numerical methods.
SalinityLead	Dynamic leading-order salinity computation using numerical methods.
SalinityFirst	Dynamic first-order salinity computation using numerical methods.
KEFittedLead	Set of modules for a vertically uniform eddy viscosity depending on the local velocity and depth, and for the roughness depending on the local velocity.
KEFittedFirst	The dependency between the eddy viscosity and roughness is drawn from relations obtained from a $k - \epsilon$ model.
KEFittedHigher	
KEFittedTruncated	
<b>package semi_analytical2DV</b>	
HydroLead	Leading-order hydrodynamics. Fully analytical in the vertical direction and numerical in the horizontal direction.
HydroFirst	First-order hydrodynamics. Fully analytical in the vertical direction and numerical in the horizontal direction.
SedimentCapacity	Leading-, first- and second-order sediment dynamics, computing the sediment capacity using analytical solutions but with numerical integration.
EquilibriumAvailability	Sediment transport/trapping, solving the bed-evolution equation for an equilibrium of the availability and erodibility of sediment (morphostatic). Solution is analytical in supply limited conditions and numerical otherwise.
DynamicAvailability	Sediment transport/trapping, integrating the bed-evolution equation for the availability and erodibility of sediment over a long time scale with varying river discharge (morphostatic). Solution is numerical.
<b>package analytical2DV</b>	
Geometry2DV	Create a two-dimensional geometry with arbitrary depth and width.
SaltHyperbolicTangent	Prescribed well-mixed salinity according to a tanh function.
SaltExponential	Prescribed well-mixed salinity according to an exponential function.
TurbulenceUniform	Prescribed vertically uniform eddy viscosity and roughness.
TurbulenceParabolic	Prescribed eddy viscosity with a parabolic vertical profile and constant roughness.

**Table 2.1:** List of modules with auxiliary function or related to computing a long-term equilibrium included in iFlow version 2.5. For modules for long-term dynamics, see the iFlow manuals.

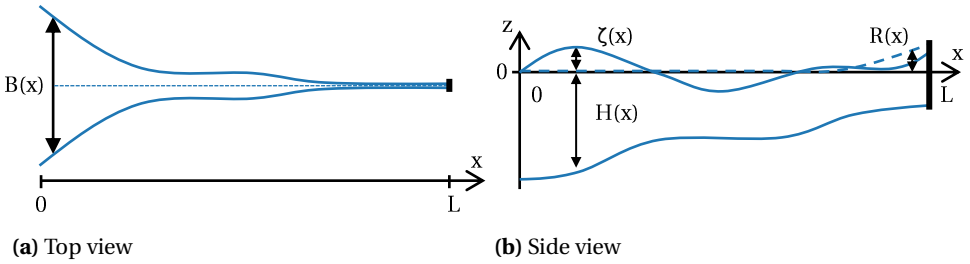


**Figure 2.2:** Model domain. The model is two-dimensional in the along-channel ( $x$ ) and vertical ( $z$ ) directions and is width-averaged. The depth and width are allowed to vary smoothly with  $x$ .

### 2.3. MODEL DOMAIN AND GRID

The iFlow core has a flexible definition of the model dimensions that allows for anything from one-dimensional to three-dimensional models. Here we discuss the standard modules in iFlow version 2.5, which are only for a two-dimensional width-averaged (2DV) model. The along-channel axis is defined as the  $x$ -coordinate and the vertical axis is defined as the  $z$ -coordinate. The length of the estuary is thus measured by following the channel between the seaward boundary  $x = 0$  and the landward boundary  $x = L$  and can be freely chosen. The width,  $B$ , and bed level,  $H$ , of the estuary can be provided as arbitrary smooth functions of  $x$ ; see Figure 2.2. The bed level  $H$  is relative to the mean sea level at the mouth (MSL) defined at  $z = 0$ . iFlow contains several built-in functions describing the depth and width, including polynomial and exponential functions. These functions and their derivatives are computed analytically to obtain maximum accuracy. Alternatively, the depth and width may be provided as a list of numerical data on a grid.

The surface level relative to  $z = 0$  is denoted by  $R + \zeta$ , where  $R$  denotes the reference level and  $\zeta$  denotes the surface elevation. The reference level  $R$  is a quick estimate of the local mean surface level, such that  $H + R$  is always positive and is a good approximation of the mean water depth. By default,  $R = 0$ , but the use of a non-zero reference level is required if the river bed is above MSL over parts of the domain. A non-zero reference level is also useful when the mean surface elevation above MSL becomes of the same order of magnitude as the depth. In such cases, the bed level alone is not a good estimate of the mean water depth. More details on the computation of  $R$  are provided in Section 2.5.3.

Each module may or may not require a numerical grid and grids may serve different purposes. Apart from using grids for (partly) numerical computations, a grid may be used to save or plot variables as numerical data. iFlow allows for using different grids in different modules or omitting a grid altogether. As a result, computations in different modules may use grids with different resolutions and the output may be stored on yet a different grid. Automatic linear interpolation of data between different grids ensures a smooth coupling of modules using different grids. Here, the standard grid module of iFlow, called *RegularGrid* is discussed. *RegularGrid* defines two grids: one computational grid used in all numerical modules and one potentially different output grid. In many cases it is useful to have an output grid with a low resolution to limit the size of the

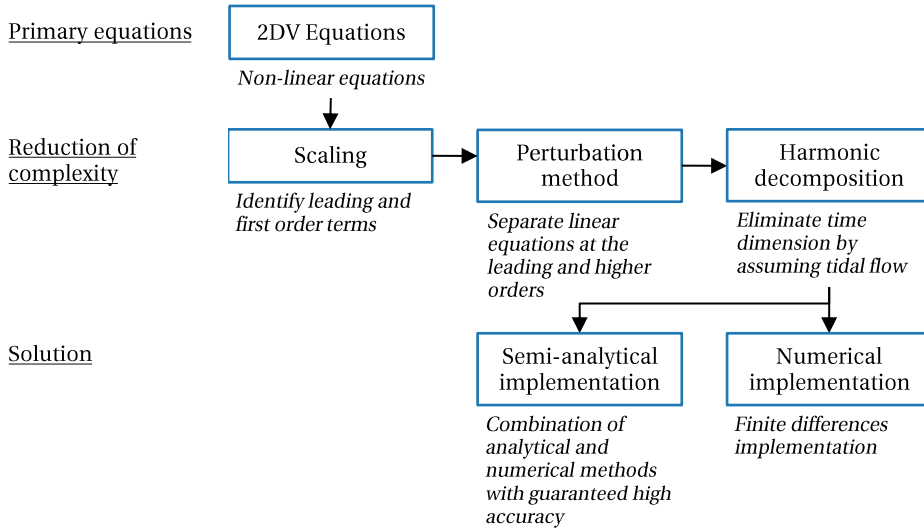


**Figure 2.3:** Flow diagram outlining the main steps taken in the derivation of the implemented equations for hydrodynamics and sediment dynamics. The fully non-linear width-averaged equations are taken through several steps of analysis to reduce the complexity of the system. Then, two implementations of this reduced system are made, each with their own advantages and disadvantages.

output data, while using a higher resolution computational grid for the benefits of the model accuracy. iFlow grids are curvi-linear and may be non-equidistant in both the  $x$  and  $z$ -direction.

## 2.4. EQUATIONS AND SOLUTION METHODS FOR HYDRODYNAMICS AND SEDIMENT DYNAMICS

The standard modules for computing the hydrodynamics and sediment dynamics fit particularly well in the iFlow philosophy as they allow for a separate analysis of the physical contributions to the total result. These analysis properties result from the perturbation approach that is used to solve the continuity, momentum and sediment balances.

The steps taken in the perturbation analysis are listed in Figure 2.3, which also forms the outline of this section. After presenting the basic width-averaged equations (Section 2.4.1), these are reduced in complexity via a scaling analysis (Section 2.4.2), perturbation approach (Section 2.4.3) and harmonic decomposition (Section 2.4.4). The perturbation approach and harmonic decomposition allow for a particularly good analysis under a set of standard forcing assumptions, which will be discussed in Section 2.4.5. Finally, we will discuss the two solution methods (semi-analytical and fully numerical) implemented in the standard modules (Section 2.4.6). Throughout the whole section we will focus on the assumptions made in this procedure and the way in which this approach helps to analyse the model results.

### 2.4.1. EQUATIONS

The water motion is described by the Reynolds-averaged width-averaged shallow water equations, that solve for the water level elevation  $\zeta(x, t)$ , horizontal velocity  $u(x, z, t)$  and vertical velocity  $w(x, z, t)$ . Here,  $t$  denotes time. We neglect the effects of Coriolis and assume that density variations are small compared to the average density, allowing for the Boussinesq approximation. The resulting momentum equation reads as (e.g. Chernetsky et al., 2010)

$$u_t + uu_x + wu_z = -g\zeta_x - g \int_z^{R+\zeta} \frac{\rho_x}{\rho_0} d\tilde{z} + (A_v u_z)_z. \quad (2.1)$$

Here,  $g$  is the acceleration of gravity,  $\rho$  is the density with reference density  $\rho_0$  and the vertical eddy viscosity is denoted by  $A_v$ . The subscripts  $x$ ,  $z$  and  $t$  in the equations denote derivatives with respect to these dimensions. The background horizontal eddy viscosity  $A_h$  has been neglected. The momentum equation has a no-stress boundary condition at the free surface and a partial slip condition at the bed

$$A_v u_z = 0 \quad \text{at } z = R + \zeta, \quad (2.2)$$

$$A_v u_z = s_f u \quad \text{at } z = -H. \quad (2.3)$$

The parameter  $s_f$  denotes the partial slip roughness coefficient. For  $s_f \rightarrow \infty$ , the partial slip condition reduces to a no-slip condition  $u = 0$ . The partial slip law becomes a quadratic bottom friction law if  $s_f$  is made dependent on the local velocity (see also Section 2.5.1).

In addition we use the width-averaged, depth-integrated continuity equation, which reads as

$$\zeta_t + \frac{1}{B} \left( B \int_{-H}^{R+\zeta} u dz \right)_x = 0, \quad (2.4)$$

with boundary conditions

$$\zeta = A \quad \text{at } x = 0, \quad (2.5)$$

$$B \int_{-H}^{R+\zeta} u dz = -Q \quad \text{at } x = L. \quad (2.6)$$

Here  $A = A(t)$  is the time-dependent tidal forcing at the seaward boundary and  $Q$  is the river discharge imposed on the landward boundary. Finally the width-averaged continuity equation reads as

$$w_z + \frac{1}{B} (Bu)_x = 0, \quad (2.7)$$

with a non-permeability condition at the bed

$$w + uH_x = 0 \quad \text{at } z = -H. \quad (2.8)$$

The sediment dynamics is described by the width-averaged sediment mass balance equation, which solves for the sediment concentration  $c(x, z, t)$  in the model domain. The

sediment is assumed to consist of non-cohesive, fine particles that have a uniform grain size (i.e. constant settling velocity) and are transported primarily as suspended load. At the surface we do not allow for transport of sediment through the water surface and at the bottom we assume that the diffusive flux equals the erosion flux  $E$ . The resulting equation is (e.g. Chernetsky et al., 2010)

$$c_t + uc_x + wc_z = w_s c_z + \frac{1}{B} (BK_h c_x)_x + (K_v c_z)_z, \quad (2.9)$$

with vertical boundary conditions

$$w_s c + K_v c_z - K_h c_x \zeta_x = 0 \quad \text{at } z = R + \zeta, \quad (2.10)$$

$$-K_v c_z - K_h c_x H_x = E \quad \text{at } z = -H \quad (2.11)$$

and horizontal boundary conditions

$$\frac{\int_0^L B a dx}{\int_0^L B dx} = a_* \quad \text{or,} \quad (2.12)$$

$$\frac{1}{H+R} \int_{-H}^{R+\zeta} c dz = c_{\text{sea}} \quad \text{at } x = 0 \text{ and} \quad (2.13)$$

$$B \int_{-H}^{R+\zeta} uc - K_h c_x = -\mathcal{F}_{\text{river}} \quad \text{at } x = L. \quad (2.14)$$

In Eq. (2.9),  $w_s$  is the settling velocity and  $K_h$  and  $K_v$  are the horizontal and vertical eddy diffusivity. Boundary condition (2.11) is valid under the assumption that  $H_x$  is much smaller than one. We assume that  $K_v$  is related to the vertical eddy viscosity coefficient  $A_v$  as  $K_v = A_v / \sigma_\rho$ , where  $\sigma_\rho$  is the Prandtl-Schmidt number that converts viscosity to diffusivity. The erosion flux  $E$  may be parametrised in two ways. The first parametrisation is related to the so-called reference concentration  $c_*$  through  $E = w_s c_*$ . With further specification of  $c_*$ , this reads as

$$E = w_s \rho_s \frac{|\tau_b(x, t)|}{\rho_0 g' d_s} \Phi(a(x)), \quad (2.15)$$

where  $\rho_s$  is the density of sediment,  $\tau_b(x, t) = \rho_0 A_v u_z$  is the bed shear stress (again assuming  $H_x \ll 1$ ),  $g' = g(\rho_s - \rho_0) / \rho_0$  is the reduced gravity,  $d_s$  is the mean grain size, and  $\Phi(a(x))$  is a function of the availability of easily erodible fine sediment on the bed  $a(x)$ . The second parametrisation, introduced in iFlow version 2.5 is related to Partheniades' formulation (e.g. Kandiah, 1974) but without critical shear stress, i.e.

$$E = M |\tau_b(x, t)| \Phi(a(x)), \quad (2.16)$$

where  $M$  is an erosion parameter. Note that Eq. (2.15) and (2.16) are equivalent if  $M = \frac{w_s \rho_s}{\rho_0 g' d_s}$ .

The function  $\Phi(a(x))$  describes how the erosion depends on the amount of sediment available on the bed. Since version 2.5, iFlow includes two options for this function. The first takes a simple linear function of the form (version 2.4 and Chernetsky et al. (2010))

$$\Phi(a(x)) = a(x). \quad (2.17)$$



The sediment availability  $a(x)$  is an unknown. Focussing on equilibrium conditions,  $a(x)$  can be determined by imposing the so-called *morphodynamic equilibrium condition* (Friedrichs et al., 1998; Huijts et al., 2006; Chernetsky et al., 2010). This condition implies that the total amount of sediment in the estuary varies on a timescale that is much longer than the timescale at which the easily erodible sediment is redistributed over the system. In other words, it is assumed that the amount of sediment in the system is a constant and we will look for the equilibrium amount and distribution of sediment in the estuary. Equilibrium in this context means that there is a balance between the tidally averaged erosion and deposition at the bottom or, equivalently, that the tidally averaged transport of sediment is divergence free. The latter is described by the morphodynamic equilibrium condition

$$\left\langle B \int_{-H}^{R+\zeta} (uc - K_h c_x) dz \right\rangle_x = 0, \quad (2.18)$$

where  $uc$  is the advective sediment transport and  $K_h c_x$  is the diffusive sediment transport. The boundary conditions to this equation are given by Eqs. (2.12)-(2.14) and are discussed at the end of this section. As the concentration  $c$  in Eq (2.18) depends linearly on the availability  $a(x)$ , the above condition is a linear equation for  $a$ .

The second option for  $\Phi$  is a non-linear function (since version 2.5)

$$\Phi(a(x)) = f(a(x)), \quad (2.19)$$

where  $f$  is a function that behaves as  $a(x)$  for small  $a$  and saturates at a value of 1 for larger  $a$ . This means that the erosion increases with the amount of sediment on the bed if there is little sediment on the bed but becomes independent of the amount of sediment on the bed if the amount of sediment on the bed is large. To solve for the equilibrium of  $a$  in this case, the morphodynamic equilibrium condition is replaced by a *sediment concentration equilibrium condition* (see also Section 1.4.2). This condition requires that the total amount of sediment *suspended* in the estuary varies on a timescale that is much longer than the timescale at which sediment is redistributed over the system. The amount of sediment on the bed may keep increasing locally in such an equilibrium state. This equilibrium is expressed as

$$f_a \left\langle B \int_{-H}^{R+\zeta} (uc - K_h c_x) dz \right\rangle_x = 0. \quad (2.20)$$

This expression is the same as the morphodynamic equilibrium condition (2.18) multiplied by the partial derivative  $f_a$  of the function  $f$  with respect to the sediment availability. In words this means that equilibrium is attained if the amount of sediment on the bed is large (i.e.  $f = 1$  and  $f_a = 0$ ) or if morphodynamic equilibrium is attained. Due to the non-linear nature of  $f$ , this equation is a non-linear equation for  $a$  which is solved analytically if  $f < 1$  everywhere in the system and numerically otherwise.

Instead of using morphodynamic or sediment concentration equilibrium conditions, one may solve for the dynamics of  $a$  on a subtidal timescale (since version 2.5). This functionality is discussed by Brouwer et al. (2018) and will not be used in this thesis.

The sediment balance equation requires two horizontal boundary conditions out of Eqs. (2.12)-(2.14). The first boundary condition offers two options. As first option (Eq. (2.12), available since version 2.4), one can prescribe the average amount of sediment on the bed in the entire estuary  $a^*$ . The relevant result of the sediment model then consists of the relative differences between concentrations at different locations along the estuary instead of the absolute magnitude of the concentration, which is prescribed. The second option (Eq. (2.13), available since version 2.5) sets the subtidal depth-averaged concentration at the seaward boundary  $c_{\text{sea}}$ . The total amount of sediment in the estuary is now computed by the model, so that the result describes both the absolute magnitude and distribution of sediment along the estuary. The second boundary condition (Eq. (2.14)) prescribes the transport of sediment from the river  $\mathcal{F}_{\text{river}}$  and is prescribed at the upstream boundary. The vertical concentration profile and tidal variation of the concentration at the upstream and downstream boundaries follows from assuming a local equilibrium sediment concentration between the bed and water column.

#### 2.4.2. SCALING & ASSUMPTIONS

The first step in the perturbation approach is the scaling of the equations. This approach uses a systematic mathematical procedure to determine the relative importance of the different terms in the equations for water motion and sediment dynamics. The most dominant terms will be called *leading-order terms*. Terms that are significantly smaller than these leading-order terms will be further categorised according to their relative importance. The most dominant terms, after separating leading-order terms, are called *first-order terms*. This categorisation continues, with all terms of second or higher order referred to here as *higher-order terms*.

The scaling requires four crucial assumptions. Firstly we assume

$$\varepsilon = \frac{\zeta}{H} \ll 1, \quad (2.21)$$

i.e. the ratio of the typical water level amplitude to the depth is much smaller than unity. The small parameter  $\varepsilon$  is used to define of which order a term is. A term is defined to be of first order if its typical relative magnitude is of order  $\varepsilon$  compared to the leading-order terms. Similarly, an  $n$ th-order term is of order  $\varepsilon^n$  with respect to the leading-order terms.

Secondly, it is assumed that the typical wave length and the typical length scale of bathymetric variations are of the same order of magnitude as the length of tidal influence into the estuary. This implies that sudden local bathymetric variations are not allowed. Rather, bathymetric changes should be smooth over the length of the estuary. Likewise, the method is restricted to long waves, such as tides. Short waves, such as wind waves, are not accounted for. As a consequence of this assumption, the non-linear advection term  $uu_x + wu_z$  in Equation (2.1) and  $uc_x + wc_z$  in Eq (2.9) scale with  $\varepsilon$ .

Thirdly, it is assumed that the horizontal density gradient is small. More precisely, the internal Froude number should be of order  $\varepsilon$  or, equivalently,  $\rho_x L_{\text{tide}} / \rho_0$  should be of order  $\varepsilon^2$ , where  $L_{\text{tide}}$  is the length of tidal influence. As a consequence, the baroclinic pressure term  $g \int_z^{R+\zeta} \frac{\rho_x}{\rho_0} d\tilde{z}$  in Equation 2.1 is of order  $\varepsilon$ .

Finally, the horizontal diffusion term  $(K_h c_x)_x$  is assumed to be of order  $\varepsilon^2$ .

### 2.4.3. PERTURBATION APPROACH & DECOMPOSITION

Instead of neglecting first- and higher-order non-linear effects, as is done in conventional linearisation techniques, the perturbation approach expands these non-linearities into a series of linear estimates. To this end, the solution variables  $u$ ,  $w$ ,  $\zeta$  and  $c$  are written as an asymptotic series ordered in the small parameter  $\varepsilon$ , i.e.

$$\begin{aligned} u &= u^0 + u^1 + u^2 + \dots, \\ w &= w^0 + w^1 + w^2 + \dots, \\ \zeta &= \zeta^0 + \zeta^1 + \zeta^2 + \dots, \\ c &= c^0 + c^1 + c^2 + \dots, \end{aligned}$$

where  $[\cdot]^0$  denotes a quantity at leading order,  $[\cdot]^1$  denotes a quantity of order  $\varepsilon$ ,  $[\cdot]^2$  order  $\varepsilon^2$  etc. In addition the eddy viscosity and diffusivity, partial slip parameter, density, tidal forcing, river discharge and settling velocity are written as similar series. These series are substituted into the equations. The resulting equations are still equivalent to the original system of equations. The analysis up to this point has merely identified what terms in the equations are of leading and higher orders.

The perturbation approach is illustrated here for the momentum and depth-averaged continuity equations for the hydrodynamics, which may be used to compute  $u$  and  $\zeta$ . A first approximation of the equations for the hydrodynamics can be made by neglecting all terms of first and higher orders. The leading-order momentum equation is formulated as

$$u_t^0 = -g\zeta_x^0 + (A_v^0 u_z^0)_z, \quad (2.22)$$

with boundary conditions

$$A_v^0 u_z^0 = 0 \quad \text{at } z = R, \quad (2.23)$$

$$A_v^0 u_z^0 = s_f^0 u^0 \quad \text{at } z = -H. \quad (2.24)$$

The leading-order depth-averaged continuity equation reads as

$$\zeta_t^0 + \frac{1}{B} \left( B \int_{-H}^R u^0 dz \right)_x = 0, \quad (2.25)$$

with boundary conditions

$$\zeta^0 = \underbrace{A^0}_{\text{tide}} \quad \text{at } x = 0, \quad (2.26)$$

$$B \int_{-H}^R u^0 dz = - \underbrace{Q^0}_{\text{river}} \quad \text{at } x = L. \quad (2.27)$$

Compared to the original equations, these leading-order equations omit the non-linear advection, density forcing and all occurrences of  $\zeta$  in the integration boundaries. These

terms feature in the first- and higher-order equations. As a result the leading-order equations have become linear and contain two forcing terms, which are named in the equation: the tidal forcing and river discharge. The linearity is a powerful property, as it allows for applying the principle of superposition. This means that the effect of the tidal forcing and river discharge may be evaluated separately and independently and may be summed to obtain the total solution. This is the principle that enables iFlow to make a decomposition of the physics into the responsible forcing mechanisms.

An improved approximation of the solution results from constructing the balance of first-order terms. Again focussing on the momentum and depth-averaged continuity equations, these form a linear set of equations for  $u^1$  and  $\zeta^1$ . The first-order momentum equation is given by

$$u_t^1 + \underbrace{u^0 u_x^0 + w^0 u_z^0}_{\text{advection}} = -g\zeta_x^1 - \underbrace{g \int_z^R \frac{\rho_x^0}{\rho_0} d\tilde{z}}_{\text{baroclinic}} + \underbrace{(A_v^0 u_z^1)_z + (A_v^1 u_z^0)_z}_{\text{eddy visc.}}, \quad (2.28)$$

with boundary conditions

$$A_v^0 u_z^1 = - \underbrace{(A_v^0 u_z^0)_z \zeta^0}_{\text{vel.-dep. asym.}} - \underbrace{A_v^1 u_z^0}_{\text{eddy visc.}} \quad \text{at } z = R, \quad (2.29)$$

$$A_v^0 u_z^1 = s_f^0 u^1 - \underbrace{A_v^1 u_z^0 + s_f^1 u^0}_{\text{eddy visc.}} \quad \text{at } z = -H. \quad (2.30)$$

The first-order depth-averaged continuity equation reads as

$$\zeta_t^1 + \frac{1}{B} \left( B \int_{-H}^R u^1 dz + \underbrace{B u_{z=R}^0 \zeta^0}_{\text{tidal return flow}} \right)_x = 0, \quad (2.31)$$

with boundary conditions

$$\zeta^1 = \underbrace{A^1}_{\text{tide}} \quad \text{at } x = 0, \quad (2.32)$$

$$B \int_{-H}^R u^1 dz = - \underbrace{Q^1}_{\text{river}} - \underbrace{B u_{z=R}^0 \zeta^0}_{\text{tidal return flow}} \quad \text{at } x = L. \quad (2.33)$$

The forcing terms to these first-order equations are defined as the known terms that do not depend on  $u^1$  or  $\zeta^1$  and are again marked by a name in the equation. The forcing mechanisms are the first-order tidal forcing  $A^1$  at the entrance, first-order river discharge  $Q^1$ , the density forcing and linear estimates of the non-linearities acting on the flow. These non-linearities include the effects of momentum advection, the tidal return flow and velocity-depth asymmetry. The tidal return flow is the flow that compensates for the mass transport due to correlations between the tidal velocity and surface variation. The velocity-depth asymmetry accounts for the effect that the velocity profile differs between ebb and flood due to different water levels. Finally, temporal or spatial variations of

Short name	Explanation	Order
<b>Hydrodynamics</b>		
Tide	Tidal amplitude forced at the seaward boundary	0 and 1
River	Constant river discharge at the landward boundary	0 (num.) or 1
Baroclinic	Forcing by the along-channel baroclinic pressure gradient	1
Advection	Effect of momentum advection $uu_x + wu_z$	1
Tidal return flow	The return flow required to compensate for the mass flux induced by tidal correlations between the velocity and water level elevation	1
Eddy viscosity	Effect of higher-order eddy viscosity contributions.	1
Velocity-depth asymmetry	Correction for the alteration of the velocity profile due to the application of the no-stress boundary condition at $z = R$ instead of the real surface $z = R + \zeta$	1
<b>Sediment dynamics</b>		
Erosion	Local resuspension at the bed	0 and 1
Spatial settling lag	Effect of sediment advection $uc_x + wc_z$	1
Surface correction	Correction because the transport across the time-dependent water surface is specified at $z = R$ instead of the real surface $z = R + \zeta$	1
Settling velocity correction	Effect of higher-order variations of the settling velocity	1
Mixing correction	Effect of higher-order variations of the eddy diffusivity	1

**Table 2.2:** Separate forcing mechanisms to the water and sediment motion and the order at which these mechanisms appear.

the leading-order eddy viscosity may be included at first-order, so that the interactions between these variations and the leading-order flow appear as a forcing at the first order. Note that some of these mechanisms appear in multiple places in the equations. As the equations are again linear, the principle of superposition allows iFlow to compute the effect of each of these forcing mechanisms separately and independently and sum them to obtain the total result. All forcing mechanisms to the leading- and first-order equations are summarised in Table 2.2.

A similar approach for the sediment balance also results in linear equations at the leading and first order, forced by different physical mechanisms. The leading-order sediment balance describes a local balance between vertical turbulent mixing and the settling of sediment. It is forced at the bed, where sediment is locally resuspended by the leading-order erosion flux  $E^0$ . This erosion rate involves the leading-order bed shear stress  $\tau_b^0$ , which is derived from the leading-order velocity. The leading-order concentration thus is the concentration locally resuspended by the leading-order tide. The first-order equation describes a similar balance between vertical diffusion and the settling of sediment but is forced by different components. Firstly, it is forced at the bed by the first-order erosion rate  $E^1$ , which represents the erosion due to the first-order bed shear stress. This involves the first-order velocity and therefore the flow caused by all mechanisms that act on the first-order hydrodynamics. Secondly, the first-order balance is forced by horizon-

tal sediment advection  $uc_x + wc_z$ , which results in what is known as spatial settling lag effects (Postma, 1954; Van Straaten and Kuenen, 1957; De Swart and Zimmerman, 2009). Thirdly, the first-order balance involves a forcing from the covariance between the sediment concentration and the surface elevation. Finally, if the eddy diffusivity and settling velocity have first-order contributions, their covariances with the leading-order concentration appear as first-order effects as well. All forcing mechanisms on the leading- and first-order sediment balances are summarised in Table 2.2. Similar to the hydrodynamics, all the contributions to the sediment concentration by different forcing terms can be evaluated separately and independently due to the principle of superposition. The ordered sediment equations are described in the manuals.

Similar to the approach outlined above for the first-order terms, higher-order approximations of both the hydrodynamics and sediment dynamics can be made by composing a balance of the terms on second, third and higher orders. It is assumed that all external forcing terms (i.e. external tidal forcing, river discharge) act on the leading and first orders. The second and higher orders therefore only contain estimates of non-linear interactions of lower order contributions. The sum of all estimates of the non-linear terms at all orders should return the total solution to the original non-linear system of equations. If the scaling assumptions are satisfied, it follows that the contributions at higher order rapidly become smaller. The solutions at leading and first order then provide a fairly accurate estimate of the total solution. The higher-order systems are nevertheless useful in cases where the scaling assumptions are only marginally satisfied or when studying a particular process that involves a non-linear interaction that appears at higher order.

#### 2.4.4. HARMONIC DECOMPOSITION

Restricting attention to the equilibrium model (see Section 2.4.1), the external forcing of the hydrodynamics in iFlow consists of a subtidal flow and a limited number of tidal constituents. In the remainder of this thesis we will assume that these tidal constituents are the  $M_2$  tide and its overtides, as these are the most common. In general, one can choose any single tidal base mode and its overtides in the model. The solution to the non-linear system of equations also consists of a subtidal component, the  $M_2$  tide and possibly infinitely many overtidal components. As the sediment dynamics is forced by the hydrodynamics, the sediment concentration is described by the same components. This means that the solution can be written as a sum of the subtidal component and these tidal constituents. However, instead of accounting for infinitely many components, the signal is truncated after  $p$  components, where  $p$  can be chosen arbitrarily. As an example, for the velocity  $u^0$  we then write

$$u^0 = \sum_{n=0}^p \text{Re} \left( \hat{u}_n^0 e^{ni\omega t} \right), \quad (2.34)$$

where  $\hat{u}_n^0$  is the complex amplitude of the  $n$ th component of  $u^0$ , where  $n = 0$  denotes the subtidal component,  $n = 1$  the  $M_2$  component,  $n = 2$  the  $M_4$  component etcetera. A similar decomposition is made for all quantities that vary on the tidal timescale.

As a consequence of this harmonic decomposition, the equations are solved for each frequency component. This eliminates the need to solve the equations by time stepping. This is a major advantage when computing (dynamic) equilibrium states of the hydro-

dynamics and sediment concentration, as iFlow can compute these states immediately. This is in contrast to time stepping models, which often need many time steps and a large computational time to go from an initial state to the equilibrium state.

Details of the equations per frequency component can be found in the manuals. For the case where the leading-order eddy viscosity, eddy diffusivity, partial slip parameter and settling velocity are constant in time, this procedure is the same as in Chernetsky et al. (2010), also see the manual on the semi-analytical model implementation. If these assumptions do not hold, the matrix-solution procedure suggested by Dijkstra (2014) is followed, also see the manual on the numerical model implementation.

#### 2.4.5. STANDARD FORCING

Under certain assumptions about the external forcing, the resulting frequency components of the solutions form an especially well-analysable set. We will call these assumptions the *standard forcing assumptions*. These are the same as in e.g. Chernetsky et al. (2010) and are the following:

1. the leading-order hydrodynamics is only forced by an  $M_2$  constituent;
2. the first-order tidal hydrodynamics is forced only by an  $M_4$  constituent;
3. the river discharge only appears at first order;
4. the eddy viscosity and partial slip parameter do not vary on the tidal timescale;
5. the settling velocity and eddy diffusivity do not vary on the tidal timescale; and
6. the leading-order density variation only contains a subtidal and  $M_4$  component.

Under these assumptions the leading-order hydrodynamics describes the linear propagation of the  $M_2$  tide and only consists of an  $M_2$  frequency. The first-order hydrodynamics consists of a subtidal component forced by the river discharge and an  $M_4$  component forced by the external tidal forcing. The density-induced flow and non-linear components appearing at first order are also described by subtidal and  $M_4$  components. The first-order flow therefore describes the sources of tidal asymmetry, both caused by external forcing and internal generation.

Assuming the standard forcing assumptions hold, the leading-order sediment dynamics contains the subtidal,  $M_4$ ,  $M_8$  etc. components. The first-order sediment dynamics conversely contains the  $M_2$ ,  $M_6$ ,  $M_{10}$  etc. components. In many examples, the leading-order and first-order concentrations are truncated after the  $M_4$  tidal component. This is because the higher harmonics beyond the  $M_4$  component are unimportant for the net transport of sediment and are therefore of less interest.

The main advantage of the standard forcing assumptions is their effect on the morphodynamic equilibrium condition, Eq. (2.18). This forms a subtidal balance of sediment transport terms at second order. Integrating Eq. (2.18) with respect to  $x$ , using the up-

stream boundary condition and substituting the ordering, this balance reads as

$$B \left\langle \int_{-H}^R u^0 c^1 + u^1 c^0 + u_{\text{river}}^1 c_{\text{river-river}}^2 - K_h c_x^0 - K_h c_{\text{river-river},x}^2 dz + u_{z=R}^0 c_{z=R}^0 \zeta^0 \right\rangle = -\mathcal{F}_{\text{river}}. \quad (2.35)$$

2

We can distinguish between three types of transport terms. The first describes the covariance between the velocity and concentration, i.e.  $\langle \int_{-H}^0 u c dz \rangle$ . The dominant covariance terms that result in a subtidal transport are  $\langle \int_{-H}^R u^0 c^1 dz \rangle$  and  $\langle \int_{-H}^R u^1 c^0 dz \rangle$ . The term  $u^0 c^1$  only generates a subtidal transport due to the covariance between the leading-order  $M_2$  flow and  $M_2$  variation of the first-order concentration. The term  $u^1 c^0$  generates transport due to  $M_4$ - $M_4$  covariance and the product of both subtidal contributions. As the model computes the effect of different physical mechanisms contributing to  $u^1$  and  $c^1$  (see Table 2.2), the transport terms can be subdivided further into the transport caused by particular physical mechanisms. This way, we obtain a subdivision of  $\langle \int_{-H}^0 u^1 c^0 dz \rangle$ , with components named after the different contributions to  $u^1$ . Likewise, the components in the subdivision of  $\langle \int_{-H}^0 u^0 c^1 dz \rangle$  are named after the contributions to  $c^1$ . One exception to this is the ‘erosion’ contribution to  $c^1$ , which is again subdivided further into the  $u^1$  velocity contributions that cause the erosion.

In addition to these terms, the model includes the subtidal transport by

$$\left\langle \int_{-H}^R u_{\text{river}}^1 c_{\text{river-river}}^2 dz \right\rangle,$$

i.e. the covariance between the river-induced velocity and the river-induced sediment resuspension. This transport is a fourth-order term according to the scaling and therefore formally does not belong in this balance. However, it typically becomes the dominant term near the end of the tidal influence where all tidally induced transport mechanisms vanish. It is therefore an important mechanism to avoid an unrealistically high degree of sediment trapping at the upstream boundary.

The second type of transport term is the covariance between the velocity, concentration and the varying water surface elevation, with dominant contribution  $u^0 c^0 \zeta^0$ . No further subdivision of this term can be made. This term represents the drift of sediment with the moving surface and is largely compensated for by the tidal return flow, which is one of the contributions to the advective transport  $\langle \int_{-H}^R u c dz \rangle$ . Therefore we will consider the transport due to this drift and the tidal return flow together as one term under the name ‘tidal return flow’.

The final type of transport terms are the terms involving the horizontal eddy diffusivity,  $\langle K_h c^0 \rangle$  and  $\langle K_h c_{\text{river-river}}^2 \rangle$ . It is assumed that the horizontal diffusivity is constant in time, so that the term  $K_h c^1$  is zero averaged over the tide. The diffusive transport thus describes horizontal background diffusion of the tide- and river-induced resuspended



sediment. Physically, this background diffusion is caused by unresolved flows such as lateral circulation.

Under the standard assumptions, the morphodynamic equilibrium condition thus yields an extensive set of sediment transport terms, which together should sum to zero. By investigating the separate transport terms, it can be inferred which of these mechanisms promote sediment export and which promote sediment import.

#### 2.4.6. SEMI-ANALYTICAL VERSUS NUMERICAL SOLUTION METHOD

The iFlow hydrodynamics and sediment dynamics modules offer two ways of solving the equations: semi-analytical and numerical. The semi-analytical method follows Chernetsky et al. (2010) and uses fully analytical formulations for the vertical velocity and sediment profiles but uses a numerical method to solve for the water level elevation. This solution method is fast and accurate but may only be applied if the forcing satisfies certain conditions. The required conditions are the standard forcing assumptions above, together with the requirement that the eddy viscosity, eddy diffusivity and settling velocity are uniform over the water column.

The numerical method was introduced, because the assumptions on the forcing in the semi-analytical method can be too restrictive for specific applications. The numerical method allows for arbitrary vertical profiles of the eddy viscosity, eddy diffusivity and settling velocity. The numerical method also allows for releasing the standard forcing assumptions. It allows any number of tidal constituents as long as they are overides of a base component, often the  $M_2$  tide. These tidal constituents may be imposed at either the leading or the first order depending on the situation. The river flow may additionally be imposed at the leading order, if appropriate. The eddy viscosity, eddy diffusivity, partial slip parameter and settling velocity are also allowed to vary in time at leading or first order. This means that the numerical model may be used with the same restrictions as the semi-analytical method, but these restrictions may be relaxed for further functionality. This is at the cost of potentially larger computational times and lower accuracy, depending on the numerical grid resolution. An overview of the differences between the restrictions in the semi-analytical and numerical methods is provided in Table 2.3.

Some of the additional functionality of the numerical method affects the sediment transport balance. The possible addition of more harmonic components leads to additional transport terms, such as a transport contribution due to the  $M_6$ - $M_6$  covariance between the velocity and concentration. When a subtidal or  $M_4$  velocity is entered at the leading-order velocity, e.g. through the river discharge or externally prescribed  $M_4$  tide, the covariance between the leading-order velocity and concentration,  $\langle \int_{-H}^0 u^0 c^0 dz \rangle$ , yields a subtidal contribution. According to the scaling, this contribution dominates over all transport contributions in Eq. 2.35, so that those contributions should no longer be considered. The term  $\langle \int_{-H}^0 u^0 c^0 dz \rangle$  in the new balance can again be subdivided according to the physical mechanisms that contribute to the velocity and concentration. However, the balance now only concerns the leading-order velocity and concentration, for which the model computes only one or two contributions (see Table 2.2). The subdivision of the transport therefore leads to much fewer terms and typically provides less insight into the underlying physics.

	<b>Semi-analytical</b>	<b>Numerical</b>
Orders hydrodynamics	Leading and first	Any
Orders sediment dynamics	Leading and first	Leading and first
Eddy viscosity/diffusivity	Vertically uniform, subtidal in leading order and $M_2$ frequency in first order	Vertical variations and leading-order and first-order time variations allowed
Bottom boundary condition	Partial slip with constant roughness in leading order and $M_2$ frequency in first order	Partial slip with time-varying roughness at leading-order and first-order
Leading-order forcing tidal components	$M_2$	Any
First-order forcing tidal components	$M_4$	Any
River discharge	First order	Leading or first order
Settling velocity	Vertically uniform, subtidal in leading order and none in first order	Vertical variations and leading-order and first-order time variations allowed

**Table 2.3:** Allowed forcing and turbulence options in the semi-analytical and numerical solution methods.

The choice to keep a simulation within the restrictions of the semi-analytical method or to extend it to the full possibilities of the numerical method thus has a direct effect on the ability to analyse the results. This is an example of the classical trade-off between model complexity and ability to analyse the results as was mentioned in the introduction. A major strength of iFlow is that it offers one software environment where one can experiment with the degree of complexity required for a simulation for a specific application.

## 2.5. INTRODUCTION TO THE MODULES FOR TURBULENCE AND SALINITY

### 2.5.1. TURBULENCE MODELS

iFlow provides a number of modules to parametrise the eddy viscosity and roughness parameter (see also Table 2.1), referred to as the turbulence model. The simplest turbulence model available is implemented in the *TurbulenceUniform* module and assumes a vertically uniform eddy viscosity and constant partial slip roughness parameter, which may only vary with the depth (Friedrichs and Hamrick, 1996; Schramkowski and De Swart, 2002), according to

$$A_v = A_{v0} \left( \frac{H + R}{H(x=0)} \right)^m, \quad (2.36)$$

$$s_f = s_{f,0} \left( \frac{H + R}{H(x=0)} \right)^n, \quad (2.37)$$

with  $A_{v0}$ ,  $s_{f,0}$ ,  $m$  and  $n$  provided as input to the model. This model may be used for the leading- and first-order eddy viscosity and partial slip parameter with different input parameters. The input parameters  $A_{v0}$  and  $s_{f,0}$  may include time-variations. This turbu-

lence model was applied in several studies, including Chernetsky et al. (2010); De Jonge et al. (2014); Wei et al. (2016). However, Schramkowski et al. (2016) showed that multiple values of the calibration parameters  $A_{v0}$  and  $s_{f,0}$  result in equivalent results. Therefore there is a degree of arbitrariness to the calibration parameters in this turbulence model.

In order to resolve this arbitrariness, iFlow includes a set of modules named *KEFitted*. These models depend only on one calibration parameter and include more physical dependencies of the eddy viscosity. These *KEFitted* turbulence modules define parametrizations for  $A_v$  and  $s_f$  derived by fitting the results of a one-dimensional numerical model with  $k - \epsilon$  closure for a large number of barotropic tidal model configurations. The turbulence closures provide a number of options. The most important option is the choice of roughness parameter to provide on input. If the roughness parameter  $s_{f,0}$  is provided, the turbulence model uses the relation

$$A_v = 0.5s_f(H + R + \zeta), \quad (2.38)$$

$$s_f = s_{f,0} \left( \frac{H + R}{H(x=0)} \right)^n, \quad (2.39)$$

This model only has the calibration parameter  $s_{f,0}$  and requires a choice for  $n$ . It thus eliminates the need to calibrate  $A_{v0}$  and  $m$ . To leading order, because it is assumed that  $\zeta \ll H + R$ , this model is the same as Eqs. (2.36)-(2.37) with  $m = 1 + n$  and  $A_{v0} = 0.5s_f(H(x=0))^m$ . This model is recommended over Eqs. (2.36)-(2.37), as it only has a single calibration parameter and thus leads to a definite best calibration parameter setting. However, note that this relation is derived for a unidirectional flow and its is assumed that any flow in another direction does not affect this relation.

Alternatively, the *KEFitted* turbulence models may be provided with a roughness parameter  $z_{00}^*$ . The formulations for the eddy viscosity and partial slip roughness then read as

$$A_v = \alpha u^*(H + R + \zeta) f_1(z_0^*), \quad (2.40)$$

$$s_f = \beta u^* f_2(z_0^*), \quad (2.41)$$

$$z_0^* = z_{00}^* \left( \frac{H + R}{H(x=0)} \right)^n. \quad (2.42)$$

where  $u^*$  is the bed friction velocity, which may be related to the depth-averaged velocity (see Burchard et al. (2011)). The parameters  $z_{00}^*$  and  $n$  should be provided as input and  $\alpha$ ,  $\beta$ ,  $f_1(z_0^*)$  and  $f_2(z_0^*)$  are known hard-coded parameters and functions obtained by fitting results of the  $k - \epsilon$  model (see the manual for details). This model therefore also contains only one calibration parameter  $z_{00}^*$  and requires a choice for  $n$ . These formulations relate the vertically uniform eddy viscosity and partial-slip parameter to the local bed shear stress velocity and water depth. As a result, the bottom boundary condition for the hydrodynamics, Eq. (2.3), has become a quadratic friction law. This model introduces non-linearity, as there now is a mutual relation between the flow velocity and the water surface elevation on the one hand and eddy viscosity and the partial slip parameter on the other hand. This non-linearity is resolved by an iteration loop over the turbulence and hydrodynamic modules, which is automatically constructed by the iFlow core as exemplified in Section 2.2. Due to the non-linearity, this model introduces more

complexity compared to the previous models and is therefore only recommended when the case at hand requires this complexity, for example because of large variations in  $u^*$  in space or time.

iFlow implements four modules that implement the above *KEFitted* relations. The *KEFittedLead*, *KEFittedFirst* and *KEFittedHigher* modules make an ordering of the above equations to determine the leading-order, first-order and higher-order eddy viscosity and partial slip parameter. The *KEFittedTruncated* module uses the sum of all computed orders of the velocity and water surface elevation to compute a total eddy viscosity and roughness parameter without ordering (i.e. a truncation method).

Finally, the *TurbulenceParabolic* turbulence model is similar to Eqs. (2.36)-(2.37) but assumes the eddy viscosity to have a parabolic profile in the vertical direction. This turbulence model assumes  $s_f \rightarrow \infty$ , so that the bottom boundary condition for the hydrodynamics reduces to a no-slip law. The roughness is instead described by a roughness height  $z_0$ . The formulations for  $A_v$  and  $z_0$  read

$$A_v = A_{v0} \left( \frac{H+R}{H(x=0)} \right)^m (z_s^* - z^*) \left( \frac{z_0}{H+R} + z^* + 1 \right), \quad (2.43)$$

$$z_0 = z_0^* \left( \frac{H+R}{H(x=0)} \right)^{n+1}. \quad (2.44)$$

The parameters  $A_{v0}$  and  $z_0^* = z_0(x=0)/H(x=0)$ ,  $m$  and  $n$  are provided as input,  $z^* = z/(H+R)$  and the dimensionless surface roughness  $z_s^*$  is determined by the model such that  $A_v$  equals  $10^{-6} \text{ m}^2/\text{s}$  at the surface, i.e. approximately the molecular viscosity. The parabolic eddy viscosity profile represents a more realistic shape in barotropic flows and therefore results in more realistically shaped velocity profiles. However, this model faces a similar degree of arbitrariness in the choice of  $A_{v0}$  and  $z_0^*$  as in Eqs. (2.36)-(2.37) and may only be used in combination with the numerical solution method.

### 2.5.2. SALINITY

The iFlow standard modules include two types of salinity models: diagnostic (i.e. prescribed) and prognostic (i.e. resolved). The diagnostic modules prescribe a subtidal vertically uniform (well-mixed) salinity that varies in the along-channel direction. The module *SalinityHyperbolicTangent* formulates this as (see also Warner et al. (2005); Talke et al. (2009))

$$s = \frac{s_{\text{sea}}}{2} \left( 1 - \tanh \left( \frac{x - x_c}{x_L} \right) \right) \quad (2.45)$$

and *SalinityExponential* formulates this as

$$s = s_{\text{sea}} \exp \left( -\frac{x}{L_s} \right). \quad (2.46)$$

The prognostic salinity model (*SalinityLead*, *SalinityFirst* modules) follows work done by McCarthy (1993) and Wei et al. (2016). The model is based on the perturbation approach, where it is assumed that the leading-order salinity consists of a subtidal vertically uniform (well-mixed) salinity. Vertical and temporal variations of the salinity appear at higher orders. For more information we refer to Wei et al. (2016).

### 2.5.3. REFERENCE LEVEL

The hydrodynamic module relies on the water depth being positive and much larger than the time varying surface elevation (see assumption 1 in Section 2.4.2). The model fails or becomes inaccurate if the bottom lies above or close to MSL. In many cases this problem can be resolved by the iFlow *ReferenceLevel* module. This module computes a quick estimate of the subtidal water level elevation based on the river-induced set-up. This is often sufficient, because the river is typically the dominant flow term in the most upstream reach, where the bottom level is highest.

The river-induced set-up is estimated numerically using the leading-order momentum and depth-averaged continuity equations, assuming it is purely forced by a constant discharge  $Q$  and the resulting water level elevation is given by  $R$ . These equations read as

$$-gR_x + (A_v u_z)_z = 0, \quad (2.47)$$

$$B \int_{-H}^R u dz = -Q. \quad (2.48)$$

This system is non-linear in  $R$  as the integral in the second equation contains  $R$  in the integration boundary and  $u$ , which depends on  $R$  according to the first equation. Nevertheless, the system can be solved without iterating by starting at the mouth and working upstream. At the mouth ( $x = 0$ ),  $R = 0$  by definition. Therefore  $R_x$  can be computed from the above system of equations. The value of  $R$  at the next grid point  $x = \Delta x$  follows from a simple first-order routine:  $R(\Delta x) = R(0) + R_x(0)\Delta x$ . The total reference level follows by repeating this procedure for all horizontal grid cells. More accurate computations of the river-induced set-up follow from the hydrodynamic modules, so that the relatively low numerical accuracy of the reference level computation will not reduce the precision of the overall result.

The reference level still depends on the eddy viscosity. If a *KEFitted* turbulence model is used, the eddy viscosity in turn depends on the reference level. To resolve this interdependency efficiently, without needing to iterate between the turbulence model and reference level module, the *KEFitted* turbulence models have a built-in routine to compute the reference level. Therefore, the *ReferenceLevel* module can be omitted when the *KEFitted* module is used.

### 2.5.4. SENSITIVITY ANALYSIS MODULE

iFlow's standard sensitivity analysis module *Sensitivity* provides a powerful analysis tool, by easily allowing a user perform a full model simulation for various values of one or more input variables. On input, the user provides the names of the variables to loop over, as well as a list with the values for these variables. A final input parameter indicates whether all combinations of parameter values should be tested or whether the values of all variables should be changed simultaneously. The iFlow core then automatically decides which modules should be included in the loop and runs these modules for all prescribed parameter settings, saving the results to a file after each loop. The sensitivity analysis is therefore a general tool that may be combined with any set of modules to loop over any set of variables and values.

## 2.6. CONCLUSIONS

iFlow provides a flexible and versatile modular environment for modelling flows and sediment transport in estuaries and tidal rivers. The model focusses on idealised approaches that allow the systematic analysis of physical processes and the sensitivity of these processes to model parameters. Due to the modular nature, iFlow offers a software environment where users can easily adjust the processes included in a simulation, thereby allowing users to adjust the degree of complexity, computational time and ability to analyse the results to a specific application. The iFlow core supports these adjustments by automatically taking care of the communication between modules, order of modules and smooth coupling of modules that use different solution methods. iFlow version 2.5 additionally includes a number of standard modules especially designed to analyse individual processes affecting the flow and sediment transport.

As the structure of iFlow can be adapted and modules can be added easily by new users, there is no such thing as a single iFlow model. Also, the provided default modules for hydrodynamics, turbulence and sediment dynamics may be replaced if this is useful for a particular application. For example, these modules may be replaced by a coupling to a complex model (e.g. as demonstrated for turbulence by Dijkstra et al., 2017) or observations. By coupling such module replacements to other modules one can construct unique model set-ups for studying a certain process or for comparing different model implementations within one modelling framework.

The future ambitions for the model involve further developments of modules for turbulence and morphology and for the transport of sediment, salinity and nutrients. Users are encouraged to contribute to this development by developing and sharing modules or sharing model applications.

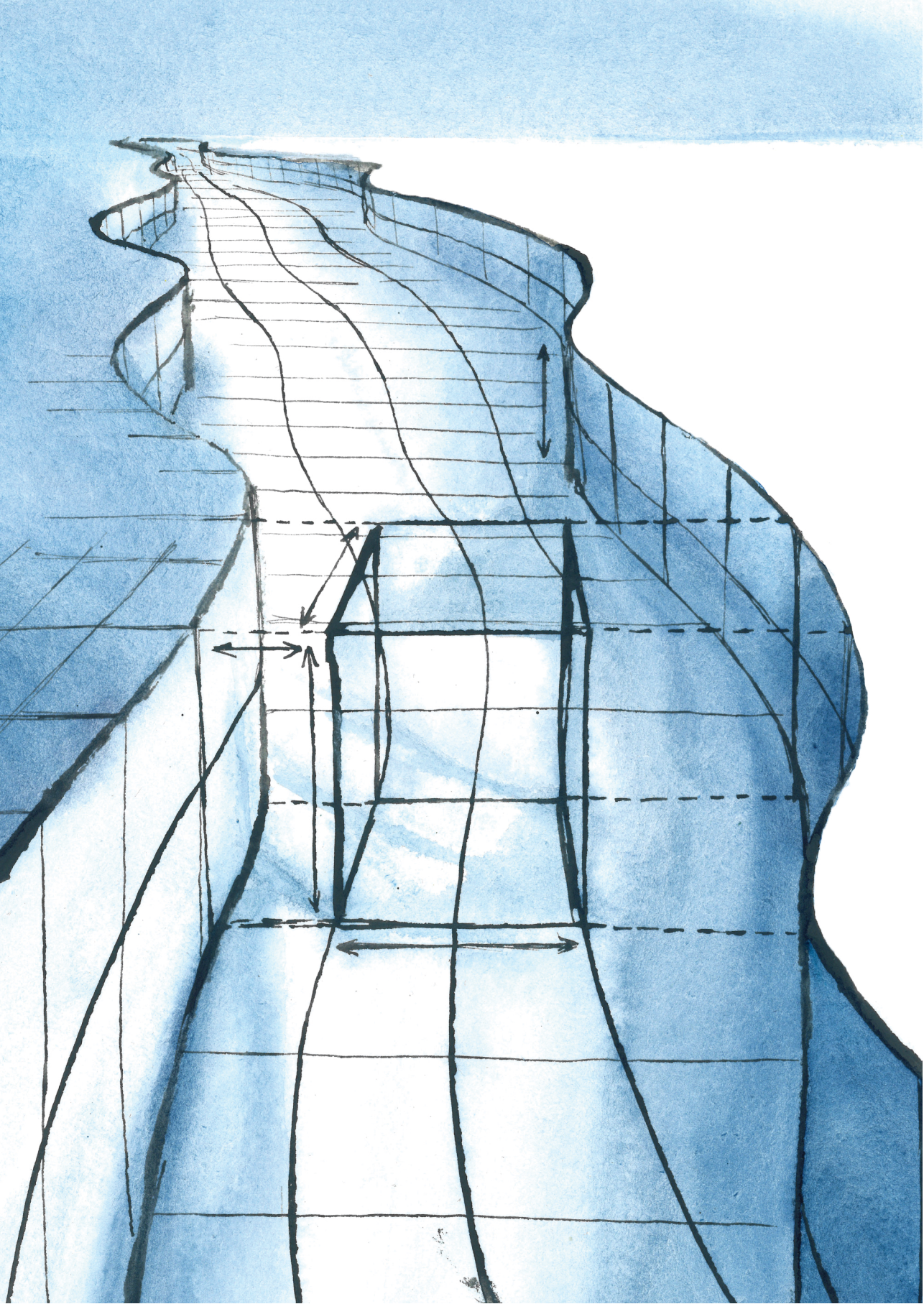
## REFERENCES

- Brouwer, R. L., Schramkowski, G. P., Dijkstra, Y. M., and Schuttelaars, H. M. (2018). Time evolution of estuarine turbidity maxima in well-mixed, tidally dominated estuaries: the role of availability- and erosion-limited conditions. *Journal of Physical Oceanography*, 48:1629–1650.
- Burchard, H., Hetland, R. D., Schulz, E., and Schuttelaars, H. M. (2011). Drivers of residual estuarine circulation in tidally energetic estuaries: Straight and irrotational channels with parabolic cross section. *Journal of Physical Oceanography*, 41:548–570.
- Cheng, P., Valle-Levinson, A., and De Swart, H. E. (2010). Residual currents induced by asymmetric tidal mixing in weakly stratified narrow estuaries. *Journal of Physical Oceanography*, 40:2135–2147.
- Chernetsky, A. S., Schuttelaars, H. M., and Talke, S. A. (2010). The effect of tidal asymmetry and temporal settling lag on sediment trapping in tidal estuaries. *Ocean Dynamics*, 60:1219–1241.
- Cloern, J. E. (1996). Phytoplankton bloom dynamics in coastal ecosystems: a review with some general lessons from sustained investigation of San Francisco Bay, California. *Reviews of Geophysics*, 34:127–168.
- Colijn, F. (1982). Light absorption in the waters of the Ems-dollard estuary and its consequences for the growth of phytoplankton and microphytobenthos. *Netherlands Journal of Sea Research*, 15:196–216.
- De Jonge, V. N., Schuttelaars, H. M., Van Beusekom, J. E. E., Talke, S. A., and De Swart, H. E. (2014). The influence of channel deepening on estuarine turbidity levels and dynamics, as exemplified by the Ems estuary. *Estuarine Coastal and Shelf Science*, 139:46–59.
- De Swart, H. and Zimmerman, J. (2009). Morphodynamics of tidal inlet systems. *Annual Review*

- of *Fluid Mechanics*, 41:203–229.
- Dijkstra, Y. M. (2014). On the effect of tidal variations of turbulent mixing on flow and salt transport in estuaries. Master's thesis, TU Delft, Delft, Netherlands.
- Dijkstra, Y. M., Schuttelaars, H. M., and Burchard, H. (2017). Generation of exchange flows in estuaries by tidal and gravitational eddy viscosity - shear covariance (ESCO). *Journal of Geophysical Research: Oceans*, 122:4217–4237.
- Friedrichs, C. T., Armbrust, B. A., and de Swart, H. E. (1998). Hydrodynamic and equilibrium sediment dynamics of shallow, funnel-shaped tidal estuaries. In Dronkers, J. and Scheffers, M., editors, *Physics of Estuaries and Coastal Seas*, pages 315–328, Rotterdam. Balkema.
- Friedrichs, C. T. and Aubrey, D. G. (1994). Tidal propagation in strongly convergent channels. *Journal of Geophysical Research: Oceans*, 99:3321–3336.
- Friedrichs, C. T. and Hamrick, J. M. (1996). Effects of channel geometry on cross sectional variations in along channel velocity in partially stratified estuaries. In Friedrichs, C. T. and Aubrey, D. G., editors, *Buoyancy effects on coastal and estuarine dynamics*, AGU, Washington D. C., pages 283–300.
- Hansen, D. V. and Rattray, M. (1965). Gravitational circulation in straits and estuaries. *Journal of Marine Research*, 23:104–122.
- Huijts, K. M. H., Schuttelaars, H. M., De Swart, H. E., and Valle-Levinson, A. (2006). Lateral entrainment of sediment in tidal estuaries: An idealized model study. *Journal of Geophysical Research: Oceans*, 111:C12016.
- Ianniello, J. P. (1977). Tidally induced residual currents in estuaries of constant breadth and depth. *Journal of Marine Research*, 35:755–786.
- Ianniello, J. P. (1979). Tidally induced residual currents in estuaries of variable breadth and depth. *Journal of Physical Oceanography*, 9:962–974.
- Kandiah, A. (1974). *Fundamental aspects of surface erosion of cohesive soils*. PhD thesis, University of California, Davis.
- McCarthy, R. K. (1993). Residual currents in tidally dominated, well-mixed estuaries. *Tellus*, 45A:325–340.
- Murray, A. B. (2003). *Prediction in Geomorphology*, chapter Contrasting the Goals, Strategies, and Predictions Associated with Simplified Numerical Models and Detailed Simulations, pages 151–165. American Geophysical Union, Washington, D. C.
- Postma, H. (1954). Hydrography of the Dutch Wadden Sea. *Archives Néerlandaises de Zoologie*, 10:405–511.
- Prandle, D. (1982). The vertical structure of tidal currents and other oscillatory flows. *Continental Shelf Research*, 1:191–2007.
- Schramkowski, G. P., Brouwer, R. L., Verwaest, T., and Mostaert, F. (2016). Geïdealiseerde processtudie van systeemovergangen naar hypertroebelheid. WP 2.2 Gevoeligheidsonderzoek en vergelijking tussen Zeeschelde en Eems. Technical Report WL2015R13\_103, Flanders Hydraulics Research, Antwerp, Belgium. In Dutch.
- Schramkowski, G. P. and De Swart, H. E. (2002). Morphodynamic equilibrium in straight tidal channels: Combined effects of the coriolis force and external overtides. *Journal of Geophysical Research: Oceans*, 107:3227.
- Schuttelaars, H. M., de Jonge, V. N., and Chernetsky, A. S. (2013). Improving the predictive power when modelling physical effects of human interventions in estuarine systems. *Ocean and Coastal Management*, 79:70–82.
- Talke, S. A., De Swart, H. E., and De Jonge, V. N. (2009). An idealized model and systematic process study of oxygen depletion in highly turbid estuaries. *Estuaries and Coasts*, 32:602–620.
- Van Straaten, L. M. J. U. and Kuenen, P. H. (1957). Accumulation of fine grained sediments in the Dutch Wadden Sea. *Netherlands Journal of Geosciences*, 19:329–354.
- Warner, J. C., Geyer, W. R., and Lerczak, J. A. (2005). Numerical modeling of an estuary: A comprehensive skill assessment. *Journal of Geophysical Research: Oceans*, 110:C05001.

- Wei, X., Schramkowski, G. P., and Schuttelaars, H. M. (2016). Salt dynamics in well-mixed estuaries: Importance of advection by tides. *Journal of Physical Oceanography*, 46:1457–1475.
- Winterwerp, J. C., Wang, Z. B., Van Brackel, A., Van Holland, G., and Kösters, F. (2013). Man-induced regime shifts in small estuaries - II: a comparison of rivers. *Ocean Dynamics*, 63:1293–1306.



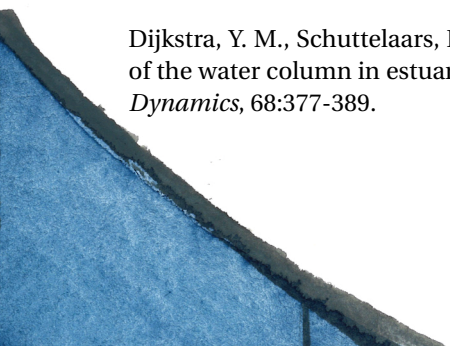




# CHAPTER 3

The hyperturbid state of the water column

The importance of hindered settling



Dijkstra, Y. M., Schuttelaars, H. M., and Winterwerp, J. C. (2018). The hyperturbid state of the water column in estuaries and rivers: the importance of hindered settling. *Ocean Dynamics*, 68:377-389.

## **Abstract**

---

Over the last few decades, some estuaries have undergone a transition to a hyperturbid state, characterised by suspended sediment concentrations of several grams per litre averaged over the water column. To improve our understanding of this transition and of naturally hyperturbid estuaries, we systematically identify the processes allowing for high suspended sediment concentrations using a water column (1DV) model. Under a range of realistic forcing conditions, the state of the water column can be characterised by one of two equilibrium states. The first is an erosion limited state, in which there still is sediment available for erosion at the bed. We find that this state only occurs with relatively low concentrations. The second is a supply limited state, in which all erodible sediment is in suspension. The concentration in this state depends entirely on the amount of sediment in the system and can potentially be very high. We identify the conditions under which the state of the water column can jump from a low to a high concentration and identify hysteresis in the transition between the two states. The mechanism responsible for this hysteresis is hindered settling.

It thus follows that hyperturbidity is only possible in a supply limited state. From this observation we derive a necessary condition for an estuarine system to make the transition from low turbidity to hyperturbidity in a 1DV context. This is an important step towards understanding why some estuaries are hyperturbid and assessing the risk that particular estuaries may become hyperturbid in the future.

---



### 3.1. INTRODUCTION

Suspended sediment concentrations in estuarine turbidity maxima range between fairly low suspended sediment concentrations of a few tens of mg/l averaged over the water column, to hyperturbid levels of several 10 g/l (Uncles et al., 2002). Apart from large variations in sediment concentrations between estuaries, there is also a large temporal variability of the sediment trapping location. The timescale of such variations ranges from the tidal timescale up to several years (Jalón-Rojas et al., 2016). Concerning the variability on a decadal timescale, it has recently been highlighted that concentrations have increased significantly in some estuaries. Examples of such estuaries are the Ems River, where the average concentration at the surface has increased from 200 mg/l in the 1950s to over 1 g/l now (e.g. Talke et al., 2009; Schuttelaars et al., 2013; De Jonge et al., 2014), and the Loire River, where the average concentration near the surface has increased from around 500 mg/l in the 1970s to several grams per litre now (Jalón-Rojas et al., 2016). This dramatic increase in suspended sediment concentration has a severe negative impact on light penetration and oxygen conditions, resulting in a strong reduction in primary production (e.g. Cloern, 1987; Talke et al., 2009).

There are strong indications that this long-term increase in sediment concentration is related to ongoing human interventions, including removal of intertidal area, deepening of navigation channels and continuous dredging to maintain the channel at navigation depth. Several studies have made this connection by using the combined knowledge of measurements and model results (Chernetsky et al., 2010; Winterwerp et al., 2013; De Jonge et al., 2014; Van Maren et al., 2015). A possible feedback mechanism that could result in such a transition was proposed by Winterwerp and Wang (2013). According to their hypothesis, channel deepening results in tidal amplification and more import of fine sediment. This sediment leads to a reduction of the drag and therefore more tidal amplification. This describes a feedback process, which may induce a strong increase in concentration, in response to a relatively small deepening. However, to date, no study has been able to validate this hypothesis by modelling the transition to a hyperturbid state as a consequence of one or multiple human interventions. Neither are the physical mechanisms featuring in the hypothesis fully understood. A better understanding of these processes is important to make well-founded management decisions in estuaries that face substantial channel deepening.

To model the transition to hyperturbidity, at least two requirements have to be met. First, it requires the availability of fine sediment. This typically requires an import of sediment into the system from the sea, the upstream part of the river or from land. Second, once a sufficient amount of sediment is available for erosion, the water motion should be able to bring and keep this sediment in suspension.

In this chapter we will focus on the second requirement: the ability of the flow to bring and keep sediment in suspension. The aim of this chapter is to gain a better understanding of the processes that allow for high suspended sediment concentrations in the water column. To this end, the physical processes relating to erosion and settling of sediment in a water column (1DV) model are systematically investigated. Although we make no explicit comparison to field data, our parametrisations for erosion and settling are semi-empirical formulations based on laboratory and field measurements. Furthermore, the

sensitivity of the results to the choice of parametrisations, parameter values, and external forcing conditions is analysed, so that the results should be globally applicable.

A lot of theoretical and experimental work has been done on individual processes acting on sediment in the water column, especially related to high concentrations or fluid mud (see e.g. Mehta (2014) for a review). The combined effect of many of these processes on sediment concentrations in water column models has been studied by for example Winterwerp (2001) and Le Hir et al. (2001). These studies have mainly focussed on stratification of the water column and the formation of lutoclines, identifying sediment-induced turbulence damping and hindered settling as the most important processes governing the amount of stratification and the formation of fluid mud from particle settling. By including these processes, they show that water column models are able to reproduce much of the behaviour of suspended sediment stratification observed in estuaries. Given this knowledge, we will not focus much on lutoclines and the structure of the suspended sediment concentration in the water column. Rather we will focus on the overall magnitude of the concentration near the bed, while accounting for stratification of the water column in our model.

The water column model is introduced in Section 3.2, focussing on the formulations for erosion and settling. We will then discuss our main result in the context of stationary flows in Section 3.3 and extend this result to tidal flows in Section 3.4. We will qualitatively discuss the consequences of different model formulations for erosion and settling in Section 3.5. Finally the main findings are summarised in Section 3.6.

### 3.2. MODEL EQUATIONS

The water motion and sediment dynamics are described by the momentum and continuity equations and the sediment mass balance equation. We concentrate on the vertical profiles of the velocity and sediment concentration. To this end, we use a water column model similar to the one used in Winterwerp (2001). The focus on vertical processes, thereby ignoring horizontal gradients, is a reasonable approximation in many estuarine systems, since vertical exchange processes are typically dominant up to leading order (see e.g. the scaling analysis in the models introduced in Chapter 2 or Chernetsky et al. (2010)).

In this section we will focus on the physical formulations used in the model, for details on the numerical implementation the reader is referred to Winterwerp and Van Kesteren (2004). We assume a hydrostatic flow in a water column with vertical coordinate  $z$  (positive upwards) that varies between the bed at  $z = -H$  and a fixed surface at  $z = 0$  (i.e. rigid lid approximation). The flow velocity  $u$  is assumed to be unidirectional and the effects of the Earth's rotation are neglected. The vertical density differences are assumed to be small compared to the actual density, allowing the use of the Boussinesq approximation. The resulting Reynolds-averaged momentum equation reads

$$u_t = -g\zeta_x + (A_v u_z)_z, \quad (3.1)$$

with boundary conditions

$$A_v u_z = 0 \quad \text{at } z = 0, \quad (3.2)$$

$$A_v u_z = \frac{\tau}{\rho_0} \quad \text{at } z = -H, \quad (3.3)$$

where  $g$  is the acceleration of gravity,  $A_v$  is the eddy viscosity,  $\tau$  is the bed shear stress and  $\rho_0$  is a reference density for water. The subscripts  $z$  and  $t$  denote derivatives with respect to space and time respectively. The model is forced by a prescribed water level gradient  $\zeta_x$ , which is either constant or varies in time. The bottom boundary condition is further rewritten using the definition  $\tau = \rho u^* |u^*|$ , where  $u^*$  is the bed-shear velocity. The bed-shear velocity follows from the flow velocity and bed roughness by assuming that the flow near the bed has logarithmic profile according to

$$\frac{u}{u^*} = \frac{1}{\kappa} \ln \left( 1 + \frac{z+H}{z_0} \right),$$

with roughness height  $z_0$  and Von Kármán coefficient  $\kappa = 0.4$ .

The eddy viscosity  $A_v$  is computed using the  $k - \varepsilon$  model and depends on the flow velocity profile and sediment-induced buoyancy destruction (see Dijkstra et al. (2016) for details on the numerical implementation of the  $k - \varepsilon$  model used here). The sediment-induced vertical density gradient is related to the sediment concentration through a linear equation of state  $\rho = \rho_w + c(1 - \rho_w/\rho_s)$ , where  $c$  is the sediment mass concentration and  $\rho_w$  and  $\rho_s$  are the densities of water and dry sediment respectively.

The sediment is assumed to consist of a single mud fraction, so that the sediment dynamics is described by

$$c_t = (w_s c + K_v c_z)_z, \quad (3.4)$$

with boundary conditions

$$w_s c + K_v c_z = 0 \quad \text{at } z = 0, \quad (3.5)$$

$$w_s c + K_v c_z = D - E \quad \text{at } z = -H, \quad (3.6)$$

where  $w_s$  is the settling velocity of sediment flocs and  $K_v$  is the vertical eddy diffusivity. The eddy diffusivity is related to the eddy viscosity through a constant Prandtl-Schmidt number as  $A_v = \frac{K_v}{\sigma_\rho}$ , with  $\sigma_\rho = 2$  (Van Maren et al., 2009).

At the bed, sediment deposits at a rate  $D$  and erodes at rate  $E$ , which are described by

$$D = w_s c_{\text{bed}}, \quad (3.7)$$

$$E = \begin{cases} \hat{E} & \text{if } S_{\text{bed}} > 0, \\ \min(\hat{E}, w_s c) & \text{if } S_{\text{bed}} = 0, \end{cases} \quad (3.8)$$

$$\hat{E} = M \max \left( 0, \frac{\tau}{\tau_c} - 1 \right). \quad (3.9)$$

The deposition rate is defined as the flux of sediment settling out from the water column on the bed. It therefore equals  $w_s c_{\text{bed}}$ , where  $c_{\text{bed}}$  is the concentration suspended in the water column just above the bed.

In order to specify the erosion rate, we first define the sediment availability. This is denoted by the *sediment stock*  $S$  (in kg per m<sup>2</sup> surface area), which is the sum of the mass of sediment per m<sup>2</sup> at the bed available for erosion, called  $S_{\text{bed}}$ , and the mass of sediment in the water column, i.e.  $S = S_{\text{bed}} + \int_{-H}^0 c \, dz$ . Next we define the *potential erosion*  $\hat{E}$  as the erosion rate provided that there is enough sediment at the bed available for erosion. The potential erosion is normally described by (semi-)empirical formulations, such as Eq. (3.9), which is referred to as Partheniades' formula (Kandiah, 1974), based on experimental work by Partheniades (1962, 1965). In this expression  $M$  is an erosion parameter and  $\tau_c$  is the critical shear stress that needs to be exceeded for erosion. For simplicity it is assumed  $M$  and  $\tau_c$  are uniform over the depth of the sediment on the bed. The consequences of relaxing these assumptions are explored qualitatively in Section 3.5.

When  $S_{\text{bed}}$  equals zero, there is no sediment at the bed that can be eroded and the erosion rate cannot be equal to the potential erosion, unless the potential erosion equals zero. This simply follows from the principle of mass conservation, i.e. the amount of sediment at the bed cannot become negative. At maximum, the erosion rate can compensate for the deposition rate, so that deposited sediment is resuspended immediately.

We will refer to conditions where  $S_{\text{bed}} > 0$  as *erosion limited*, as the erosive strength of the flow limits the maximum erosion rate in this state. In literature this is sometimes referred to as erosion rate limited. The condition  $S_{\text{bed}} = 0$  is referred to as *supply limited*, as it is the sediment supply that limits the erosion rate (e.g. Scully and Friedrichs, 2007; Winterwerp et al., 2012). In literature this is alternatively referred to as depth limited, expressing that the erosion has reached a depth below which sediments are too consolidated to be suspended given the present flow conditions. In this research we will show that these two states lead to a clearly different behaviour of the water column. Which of the two states a water column is in, depends dynamically on the flow and the parameters in the erosion model. In our model simulations we prescribe the sediment stock  $S$ . Whether the model is in an erosion or supply limited state given this stock, follows as a model result.

When the concentrations in the water column are high, interactions between sediment particles and the ambient water reduce the effective settling velocity. To account for these effects, we use the hindered settling formulation proposed by Richardson and Zaki (1954). Their formulation is based on the reasoning that high-concentration suspensions increase the drag exerted on particles by the water that flows through the narrow space between the settling particles. Their parametrisation reads

$$w_s = w_{s,0}(1 - \phi)^m, \quad (3.10)$$

where  $w_{s,0}$  is the settling velocity of a single sediment floc and  $\phi$  the volumetric concentration of flocs defined as  $c/c_{\text{gel}}$ . The gelling concentration  $c_{\text{gel}}$  is the concentration at which the sediment flocs form a self-supporting network. The parameter  $m$  is determined from experiments and assumes values between 2.4 and 4.7 for coarse to fine

particles. The value  $m = 5$ , often used in practice for fine sediment, is taken as the default value in this article. The effect of other choices for  $m$  will be discussed in Section 3.5.

The model is solved numerically using 400 staggered grid cells and a time step of 5 seconds. The parameters for this model are assigned default values, which are presented in Table 3.1.

Symbol	Explanation	Value
$H$	Depth	10 m
$z_0$	Roughness height	$10^{-4}$ m
$M$	Erosion parameter	$2 \cdot 10^{-3}$ g/l m/s
$\tau_c$	Critical shear stress	0.1 Pa
$c_{\text{gel}}$	Gelling concentration	100 g/l
$w_{s,0}$	Clear-water settling velocity	$2 \cdot 10^{-3}$ m/s

**Table 3.1:** Model configuration in all experiments unless denoted otherwise.

### 3.2.1. DIMENSIONLESS EROSION PARAMETER

It is illustrative to consider a stationary flow and assume there is an abundant sediment supply (i.e.  $S = \infty$ ,  $S_{\text{bed}} = \infty$ ). Under these assumptions,  $u_t = 0$ ,  $c_t = 0$  and  $E = \hat{E}$ . Integrating the sediment concentration equation (3.4) between  $z = -H$  and 0, it follows that deposition balances the potential sediment erosion, i.e.  $D = \hat{E}$ . Substituting Eq. (3.7) for  $D$  and Eq. (3.9) for  $\hat{E}$ , together with Expression (3.10) for hindered settling and using  $\phi = c/c_{\text{gel}}$ , the condition  $D = \hat{E}$  can be written as

$$(1 - \phi_{\text{bed}})^m \phi_{\text{bed}} = \underbrace{\frac{M}{w_{s,0} c_{\text{gel}}} \left( \frac{\tau}{\tau_c} - 1 \right)}_{\hat{E}} \quad (\tau > \tau_c), \quad (3.11)$$

which relates the near-bed concentration  $\phi_{\text{bed}}$  (on the left-hand side) to a quantity that is defined as the *dimensionless erosion parameter*  $\hat{E}$ . In the results presented in the next sections, we will use the dimensionless erosion parameter to characterise the possible equilibrium states of the water column and show that this parameter is also useful in a context of non-stationary flows.

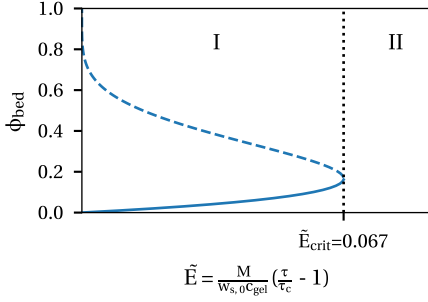
## 3.3. RESULTS FOR STATIONARY FLOWS

### 3.3.1. ABUNDANT SEDIMENT SUPPLY

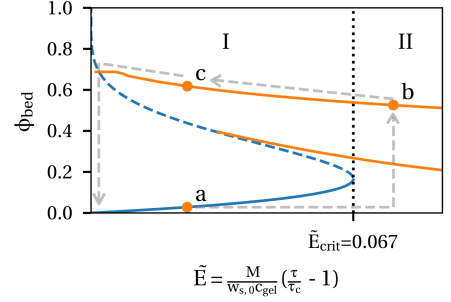
We first assume a stationary flow with an abundant supply of sediments, so that Eq. (3.11) defining  $\hat{E}$  holds. This expression is a non-linear algebraic equation for  $\phi_{\text{bed}}$  that only depends on the bed shear stress  $\tau$  and a number of model parameters. The bed shear stress follows by vertically integrating the momentum balance (3.1) and using the corresponding boundary conditions. It then follows that  $\tau = \rho_0 g H \zeta_x$ . As the model is forced by  $\zeta_x$ ,  $\tau$  is known a priori. Hence  $\phi_{\text{bed}}$  can be obtained by resolving near-bed processes, without solving for the entire water column. Thus  $\phi_{\text{bed}}$  does not depend on turbulence in the water column.

Figure 3.1 shows the resulting equilibrium near-bed concentration  $\phi_{\text{bed}}$  as a function of





**Figure 3.1:** Equilibrium conditions for the near-bed dimensionless concentration  $\phi = \frac{c}{c_{\text{gel}}}$  for a stationary flow. In range I the solid line indicates a stable equilibrium and the dashed line indicates an unstable equilibrium. No equilibrium exists in range II, where the concentration may theoretically increase without bounds.



**Figure 3.2:** Equilibrium conditions for the near-bed dimensionless concentration for a stationary flow as in Figure 3.1, with the addition of supply limited branches for two different values of the stock, indicated by the orange lines. The lower orange line corresponds to  $S = 15 \text{ kg/m}^2$ , the upper orange line corresponds to  $S = 150 \text{ kg/m}^2$ . On these lines all available sediment is suspended in the water column. The arrows illustrate how a system can jump from one branch to another for increasing  $\tilde{E}$  (from point a to b) and decreasing  $\tilde{E}$  (from b to c and further).

$\tilde{E}$ . We distinguish between two regions in this graph. In region I ( $0 < \tilde{E} < \tilde{E}_{\text{crit}}$ ), two solutions for the near-bed concentration exist. However, linear stability analysis shows that only the solution depicted by the solid line is a stable solution, meaning that a system close to the equilibrium state evolves towards its equilibrium over time. The near-bed concentrations on this stable solution branch have values up to  $\phi = 0.16$ . These concentrations can be high (up to 16 g/l assuming a gelling concentration of 100 g/l) but are significantly smaller than the gelling concentration. The dashed line depicts an unstable solution, meaning that a system close to, but not exactly in, this state will move away from it over time.

The behaviour of the solution if it is not in equilibrium is best seen from the depth-integrated concentration equation Eq. (3.4)

$$\int_H^0 c_t dz = E - D.$$

Left of the equilibrium curve  $D > E$ , the depth-integrated concentration decreases over time. Conversely, on the right of the equilibrium curve,  $E > D$  and the concentration increases over time. Correspondingly, if the near-bed concentration is above the unstable equilibrium (dashed line), the system will continue to erode sediment and, within this model, the concentration will increase without bound.

In region II ( $\tilde{E} > \tilde{E}_{\text{crit}}$ ) we are on the right of the equilibrium curve and the concentration

continues to increase, regardless of the initial concentration. This is possible because of the effects of hindered settling: as the concentration increases due to erosion, hindered settling leads to a decrease in the settling velocity and therefore in the rate of sediment deposition. As a consequence, the net erosion rate of the system increases leading to a further increase of the concentration and reduction of the deposition.

The change in model behaviour as one moves from region I into II is known mathematically as a bifurcation. This bifurcation exists, because the left-hand side of Eq. (3.11), which represents a dimensionless deposition flux  $\frac{w_s c}{w_{s,0} c_{gel}}$ , has a maximum. If  $\phi$  is small, the deposition flux increases with  $\phi$ , as the settling velocity is virtually constant and the sediment concentration increases. However, if  $\phi$  is large, hindered settling has such a strong effect in decreasing the settling velocity, that the total deposition flux decreases with increasing  $\phi$ .

### 3.3.2. LIMITED SEDIMENT AVAILABILITY

By limiting the sediment stock, the suspended sediment concentrations remain finite for all time. If all the available sediment is suspended in the water column, the solution cannot be computed from the near-bed balance  $E = D$ . This is because  $E$  reduces to  $D$  in this state (see the definition of erosion Eq. (3.8)) and the bottom boundary condition becomes trivial. In this case, the restricting condition reads as  $S = \int_{-H}^0 c \, dz$ , i.e. all sediment is suspended in the water column. This means that the near-bed concentration depends on the distribution of the sediment over the water column and thus on both the turbulence profile and hindered settling. Hence, the near-bed concentration follows from the water column model. We have conducted 40 model experiments with different values for the water level gradient but otherwise default values (Table 3.1). We start with the largest water level gradient and run the model for a sufficiently long time, until a stationary state is attained. Next, the water level gradient is decreased and the model is run again, using the result of the previous experiment as initial condition. This ensures that the solution remains on the supply limited branch provided this branch still exists.

The equilibria are shown in Fig. 3.2. The equilibrium branches in Section 3.3.1 are still present and are shown in blue. Added to this are two new (orange) branches which result from setting a finite stock  $S$  of 15 (lower branch) and 150 kg/m<sup>2</sup> (upper branch). On these branches, all available sediment is suspended in the water column, preventing a further increase in concentration. This equilibrium is therefore referred to as *supply limited*, corresponding to the definition of supply limited given in Section 3.2 for the erosion rate. Naturally, a larger value of the stock leads to larger values of  $\phi_{bed}$ . Regardless of the stock, the supply limited solution exists for all values of  $\tilde{E}$  in region II, so that the concentration is bounded for all model settings. It also extends into region I, where it ceases to exist when it crosses the erosion limited solution. At this point, the flow velocity and effect of hindered settling are no longer sufficient to keep all the available sediment in suspension and the concentration reduces towards the stable blue branch. On the blue branch, some of the available sediment remains on the bed and the suspended sediment concentration is restricted by the ability of the flow to erode and keep sediment in suspension. This is referred to as an *erosion limited* equilibrium, also corresponding to the definition of erosion limited in Section 3.2.

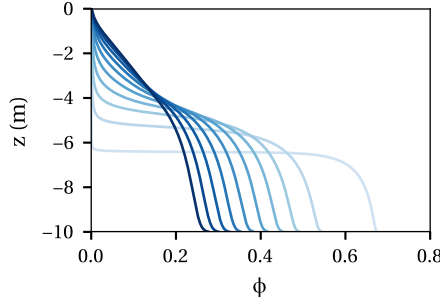


**Figure 3.3:** Vertical profiles of the sediment concentration along the supply limited branch with  $S = 150 \text{ kg/m}^2$ . The profiles are plotted for a range of values of  $\zeta_x$  from 0 to  $5 \cdot 10^{-5}$ . Correspondingly  $\tilde{E}$  ranges from 0 to 0.5. The colours indicate increasing  $\zeta_x$  or increasing  $\tilde{E}$  (i.e. light colours: small  $\zeta_x$ , dark colours: large  $\zeta_x$ ).

The supply limited solutions are down-sloping curves. The near-bed concentration decreases with increasing  $\tilde{E}$  because we vary  $\zeta_x$  in the model experiments. This not only leads to a variation in  $\tilde{E}$  via the bed shear stress but also to a variation in the rate of mixing of the water column. As a result, a larger  $\tilde{E}$  coincides with a more well-mixed water column. As the same amount of sediment is in suspension for all solutions on the branch, the near-bed concentration decreases as  $\tilde{E}$  increases. This is also illustrated by the vertical sediment profiles plotted in Figure 3.3, where the colours from light to dark are obtained by increasing  $\tilde{E}$  from 0.015 to 0.15.

The distinction between erosion and supply limited equilibrium states has profound implications for hyperturbidity. Near-bed concentrations associated with hyperturbidity are of the order of the gelling concentration. However, the maximum near-bed concentration in a stable erosion limited state is only approximately  $\phi_{\text{bed}} = 0.16$  according to this model, one order of magnitude smaller than the gelling concentration. In order for a system to be hyperturbid, it therefore needs to be supply limited. A water column can only be supply limited with  $\phi_{\text{bed}} > 0.16$  if it satisfies the criterion  $\tilde{E} > \tilde{E}_{\text{crit}}$ , or has satisfied this criterion at some point in its history and has stayed on a supply limited equilibrium branch with high concentrations (see below).

Figure 3.2 also has profound implications for the ways in which a transition between branches occurs. Consider a system on the erosion limited stable equilibrium branch (e.g. at point a in the figure). Next consider some change to, for example, the bed shear stress such that  $\tilde{E}$  increases beyond  $\tilde{E}_{\text{crit}}$ . The system will then evolve over time to a supply limited equilibrium (e.g. at point b). If there is a sufficient amount of sediment available, this leads to a catastrophic increase in concentration. If the change to  $\tilde{E}$  is completely reversed, the potential erosion is still larger than the deposition. Therefore, all sediment remains suspended in the water column and the system remains on the supply limited branch, with even higher concentrations near the bed (point c). A transition back to the erosion limited equilibrium branch will only happen if  $\tilde{E}$  is further reduced to below the point where the supply limited branch starts. The erosion and supply limited branches thus describe hysteresis between the transition from low to high concentrations and back.

### 3.4. EXTENSION TO TIDAL FLOWS

#### 3.4.1. INSTANTANEOUS RESULTS

The instantaneous bed shear stress in tidal flows varies from its maximum at peak ebb or flood to virtually zero at slack tide. As a result, the near-bed sediment concentration varies over the tidal cycle. To demonstrate this, we force the water column model by a tidally varying water level gradient consisting only of an  $M_2$  tidal constituent:

$$\zeta_x = |\zeta_x| \cos(\omega t),$$

where  $|\zeta_x|$  denotes the amplitude of the forcing and  $\omega$  is the angular frequency of the  $M_2$  tide.

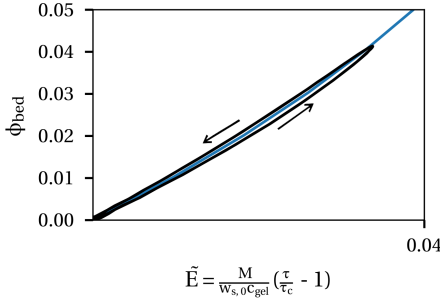
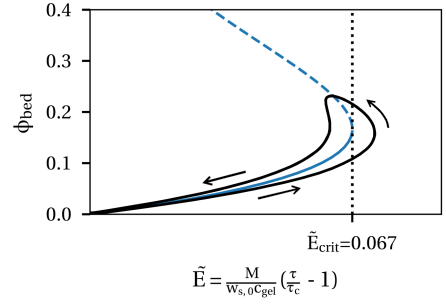
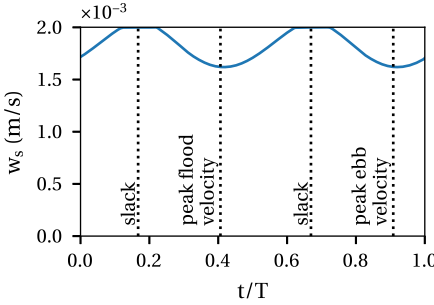
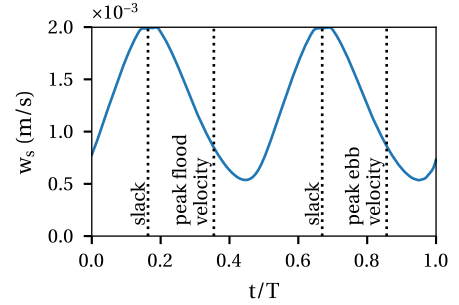
Figure 3.4 shows model results for  $|\zeta_x| = 10^{-5}$  (left) and  $2.1 \cdot 10^{-5}$  (right), an infinite sediment supply and all other variables having their default values (Table 3.1). The figure shows the temporal evolution of the near-bed volumetric concentration as a function of the dimensionless erosion parameter during half a tidal cycle from slack tide to peak tide and back to slack tide. The solid and dashed blue lines in the figure indicate the stationary equilibrium and are identical to the solution in Figure 3.1 obtained for stationary forcing conditions. In Figure 3.4a, the tidal forcing is small, leading to a small concentration and small amplitude of the dimensionless erosion parameter. The tidal signal is always close to the solid line that indicates the stationary equilibrium. Therefore it is concluded that the change of the concentration during the tidal period is small enough to adjust to the stationary equilibrium at all time.

Figure 3.4b shows the temporal variation of the near-bed concentration for a larger tidal forcing. The concentration now deviates significantly from the stationary equilibrium. During accelerating tide, the concentration increases but remains below the stationary equilibrium concentration. Conversely, during most of the decelerating tide, the concentration decreases but remains above the equilibrium concentration. At peak tide, the maximum value of  $\bar{E}$  is attained and  $\bar{E}$  exceeds  $\bar{E}_{\text{crit}}$ , allowing for an unbounded increase of the concentration. After peak tide,  $\bar{E}$  still exceeds  $\bar{E}_{\text{crit}}$  for some time resulting in a further increase of the near-bed concentration, even though the bed shear stress already decreases. The increase of the concentration only stops when the pair  $(\phi_{\text{bed}}, \bar{E})$  crosses the unstable stationary equilibrium (dashed line), well after peak tide. Within the remainder of the time until slack tide, the concentration reduces to almost zero. Therefore there is no net change of the concentration over the tidal cycle.

Figures 3.4c and 3.4d visualise the same experiments in a different way, by plotting the effective settling velocity versus  $t/T$ , where  $T$  is one tidal period. For the weak tidal forcing, the variation in settling velocity is weak and in phase with the tidal velocity near the bed. For the stronger tidal forcing, the variation in settling velocity is stronger and we again see that the lowest settling velocity (highest concentration) is attained after peak tidal velocity.

#### 3.4.2. TIDALLY AVERAGED RESULTS

Even though the concentration varies over the tidal cycle, we are mainly interested in the average behaviour over a tidal cycle. Therefore, we will further consider the tidally averaged concentration. It is not possible to find a relation between the tidally averaged

(a)  $\tilde{E} - \phi$  for  $|\zeta_x| = 10^{-5}$ (b)  $\tilde{E} - \phi$  for  $|\zeta_x| = 2.1 \cdot 10^{-5}$ (c)  $w_s$  for  $|\zeta_x| = 10^{-5}$ (d)  $w_s$  for  $|\zeta_x| = 2.1 \cdot 10^{-5}$ 

**Figure 3.4:** Top: instantaneous values of  $\phi_{\text{bed}}$  and  $\tilde{E}$  for half a period of an  $M_2$  tidal wave for two forcing strengths. This is compared to the stationary equilibrium branch (blue line). At slack tide,  $\tilde{E} = 0$ , while  $\tilde{E}$  is at its maximum for peak flood and ebb velocities. Bottom: the same simulations but now visualising the effective settling velocity versus dimensionless time over one  $M_2$  tidal cycle.

near-bed concentration  $\langle \phi_{\text{bed}} \rangle$  and the tidally averaged dimensionless erosion parameter  $\langle \tilde{E} \rangle$  only on the basis of near-bed processes, as was the case in stationary flows (see Appendix 3.A for details). Therefore, the water column model has to be solved for different tidal forcing conditions.

In these experiments, we force the water motion by a prescribed tidally varying water level gradient, an infinite stock and use the default parameter values (Table 3.1). Each experiment for one value of  $|\zeta_x|$  is allowed a sufficiently long spin-up time to attain periodic conditions, resulting in a single equilibrium value of  $\langle \tilde{E} \rangle$  and  $\langle \phi_{\text{bed}} \rangle$ . The branch of stable equilibrium states is constructed by repeating this procedure for various water level gradient amplitudes. The unstable equilibrium branch is, by definition, never obtained using time-integration models. Nevertheless this branch can be inferred from the model by introducing a limited sediment availability. As demonstrated in Figure 3.2 for stationary flows, a limited sediment availability results in a new branch of stable supply

limited equilibrium solutions. This branch exists at all values of  $\bar{E}$  on the right side of the equilibrium curve. By running the model for various values of the sediment availability and water level gradient amplitude, we find various supply limited branches. The left-most endpoints of these supply limited branches mark the location where they cross the unstable equilibrium. This way, the unstable equilibrium solution can be reconstructed. Here, this reconstruction procedure is done using over 4000 model simulations with the  $M_2$  water level gradient amplitude  $|\zeta|_x$  varying between 0 and  $5 \cdot 10^{-5}$  and the sediment stock varying between 5 and  $400 \text{ kg/m}^2$ .

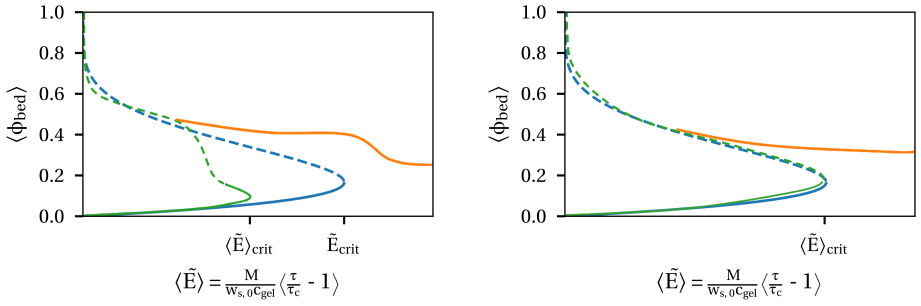
The solution is plotted in Figure 3.5a (green line), together with one supply limited branch corresponding to a sediment stock of  $15 \text{ kg/m}^2$  (orange line). For small values of  $\langle \bar{E} \rangle$  the stable erosion limited branch (solid green line) corresponds closely to the stationary equilibrium branch (solid blue line). This is because the concentrations are small and are almost equal to the stationary equilibrium concentration throughout every instance of the tidal cycle (cf. Figure 3.4a). For increasing  $\langle \bar{E} \rangle$ , the tidal and stationary branches start to differ. For these settings it is found that  $\langle \bar{E} \rangle_{\text{crit}}$  is smaller in the tidal case than in the stationary case. To see why this is possible, consider some value of  $\langle \bar{E} \rangle$ . The instantaneous value of  $\bar{E}$  is smaller than  $\langle \bar{E} \rangle$  during approximately half of the tidal cycle and larger during the remainder of the tidal cycle. If  $\langle \bar{E} \rangle$  is sufficiently large, the instantaneous  $\bar{E}$  also exceeds the instantaneous  $\bar{E}_{\text{crit}}$  for some smaller time interval of the tidal cycle. If, during this time interval, the concentration increases so much that the concentration cannot decrease back during the remainder of the tidal cycle, the average concentration keeps increasing over time and no equilibrium condition can be found. This means we must have passed the critical point. It depends on the model settings how long  $\bar{E}$  has to exceed  $\bar{E}_{\text{crit}}$  before this happens.

To illustrate this, Figure 3.5b shows the erosion limited equilibrium branches and a supply limited branches ( $S = 100 \text{ kg/m}^2$ ) for a different set of parameter values. We have decreased the erosion parameter  $M$  to  $2 \cdot 10^{-4} \text{ g/l m/s}$  and increased the range of  $|\zeta_x|$  between 0 and  $5 \cdot 10^{-4}$ . Compared to the default value of  $M$ , a larger  $|\zeta_x|$  and thus a higher degree of vertical mixing is required to suspend the same amount of sediment. Firstly, this leads to a more uniform distribution of the sediment over the water column. Therefore a much higher stock is required to find a supply limited branch at similar values of  $\phi_{\text{bed}}$  compared to the results shown in Figure 3.5a. Secondly, the value of  $\langle \bar{E} \rangle_{\text{crit}}$  in Figure 3.5b is almost the same as the instantaneous critical value and significantly larger than the critical value in Figure 3.5a. As this concerns the tidal average in a symmetric tide, this implies that the instantaneous  $\bar{E}$  exceeds the stationary critical value for almost half the tidal cycle. However, in this time, the concentration does not increase so much that it cannot return to low values around slack tide. In other words, the timescale for the concentration to change is longer.

This can be explained from a rough scaling analysis of the depth-integrated version of Eq. 3.4. After applying the boundary conditions, this equation reads as

$$\left( \int_{-H}^0 c \, dz \right)_t + w_s c_{\text{bed}} - \hat{E} = 0. \quad (3.12)$$

Let  $\bar{C}$  denote a typical depth-averaged concentration and  $T$  denote a timescale at which



(a) Default settings, with  $|\zeta_x|$  varying between 0 and  $5 \cdot 10^{-3}$ . The supply limited curve (orange) is for a stock of  $15 \text{ kg/m}^2$ . (b) Reduced erosion parameter  $2 \cdot 10^{-4} \text{ g/l m/s}$  and increased  $|\zeta_x|$  between 0 and  $5 \cdot 10^{-4}$ . The supply limited curve (orange) is for a stock of  $100 \text{ kg/m}^2$ .

**Figure 3.5:** Equilibrium values of the tidally averaged near-bed concentration for an  $M_2$  tidal flow constructed by varying  $|\zeta_x|$ . The green line indicates the erosion limited stable (solid line) and unstable (dashed line) branches. The orange line indicates a supply limited branch for a given sediment supply. For reference, the blue line indicates the stationary erosion limited equilibrium branches and is the same as in Figure 3.1.

the average concentration changes, then  $\frac{H\hat{C}}{T} \sim -w_s c_{\text{bed}} + \hat{E}$ , i.e.

$$T \sim \frac{H\hat{C}}{-w_s c_{\text{bed}} + \hat{E}}.$$

The depth-averaged concentration scales with the near-bed concentration and with some increasing function of the eddy diffusivity. In other words, an increase in the eddy diffusivity at the same near-bed concentration leads to an increase in the depth-averaged concentration. Therefore, at the same near-bed concentration and potential erosion, a higher degree of mixing of the water column leads to a higher value of  $\hat{C}$  and thus a larger timescale for the concentration to change. For an even larger tidal forcing and smaller erosion parameter,  $\langle \tilde{E} \rangle_{\text{crit}}$  can exceed  $\tilde{E}_{\text{crit}}$ .

Though the horizontal axis of Figure 3.5 shows the dimensionless erosion parameter, the model results were obtained by varying the water level amplitude. A change in the water level gradient amplitude not only affects  $\tilde{E}$  through the bed shear stress but also affects the rate of mixing of the water column. A variation of another parameter, such as the erosion parameter only affects  $\tilde{E}$  and not the rate of mixing. Figure 3.6 again shows the stable and unstable equilibrium solution branches but now obtained by varying the erosion parameter  $M$  at a fixed value of  $|\zeta_x|$  of  $10^{-4}$ . The orange supply limited branch corresponds to  $S = 100 \text{ kg/m}^2$ . Similar to Figure 3.5b,  $\langle \tilde{E} \rangle_{\text{crit}}$  is close to the stationary critical value, because the tidal forcing is relatively large and the timescale for the concentration to change is relatively long. The main difference with the figures found before is the shape of the supply limited branches. These are more flat or even slightly upward sloping. This is because a change in  $\tilde{E}$  now does not coincide with enhanced or decreased

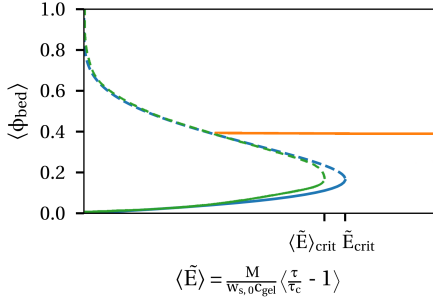


**Figure 3.6:** Similar to Figure 3.5a but now for  $|\zeta_x| = 10^{-4}$ ,  $S = 100 \text{ kg/m}^2$  and varying erosion parameter  $M$ . Because  $M$  is varied instead of  $|\zeta_x|$ , the supply limited branch is no longer downward sloping.

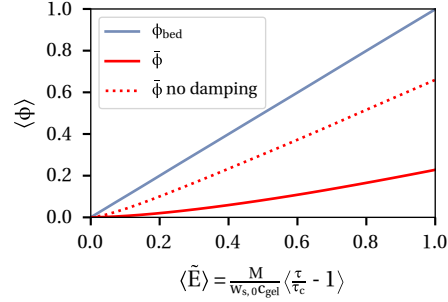


**Figure 3.7:** Relation between  $\langle \phi_{\text{bed}} \rangle$  and the tidally averaged dimensionless erosion parameter if hindered settling is removed from the model. The blue line shows the near-bed concentration. The red line shows the depth-averaged concentration, compared to the depth-averaged concentration if both hindered settling and sediment-induced damping are omitted (red dotted line). The figure is obtained by varying the tidal  $M_2$  amplitude of  $\zeta_x$  in the model.

mixing of the water column; the vertical distribution of sediment remains the same at different values of  $\tilde{E}$ .

### 3.4.3. ROLE OF HINDERED SETTLING

In a tidal flow, the instantaneous sediment concentration changes constantly in the direction of the stationary equilibrium or keeps increasing if a stationary equilibrium does not exist. The essential mechanism explaining the bifurcation in the stationary case therefore also explains the bifurcation in the tidal case. This mechanism is hindered settling. Additional to hindered settling, inertia is important in tidal flows: the instantaneous  $\tilde{E}$  needs to exceed  $\tilde{E}_{\text{crit}}$  for a sufficiently long time for the concentration to move away from the erosion limited equilibrium.

In order to further support the conclusion that hindered settling is essential for the bifurcation, we again consider the depth-integrated sediment balance Eq. (3.12) without hindered settling. We assume a dynamic tidal equilibrium exists and take the tidal average. The result reads

$$\langle \phi_{\text{bed}} \rangle = \underbrace{\left\langle \frac{M_0}{w_{s,0} c_{\text{gel}}} \max \left( 0, \frac{\tau}{\tau_c} - 1 \right) \right\rangle}_{\tilde{E}}, \quad (3.13)$$

i.e. the tidally averaged near-bed concentration depends linearly on the dimensionless erosion parameter and does not depend on the rate of turbulent mixing of the water



column. For comparison, the solution with hindered settling leads to the non-linear relation  $\langle (1 - \phi_{\text{bed}})^m \phi_{\text{bed}} \rangle = \langle \tilde{E} \rangle$  (see Eq. (3.20) in Appendix 3.A). The solution without hindered settling is plotted in Figure 3.7 (blue line). Clearly, there is no bifurcation. High near-bed concentrations of the order of the gelling point can nevertheless be attained but only at values of  $\langle \tilde{E} \rangle$  which are one order of magnitude larger than in the case with hindered settling (compare  $\tilde{E}_{\text{crit}} = 0.067$ ).

The figure also shows the depth- and time-averaged concentration without hindered settling, with and without sediment-induced turbulence damping (red solid line and red dotted line respectively). In these experiments, all parameters have their default values (Table 3.1), the stock is infinite and the variation of  $\langle \tilde{E} \rangle$  is obtained by varying  $|\zeta_x|$ . The figure shows that sediment-induced turbulence damping has a significant effect by reducing the depth-averaged concentration compared to the situation without turbulence damping. It also shows that turbulence damping alone does not lead to any bifurcations.

### 3.5. DISCUSSION

In this section we investigate the sensitivity of the model results to different parametrisations and parameter choices. In section 3.5.1 we discuss several formulations and parameter choices related to hindered settling. In Section 3.5.2 we look at several formulations for erosion. Finally, the role of flocculation is discussed in Section 3.5.3. An exhaustive discussion of each available formulation is beyond the scope of this study, but the influence of different parametrisations will be at least qualitatively discussed and the methodology to perform an in-depth analysis will be indicated where deemed necessary.

#### 3.5.1. OTHER PARAMETRISATIONS OF HINDERED SETTLING

The existence of a limit point when the erosion parameter attains a critical value, depends crucially on hindered settling. Three parametrisations of hindered settling prevail in literature. The first is the formulation proposed by Richardson and Zaki (1954) (see Eq. (3.10)), in which the parameter  $m$  is empirical and still needs to be chosen. Laboratory measurements indicate  $m$  is likely between 2 and 5. The second formulation is by Dankers and Winterwerp (2007). It reads

$$w_s = w_{s,0} \frac{(1 - \phi)^m (1 - \phi_p)}{1 + 2.5\phi}. \quad (3.14)$$

Here  $\phi_p$  is the volumetric concentration of primary particles, defined as  $c/\rho_s$ , with  $\rho_s$  the dry density of the soil. Dankers and Winterwerp (2007) propose  $m = 2$  after a comparison to measurements. The third formulation is by Toorman and Berlamont (1993), in which we neglect the contribution related to consolidation and rewrite to our notation as

$$w_s = w_{s,0} e^{-\alpha\phi}, \quad (3.15)$$

where  $\alpha$  is an empirical parameter. Mehta (2014) summarises data from three studies, with  $\alpha$  ranging between 5.5 and 8. Here we use  $\alpha = 7$ , but the results are qualitatively the same for all values in this range.

Figure 3.8 shows the stable and unstable erosion limited branches in a stationary flow for various values of  $m$  in Eq. (3.10),  $m = 2$  in Eq. (3.14) and  $\alpha = 7$  in Eq. (3.15). All

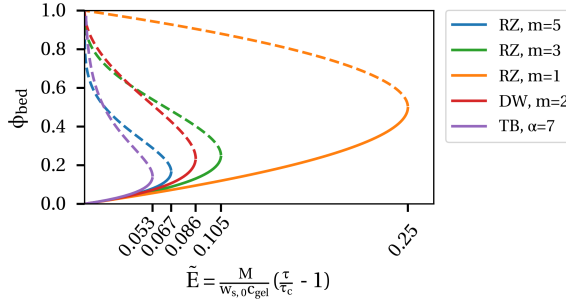


**Figure 3.8:** Stationary equilibrium branches for different parametrisations of hindered settling. The lines marked RZ refer to the Richardson and Zaki (1954) formulation (3.10) for different values of the parameter  $m$ . The line marked DW refers to the Dankers and Winterwerp (2007) formulation (3.14). The line marked TB refers to the Toorman and Berlamont (1993) formulation (3.15). All formulations essentially display the same characteristic of a bifurcation point separating a stable and unstable branch. The tick marks on the horizontal axis show the location of the bifurcation point on the RZ and TB curves.

curves show the same characteristics as found before: the existence of a bifurcation point, where one stable and one unstable solution branch meet. The various curves only differ in the value of the critical dimensionless erosion parameter and the corresponding near-bed concentration.

As was explained in Section 3.3, the necessary condition for the existence of a bifurcating solution is the existence of a maximum of the settling flux. This is obtained for all hindered settling parametrisations studied here. For the Richardson and Zaki (1954) formulation this bifurcation point can be easily derived to occur at  $\phi_{\text{bed}} = \frac{1}{m+1}$ . The value of  $\hat{E}_{\text{crit}}$  can also be expressed analytically in terms of  $m$  and is given by  $\left(\frac{m}{m+1}\right)^m \frac{1}{m+1}$ .

### 3.5.2. OTHER DESCRIPTIONS OF EROSION

Although much experimental work has been done on erosion, there is no consensus on the best mathematical description of erosion (e.g Sanford and Maa, 2001; Mehta, 2014). One popular formulation for erosion can be generalised as

$$\hat{E} = M(\tilde{z}, t) \max\left(0, \frac{\tau(t)}{\tau_c(\tilde{z}, t)} - 1\right)^n, \quad (3.16)$$

where  $\tilde{z}$  indicates the depth of erosion relative to the bottom of the water column ( $z = -H$ ). Many variations on this model exist in which the time and/or depth dependence of the erosion parameter  $M$  or critical shear stress are omitted. The time and depth dependence of  $\tau_c$  is often associated with consolidation but may also be related to biological influence (e.g. Le Hir et al., 2007). The erosion parameter  $M$  is often kept constant over time and depth but may be allowed to vary related to sediment composition or consolidation (e.g. Sanford and Maa, 2001). Often  $n = 1$ ,  $M(\tilde{z}, t) = M$  and  $\tau_c(\tilde{z}, t) = \tau_c$  are chosen for practical reasons. In this case, this formulation is typically associated with well-consolidated soils (referred to as type II erosion). Another formulation for erosion

reads

$$\hat{E} = E_f(\tilde{z}, t) \exp \left( \alpha \left( \frac{\tau_b(t)}{\tau_c(\tilde{z}, t)} - 1 \right) \right). \quad (3.17)$$

This form is sometimes favoured for unconsolidated soils (referred to as type I erosion), where the strength varies with depth.

The results presented in this chapter do not hold for all forms of the general erosion formulations Eq. (3.16) and (3.17) with arbitrary  $t$  or  $z$  dependence. It depends on the exact formulation if the same qualitative results hold. We will not go into the effect of choosing any particular form of these general erosion formulations, as there is not one standard form other than Partheniades' formulation, which is used throughout this chapter. The purpose of this section is to show that the same methods applied in this chapter can be applied to study many forms of the erosion formulation. This mainly requires a suitable redefinition of  $\tilde{E}$ . We will illustrate how one may determine  $\tilde{E}$  and the existence of a bifurcation point in this case by a simple example.

Consider a stationary flow forced by a constant water level slope. Let the critical shear strength increase with depth, e.g. due to consolidation, and let the erosion be described by (3.16) with  $n = 1$ . The condition for the equilibrium near-bed concentration of Eq. (3.11) is modified to

$$(1 - \phi_{\text{bed}})^m \phi_{\text{bed}} = \frac{M}{w_{s,0} c_{\text{gel}}} \left( \frac{\tau}{\tau_c(\tilde{z})} - 1 \right).$$

Reordering this expression yields

$$\left( (1 - \phi_{\text{bed}})^m \phi_{\text{bed}} + \frac{M}{w_{s,0} c_{\text{gel}}} \right) \tau_c(\tilde{z}) = \underbrace{\frac{M}{w_{s,0} c_{\text{gel}}}}_{\tilde{E}} \tau, \quad (3.18)$$

where all terms depending on  $\phi$  are on the left-hand side, including  $\tau_c$ , which depends on  $\phi$  through  $\tilde{z}$ . Within this formulation, the right-hand side should be considered as the dimensionless erosion parameter, i.e.  $\tilde{E} = \frac{M_0}{w_{s,0} c_{\text{gel}}} \tau$ . Eq. (3.18) has a bifurcation point if the left-hand side of this expression has a maximum. Whether this is the case depends on the relation between the critical shear stress and  $\phi_{\text{bed}}$ . If a maximum to the left-hand side of Eq. (3.18) exists, the results of this study also hold qualitatively for this erosion formulation. If there is no such maximum, the stable erosion limited solution branch exists for all values of  $\tilde{E}$ . High concentrations can then be attained for erosion limited conditions and no hysteresis is observed in the transition between low and high concentration states.

### 3.5.3. ROLE OF FLOCCULATION

Fine cohesive sediments are known to flocculate. The size and settling velocity of sediment flocs may differ of that of the primary sediment particles by several orders of magnitude. It is known that the degree of flocculation depends on the concentration of primary particles and shear stress in the water column. Therefore the flocculation also varies with  $\phi_{\text{bed}}$  and  $\tilde{E}$  and is expected to modify the equilibrium curves in  $\phi_{\text{bed}}-\tilde{E}$  space.

Experiments on flocculation show that the settling velocity of the sediment increases due to flocculation processes but only up to values of  $\phi$  around 0.1 (see e.g. Figure 5.3 of Winterwerp and Van Kesteren, 2004, and references therein). For higher volumetric concentrations, hindered settling takes over and dominates the settling velocity. Therefore it is expected that flocculation only modifies the shape of the erosion limited equilibrium branch in the  $\phi_{\text{bed}} - \bar{E}$  diagram. Taking  $w_{s,0}$  as the settling velocity of flocs at  $\bar{E} = \bar{E}_{\text{crit}}$ , the unstable branch and  $\bar{E}_{\text{crit}}$  are hardly affected by flocculation. Flocculation is therefore not expected to have any important implications for the results found in this chapter.

### 3.5.4. NECESSITY OF HINDERED SETTLING TO REPRODUCE HIGH CONCENTRATIONS

The theory developed in this work helps to explain why some estuaries and coastal systems can support very high suspended sediment concentrations, while the bed shear stress is not particularly high. Here we demonstrate this using two examples. The first is of the Amazon shelf, with concentrations of more than 100 g/l (Kineke and Sternberg, 1995), while the average bed shear stresses are estimated by model studies to be of the order of 1 Pa (Gabioux et al., 2005). The second example is the Ems River Estuary, where concentrations of over 30 g/l have been observed (Talke et al., 2009), while bed shear stresses are up to 2 Pa (Van Maren et al., 2015). We compute the order of magnitude of the tide-averaged dimensionless erosion parameter for these systems, using its definition Eq. (3.11). The erosion parameter  $M$  is a calibration parameter in most models. The critical bed shear stress  $\tau_c$  can be measured but has a significant measurement uncertainty and natural variability. However, both parameters have a well-established range of typical values. We estimate  $M$  to be of the order of  $10^{-4} - 10^{-3}$  g/l m/s and  $\tau_c$  in the range  $10^{-1} - 10^1$  Pa (see e.g. Partheniades (2010)). We assume a typical order of magnitude of the settling velocity of 1 mm/s and  $c_{\text{gel}}$  of 100 g/l. For the Amazon shelf and the Ems River this means that typical values of  $\langle \bar{E} \rangle$  are  $10^{-3}$  to  $10^{-1}$ .

If the effects of hindered settling were not included in the model, the mean value of  $\bar{E}$  equals the mean near-bed volumetric concentration (also see Eq. (3.13)). This means that  $\phi$  can at maximum attain concentrations of around  $10^{-1}$ , corresponding to 10 g/l with the current choice of the gelling concentration. This is much lower than the concentrations observed on the Amazon shelf and also lower than the concentrations observed in the Ems River. Without hindered settling the observed concentrations can therefore not be reproduced using realistic parameter settings. In a model that includes the effects of hindered settling, the only requirement for obtaining high concentrations is that  $\langle \bar{E} \rangle$  exceeds  $\langle \bar{E} \rangle_{\text{crit}}$ , which is of the order of magnitude of  $\bar{E}_{\text{crit}} = 0.067$ . This value is within the range of typical values

Apart from requiring a sufficiently high  $\langle \bar{E} \rangle$ , high concentrations also require a large supply of sediment. In estuaries like the Ems, where the sediment mainly enters at the mouth of the estuary, this requires a strong trapping of sediment. This trapping depends on the along-channel dynamics of the system and has not been investigated in this study. The role of hindered settling on the trapping behaviour of systems like the Ems thus still needs to be investigated.

### 3.6. CONCLUSIONS

Over the last several decades, some estuaries have undergone a transition from low or average turbidity levels to a so called hyperturbid state. In order to improve our understanding of this transition, we have systematically identified the essential processes that allow for high suspended sediment concentrations in an estuarine water column. We adopt a framework where we characterise the dynamic equilibrium state of the water column as either erosion or supply limited. In the erosion limited state, the concentration is bounded by the ability of the flow to erode and keep sediment in suspension. In the supply limited state, all available sediment is suspended in the water column, so that the maximum concentration is bounded by the amount of sediment available in the system.

The behaviour of the water column in these equilibrium states can be described in terms of a time-averaged dimensionless erosion parameter  $\langle \tilde{E} \rangle$ , which parametrises the rate of erosion. If  $\langle \tilde{E} \rangle$  is above some threshold  $\langle \tilde{E} \rangle_{\text{crit}}$ , only the supply limited equilibrium exists and the actual concentration entirely depends on the amount of sediment in the system. This potentially allows for extremely high concentrations. For values of  $\langle \tilde{E} \rangle$  below the threshold, both types of equilibria may exist. Provided the sediment supply is sufficiently large, this implies that the flow can be in one of two states: an erosion limited state with relatively low concentrations and a supply limited solution with relatively high concentrations. The actual state of the system depends on its history. If a system is in the low concentration, erosion limited state, it can only jump to the supply limited state if  $\langle \tilde{E} \rangle$  increases beyond the threshold value. This might result in a dramatic increase in concentration. The jump back from the supply limited to the erosion limited state only happens for  $\langle \tilde{E} \rangle$  significantly smaller than the threshold, so that there is hysteresis in the transition between the two equilibrium states.

The threshold value of  $\langle \tilde{E} \rangle$  and the hysteresis in the transition between states exist because of the effects of hindered settling. These phenomena therefore disappear if hindered settling is not taken into account, strongly altering the behaviour of the model. Hindered settling allows for a positive feedback loop that might lead to a catastrophic increase in concentration if  $\langle \tilde{E} \rangle$  exceeds the threshold. An investigation into the different formulations and parameter values parametrising hindered settling shows that this behaviour is a robust characteristic of all known formulations for hindered settling. Sediment-induced damping of turbulence is often thought to be an essential mechanism promoting a sudden transition between states of low and high sediment concentration but is found to play no essential role in the behaviour identified here. However, it is important for the vertical distribution of sediment over the water column and quantitative determination of the threshold value for  $\langle \tilde{E} \rangle$  in tidal flows.

The high suspended sediment concentrations observed in some estuaries are only possible in a supply limited state. Therefore it can be concluded that hyperturbid systems should at least satisfy the criterion  $\langle \tilde{E} \rangle > \langle \tilde{E} \rangle_{\text{crit}}$  or have satisfied this criterion at some point in the past. This observation is an important step towards the understanding of why some systems have become hyperturbid and the assessment of the risk that a particular non-hyperturbid system may become hyperturbid in the future.

### 3.A. VERTICAL COUPLING OF THE NEAR-BED CONCENTRATION IN NON-STATIONARY FLOWS

For stationary flows, the near bed concentration can be obtained simply by considering the local balance of erosion and deposition at the bed, without solving for the entire water column. In this appendix we will show that this is no longer possible in non-stationary flows. Let us assume an abundant sediment supply ( $S_{\text{bed}} = \infty$ ) and consider the sediment balance of Eq. (3.4). Dividing by  $c_{\text{gel}}$ , integrating this balance between  $z = -H$  and 0 and using the boundary conditions yields

$$\left( \int_{-H}^0 \phi dz \right)_t + w_s \phi_{\text{bed}} - \frac{\hat{E}}{c_{\text{gel}}} = 0. \quad (3.19)$$

We will assume periodic conditions for the flow and concentrations and take the time-average of the above expression. Next, substituting the expressions for the erosion (3.9) and hindered settling (3.10) and dividing by  $c_{\text{gel}}$ , yields

$$\langle (1 - \phi_{\text{bed}})^m \phi_{\text{bed}} \rangle = \left\langle \frac{M_0}{w_{s,0} c_{\text{gel}}} \max \left( 0, \frac{\tau}{\tau_c} - 1 \right) \right\rangle, \quad (3.20)$$

where  $\langle \cdot \rangle$  denotes the tidal average. Due to the non-linearity of this expression, the average concentration  $\langle \phi_{\text{bed}} \rangle$  cannot be directly inferred from the left-hand side of the equation, without knowledge on the tidally varying signal of  $\phi_{\text{bed}}$ . The tidally varying  $\phi_{\text{bed}}$  follows from Eq. (3.19), which involves an integral over the entire water column. Therefore, the full water column model is required to solve for the average near-bed concentration in non-stationary flows.

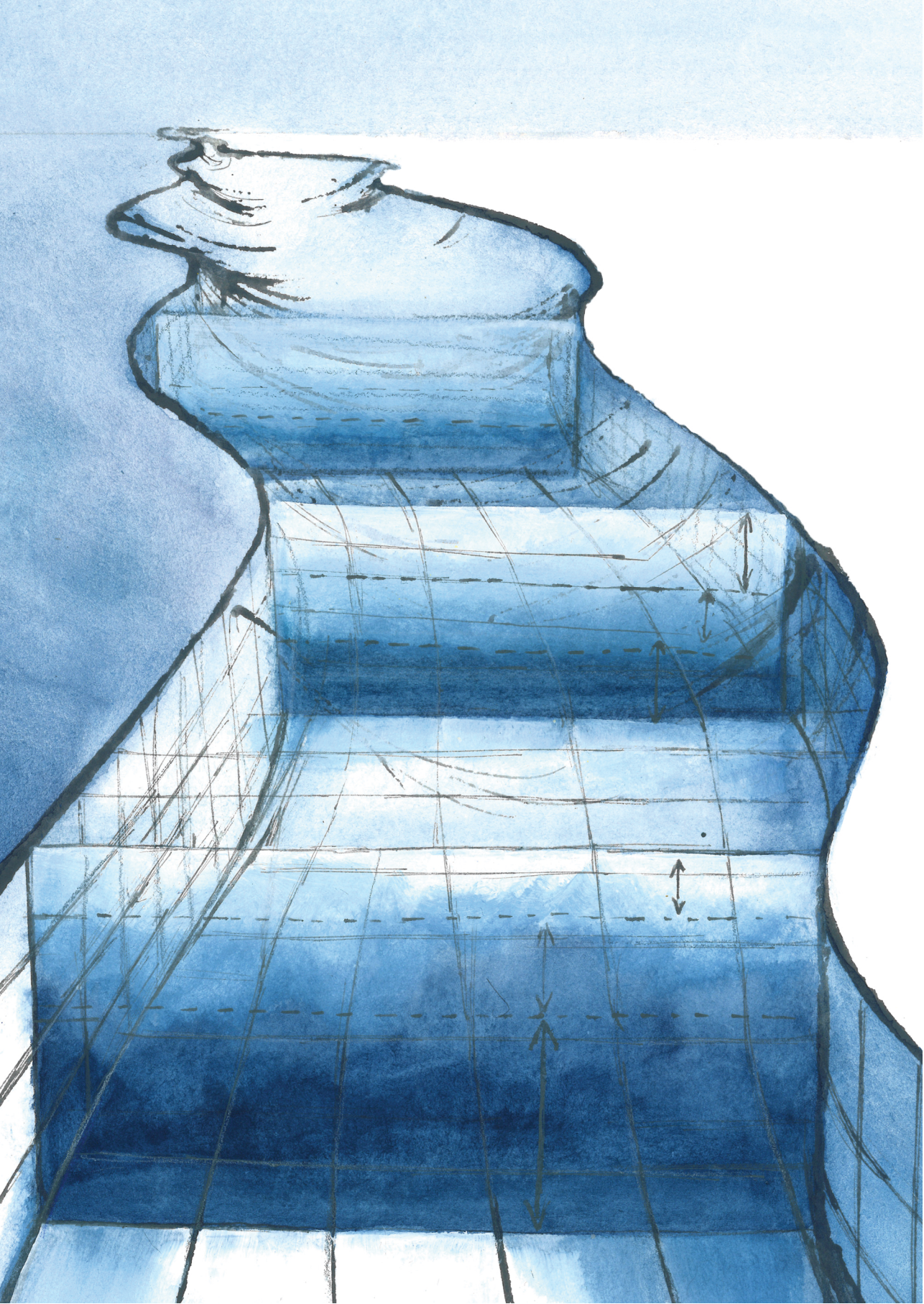
## REFERENCES

- Chernetsky, A. S., Schuttelaars, H. M., and Talke, S. A. (2010). The effect of tidal asymmetry and temporal settling lag on sediment trapping in tidal estuaries. *Ocean Dynamics*, 60:1219–1241.
- Cloern, J. E. (1987). Turbidity as a control on phytoplankton biomass and productivity in estuaries. *Continental Shelf Research*, 7:1367–1381.
- Dankers, P. J. T. and Winterwerp, J. C. (2007). Hindered settling of mud flocs: Theory and validation. *Continental Shelf Research*, 27:1893–1907.
- De Jonge, V. N., Schuttelaars, H. M., Van Beusekom, J. E. E., Talke, S. A., and De Swart, H. E. (2014). The influence of channel deepening on estuarine turbidity levels and dynamics, as exemplified by the Ems estuary. *Estuarine Coastal and Shelf Science*, 139:46–59.
- Dijkstra, Y. M., Uittenbogaard, R. E., Van Kester, J. A. T. M., and Pietrzak, J. D. (2016). Improving the numerical accuracy of the  $k - \epsilon$  model by a transformation to the  $k - \tau$  model. *Ocean Modelling*, 104:129–142.
- Gabioux, M., Vinzon, S. B., and Paiva, A. M. (2005). Tidal propagation of fluid mud layers on the Amazon shelf. *Continental Shelf Research*, 25:113–125.
- Jalón-Rojas, I., Schmidt, S., Sottolichio, A., and Bertier, C. (2016). Tracking the turbidity maximum zone in the Loire Estuary (France) based on a long-term, high-resolution and high-frequency monitoring network. *Continental Shelf Research*, 117:1–11.
- Kandiah, A. (1974). *Fundamental aspects of surface erosion of cohesive soils*. PhD thesis, University of California, Davis.
- Kineke, G. C. and Sternberg, R. W. (1995). Distribution of fluid muds on the amazon continental shelf. *Marine Geology*, 125:193–233.
- Le Hir, P., Bassoullet, P., and Jestin, H. (2001). *Coastal and Estuarine Fine Sediment Processes*, chapter Application of the continuous modeling concept to simulate high-concentration suspended sediment in a macrotidal estuary, pages 229–247. Elsevier Science.
- Le Hir, P., Monbet, Y., and Orvain, F. (2007). Sediment erodibility in sediment transport modeling: Can we account for biota effects? *Continental Shelf Research*, 27:1116–1142.

- Mehta, A. J. (2014). *An introduction to the hydraulics of fine sediment transport*. World Scientific.
- Partheniades, E. (1962). *A study of erosion and deposition of cohesive soils in salt water*. PhD thesis, Univ. of Calif., Berkely.
- Partheniades, E. (1965). Erosion and deposition of cohesive soils. *J. Hydraul. Div. Am. Soc. Civ. Eng.*, 91:105–139.
- Partheniades, E. (2010). *Cohesive Sediments in Open Channels. Properties, Transport, and Applications*. Elsevier.
- Richardson, J. F. and Zaki, W. N. (1954). Sedimentation and fluidisation: part 1. *Transactions of the Institution of Chemical Engineers*, 32:35–53.
- Sanford, L. P. and Maa, J. P.-Y. (2001). A unified erosion formulation for fine sediments. *Marine Geology*, 179:9–23.
- Schuttelaars, H. M., de Jonge, V. N., and Chernetsky, A. S. (2013). Improving the predictive power when modelling physical effects of human interventions in estuarine systems. *Ocean and Coastal Management*, 79:70–82.
- Scully, M. E. and Friedrichs, C. T. (2007). Sediment pumping by tidal asymmetry in a partially mixed estuary. *Journal of Geophysical Research*, 112(C07028).
- Talke, S. A., De Swart, H. E., and Schuttelaars, H. M. (2009). Feedback between residual circulations and sediment distribution in highly turbid estuaries: an analytical model. *Continental Shelf Research*, 29:119–135.
- Toorman, E. A. and Berlamont, J. E. (1993). Nearshore and estuarine cohesive sediment transport. In Mehta, A. J., editor, *Mathematical Modeling of cohesive sediment settling and consolidation*, pages 148–184. American Geophysical Union.
- Uncles, R. J., Stephens, J. A., and Smith, R. E. (2002). The dependence of estuarine turbidity on tidal intrusion length, tidal range and residence time. *Continental Shelf Research*, 22:1835–1856.
- Van Maren, D. S., Winterwerp, J. C., and Vroom, J. (2015). Fine sediment transport into the hyper-turbid lower Ems River: the role of channel deepening and sediment-induced drag reduction. *Ocean Dynamics*, 65:589–605.
- Van Maren, D. S., Winterwerp, J. C., Wu, B. S., and Zhou, J. J. (2009). Modelling hyperconcentrated flow in the Yellow River. *Earth Surface Processes and Landforms*, 34:596–612.
- Winterwerp, J. C. (2001). Stratification effects by cohesive and noncohesive sediment. *Journal of Geophysical Research: Oceans*, 106:22559–22574.
- Winterwerp, J. C. and Van Kesteren, W. G. M. (2004). *Introduction to the Physics of Cohesive Sediment Dynamics in the Marine Environment*. Developments in sedimentology, 56. Elsevier.
- Winterwerp, J. C., Van Kesteren, W. G. M., Van Prooijen, B. C., and Jacobs, W. (2012). A conceptual framework for shear flow-induced erosion of soft cohesive sediment beds. *Journal of Geophysical Research: Oceans*, 117:C10020.
- Winterwerp, J. C. and Wang, Z. B. (2013). Man-induced regime shifts in small estuaries - I: theory. *Ocean Dynamics*, 63:1279–1292.
- Winterwerp, J. C., Wang, Z. B., Van Brackel, A., Van Holland, G., and Kösters, F. (2013). Man-induced regime shifts in small estuaries - II: a comparison of rivers. *Ocean Dynamics*, 63:1293–1306.



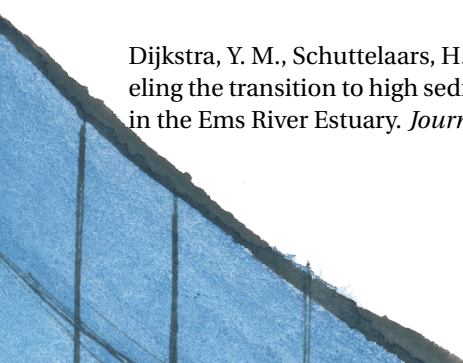






# CHAPTER 4

Modelling the transition to high sediment concentrations as a response to channel deepening in the Ems River Estuary



Dijkstra, Y. M., Schuttelaars, H. M., Schramkowski, G. P., and Brouwer, R. L. (2019). Modeling the transition to high sediment concentrations as a response to channel deepening in the Ems River Estuary. *Journal of Geophysical Research: Oceans*, 124:1-17.

## Abstract

---

Many estuaries are strongly modified by human interventions, including substantive channel deepening. In the Ems River Estuary (Germany, Netherlands), channel deepening between the 1960s and early 2000s coincided with an increase in the maximum near-bed suspended sediment concentration from moderate ( $\sim 1 \text{ kg/m}^3$ ) to high ( $> 10 \text{ g/m}^3$ ). In this study the observed transition in the suspended sediment concentration in the Ems is qualitatively reproduced by using an idealized width-averaged iFlow model. The model is used to reproduce observations from 1965 and 2005 by only changing the channel depth between the years. Model results show an increase in sediment concentrations from approximately  $1\text{--}2 \text{ kg/m}^3$  to  $20\text{--}30 \text{ kg/m}^3$  near the bed between 1965 and 2005 if the river discharge is below  $70 \text{ m}^3/\text{s}$ , which holds approximately 60% of the time. Thereby, this study for the first time provides strong evidence for earlier published hypotheses that channel deepening was the main driver of the increased sediment concentrations in the Ems.

The results are explained using two aspects: sediment transport (longitudinal processes) and local resuspension (vertical processes). The magnitude of the sediment import increased, because a combination of channel deepening and sediment-induced damping of turbulence increased the  $M_2$ - $M_4$  tidal asymmetry. This effect is particularly strong, because the  $M_4$  tide evolved to a state close to resonance. All imported sediment is kept in suspension when it is assumed that resuspension is sufficiently efficient, which depends on the value of the erosion parameter used and inclusion of hindered settling in the model.

---



## 4.1. INTRODUCTION

Estuaries are known to be efficient sediment traps, with sediment concentrated in one or more estuarine turbidity maxima (ETM). The maximum sediment concentrations in such ETM typically range between 0.1 and over 10 kg/m<sup>3</sup> and may be several times to orders of magnitude higher than in the surrounding waters. Several examples exist of estuaries that underwent a strong increase in the sediment concentration in their ETM, including the Ems (Germany, Netherlands) and Loire (France) Rivers (Winterwerp et al., 2013). Such a transition has severe consequences for the ecological functioning of the estuary, as high suspended sediment concentrations are associated with a strong reduction in oxygen levels (e.g. Uncles et al., 1998; Talke et al., 2009a) and primary production (Cloern, 1987). The increased sediment concentration in both the Ems and Loire Rivers is hypothesised to be due to man-made changes to the estuary in the last several decades, most notably deepening of the shipping channel (Winterwerp and Wang, 2013). Considering the large-scale deepening projects in many estuaries around the world, it is important to understand the effect of channel deepening on the sediment concentration in the Ems and Loire, to assess if a similar large increase in sediment concentration can happen in other estuaries as well.

In this study we focus on the Ems River Estuary, see Fig. 4.1. In the 1950s, the ETM in the Ems River was located approximately between Pogum and Terborg (km 15-25), with typical concentrations at the surface estimated around 0.1-0.2 kg/m<sup>3</sup> (De Jonge et al., 2014) and at the bed around 0.5-2 kg/m<sup>3</sup> (Dechend, 1950). After dredging operations that occurred between 1960 and 1994, the ETM had moved upstream and had become a wide turbidity zone between approximately Pogum/Terborg (km 15-25) and the tidal weir at Hebrum (km 64). Typical sediment concentrations in this ETM are 1-4 kg/m<sup>3</sup> at the surface (De Jonge et al., 2014) and 10-100 kg/m<sup>3</sup> near the bed (Talke et al., 2009b; Wang, 2010; Papenmeier et al., 2013; Becker et al., 2018).

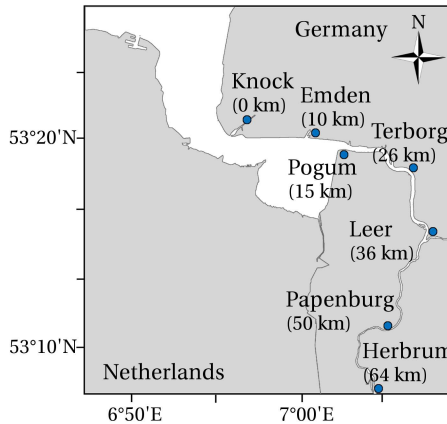


**Figure 4.1:** The Ems River Estuary, located in Northern Germany and Netherlands discharging into the Wadden Sea-North Sea. Our model domain is from Knock to the tidal weir at Hebrum, 64 km from Knock.

Several modelling studies have focussed on this transition in the sediment concentration in the Ems. All studies to date have done so by calibrating their model separately for conditions before and after the transition. Using various models ranging from highly idealised to complex, it was found that a lower roughness is required to calibrate to conditions after the transition to high sediment concentrations (Chernetsky et al., 2010; Winterwerp et al., 2013; Van Maren et al., 2015). Using an idealised model and simultaneously deepening the channel and lowering the roughness, Chernetsky et al. (2010) and De Jonge et al. (2014) qualitatively reproduced the upstream shift in the ETM position. However, as their model assumed a prescribed amount of sediment in the estuary, they could not draw conclusions about the increase of the sediment concentration. Using a numerical three-dimensional model calibrated to recent conditions (year 2005), Weilbeer (2007) and Van Maren et al. (2015) obtained concentrations up to  $10 \text{ kg/m}^3$  near the bed in the ETM, thereby demonstrating that it is possible to find high sediment concentrations in the model under suitable hydrodynamic conditions. However, in order to dynamically model the actual transition, the reduced roughness and increase in concentration should not follow from recalibration but have to be resolved by the model itself. It is thought that the reduced roughness is caused by damping of turbulence and bed friction by the high sediment concentrations (Winterwerp and Wang, 2013). Winterwerp and Wang (2013) and Van Maren et al. (2015) go one step further and hypothesise about the existence of a positive feedback loop, where a high sediment concentration leads to a reduction of the hydraulic roughness, which in turn leads to the import of more sediment. However, no study to date has shown that deepening of the estuary indeed leads to a highly increased import and trapping of sediment, nor has it been shown that this imported sediment is indeed able to reduce the hydraulic roughness to the extent necessary to match observations.

The goal of this study is to show whether channel deepening alone can be responsible for the transition from low to high sediment concentrations in the Ems and what physical mechanisms underlie this transition. This is done by extending and using the idealised width-averaged process-based iFlow model (Chapter 2). Focus of the study is on the qualitative characteristics of the dynamic equilibrium state of the sediment concentration estuary for conditions of 1965 and 2005 (i.e. before and after the deepening operations) and the physical processes essential to establish this state. The model is calibrated only to conditions before deepening, and the model results after deepening are systematically analysed for different parameters to verify the robustness of the results.

A short description of the iFlow model and the extensions is given in Section 4.2. Section 4.3 presents the data used to set-up the model. The results of the 1965 and 2005 cases for default parameter settings are presented in Section 4.4 and further analysed in Section 4.5. The sensitivity of the results to several model parameters is discussed in Section 4.6. Finally, the conclusions are summarised in Section 4.7.

## 4.2. MODEL

The framework used for this study is an extended version of the *iFlow* model described in Chapter 2. iFlow is a width-averaged idealized model that solves for the continuity and momentum equations for the water motion and the mass balance equation for sediment. Several assumptions are made to speed up the model and allow for detailed

analysis of the most important processes in the equations. First, it is assumed that the estuarine geometry can be parametrised by smoothed width and depth profiles, ignoring bathymetric variations on length scales much smaller than the length of the estuary. Second, it is assumed that the water surface elevation is small compared to the mean depth. This allows the use of scaling and perturbation methods, which leads to systems of mathematical equations that can be solved at low computational costs. Furthermore, it allows for making a decomposition of the water motion and sediment transport into contributions by individual physical forcing mechanisms. Third, the model resolves only the subtidal,  $M_2$  and  $M_4$  contributions to the water motion and sediment dynamics, imposing an  $M_2$  tide and an  $M_4$  tide at the mouth and a constant river discharge at the head of the estuary. The subtidal and tidal contributions are computed for a dynamic equilibrium. This means that the water motion and sediment concentration are allowed to vary on a tidal timescale but not on a subtidal timescale. Considering dynamic equilibrium prevents spin-up time, hence strongly reducing the computation time compared to models based on time stepping routines. Below, we discuss the elements of the model that are changed or added to the version presented in Chapter 2 in more detail.

The first change to the iFlow model is the parametrisation of the erosion rate  $E$ , which here represents erosion of a soft nonconsolidated layer of fine sediments on top of a nonerodible layer. The erosion rate is written as the product of the potential erosion  $\hat{E}$  and the erodibility  $f$  (Chapter 3 and Brouwer et al. (2018)), that is,

$$E = \hat{E} f. \quad (4.1)$$

The potential erosion  $\hat{E}$  is the erosion rate assuming an abundant availability of sediment. The potential erosion is parametrised using the formulation of Partheniades (Kandiah, 1974) but assuming a negligible critical shear stress

$$\hat{E} = M |\tau_b|. \quad (4.2)$$

The parameter  $M$  is an erosion parameter, and  $\tau_b$  represents the bed shear stress. The erodibility  $f$  takes values between 0 and 1 to account for the amount of sediment on the bed. If no easily erodible sediment is available at the bed at any time during the tidal cycle,  $f = 0$  and consequently the erosion is zero. If easily erodible sediment is available at the bed during the entire tidal cycle,  $f$  equals one and  $E = \hat{E}$ . If easily erodible sediment is available at the bed only during a part of the tidal cycle,  $f$  takes a value between 0 and 1 (see Brouwer et al., 2018, for an elaborate discussion and derivation of the erodibility).

As a second extension to the model, the sediment settling velocity is allowed to vary along the channel due to the effects of hindered settling (Richardson and Zaki, 1954). Here we use a parametrisation of hindered settling in which the settling velocity in each water column is based on the subtidal near-bed sediment concentration, according to

$$w_s = w_{s,0} \left\langle 1 - \frac{c_{\text{bed}}}{c_{\text{gel}}} \right\rangle^5. \quad (4.3)$$

Hence,  $w_s$  does not vary on the tidal timescale and is depth uniform. For concentrations much lower than the gelling concentration  $c_{\text{gel}}$ ,  $w_s$  equals the prescribed clear-water settling velocity  $w_{s,0}$ .

The third and final extension to the model is a dependency between the eddy viscosity, eddy diffusivity, and bed friction parameter and the sediment concentration, parametris- ing the effects of sediment-induced turbulence damping. The eddy viscosity and eddy diffusivity are assumed to be constant over a tidal cycle and are depth uniform. They are parametrised as functions of the depth-averaged velocity  $U(x, t)$ , the depth (consisting of the bed level  $H$ , reference surface level  $R$  and surface elevation  $\zeta$ ), and the depth- averaged gradient Richardson number  $Ri(x, t)$ :

$$A_v = \left\langle c_{v,1}(z_0^*) U(H + R + \zeta) F(\overline{Ri}) \right\rangle, \quad (4.4)$$

$$K_v = \left\langle \frac{c_{v,1}(z_0^*)}{\sigma_\rho} U(H + R + \zeta) G(\overline{Ri}) \right\rangle. \quad (4.5)$$

The coefficient  $c_{v,1}$  is a drag coefficient that depends on a dimensionless roughness height  $z_0^* = \frac{z_0}{H}$  (see Chapter 2) and  $\sigma_\rho$  is the Prandtl-Schmidt number, which is set to 1 by default. The functions  $F$  and  $G$  are based on the damping functions suggested by Munk and Anderson (1948), using the depth-averaged Richardson number  $\overline{Ri}$  instead of the bulk Richardson number. The damping functions read

$$F(\overline{Ri}) = \left(1 + 10\overline{Ri}\right)^{-1/2}, \quad (4.6)$$

$$G(\overline{Ri}) = \left(1 + 3.33\overline{Ri}\right)^{-3/2}, \quad (4.7)$$

with the gradient Richardson number is defined as

$$Ri = -\frac{g\beta_c}{\rho_0} \frac{c_z}{u_z^2 + u_{z,\min}^2}.$$

Here  $\beta_c = 1 - \rho_0/\rho_s$  is the conversion factor from sediment concentration to density, where  $\rho_0$  is the clear-water density (assumed equal to  $1000 \text{ kg/m}^3$ ) and  $\rho_s$  is the dry sed- iment density (assumed equal to  $2650 \text{ kg/m}^3$ ). The variable  $u_z$  is the vertical gradient of the along-channel velocity and  $u_{z,\min}$  represents a background shear to parametrise flows that are not accounted for (e.g. lateral flows, wind-driven flow and small-scale cir- culations), nonlocal turbulence production and inertia in turbulence dissipation. Prac- tically, it prevents the Richardson number from becoming unrealistically large.

The bed shear stress used to compute the friction felt by the water motion,  $\tau_{b,w}$ , is parametrised using an expression that captures the qualitative effect of a quadratic fric- tion law

$$\tau_{b,w} = s_f u_{\text{bed}}, \quad (4.8)$$

where  $u_{\text{bed}}$  is the velocity near the bed and  $s_f$  is a partial slip parameter that depends on the depth-averaged velocity  $U$ , defined as (see also Chapter 2)

$$s_f = \left\langle c_{v,2}(z_0^*) c_D U \right\rangle. \quad (4.9)$$

The function  $c_{v,2}$  is a drag coefficient that depends on  $z_0^*$  and  $c_D$  is a reduced-drag coeffi- cient, which accounts for the deformation of the logarithmic boundary layer due to sedi- ment stratification. As the model does not resolve the bottom-most part of this boundary

layer, the deformation of this boundary layer needs to be accounted for in the bed friction parametrisation. This is done through a reduced-drag coefficient following studies by Adams and Weatherly (1981), Friedrichs et al. (2000) and Wang (2002). This reduced drag coefficient is expressed as

$$c_D = (1 + A \langle Rf_{bed} \rangle)^{-2}, \quad (4.10)$$

with the parameter  $A$  empirically determined by the aforementioned studies and set to 5.5. The parameter  $Rf_{bed}$  is the flux Richardson number near the bed, which reads

$$Rf_{bed} = \frac{K_v}{A_v} Ri_{bed}.$$

To avoid a drag reduction that is much stronger than has been observed in laboratory studies, the value of  $Rf_{bed}$  is limited to a maximum value  $Rf_{max} = 2$ . A flux Richardson number of 2 may still seem large compared to the often mentioned critical value around 0.25. However, the Richardson number must be interpreted differently in this model, as our turbulence model does not produce a sudden strong reduction of turbulent mixing at Richardson numbers near its theoretical critical value. As a result the model allows for much larger Richardson numbers.

Whereas the bed shear stress for the water motion parametrises the friction generated in the lowest part of the bottom boundary layer, the bed shear stress that generated sediment erosion  $\tau_b$  strictly applies to the water-bed interface. Therefore, near-bed stratification should not be accounted for in the bottom boundary condition for sediment. Therefore  $\tau_b$ , used in the erosion formulation (4.2), is parametrised as

$$\tau_b = s_s u_{bed}, \quad (4.11)$$

where  $s_s$  is equal to  $s_f$  with  $c_D = 1$ .

The use of a depth-averaged and tide-averaged eddy viscosity, eddy diffusivity and settling velocity, combined with the iFlow solution procedure (see Chapter 2), allows for semianalytical solutions to the hydrodynamic and sediment concentration equations. The solution procedure is summarised in the flow diagram of Fig. 4.2. Given the turbulence and drag parameters, the vertical profiles of the velocity are computed analytically. They still depend on the water levels, which are computed numerically. The water motion is used as input to the sediment dynamics, where the vertical variation of the sediment concentration is computed analytically and depends on the erodibility  $f$ . The erodibility is computed analytically if  $f < 1$  everywhere and numerically otherwise. Using the sediment concentrations, new values for the settling velocity (Eq. (4.3)), turbulence and drag parameters (Eqs. (4.4)-(4.5), (4.9)) are obtained. This is iterated until the settling velocity and turbulence parameters have a relative change per iteration of less than  $10^{-4}$ . For the numerical computation of the water level and erodibility, a second-order finite differences method is used on an equidistant grid containing 250 grid cells.

### 4.3. THE EMS IN 1965 AND 2005

The Ems River Estuary consists of the lower Ems estuary on the Dutch-German border, the shallow Dollard Bay, the upper Ems estuary and tidal river in Germany. Following



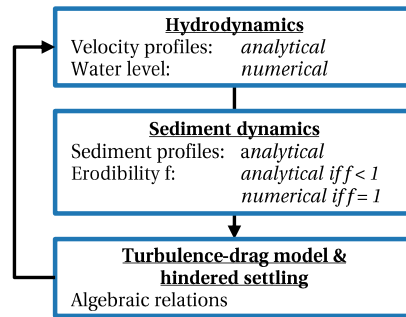


**Figure 4.2:** Summary of the model components (boxes) and the solution methods (in *italics*), indicating the iteration over the components by arrows.

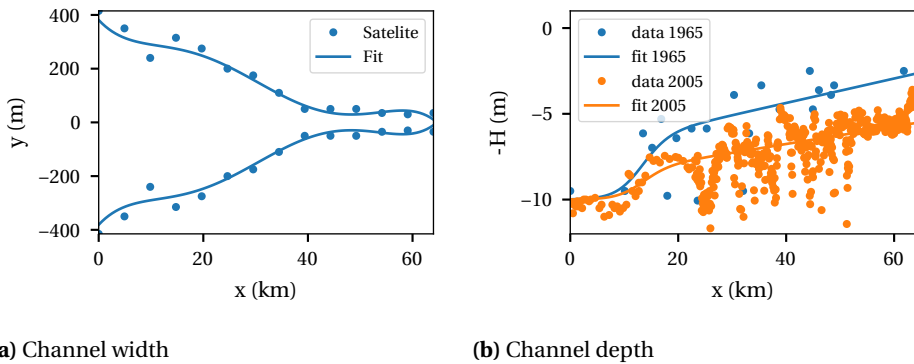


**Figure 4.3:** a) Channel width estimated from satellite images and a smooth fit used in the model. b) Measured channel depth in 1965 (Janssen, 1968) and 2005 (WSA Emden, see also De Jonge et al. (2014)) with smooth fits used in the model.

earlier studies by Chernetsky et al. (2010) and Van Maren et al. (2015), we focus on the upper estuary and tidal river, see Fig. 4.1. This part of the river stretches from Knock to a tidal weir at Herbrum and has a total length of 64 km.

The width of the estuary is estimated from satellite images and is fitted by a smooth polynomial curve, see Fig. 4.3a. Shallow areas and the Dollard bay have been ignored. It is assumed that the width is the same between 1965 and 2005, because most of the narrowing works and land reclamations were done before 1965. The depth of the channel in 1965 is derived from Janssen (1968), see also De Jonge et al. (2014). Channel depth data for 2005 were obtained from WSA Emden and were presented earlier by De Jonge et al. (2014). Both sets of depth measurements and smooth curve fits for use in the model are plotted in Fig. 4.3b. The smooth fits average over the large-scale dunes with typical amplitudes of 2-3 m and lengths of 5-10 km. Hence, the model does not resolve their effect on the dynamics of the water and sediment.

	Parameter		1965	2005
Hydrodynamics	$A^0$	$M_2$ water level amplitude at x=0	1.34 m	1.40 m
	$A^1$	$M_4$ water level amplitude at x=0	0.18 m	0.21 m
	$\phi^0$	$M_2$ water level phase at x=0	0	0
	$\phi^1$	$M_4$ water level phase at x=0	-178 deg	-171 deg
	$Q$	River discharge	30-150 m <sup>3</sup> /s	
Salinity	$s_{\text{sea}}$	Seaward salinity	30 psu	
	$x_c$	Translation (depends on Q)	4.9 to -4.2 km	
	$x_l$	Salt intrusion length scale (depends on Q)	13.5 to 10.4 km	
Sediment	$c_{\text{sea}}$	depth-averaged subtidal concentration at x=0	0.1 kg/m <sup>3</sup>	
	$K_h$	Horizontal eddy diffusivity	100 m <sup>2</sup> /s	
	$M$	Erosion parameter	0.02 s/m	
	$w_{s,0}$	Clear-water settling velocity	1 mm/s	
	$c_{\text{gel}}$	Gelling concentration	100 kg/m <sup>3</sup>	
Turbulence	$\sigma_\rho$	Prandtl-Schmidt number (= $A_v/K_v$ for $Ri = 0$ )	1	
	$u_{z,\text{min}}$	Velocity gradient for background turbulence production	0.03 1/s	

**Table 4.1:** Default model parameters for the Ems in 1965 and 2005.

Observed water levels are used to determine the tidal forcing at the seaward boundary in the model, to calibrate the 1965 model and to validate the results of the 2005 model. For 1965, the observed water level amplitude is derived from tidal curves for a mean tide drawn in a report of the German Federal Waterways Engineering and Research Institute (BAW, 1967). The  $M_2$  and  $M_4$  tidal amplitudes and relative phases are derived from this by a spectral analysis, but the tidal phase difference between the stations could not be derived. The 2005 data set is available from the Lower Saxony state department for water management, coastal and nature conservation (NLWKN) as a high-resolution time series of almost the entire year. The year-averaged  $M_2$  and  $M_4$  tidal amplitude and phase are derived using complex demodulation (e.g. Jalón-Rojas et al., 2016), thereby averaging over the spring-neap cycle and seasonal variations. From the observations we derive the model forcing at the seaward boundary, see Table 4.1.

The river discharge of the Ems River is measured at Versen, a station approximately 40 km upstream from the weir at Herbrum. Taking the average of daily discharge measurements between 1987 and 2006, we find a year-averaged discharge of 80 m<sup>3</sup>/s, a summer-averaged (Jul-Sep) discharge of 40 m<sup>3</sup>/s and a winter-averaged (Jan-Mar) discharge of 150 m<sup>3</sup>/s. It is assumed that the average discharge remained the same between 1965 and 2005. At Leer (km 36), the river Leda enters the Ems. This river has a small but significant discharge, which is neglected in this study.

Following Talke et al. (2009a) we assume that the salinity is well-mixed and may be de-

scribed diagnostically by a hyperbolic tangent profile. The length of the salt intrusion and salinity at the mouth depend on the discharge (see Table 1 in Talke et al. (2009a)). The salinity profile reads

$$s = \frac{s_{\text{sea}}}{2} \left( 1 - \tanh \left( \frac{x - x_c}{x_L} \right) \right), \quad (4.12)$$

where  $s_{\text{sea}} = 30$  psu. For year-averaged conditions,  $x_c = -3.5$  km and  $x_L = 11.5$  km.

We prescribe a depth-averaged subtidal suspended sediment concentration of  $0.1 \text{ kg/m}^3$  at the seaward boundary (Talke et al., 2009b) and assume that this has not changed between 1965 and 2005. This seems a conservative estimate, as the concentration has likely increased in the lower Ems Estuary after 1965 (De Jonge et al., 2014). We choose a horizontal eddy diffusivity  $K_h = 100 \text{ m}^2/\text{s}$  and have verified that the model results are insensitive to the exact value of this parameter. For the gelling concentration we choose a default value of  $100 \text{ kg/m}^3$ . For the settling velocity, erosion parameter, Prandtl-Schmidt number and background turbulence production  $u_{z,\min}$  we choose default values given in Table 4.1. The effect of varying these parameter values is demonstrated in Section 4.6. The default setting for the settling velocity  $w_{s,0} = 1 \text{ mm/s}$  and the erosion parameter  $M = 0.02 \text{ s/m}$  correspond to those used by Van Maren et al. (2015), where our  $M$  corresponds to their  $M/\tau_c$ . The default parameter settings are summarised in Table 4.1.

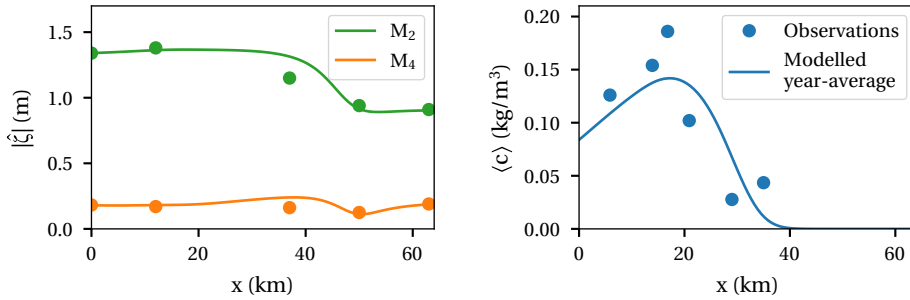
## 4.4. MODEL CALIBRATION AND RESULTS

### 4.4.1. MODEL CALIBRATION

The 1965 model with the default parameter settings (Table 4.1) and year-averaged discharge ( $Q = 80 \text{ m}^3/\text{s}$ ) is calibrated against the  $M_2$  water level amplitude measurements, resulting in an optimal value of the dimensionless roughness height of  $z_0^* = 0.0093$ . The resulting water level amplitudes of the two main tidal constituents are plotted in Figure 4.4a. As the 1965 modelled  $M_2$  water level is calibrated to the measurements, it is to be expected that this yields good correspondence. Also the  $M_4$  tide in 1965 corresponds well to the measurements, giving confidence that the most important hydrodynamic processes are captured.

Little data are available for calibrating the sediment concentrations in 1965. Therefore, parameter values in the sediment model ( $w_{s,0}$ ,  $c_{\text{sea}}$  and  $M$ ) are not calibrated to best fit the measurements but are based on previous studies. As an indication of the fit between model and observations, we have used data from 1954 presented by De Jonge et al. (2014), which are supposed to represent yearly mean surface concentrations, but the exact conditions under which they were obtained are unknown. The data show an ETM around km 20 with maximum surface sediment concentrations around  $0.2 \text{ kg/m}^3$  (see Fig. 4.4b). The model results show a similar location of the ETM and magnitude of the surface concentration compared to the observations.

The parameter values are fixed for all discharge values and used for both the 1965 and 2005 cases. The model is thus *not* recalibrated for the 2005 case. The 2005 case therefore only differs from the 1965 case by the level of the bed and some minor changes to the  $M_2$  and  $M_4$  tidal amplitude and phase at the mouth to make it easier to compare to measurements. It has been verified that the changes to the forcing at the mouth have a



(a) Water level amplitude for 1965 for the two main tidal constituents  $M_2$  and  $M_4$  during year-average discharge conditions ( $Q = 80 \text{ m}^3/\text{s}$ ). The lines represent model results. The dots are reported observed water levels under average conditions (BAW, 1967).

(b) Subtidal surface sediment concentration in 1965 from the model (blue line) for equilibrium conditions corresponding to year-averaged conditions. The model results are compared to the year average of observations from 1954 presented by De Jonge et al. (2014). Note that the number of observations in 1954 is very limited.

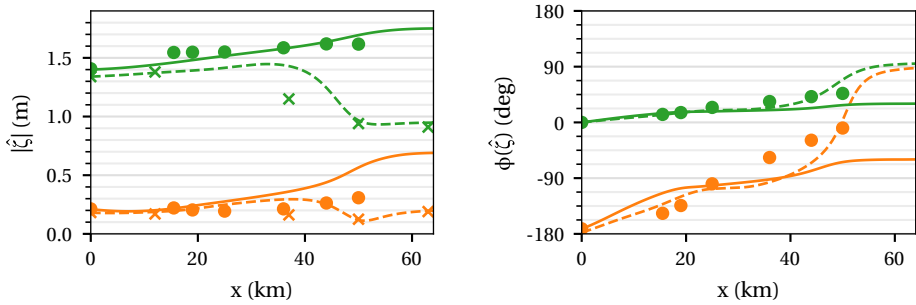
**Figure 4.4:** Water levels and sediment concentrations from the model results (lines) and observations (dots) for the calibration of the 1965 case for year-averaged discharge conditions.

negligible influence on the results. Below we discuss the results of both cases for various discharge conditions.

#### 4.4.2. RESULTS FOR A LOW RIVER DISCHARGE

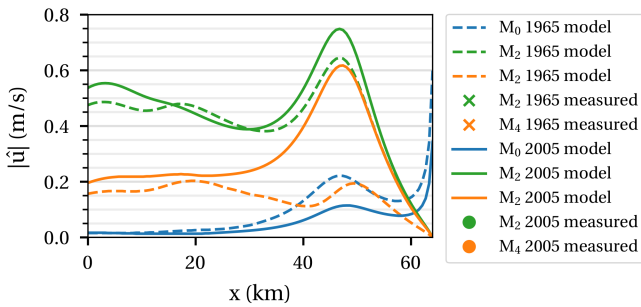
First, focussing on the the average summer river discharge of  $Q = 40 \text{ m}^3/\text{s}$ , the water level amplitude and phase for both 1965 and 2005 are plotted in Figs. 4.5a-4.5b. The water level for the 1965 case is almost the same as in Fig. 4.4a for the year-averaged river discharge. This is because the river-induced velocity is much smaller than the tidal velocity and the sediment concentration has little influence on the damping of turbulence in this case. The 2005  $M_2$  water level shows strong amplification compared to 1965 and the tidal wave travels faster through the estuary (i.e. smaller phase difference between the mouth and the weir). This observation is consistent with earlier modelling studies by, e.g., Chernetsky et al. (2010) and Winterwerp et al. (2013). However, the amplification and the wave celerity of the  $M_2$  tide seem to be slightly overestimated. Observations indicate that the  $M_4$  water level amplitude has amplified as well and that the  $M_4$  tidal wave travels faster through the estuary. This is reproduced but overestimated by the model.

Concerning the flow velocity (Fig. 4.5c), the cross-sectionally averaged  $M_2$  flow velocity has only increased by at most 20% between 1965 and 2005. The  $M_4$  flow velocity on the other hand has increased by more than 100% between 1965 and 2005 in the area between 40 and 60 km. Additionally, the subtidal (i.e.  $M_0$ ) velocity has decreased in this area by up to 40%.

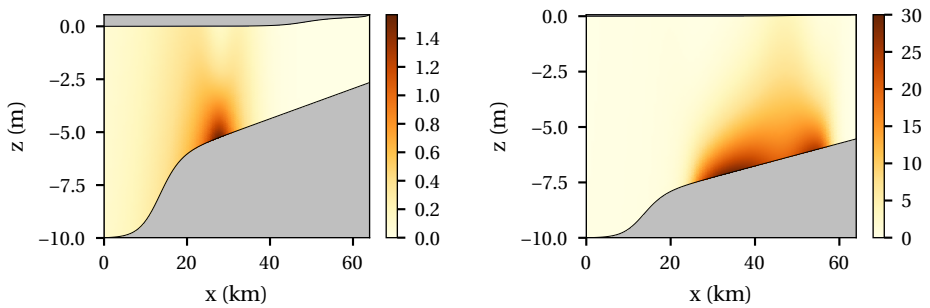


(a) Water level amplitude

(b) Water level phase



(c) Depth-averaged width-averaged along-channel flow velocity amplitude



(d) Sediment concentration 1965 ( $\text{kg/m}^3$ )

(e) Sediment concentration 2005 ( $\text{kg/m}^3$ )

**Figure 4.5:** Model results for the 1965 and 2005 cases with summer average discharge,  $Q = 40 \text{ m}^3/\text{s}$ .

Fig. 4.5d shows the modelled subtidal sediment concentration in 1965. It shows that the ETM is located around km 25 in 1965, with concentrations of up to  $1.5 \text{ kg/m}^3$  near the bed and concentrations under  $0.3 \text{ kg/m}^3$  at the surface. The relatively large difference between bottom and surface concentrations is related to sediment-induced turbulence

damping in the ETM, which keeps the sediment confined to the bed. As the ETM remains narrow, this damping of turbulence acts locally and thus has a negligible effect on the water motion. The order of magnitude of the near-bed concentration of  $1.5 \text{ kg/m}^3$  seems realistic in comparison to observations of  $1\text{--}2 \text{ kg/m}^3$  near the bed between Emden (km 10) and Terborg (km 26) in 1949 reported by Dechend (1950).

In the 2005 case (Fig. 4.5e), the ETM became wide, covering an area between km 25 and 60. Near-bed concentrations increased up to  $30 \text{ kg/m}^3$ . Concentrations at the surface range from 1 to  $4 \text{ kg/m}^3$  between km 35 and 60. These results capture the qualitative characteristics of the observed ETM; observations made by Talke et al. (2009b) during one cruise in 2006 show sediment concentrations near the bed of  $10\text{--}30 \text{ kg/m}^3$  and near the surface of approximately  $1 \text{ kg/m}^3$  in the entire zone between km 35 and 60. Similar or higher near-bed concentrations and fluid mud have been observed by Wang (2010), Papenmeier et al. (2013), Winterwerp et al. (2017) and Becker et al. (2018). De Jonge et al. (2014) reports observed surface concentrations locally exceeding  $3 \text{ kg/m}^3$ .

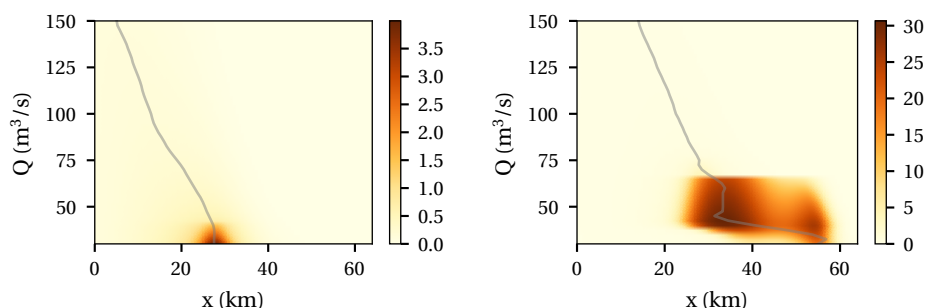
Comparing the modelled concentrations between 1965 and 2005, the maximum near-bed concentration in the domain has gone up by a factor of 20, while the maximum near-surface concentration has increased by a factor of 14. The amount of sediment suspended in the estuary, in the model, has increased by a factor of 8 from approximately 40 to 300 thousand metric tons.

#### 4.4.3. SENSITIVITY TO THE RIVER DISCHARGE

The sensitivity of the model results to the river discharge is investigated by varying the discharge between  $30$  and  $150 \text{ m}^3/\text{s}$ . In each experiment, the discharge is assumed to be constant and the resulting water motion and sediment concentration are in dynamic equilibrium. Fig. 4.6 shows the resulting near-bed suspended sediment concentration as a function of the along-channel distance (horizontal axis) and the river discharge (vertical axis). The grey line in the figures indicates the location of the maximum near-bed concentration in the ETM.

In 1965 the ETM is narrow and located around km 25–30 for discharges below  $60 \text{ m}^3/\text{s}$ . At these low discharges, near-bed concentrations of several  $\text{kg/m}^3$  occur, which correspond to surface concentrations around  $0.2\text{--}0.4 \text{ kg/m}^3$ . For discharges below  $30 \text{ m}^3/\text{s}$ , concentrations are locally up to  $4 \text{ kg/m}^3$  near the bed. It is unlikely that such conditions were ever attained, as such discharges only occurred for 10% of the time. For discharges exceeding  $70 \text{ m}^3/\text{s}$ , the ETM moves downstream and the maximum near-bed concentration rapidly decreases below  $1 \text{ kg/m}^3$ . The  $M_2$  and  $M_4$  water level elevation (not shown) is almost independent of the river discharge.

In 2005 we find a wide ETM with high concentrations exceeding  $30 \text{ kg/m}^3$  for discharges between  $35$  and  $70 \text{ m}^3/\text{s}$ . For lower discharges, we also find high concentrations but more concentrated at the landward side of the estuary. Conditions with discharges below  $70 \text{ m}^3/\text{s}$  occur approximately 60% of the time with uninterrupted periods of several months each year, making it is probable that such concentrations could indeed be attained. For discharges above  $70 \text{ m}^3/\text{s}$  (approximately 40% of the time) the high concentrations disappear and only a narrow ETM with much lower concentrations remains.



(a) Subtidal near-bed concentration in 1965 (b) Subtidal near-bed concentration in 2005  
(kg/m<sup>3</sup>) (kg/m<sup>3</sup>)

**Figure 4.6:** Near-bed modelled sediment concentration along the channel (horizontal axis) for a various long-term constant discharge values (vertical axis) for the 1965 and 2005 cases. The grey line indicates the location of the ETM.

For these high discharges, concentrations are only marginally higher than for the same discharge conditions in 1965. Additionally, the tidal amplification is much less than in Fig. 4.5a. Although observations of sediment concentrations show a marked decrease of the suspended sediment concentration at high river discharge (Winterwerp et al., 2017), the modelled concentrations are much lower than observed. The modelled reduction in tidal amplification is not observed. The model therefore does not seem to capture the observed characteristics of the water motion and sediment dynamics at  $Q > 70 \text{ m}^3/\text{s}$ .

The results show that the transition from a narrow ETM with relatively low concentrations in 1965 to a wide ETM with much higher concentrations in 2005 may be reproduced by only increasing the channel depth for long-term discharges below  $70 \text{ m}^3/\text{s}$ . The model does not reproduce the transition if the discharge is higher, see Section 4.7 for a more detailed discussion of this.

#### 4.5. ANALYSIS OF THE RESULTS

We will look closer at the physical processes that allow for the transition from moderate concentrations in 1965 to high concentrations in a wide ETM in 2005 for discharges below  $70 \text{ m}^3/\text{s}$ . We consider two aspects:

1. *Sediment trapping (along-channel processes)*. The amount of sediment that can be contained within the estuary by the flow and sediment dynamics.
2. *Local resuspension (vertical processes)*. The amount of sediment that can potentially be brought into suspension given the erosion properties of the bed and the strength of the flow.

These aspects are discussed separately in Sections 4.5.1 and 4.5.2.



#### 4.5.1. SEDIMENT TRAPPING

In order to analyse the processes resulting in sediment trapping, we will look at the various contributions to the suspended sediment transport. The suspended sediment transport  $\mathcal{T}$  is written as the sum of the advective and diffusive transport integrated over the cross-section, i.e.

$$\mathcal{T} = \left\langle B \int_{-H}^{R+\zeta} uc - K_h c_x dz \right\rangle, \quad (4.13)$$

where  $B$  is the width,  $u$  is the along-channel velocity,  $c$  is the sediment concentration,  $c_x$  is the along-channel sediment concentration gradient and  $K_h$  is the prescribed horizontal eddy diffusivity (see Table 4.1). Between 1965 and 2005, the flow velocity, sediment concentration and location of the ETM have changed (e.g. see Fig. 4.5). Hence, there are so many differences in the sediment transport in 1965 and 2005 that a comparison of the sediment transport processes between the years does not give much insight.

To overcome this problem we look at the *the transport capacity*: the sediment transport  $\mathcal{T}$  that would occur if there were an abundance of sediment on the bed everywhere in the estuary (i.e.  $f = 1$  everywhere) given the modelled hydrodynamic conditions (flow velocity and turbulence field) and sediment parameters (effective settling velocity and erosion parameter). A formal mathematical definition is given in Appendix 4.A. The transport capacity shows the tide-averaged initial redistribution of a uniform layer of sediment on the bed. Unlike the total sediment transport, the transport capacity depends mainly on the hydrodynamic conditions and sediment parameters and only indirectly on the location of the ETM and magnitude of the sediment concentration. As a result, the comparison between results of 1965 and 2005 is not complicated by the changed location of the ETM and large increase in sediment concentration and gives more insight. Furthermore, the transport capacity gives information about the trapping locations, because the convergence and divergence points of the transport capacity (i.e. locations where the transport capacity is zero) correspond to the maxima and minima in  $f$ .

**CONTRIBUTIONS TO THE TRANSPORT CAPACITY** iFlow distinguishes several contributions to the transport capacity related to different physical mechanisms. The five most important contributions for the 1965 and 2005 cases are plotted in Fig. 4.7. Before comparing the transport capacities between the years, we introduce the physical mechanisms of these contributions are related to the following:

- The *external  $M_4$  tide* contribution is due to tidal asymmetry caused by the  $M_2$  tide and  $M_4$  tide entering the estuary at the mouth. This contribution to the  $M_4$  tide is generated outside the estuary on the shallow shelf and propagates through the estuary, causing asymmetry in the velocity during ebb and flood and therefore net sediment transport.
- The *tidal return flow* contribution is the transport capacity due to Stokes drift and the corresponding return flow. The Stokes drift is associated with sediment import. At least partly compensating this import, the return flow velocity contains a subtidal contribution which typically causes export of sediment. Additionally, the return flow velocity has an  $M_4$  contribution, which may cause import or export of sediment, depending on the phase-lag with the  $M_2$  tide.

- The *sediment advection* contribution represents the transport due to spatial settling lag (see e.g. Van Straaten and Kuenen, 1957; De Swart and Zimmerman, 2009). This contribution tends to transport sediment toward along-channel minima in the tidal velocity amplitude.
- The *river* contribution consists of two parts: the river-induced flushing of tidally resuspended sediment and the transport due to the tidal asymmetry caused by the tide-river interaction. Both contributions cause an export of sediment
- The *river-river* contribution represents the river-induced flushing of sediment resuspended by the river flow. This contribution is therefore independent of the tide and causes sediment export close to the landward boundary, where the river-induced flow dominates over the tidal flow.

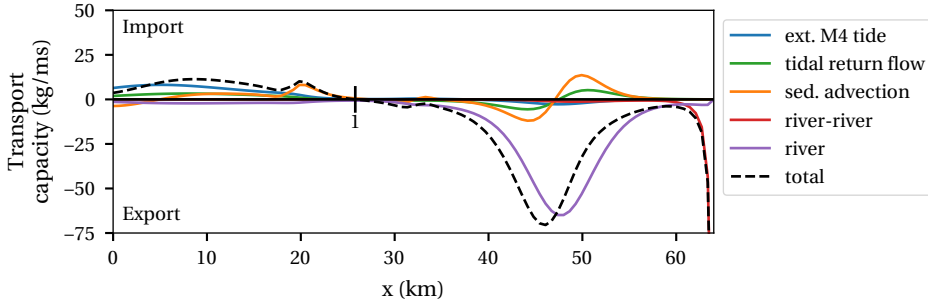
4

**COMPARISON OF THE TRANSPORT CAPACITY IN 1965 AND 2005** In 1965 and 2005 the total transport capacity (black dashed lines in Fig. 4.7) is positive (i.e. directed upstream) in the first 25 and 35 km, respectively, and negative (i.e. directed downstream) from there to km 45. This convergence leads to the development of an ETM around km 25 and 35 (number 1 in the figure). In 1965, the transport capacity is negative upstream from km 45. In 2005, however, the transport capacity is positive between km 45 and 57, leading to a second convergence zone around km 57 (number 2 in the figure). These two trapping zones appear in Fig. 4.5e as one large ETM zone stretching from km 25 to 60.

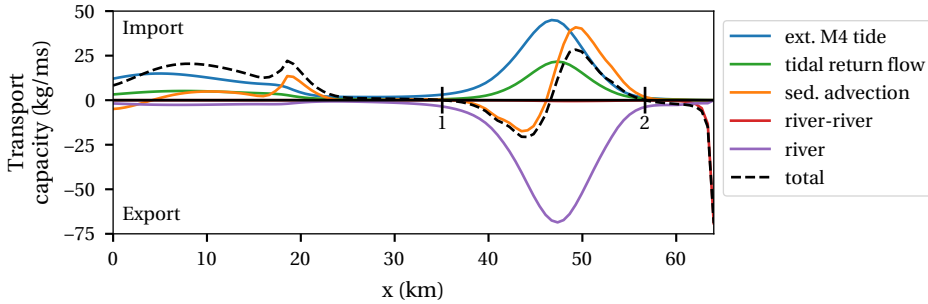
The dominant exporting transport contribution in both years is the river discharge. Import is mainly caused by the contributions due to the external  $M_4$  tide and tidal return flow (see Section 4.5.1). The most important difference between 1965 and 2005 is the large increase of these importing contributions between km 35 and 57. This increase is related to the increase in the  $M_4$  velocity amplitude (c.f. Fig. 4.5c). In addition, the phase difference between the  $M_2$  tidal velocity and erosion asymmetry due to the external  $M_4$  tide and  $M_4$  tidal return flow has become more favourable for import (not shown).

**ROLE OF SEDIMENT-INDUCED TURBULENCE DAMPING** The strong effect of sediment-induced turbulence damping in the Ems cannot be captured in a specific contribution to the transport capacity, because it is strongly and mutually dependent on the flow and sediment concentration. To capture the effect of sediment-induced damping on the sediment trapping we therefore compare results with and without it. Sediment-induced damping is turned off by setting  $F$ ,  $G$  and  $c_D$  in Eqs. (4.4), (4.5) and (4.10) equal to 1.

Fig. 4.8 shows the resulting maximum near-bed concentration along the channel versus the river discharge. This shows moderate sediment concentrations, with concentrations not exceeding  $1.2 \text{ kg/m}^3$  even for a low discharge of  $30 \text{ m}^3/\text{s}$ . Compared to 1965, the maximum sediment concentrations in 2005 are higher and the ETM is found more upstream. However, the level of the sediment concentration in 2005 and the changes between 1965 and 2005 are much smaller than in the case with sediment-induced turbulence damping (cf. Fig. 4.6). Without sediment-induced turbulence damping, concentrations remain moderate and the observed transition in sediment concentration between 1965 and 2005 is not reproduced.



(a) 1965

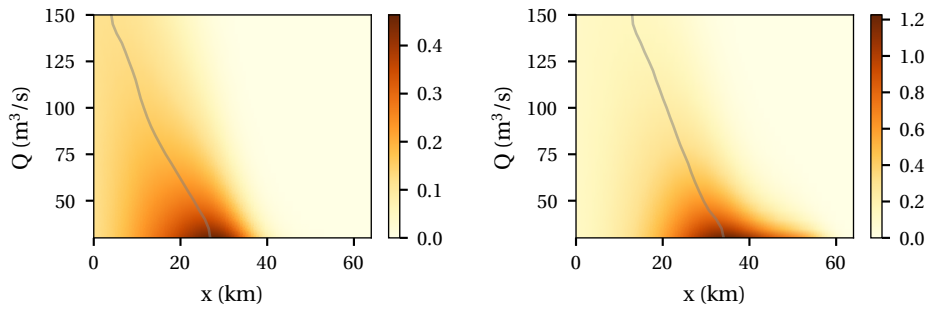


(b) 2005

**Figure 4.7:** Sediment transport capacity per metre width (and integrated over depth) for 1965 (a) and 2005 (b) for summer average discharge conditions ( $Q = 40 \text{ m}^3/\text{s}$ ). The five most important contributions to the transport capacity are plotted, as well as the sum of all modelled contributions (black dashed line). Downward sloping zero-crossings of the total transport capacity indicate a convergence zone and are marked by a vertical line and number.

**RESONANCE** The previous sections demonstrate that the increase in the  $M_4$  tidal velocity amplitude in combination with sediment-induced turbulence damping is essential for the increase in sediment concentrations between 1965 and 2005. The reason that this effect is so strong is better explained by looking at the resonance characteristics. Resonance is a state of maximum tidal amplification. Hence, when an estuary is close to resonance, the water level amplitude becomes very sensitive to changes in the characteristics of the estuary. Here we will take this as a proxy for sensitivity of the tidal velocity amplitude as well. Whether an estuary is in resonance depends on various parameters including the depth, friction (i.e. effect of eddy viscosity and bed friction) and length and is furthermore different for each tidal constituent.

We take the depth and friction of the Ems estuary in 1965 and 2005 and derive the length at which the estuary would be in resonance for the  $M_2$  and  $M_4$  tide, that is, the *resonance length*. This is done on the basis of a simple one-dimensional hydrodynamic model for the linear wave propagation of the externally forced  $M_2$  and  $M_4$  tide (see e.g. Friedrichs, 2010). Results are summarised in Table 4.2.



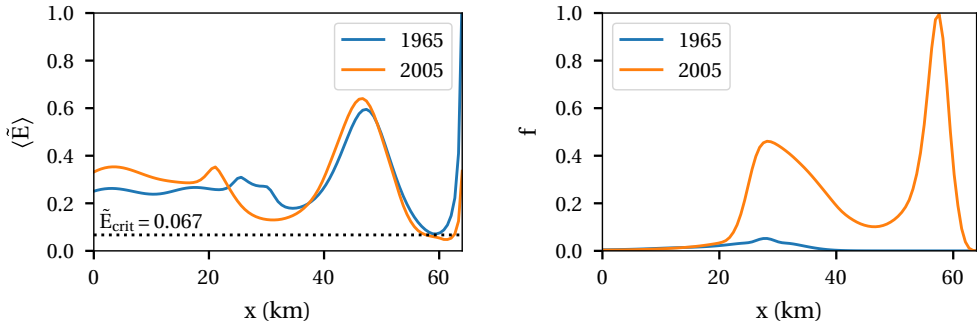
(a) Subtidal near-bed concentration in 1965 (b) Subtidal near-bed concentration in 2005  
(kg/m<sup>3</sup>) (kg/m<sup>3</sup>)

**Figure 4.8:** Near-bed modelled sediment concentration along the channel (horizontal axis) for a various long-term constant discharge values (vertical axis) for the 1965 and 2005 cases without sediment-induced reduction of the bed roughness, eddy viscosity and eddy diffusivity. Sediment concentrations are much lower than in Fig. 4.6 with sediment-induced turbulence damping and no strong transition is observed between 1965 and 2005.

Case	Resonance length	
	$M_2$ tide	$M_4$ tide
1965	39 km	37 km
2005 with friction as in 1965	55 km	51 km
2005 with friction as in 2005	72 km	63 km

**Table 4.2:** Computed resonance lengths for the  $M_2$  and  $M_4$  tide in the cases of 1965 and 2005 for a friction parameter calibrated for 1965 and 2005. A resonance length close to the actual length of 64 km indicates that the tidal amplitude is very sensitive to changes in depth or friction.

In 1965, we find a resonance length of 39 and 37 km for the  $M_2$  and  $M_4$  tide, respectively. This is very short, because the estuary is strongly friction dominated; the tide becomes damped by friction for larger length. When deepening the estuary to 2005 depth but keeping friction as in 1965, the resonance length increases, explaining part of the amplification of the  $M_2$  and  $M_4$  tide between 1965 and 2005. When also changing the friction to 2005 conditions, representing the sediment-induced damping of turbulence, the resonance length increases further. The resonance length for the  $M_2$  tide increases beyond the actual length of the estuary. Hence, the  $M_2$  is not closer to resonance than with the 2005 depth and 1965 friction. Nevertheless, the  $M_2$  tide amplifies somewhat more because of the reduced friction. The transport contribution due to the tidal return flow is related to the  $M_2$  tide and is larger because of the amplification of this  $M_2$  tide. The resonance length of the  $M_4$  tide on the other hand is very close to resonance. It therefore amplifies not only because of the reduced friction but also because of resonance. The transport contribution due to the external  $M_4$  tide has therefore become much larger.



(a) The dimensionless erosion parameter (See Eq. (4.14)) and its threshold value 0.067. If  $\langle \tilde{E} \rangle$  exceeds the threshold, local resuspension does not restrict the maximum suspended sediment concentration.

(b) The erodibility  $f$ , which is a measure for the availability of easily erodible sediment. A value  $f < 1$  indicates that sediment availability is limiting the sediment concentration, while  $f = 1$  indicates that local resuspension is limiting the sediment concentration.

4

**Figure 4.9:** Dimensionless erosion parameter  $\tilde{E}$  and erodibility  $f$  for 1965 and 2005 with average summer discharge ( $Q = 40 \text{ m}^3/\text{s}$ ).

#### 4.5.2. LOCAL RESUSPENSION CRITERION

The second aspect important for understanding the dynamics of the suspended sediment concentration is the ability of the flow to keep sediment in suspension by erosion or resuspension. In Chapter 3 it was derived that the maximum concentration that may be locally resuspended is related to a dimensionless erosion parameter  $\tilde{E}$ . For our erosion formulation (Eq. (4.2)), this parameter is expressed as

$$\tilde{E} = \frac{M|\tau_b|}{w_{s,0}c_{\text{gel}}}. \quad (4.14)$$

Using the hindered settling parametrisation of Eq. (4.3), the maximum concentration is limited to a value that depends on the tidally averaged dimensionless erosion parameter  $\langle \tilde{E} \rangle$  if  $\langle \tilde{E} \rangle$  is smaller than a threshold value of 0.067 (see Chapter 3 for details). This maximum cannot exceed 16% of the gelling concentration, that is,  $16 \text{ kg/m}^3$  in our case. If  $\langle \tilde{E} \rangle > 0.067$  there is no restriction to the concentration that can be maintained by resuspension. This is because of a positive feedback, where hindered settling leads to reduced deposition rates and hence a larger net erosion (=erosion-deposition).

Fig. 4.9a show  $\langle \tilde{E} \rangle$  for the 1965 and 2005 cases for the average summer discharge, together with the threshold value. The tidally averaged dimensionless erosion parameter is well over the threshold in most of the domain. In those locations, all the available sediment is resuspended at least during some part of the tide. Only in 2005 between 59 and 62 km does  $\langle \tilde{E} \rangle$  drop below the threshold value, where it may restrict the maximum concentration.

Whether the maximum sediment concentration is indeed restricted by local resuspension follows from the erodibility, see Fig. 4.9b. If  $f < 1$  everywhere in the estuary, it is said that the estuary is in an *availability* (or *supply*) *limited* state and the concentration is limited by the amount of sediment trapping. A value  $f = 1$  indicates that some easily erodible sediment remains on the bed during the entire tidal cycle and local resuspension is limiting there. This state is called *erosion* (or *erosion rate*) *limited*. In an erosion limited state, the estuary imports sediment, which is deposited in the area where  $f = 1$ , leading to a growing bottom pool (Brouwer et al., 2018). Since the local growing bottom pool acts as a sediment sink, even a small area with  $f = 1$  leads to lower concentrations in equilibrium elsewhere in the estuary. Fig. 4.9b shows that  $f < 1$  along the entire estuary in both years, although only marginally in 2005. Hence, it is concluded that sediment trapping is the limiting mechanism, even in the small area between km 59 and 62 in 2005, where sediment resuspension could theoretically be limiting.

#### 4.6. SENSITIVITY

To explore the robustness of the results to different parameter choices, we present the effect of choosing different values for the clear-water settling velocity and erosion parameter, which are two of the least constrained parameters in the model.

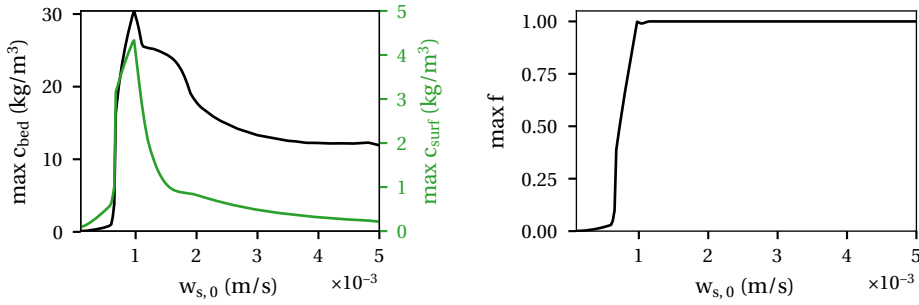
##### 4.6.1. SENSITIVITY TO THE SETTLING VELOCITY

To test the sensitivity of the model results to the clear-water settling velocity,  $w_{s,0}$  is varied between 0.1 to 5 mm/s. The resulting maximum near-bed and surface concentrations in 2005 are shown in Fig. 4.10, using the default settings for 2005 for all other parameters (see Table 4.1) and using the average summer discharge of 40 m<sup>3</sup>/s. The maximum concentration is small for settling velocities below 0.5 mm/s. At such settling velocities, the sediment behaves like a wash load and will not be trapped inside the estuary. Hence, sediment trapping is limiting the sediment concentration. This is confirmed in Fig. 4.10b, which shows that  $f < 1$  everywhere in the estuary if  $w_{s,0} < 0.5$  mm/s. Around  $w_{s,0} = 0.5$  mm/s, a sharp transition to high sediment concentrations is found due to the strong feedback effect of sediment-induced turbulence damping. For  $w_{s,0}$  between 0.5 and 1 mm/s, the maximum concentration increases with  $w_{s,0}$ . Sediment trapping is still limiting, but more sediment is trapped as the settling velocity increases. The maximum concentration decreases again if the settling velocity exceeds 1 mm/s. As shown in Fig. 4.10b, this is because local resuspension becomes limiting ( $f = 1$ ), as the dimensionless erosion parameter  $\tilde{E}$  decreases with increasing  $w_{s,0}$  by definition (see Eq. (4.14)). Under these erosion limited conditions, sediment deposits at the edges of the wide ETM zone near km 60 and 30 and forms two growing pools of sediment.

##### 4.6.2. SENSITIVITY TO THE EROSION PARAMETER

The dimensionless erosion parameter  $\tilde{E}$  is linearly proportional to the erosion parameter  $M$  (Eq. (4.14)). Hence, the estuary becomes erosion limited at small values of the erosion parameter  $\tilde{E}$ . If the ETM location remains the same for different values of  $M$ , the maximum concentration scales linearly with  $M$ . When  $M$  becomes sufficiently large so that the estuary becomes supply limited, the maximum concentration is independent of  $M$ . At what value of  $M$  this occurs, depends on the conditions.

Model results obtained by varying both the erosion parameter and the river discharge



(a) Subtidal near-bed (black) and surface (b) Erodibility. (green) concentration

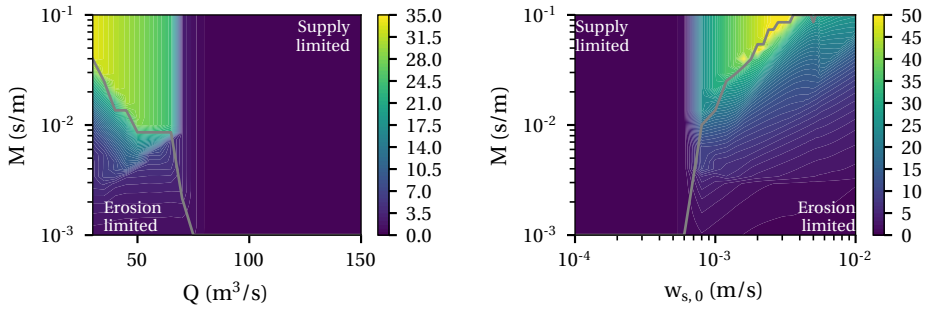
**Figure 4.10:** Sensitivity of the model results in 2005 with average summer discharge ( $Q = 40 \text{ m}^3/\text{s}$ ) to the clear-water settling velocity.

are presented in Fig. 4.11a. The grey line indicates the transition point between erosion and supply limited conditions. For each value of the river discharge, the concentration increases with increasing  $M$  up to the point where the estuary becomes supply limited and the concentration becomes independent of  $M$ . The figure shows high concentrations in the upper-left corner, i.e. for high erosion parameters and low river discharges. If the river discharge is high, the sediment trapping is too weak to attain high sediment concentrations regardless of the value of  $M$ .

Results of a sensitivity study over the clear-water settling velocity and the erosion parameter for fixed discharge  $Q = 40 \text{ m}^3/\text{s}$  are presented in Figure 4.11b. For each value of the settling velocity, we again see that the maximum sediment concentration increases with  $M$  up to the point where the estuary becomes supply limited. Additionally, for each value of the erosion parameter, we see that the sediment concentration has a maximum for some value of the settling velocity. For low erosion parameters this maximum occurs for settling velocities around  $0.5 \text{ mm/s}$  but with low maximum concentrations. For high values of the erosion parameter, the maximum concentrations occur for settling velocities around  $2$  to  $3 \text{ mm/s}$  and can attain values up to  $50 \text{ kg/m}^3$ .

#### 4.7. DISCUSSION AND CONCLUSIONS

It is demonstrated that deepening of the channel in the Ems River can indeed be responsible for the transition from low to high sediment concentrations using the width-averaged idealised process-based iFlow model. The model was used to simulate two scenarios representing 1965 and 2005, which only differ in the channel depth. Between 1965 and 2005 we find a strong amplification of the tidal water level, a strong increase in the suspended sediment concentration, an upstream movement and a widening of the ETM to an area between  $25$  and  $60 \text{ km}$  upstream from Knock. These features show good qualitative correspondence to observations. Since the model results represent dynamic equilibrium conditions, we draw conclusions on the long-term change of the state of the estuary, not on the sequence of events and timescale of the changes. As the transition



(a) Maximum sediment concentration as a function of  $M$  and  $Q$  (kg/m³) (b) Maximum sediment concentration as a function of  $M$  and  $w_{s,0}$  (kg/m³)

**Figure 4.11:** Sensitivity of the near-bed subtidal sediment concentration in the 2005 case to  $M$ ,  $Q$  and  $w_{s,0}$ . The grey line marks the transition between erosion and supply limited conditions.

from low to high concentrations is found for discharges below 70 m³/s, which occur on average 60% of the time, it seems likely that the modelled equilibrium conditions can indeed be attained. Therefore, we are confident that the model provides a good qualitative representation of the physical mechanisms that govern the transition.

The physical mechanisms responsible for the transition to high sediment concentrations are analysed by analysing sediment transport and resuspension. It is shown that the most important mechanisms responsible for increased sediment import into the estuary after deepening are amplification of the  $M_4$  tidal velocity and sediment-induced damping of turbulence. The increased  $M_4$  tidal velocity increased the tidal asymmetry leading to more import of sediment. Together with sediment-induced damping of turbulence, this results in a positive feedback thereby confirming the hypothesis of the existence of such a feedback by Winterwerp and Wang (2013). It is furthermore found in this study that the combination of deepening and sediment-induced damping of turbulence brought the  $M_4$  tide close to resonance, hence explaining why the import of sediment is so much stronger after deepening compared to the situation before deepening. It has been assumed that resuspension from the bed is efficient by choosing a high value of the erosion parameter and by including hindered settling in the model. This ensures that all the imported sediment can be kept in suspension by the flow, explaining the increase in suspended sediment concentration.

Once the transition to high sediment concentrations has occurred, the model lacks several physical processes that are essential to describe the sediment dynamics. This shows in the 2005 model results by an overestimation of the  $M_4$  tidal water level amplitude and insufficient vertical structure to capture the observed distinct fluid mud layers (e.g. Becker et al., 2018). Furthermore, while lower sediment concentrations are observed during periods of high discharges (Winterwerp et al., 2017), the strong flushing found in the model for discharges higher than 70 m³/s does not correspond to the observations. The model therefore lacks mechanisms that retain the fluid mud during periods of high



discharges. Possible mechanisms that need to be included for a better description of the 2005 state are a critical shear stress for erosion, multiple sediment fractions, internal dynamics (i.e. the effect of a temporally variable density structure on the eddy viscosity and eddy diffusivity) (Winterwerp et al., 2017; Becker et al., 2018) and dynamic effects that resolve the timescale for depleting a bottom pool of sediment (e.g. Schoellhamer, 2011).

The physical mechanisms investigated in this study occur in many estuaries, but their response to deepening is not necessarily the same in other estuaries. The feedback between amplification of the  $M_4$  tidal velocity and sediment-induced turbulence damping relies on the  $M_4$  tide evolving toward resonance and depends on the phase difference between the  $M_2$  and  $M_4$  tide, which may be different in other estuaries. Additionally, the  $M_2$ - $M_4$  tidal asymmetry that is essential for sediment transport in the Ems, may not be essential in other estuaries. Furthermore, sediment resuspension may be limiting instead of sediment trapping in some other estuaries. Therefore, to establish if a similar transition to high sediment concentrations can occur in another estuary, it needs to be investigated whether sediment transport or resuspension is limiting, what sediment transport processes are important and how these processes respond to deepening.

#### 4.A. FORMAL DEFINITION OF THE TRANSPORT CAPACITY

The transport capacity used in Section 4.5 can be formally defined from the sediment transport  $\mathcal{T}$ . For convenience we repeat Eq. (4.13) describing  $\mathcal{T}$ ,

$$\mathcal{T} = \left\langle B \int_{-H}^{R+\zeta} uc - K_h c_x dz \right\rangle. \quad (4.15)$$

This expression is rewritten using iFlow's approximation of the sediment concentration (see also Brouwer et al., 2018)

$$c = \hat{c}^f f + \hat{c}^{fx} f_x. \quad (4.16)$$

Here  $f$  is the erodibility (see Section 4.2), which is a measure between 0 and 1 for the abundance of sediment available at the bed for erosion. The quantity  $\hat{c}^f$  is the sediment concentration suspended at capacity conditions. The term *capacity conditions* indicates the maximum concentration that can be supported by the flow, assuming an abundant availability of sediment. Indeed, according to Eq. (4.16) the concentration  $c$  equals  $\hat{c}^f$  if there is an abundance of sediment, that is,  $f = 1$  everywhere (resulting in  $f_x = 0$ ). The quantity  $\hat{c}^{fx}$  represents the along-channel sediment dispersion by tidal advection at capacity conditions. Combining Eq. (4.15) and Eq. (4.16) yields a new expression for the sediment transport

$$\mathcal{T} = \left\langle \underbrace{B \int_{-H}^{R+\zeta} (u\hat{c}^f - K_h \hat{c}_x^f) f}_{\text{Transport capacity}} - (\hat{c}^{fx} + K_h \hat{c}_x^f) f_x dz \right\rangle. \quad (4.17)$$

The *transport capacity*  $T$  is now defined as the first term divided by  $f$ , that is,

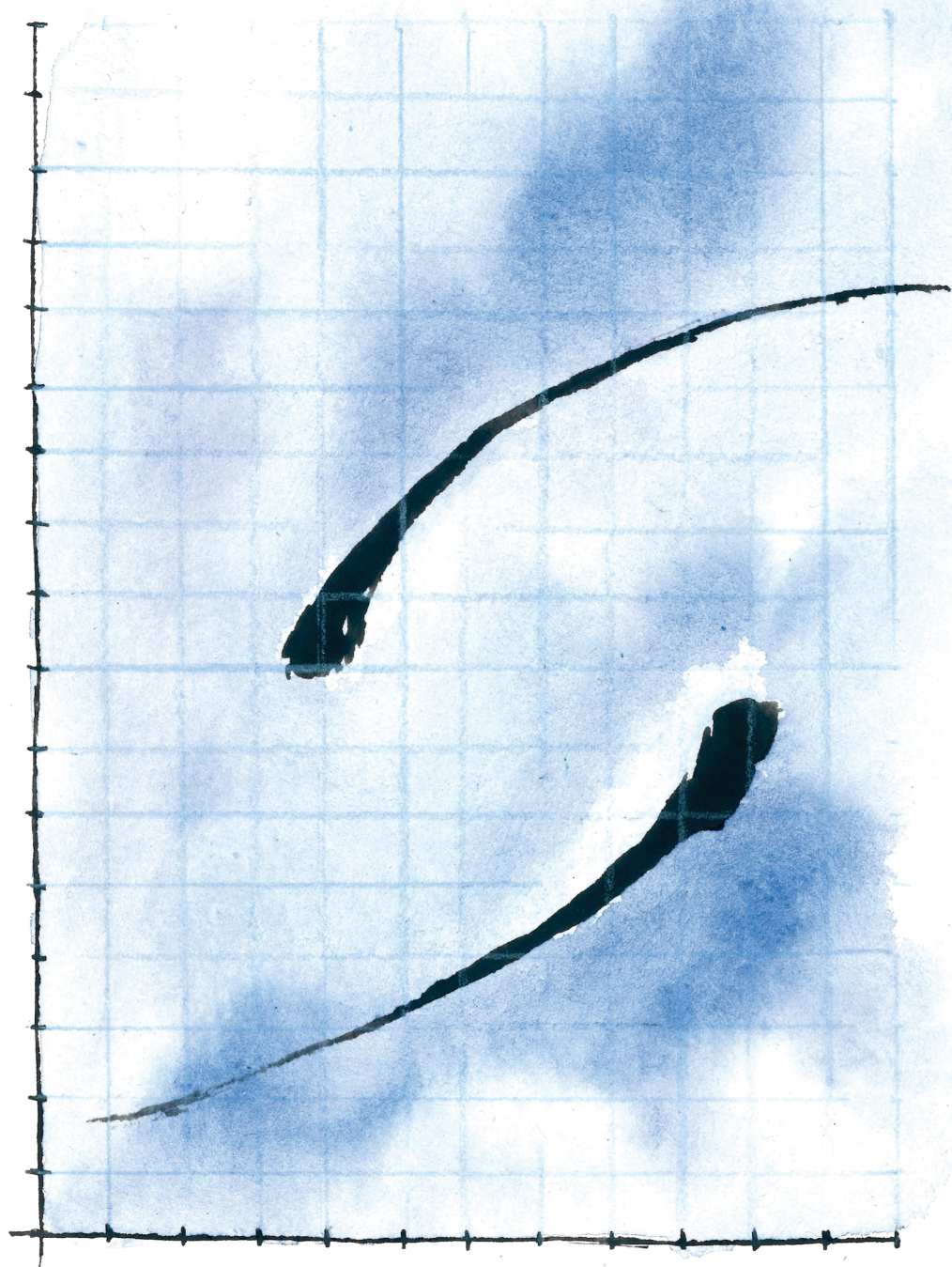
$$T = \left\langle B \int_{-H}^{R+\zeta} u\hat{c}^f - K_h \hat{c}_x^f dz \right\rangle. \quad (4.18)$$

This definition is consistent with the transport function  $T$  used by Chernetsky et al. (2010).

## REFERENCES

- Adams, C. E. and Weatherly, G. L. (1981). Some effects of suspended sediment stratification on an oceanic bottom boundary layer. *Journal of Geophysical Research: Oceans*, 86:4161–4172.
- BAW (1967). Modellversuche für die Ems. Technical report, Bundesanstalt für Wasserbau, Hamburg. in German.
- Becker, M., Maushake, C., and Winter, C. (2018). Observations of mud-induced periodic stratification in a hyperturbid estuary. *Geophysical Research Letters*, 45:5461–5469.
- Brouwer, R. L., Schramkowski, G. P., Dijkstra, Y. M., and Schuttelaars, H. M. (2018). Time evolution of estuarine turbidity maxima in well-mixed, tidally dominated estuaries: the role of availability- and erosion-limited conditions. *Journal of Physical Oceanography*, 48:1629–1650.
- Chernetsky, A. S., Schuttelaars, H. M., and Talke, S. A. (2010). The effect of tidal asymmetry and temporal settling lag on sediment trapping in tidal estuaries. *Ocean Dynamics*, 60:1219–1241.
- Cloern, J. E. (1987). Turbidity as a control on phytoplankton biomass and productivity in estuaries. *Continental Shelf Research*, 7:1367–1381.
- De Jonge, V. N., Schuttelaars, H. M., Van Beusekom, J. E. E., Talke, S. A., and De Swart, H. E. (2014). The influence of channel deepening on estuarine turbidity levels and dynamics, as exemplified by the Ems estuary. *Estuarine Coastal and Shelf Science*, 139:46–59.
- De Swart, H. and Zimmerman, J. (2009). Morphodynamics of tidal inlet systems. *Annual Review of Fluid Mechanics*, 41:203–229.
- Dechend, W. (1950). Die geologischen Untersuchungen in der Ems. Technical report, WSA Emden. In German.
- Friedrichs, C. T. (2010). *Contemporary issues in estuarine physics*, chapter Barotropic tides in channelized estuaries, pages 27–61. Cambridge University Press, Cambridge, UK.
- Friedrichs, C. T., Wright, L. D., Hepworth, D. A., and Kim, S. C. (2000). Bottom-boundary-layer processes associated with fine sediment accumulation in coastal seas and bays. *Continental Shelf Research*, 20:807–841.
- Jalón-Rojas, I., Schmidt, S., Sottolichio, A., and Bertier, C. (2016). Tracking the turbidity maximum zone in the Loire Estuary (France) based on a long-term, high-resolution and high-frequency monitoring network. *Continental Shelf Research*, 117:1–11.
- Janssen, T. (1968). Das Elend des Emderfahrwassers und seine Beseitigung. Technical report, Verlag Ostfriesische Landschaft, Aurich. p.26.
- Kandiah, A. (1974). *Fundamental aspects of surface erosion of cohesive soils*. PhD thesis, University of California, Davis.
- Munk, W. H. and Anderson, E. R. (1948). Notes on a theory of the thermocline. *Journal of Marine Research*, 7:276–295.
- Papenmeier, S., Schrottke, K., Bartholomä, A., and Flemming, B. W. (2013). Sedimentological and rheological properties of the water-solid bed interface in the Weser and Ems Estuaries, North Sea, Germany: Implications for fluid mud classification. *Journal of Coastal Research*, 29:797–808.
- Richardson, J. F. and Zaki, W. N. (1954). The sedimentation of a suspension of uniform spheres under conditions of viscous flow. *Chemical Engineering Science*, 8:65–78.
- Schoellhamer, D. H. (2011). Sudden clearing of estuarine waters upon crossing the threshold from transport to supply regulation of sediment transport as an erodible sediment pool is depleted: San Francisco Bay, 1999. *Estuaries and Coasts*, 34(5):885–899.
- Talke, S. A., De Swart, H. E., and De Jonge, V. N. (2009a). An idealized model and systematic process study of oxygen depletion in highly turbid estuaries. *Estuaries and Coasts*, 32:602–620.
- Talke, S. A., De Swart, H. E., and Schuttelaars, H. M. (2009b). Feedback between residual circulations and sediment distribution in highly turbid estuaries: an analytical model. *Continental Shelf Research*, 29:119–135.
- Uncles, R. J., Joint, I., and Stephens, J. A. (1998). Transport and retention of suspended particulate matter and bacteria in the Humber-Ouse Estuary, United Kingdom, and their relationship to

- hypoxia and anoxia. *Estuaries*, 21:597–612.
- Van Maren, D. S., Winterwerp, J. C., and Vroom, J. (2015). Fine sediment transport into the hyper-turbid lower Ems River: the role of channel deepening and sediment-induced drag reduction. *Ocean Dynamics*, 65:589–605.
- Van Straaten, L. M. J. U. and Kuenen, P. H. (1957). Accumulation of fine grained sediments in the Dutch Wadden Sea. *Netherlands Journal of Geosciences*, 19:329–354.
- Wang, L. (2010). *Tide Driven Dynamics of Subaqueous Fluid Mud Layers in Turbidity Maximum Zones of German Estuaries*. PhD thesis, University of Bremen.
- Wang, X. H. (2002). Tide-induced sediment resuspension and the bottom boundary layer in an idealized estuary with a muddy bed. *Journal of Physical Oceanography*, 32:3113–3131.
- Weilbeer, H. (2007). Numerical simulation and analyses of sediment transport processes in the Ems-Dollard estuary with a three-dimensional model. In Kusuda, T., Yamanishi, H., Spearman, J., and Gailani, J. Z., editors, *Sediment and Ecohydraulics: INTERCOH 2005*, pages 447–463. Elsevier.
- Winterwerp, J. C., Vroom, J., Wang, Z. B., Krebs, M., Hendriks, E. C. M., Van Maren, D. S., Schrottke, K., Borgsmüller, C., and Schöl, A. (2017). SPM response to tide and river flow in the hyper-turbid Ems River. *Ocean Dynamics*, 67:559.
- Winterwerp, J. C. and Wang, Z. B. (2013). Man-induced regime shifts in small estuaries - I: theory. *Ocean Dynamics*, 63:1279–1292.
- Winterwerp, J. C., Wang, Z. B., Van Brackel, A., Van Holland, G., and Kösters, F. (2013). Man-induced regime shifts in small estuaries - II: a comparison of rivers. *Ocean Dynamics*, 63:1293–1306.



# CHAPTER 5

A regime shift from low to high sediment concentrations in a tide-dominated estuary

Dijkstra, Y. M., Schuttelaars, H. M., and Schramkowski, G. P. (*Accepted to Geophysical Research Letters*). A regime shift from low to high sediment concentrations in a tide-dominated estuary.

## Abstract

---

Many estuaries are strongly deepened to improve navigation, with sometimes large and poorly understood consequences to suspended sediment dynamics. To improve understanding of such large changes, we study the Ems River Estuary, where a *regime shift* from low to high sediment concentrations was observed after deepening. The aim of this study is to improve understanding of the development of the sediment concentration regime over time and estimate the associated timescale. Using the idealised width-averaged iFlow model, we identify the co-existence of two distinct stable equilibrium regimes representing low and high sediment concentrations, qualitatively matching the regimes observed in the Ems. Depending on the river discharge, a critical depth profile is identified at which the regime shifts. By combining the model results and long-term observations of the tidal range, first indications of the regime shift are observed around 1989, taking approximately 6-7 years to develop.

---



## 5.1. INTRODUCTION

Rapid changes in the long-term average suspended sediment concentration have been observed in several estuaries, including the Ems (Germany, Netherlands), Loire (France) and Yangtze (China) Rivers. These changes are probably driven in large part by human activity, including dam construction, removal or restoration of intertidal area, port development and channel deepening. A sudden transition of a long-term average state or *regime* of a system, such as an estuary, is called a *regime shift* (e.g. Scheffer et al., 2001). Typically, a regime shift is accompanied by a shift in the dominant processes and occurs on a timescale that is much shorter than that of natural variability. This short timescale makes regime shifts a particularly challenging aspect in marine ecosystem management, because it leaves little time to develop measures to mitigate negative effects associated with a regime shift after the first adverse changes to the ecosystem have been observed (e.g. Biggs et al., 2009). Moreover, forecasting a regime shift using computational models is challenging, as it is unclear if process parametrisations and parameter values chosen in these models are sufficient to describe a regime shift. Therefore, to assess what systems are susceptible to a regime shift and if such a regime shift can be recognised in time to mitigate negative effects, it is necessary to systematically analyse examples of observed regime shifts and investigate the underlying physical processes and associated timescales.

In this study we focus on the lower Ems River, where the regime shifted from low to high suspended sediment concentrations following extensive channel deepening. Between the 1950s-1960s and early 2000s, deepening of the estuary led to an increase in the suspended sediment concentration by at least one order of magnitude at the water surface, from 100-200 mg/l to 1-2 g/l (De Jonge et al., 2014) and at the bed from 1-2 g/l (Dechend, 1950) to 30-200 g/l (Talke et al., 2009b; Wang, 2010; Papenmeier et al., 2013; Becker et al., 2018). Additionally, the estuarine turbidity maximum (ETM) has moved upstream and widened, presently covering an area of over 40 km between Gandersum (km 20) and Herbrum (km 64), see Fig. 5.1. We thus define the regime shift in the Ems as the transition from a single narrow ETM, where fluid mud may have been present only briefly and locally, to a wide ETM, where fluid mud and high sediment concentrations are found during a large part of the year.

Due to a lack of historical observations of the sediment concentration, little is known about the moment the regime shifted and the timescale associated with this regime shift. Using a three-dimensional numerical model, Van Maren et al. (2015) reproduced some characteristics of the observed sediment concentration in the Ems in several years between 1945 and 2005 but only by recalibrating the model for each year, so that they could not dynamically model the sediment concentration over the course of the decades. Therefore current knowledge about the regime shift in the Ems is based on more indirect and idealised models. Winterwerp et al. (2013) and De Jonge et al. (2014) inferred the time-development of the sediment concentration by reconstructing the apparent friction in the estuary using observed water levels and a hydrodynamic model, reasoning that increasing sediment concentrations lead to a decreasing friction. In this way, Winterwerp et al. (2013) found a gradual decrease of the friction over time since 1960. De Jonge et al. (2014) also found a gradual decrease of friction over time since the 1960s but with the strongest reduction of friction between 1981 and 1992. However, as these

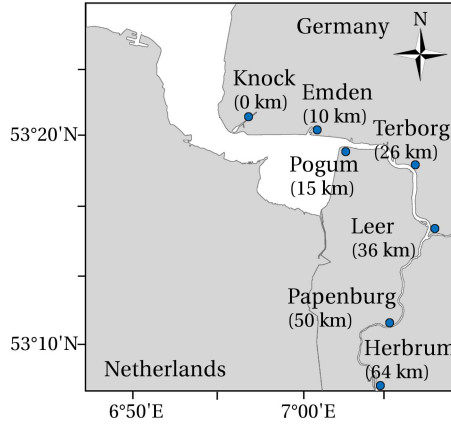


**Figure 5.1:** Map of the Lower Ems River (Germany) from Knock to the tidal weir at Herbrum.

5

idealised models did not resolve the effect of sediment on friction dynamically, they could only model individually calibrated states for different years, not the transition processes over time.

The aim of this study is to better identify how the sediment concentration regime in the Ems changed over time, and thereby estimate the starting time and timescale of the regime shift. This is done by using the width-averaged idealised iFlow model (Section 5.2). In Chapter 4, this model was used to reproduce the qualitative characteristics of the water motion and sediment concentration in the Ems in 1965 (before the regime shift) and 2005 (after the regime shift). This was done by only changing the channel depth, dynamically modelling the water motion, sediment concentration and including the influence of the suspended sediment concentration on friction. Their study focussed on the difference in dominant physical processes before and after the regime shift and did not look at the transition in time. Here, the same model is used to compute dynamic equilibrium sediment concentrations, i.e. the regime, as a function of the river discharge and channel depth, representing the conditions in the years between 1965 and 2005 (Section 5.3) and for the first time demonstrating the existence of multiple coexisting sediment concentration regimes. By combining the modelled regimes with observations, it is estimated when the observations start to deviate from the low sediment concentration regime and move towards the high concentration regime, allowing the estimate of the starting time and timescale of the regime shift (Section 5.4). The interpretation of these results for the Ems and for other estuaries is discussed in Section 5.5. Finally, the main findings are summarised in Section 5.6.

## 5.2. MODEL AND CASE SET-UP

### 5.2.1. THE iFLOW MODEL FOR THE EMS

The iFlow model is a width-averaged model for tide-dominated estuaries that solves for an approximation of the non-linear continuity, momentum, and suspended sediment equations using scaling and perturbation methods (see Chapter 2 and Brouwer et al.



(2018). The model additionally resolves sediment-induced damping of turbulence and hindered settling, assuming that the eddy viscosity, eddy diffusivity and sediment settling velocity are depth-uniform and time-independent (Chapter 4).

The geometry of the Ems River is represented by a smooth width and depth profile along the estuary, resolving estuary-scale geometric variations. The water motion is forced by an  $M_2$  and  $M_4$  tide at the seaward boundary based on the average of observations from 2005, with an amplitude of 1.4 and 0.21 m, respectively, and with a relative phase difference of -172 degrees. These tidal conditions are representative for historic conditions as well (cf. Chapter 4). Fresh water enters at the landward boundary, with summer, winter and yearly average values of 40, 150 and 80 m<sup>3</sup>/s, respectively, based on 1987-2006 average measurements at Versen. At the seaward boundary at Knock (Fig. 5.1), a tide-averaged, depth-averaged sediment concentration of 0.1 kg/m<sup>3</sup> is imposed. This is representative of historic conditions but is a conservative estimate for recent conditions (De Jonge et al., 2014; BfG, 2017). However, since little is known about the time-development of the sediment concentration at Knock, we choose to use a value of 0.1 kg/m<sup>3</sup> for all years. It is assumed that no sediment enters the estuary from the watershed, because the average sediment concentration in the non-tidal river is only 20-40 mg/l (NLWKN, 2008). Sediment is represented as a single fraction with an erosion coefficient of 0.02 s/m, a gelling concentration of 100 kg/m<sup>3</sup> and a clear-water settling velocity of 1 mm/s. The settling velocity only varies due to the effects of hindered settling. Salinity is included in the model as a concentration that varies in the along-channel direction and is dependent on the river discharge but is uniform in depth and constant in time (Talke et al., 2009a). The model resolves the  $M_2$ ,  $M_4$  and subtidal water motion (horizontal velocity  $u$ , vertical velocity  $w$  and surface elevation  $\zeta$ ) and sediment concentration  $c$  in the vertical and along-channel dimension in dynamic equilibrium. Here dynamic equilibrium is defined as a state in which the water motion and sediment concentration vary on the tidal timescale but not on the subtidal timescale (see definitions in Chapter 1). To reach such an equilibrium, the model computes the amount of sediment in the model domain, based on the boundary conditions, flow and sediment transport.

### 5.2.2. SCHEMATISATION OF THE DEPTH

Between 1965 and 1995, the estuary between Emden and Papenburg has been deepened sequentially from 5 m below MHW (1961-1962), to 5.7 m (1984-1985), 6.3 m (1991), 6.8 m (1993) and finally to 7.3 m below MHW (1994-1995) (Lange, 2007; Krebs and Weilbeer, 2008). Observations of the thalweg depth in 1965, 1981, 1990, 1992 and 2005 are reported by De Jonge et al. (2014). Notably, the channel is up to 1.5 m deeper in 1981 than in 1965, even though there was no official deepening campaign within this period. This was possibly a response to engineering works in the outer estuary and building of dikes and dams. We use these observations as a motivation to approximate the deepening of the Ems as a gradual process, rather than a sequential process.

The continuous depth development between 1965 and 2005 is approximated by taking smooth depth profiles fitted to the observations in 1965 and 2005,  $d_{1965}(x)$  and  $d_{2005}(x)$ , used in Chapter 4. The depth in the intermediate years,  $d_{yr}$ , is defined as a linear combi-

nation of the depth in 1965 and 2005, i.e.

$$d_{\text{yr}}(x; \alpha) = (1 - \alpha)d_{1965}(x) + \alpha d_{2005}(x), \quad (5.1)$$

where  $\alpha$  is a bed profile parameter that follows from fitting the observed depth of 1981, 1990 and 1992 to Eq. (5.1) in a least-squares sense. This yields a different value of  $\alpha$  for each year. The value of  $\alpha$  increases monotonically over time but not at a constant rate in each time interval, see Fig. 5.2a. The depth observations and fits per year are plotted in Fig. 5.2b-5.2f. The fitted profiles do not capture the strong scatter in depth-observations related to large dunes and troughs but qualitatively capture the estuary-scale characteristics of the depth.

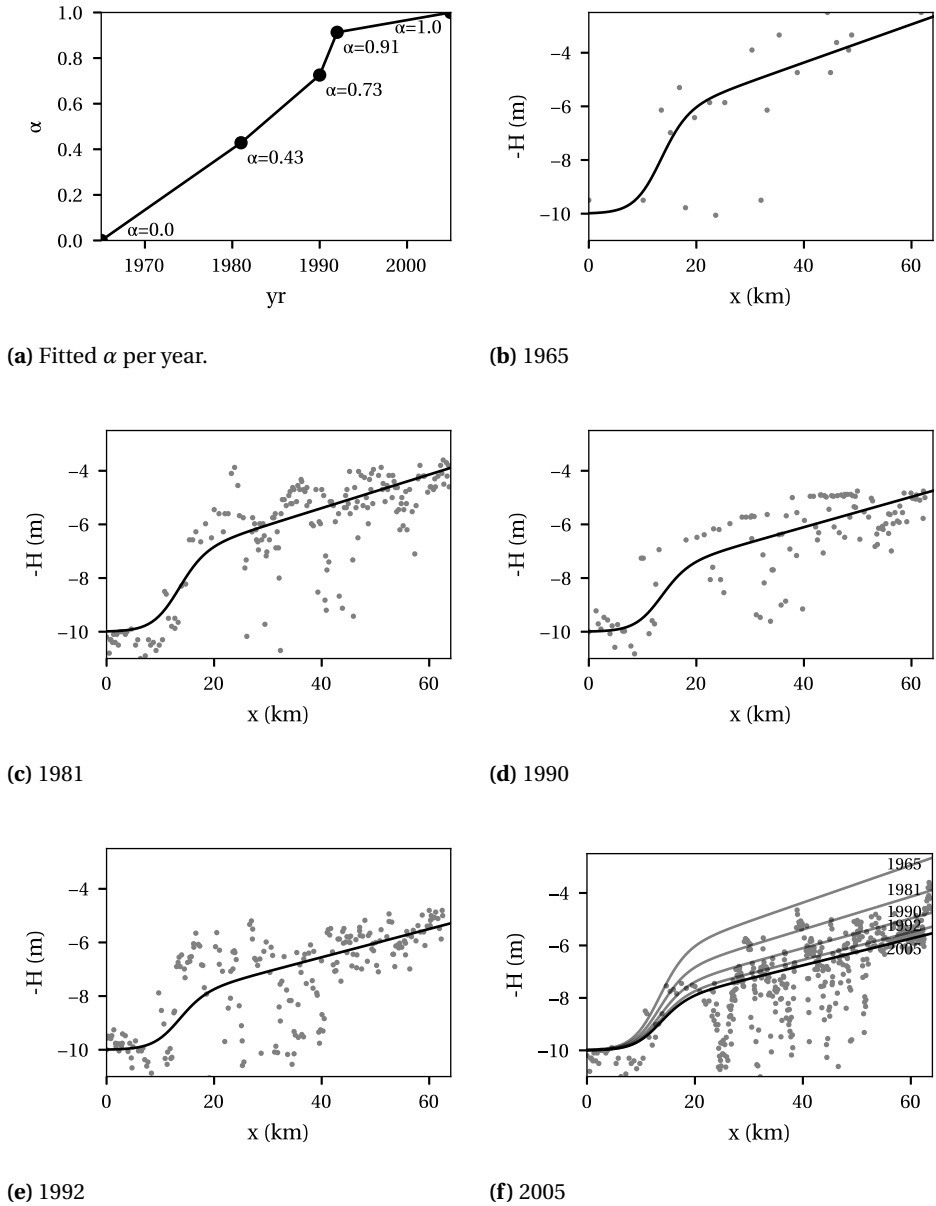
### 5.2.3. SET-UP OF THE MODEL EXPERIMENTS

The model is only calibrated to observed tidal amplitudes in 1965 ( $\alpha = 0$ ) and is not recalibrated when used for other years. Model experiments are conducted by varying the bed profile parameter  $\alpha$  between 0 and 1 and taking a fixed river discharge  $Q$  that is varied between 30 and 150 m<sup>3</sup>/s, keeping all other model parameters the same. The result of each model experiment consists of a spatially and tidally varying water motion and sediment concentration in dynamic equilibrium. The stable dynamic equilibria are obtained by continuation in  $\alpha$ . This procedure is repeated two times: for increasing and decreasing  $\alpha$ .

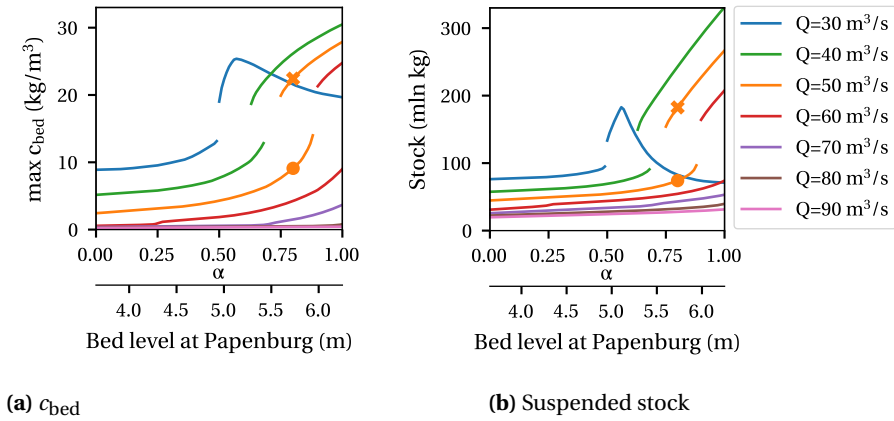
## 5.3. MODEL RESULTS

Fig. 5.3 shows the maximum near-bed tidally averaged sediment concentration (Fig. 5.3a) and the total amount of sediment suspended in the estuary, i.e. the *suspended sediment stock* (Fig. 5.3b), as a function of  $\alpha$  for various  $Q$ . When keeping  $Q < 60$  m<sup>3</sup>/s and for increasing  $\alpha$ , the near-bed sediment concentration and stock gradually increase up to a critical value of  $\alpha$ . For  $\alpha$  larger than this critical value, the near-bed concentration and stock jump to much larger values; the solution jumps to a different branch. The existence of two branches and the abrupt jump is related to a strong positive feedback between sediment-induced turbulence damping and sediment import by the  $M_2 - M_4$  tidal asymmetry, elaborated on in Chapter 4: if the suspended sediment concentration is sufficiently low (lower branch), this feedback is weak. For sufficiently high sediment concentrations (upper branch), however, this feedback dominates the sediment dynamics. On the upper branch, the sediment concentration and stock keep increasing when further increasing  $\alpha$ . Only for very low discharges ( $Q \sim 30$  m<sup>3</sup>/s) does a further increase of  $\alpha$  leads to a decrease in the suspended sediment concentration and stock. This is because sediment is pushed closer to the upstream boundary, where it deposits on the bed and cannot be kept in suspension due to the low flow velocities.

Examples of the spatial distribution of sediment corresponding to the branches are plotted in Fig. 5.3c-5.3d. The lower branch of equilibrium solutions corresponds to a single narrow ETM located around km 20-30 (Fig. 5.3c), characteristic of historical conditions in the Ems. The upper branch of solutions corresponds to a double ETM near km 30 and 60 (Fig. 5.3d), with high concentrations in the entire zone between the two ETM, characteristic for current conditions. We thus define the two branches as different regimes and the transition between the branches as a regime shift (cf. definition in Section 5.1).

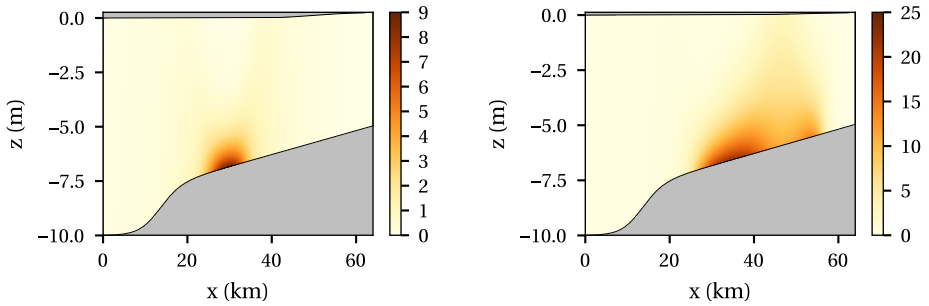


**Figure 5.2:** Evolution of the bed profile in the Ems, with in (a) the development of the bed profile parameter  $\alpha$  (Eq. (5.1)) over time, obtained by fitting to observed depths in 1965, 1981, 1990, 1992 and 2005. In (b)-(f) the resulting smooth fitted depth profiles (solid lines) in these years are plotted together with observed thalweg depth (dots). (f) additionally shows the smooth fitted profiles of the other years for comparison.



(a)  $c_{bed}$

(b) Suspended stock



(c) Subtidal sediment concentration (in  $\text{kg/m}^3$ ) for settings corresponding to the orange circle in (a)-(b). (d) Subtidal sediment concentration (in  $\text{kg/m}^3$ ) for settings corresponding to the orange cross in (a)-(b).

**Figure 5.3:** Modelled dynamic equilibrium solution for the maximum near-bed concentration (a) and total amount of suspended sediment (b) as a function of the bed profile parameter  $\alpha$  and river discharge  $Q$ . For  $Q < 70 \text{ m}^3/\text{s}$ , two branches of solutions are found characterising low and high sediment concentration regimes. The branches overlap for specific  $\alpha$  and  $Q$  and the transition between the two branches is discontinuous. Two distributions of the subtidal sediment concentration are plotted in (c) and (d) for  $Q = 50 \text{ m}^3/\text{s}$  and  $\alpha = 0.8$ , corresponding to the lower branch ((c), orange circle in (a)-(b)) and upper branch ((d), orange cross in (a)-(b))

The two branches can overlap for specific  $\alpha$  and  $Q$ , e.g. for  $Q = 50 \text{ m}^3/\text{s}$  they overlap for  $\alpha$  between 0.75 and 0.9. Thus, there is a range of values of  $\alpha$  and  $Q$  for which multiple equilibrium solutions exist. Therefore if, given a constant  $Q$ , the equilibrium state of the estuary evolves from the lower to the upper branch, the depth needs to be decreased in order to evolve back to the lower branch again, thus creating hysteresis in the model behaviour for increasing and decreasing depth. Mathematically, such behaviour is known as a double saddle-node bifurcation.

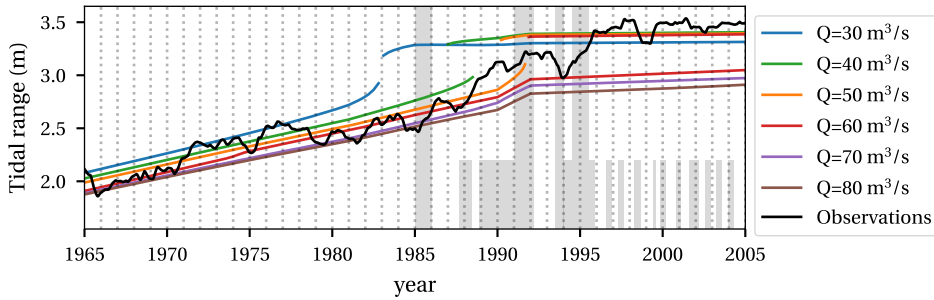


**Figure 5.4:** The observed 28-day averaged tidal range in Papenburg (black line) and modelled equilibrium solutions for the tidal range (approximated as twice the  $M_2$  tidal amplitude) in Papenburg as a function of time and  $Q$ . The model results are obtained by varying the bed profile parameter  $\alpha$  and then relating  $\alpha$  to the year using Fig. 5.2a. The model results shows two branches of solutions corresponding to the branches of low and high sediment concentrations in Fig. 5.3. The tall grey bands in the figure indicate the times of the official deepening campaigns. The smaller grey bands indicate the times of maintenance dredging since 1985 according to Lange (2007).

#### 5.4. THE TRANSITION PROCESS IN TIME

While the equilibrium state makes sudden transitions between the two identified regimes as a function of the river discharge and depth, the actual state of the estuary constantly adapts to this equilibrium by gradually importing or exporting sediment. This adaptation takes time and the timescale of this process cannot be identified from model. Therefore, information about the adaptation timescale is obtained by comparing the modelled equilibrium state to observations. Since there are too few observations of the historical evolution of the sediment concentration, we cannot infer information about adaptation time scales directly from sediment concentration measurements. However, an increasing sediment concentration leads to sediment-induced damping of turbulence, which can be observed as an increasing tidal range. As high time-resolution measurements of the tidal range are available since the 1950s, we use the tidal range to estimate the adaptation time scale.

The observed 28 day-averaged tidal range in Papenburg (km 50) between 1965 and 2005 is shown by the black line in Fig. 5.4. The modelled equilibrium tidal range in Papenburg, approximated as twice the  $M_2$  tidal amplitude, is shown by the coloured lines for various values of the river discharge. The model results show a lower branch, which corresponds to the low concentration regime (Section 5.3), characterised by a single narrow ETM, and an upper branch, which corresponds to the high concentration regime, characterised by two ETM and a wide highly turbid zone.

The observations indicate that the tidal range increased gradually between 1965 and 1989, even though there is a significant year-to-year fluctuation. These fluctuations remain roughly within the range of modelled tidal ranges on the lower branch using  $Q$  between 30 and 150  $\text{m}^3/\text{s}$ . As stated above, this lower branch corresponds to the lower branch of sediment concentrations with gradually increasing concentration in one narrow ETM around km 20-30. This is supported by observations of the sediment concen-

tration in the 1970s (De Jonge et al., 2014), which place the ETM around this location, and records of the bed material composition along the estuary in 1989 (BfG, 2017), which show mostly small amounts of fines ( $< 63 \mu\text{m}$ ) in the bed, except around km 20-30.

Between 1989 and 1994, the observed tidal range diverges from the modelled tidal range on the lower branch, marking the onset of the regime shift. Observational evidence seems to support 1989 as the starting year of the regime shift. Lange (2007) and references therein report a 7-fold increase in the dredging volume near Herbrum, comprising higher ratios of mud following the spring of 1989. Furthermore, De Jonge et al. (2014) report observed surface concentrations in 1992-1993, which are similar to those in 2005. Nevertheless, water quality between 1990 and 1993 was still assessed as 'moderately-critically burdened' (*German: mäßig-kritisch belastet*), indicating good biodiversity and oxygen conditions, better than any other German tidal river at the time (Lange, 2007).

The observed tidal range first attains levels matching the modelled tidal range on the upper equilibrium branch in 1994-1995 and observations remain close to this branch after 1995. This implies that the high sediment concentration regime prevails throughout these years. After 1995, hypoxic conditions were measured over prolonged times (Talke et al., 2009a), the water quality in 2004 was described as 'strongly-excessively polluted' (*German: stark-übermäßig verschmutzt*) (Lange, 2007), and sediment concentrations measured since 2006 show levels of 30-200 g/l (Talke et al., 2009b; Wang, 2010; Papenmeier et al., 2013; Becker et al., 2018).

The development of the observed tidal range in the transition years 1989-1995 gives an indication about the typical timescales required to adapt to changing regimes. In these years, the equilibrium associated with high sediment concentrations only exists for low discharges ( $Q < 50 - 70 \text{ m}^3/\text{s}$ ), while the equilibrium associated with low sediment concentrations is the only equilibrium for larger discharges. The observed tidal range is between the two equilibrium branches and does not show large seasonal oscillations between these two branches, known as *flickering* (e.g. Scheffer et al., 2009), related to seasonal variations in the river discharge. This indicates that the timescale to adapt to new equilibrium conditions is considerably larger than a season. In other words, both sediment import and flushing of accumulated sediment happen on a timescale that is longer than the few months of consistently low and high river discharge that occur each year. Furthermore, the figure indicates that regime shift occurs between 1989 and 1995, meaning that adaptation timescale is less than seven years. This is much shorter than the timescale of decades hypothesised by Winterwerp et al. (2013). As the deepening operations followed each other within the timescale of the regime shift, one could argue that the timescale of the regime shift changed while it was unfolding but remained of the order of several years.

## 5.5. DISCUSSION

### 5.5.1. MODEL INTERPRETATION AND LIMITATIONS

The state of the Ems since the regime shift is characterised by a thick layer of fluid mud with concentrations of up to several tens to hundreds grams per litre. Due to the model simplifications, including the assumption of a depth uniform, time-independent eddy viscosity and eddy diffusivity, the iFlow model cannot reproduce the specific behaviour

associated with such a strongly layered system. As a result, the model disregards some potentially essential sediment processes in this highly turbid regime (e.g. Becker et al., 2018; Winterwerp et al., 2017). However, the model is expected to capture the essential sediment transport processes in the low-concentration regime. The model results should therefore be interpreted as a model extrapolation of the processes essential in the low-concentration regime to a larger depth. The results show under what conditions these processes allow for the onset of a regime shift. After the regime shift, the model results cannot be expected to represent all the essential processes.

The conclusion that transitional behaviour took place over a timescale of several years strongly motivates study into the seasonal behaviour during the transition period. Such a study is necessary to get a better understanding of the dynamic processes causing the sediment to remain in the estuary during times of high discharges, which cannot be captured in our equilibrium model.

### 5.5.2. IMPLICATIONS FOR OTHER ESTUARIES

While channel deepening has led to highly increased sediment concentrations in the Ems, we stress that it is not generally true that channel deepening implies sediment import and higher sediment concentrations as was hypothesised by Winterwerp and Wang (2013). As shown by Dijkstra et al. (2019) the effect of channel deepening on the sediment concentration strongly depends on the physical mechanisms that dominate the sediment dynamics and the effect of deepening on each of these mechanisms. The Loire River is thought to have become hyperturbid over time as a consequence of deepening, but this is yet to be proven (Winterwerp et al., 2013). On the other hand, an example where models have shown that deepening does not lead to large increase of the sediment concentrations are provided by e.g. van Maanen and Sottolichio (2018) for the Gironde Estuary. This suggests that system specific modelling of individual estuaries is essential to determine the effect of deepening on the sediment concentration.

## 5.6. CONCLUSIONS

Using the idealised width-averaged iFlow model representing the lower Ems River, we investigated the development of the dynamic equilibrium sediment concentration as a function of the channel depth and river discharge. For sufficiently low river discharge ( $Q < 70 \text{ m}^3/\text{s}$ , approximately 60% of the time), we found two types of dynamic equilibria or regimes. The first regime is characterised by one narrow ETM around km 20-30 and generally moderate sediment concentrations. The second regime is characterised by two ETM, which together form a wide ETM zone between roughly km 30 and 60, with high sediment concentrations in the entire zone. The dynamics in this regime is dominated by sediment-induced reduction of turbulence, which is also expressed in amplification of the tidal range. This study is the first to show that both regimes coexist for certain depth profiles. The regime shifts from the low to the high concentration regime when the estuary becomes deeper than a discharge-dependent critical channel depth.

From a comparison between the model results and long-term observations of the tidal range in Papenburg, the timescale of the regime shift was found to be much shorter than thought earlier, taking a few years since 1989 instead of decades. The available historical observations of sediment concentrations support this timescale estimate.

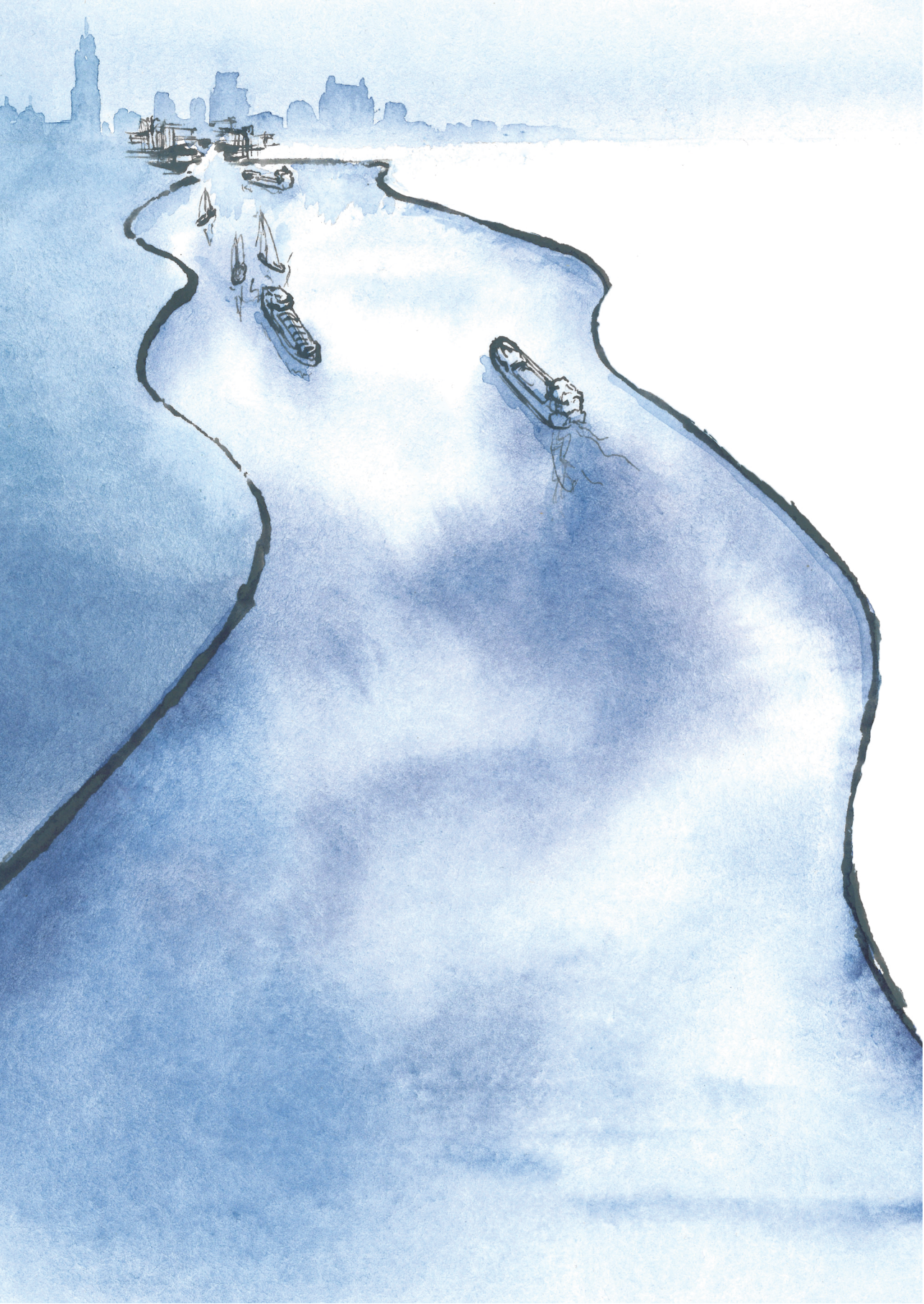


## REFERENCES

- Becker, M., Maushake, C., and Winter, C. (2018). Observations of mud-induced periodic stratification in a hyperturbid estuary. *Geophysical Research Letters*, 45:5461–5469.
- BfG (2017). Sedimentmanagementkonzept Tideems. Gutachten im Auftrag des WSA Emden. Technical Report BfG-Bericht 1944, Bundesanstalt für Gewässerkunde, Koblenz. In German.
- Biggs, R., Carpenter, S. R., and Brock, W. A. (2009). Turning back from the brink: Detecting an impending regime shift in time to avert it. *Proceedings of the National Academy of Sciences*, 106:826–831.
- Brouwer, R. L., Schramkowski, G. P., Dijkstra, Y. M., and Schuttelaars, H. M. (2018). Time evolution of estuarine turbidity maxima in well-mixed, tidally dominated estuaries: the role of availability- and erosion-limited conditions. *Journal of Physical Oceanography*, 48:1629–1650.
- De Jonge, V. N., Schuttelaars, H. M., Van Beusekom, J. E. E., Talke, S. A., and De Swart, H. E. (2014). The influence of channel deepening on estuarine turbidity levels and dynamics, as exemplified by the Ems estuary. *Estuarine Coastal and Shelf Science*, 139:46–59.
- Dechend, W. (1950). Die geologischen Untersuchungen in der Ems. Technical report, WSA Emden. In German.
- Dijkstra, Y. M., Schuttelaars, H. M., Schramkowski, G. P., and Brouwer, R. L. (2019). Modeling the transition to high sediment concentrations as a response to channel deepening in the Ems River Estuary. *Journal of Geophysical Research: Oceans*, 124:1–17.
- Krebs, M. and Weilbeer, H. (2008). Ems-Dollart Estuary. *Die Küste*, (74):252–262.
- Lange, J. (2007). Ausbau der Unterems. Eine Chronik der Maßnahmen seit 1984 mit einer Bewertung der Umweltfolgen. Technical report, WWF Germany, Frankfurt. In German.
- NLWKN (2008). Deutsches Gewässerkundliches Jahrbuch Weser- und Emsgebiet 2005. Technical report.
- Papenmeier, S., Schrottke, K., Bartholomä, A., and Flemming, B. W. (2013). Sedimentological and rheological properties of the water-solid bed interface in the Weser and Ems Estuaries, North Sea, Germany: Implications for fluid mud classification. *Journal of Coastal Research*, 29:797–808.
- Scheffer, M., Bascompte, J., Brock, W. A., Brovkin, V., Carpenter, S. R., Dakos, V., Held, H., van Nes, E. H., Rietkerk, M., and Sugihara, G. (2009). Early-warning signals for critical transitions. *Nature*, 461:53–59.
- Scheffer, M., Carpenter, S., Foley, J. A., Folke, C., and Walker, B. (2001). Catastrophic shifts in ecosystems. *Nature*, 413(6856):591–596.
- Talke, S. A., De Swart, H. E., and De Jonge, V. N. (2009a). An idealized model and systematic process study of oxygen depletion in highly turbid estuaries. *Estuaries and Coasts*, 32:602–620.
- Talke, S. A., De Swart, H. E., and Schuttelaars, H. M. (2009b). Feedback between residual circulations and sediment distribution in highly turbid estuaries: an analytical model. *Continental Shelf Research*, 29:119–135.
- van Maanen, B. and Sottolichio, A. (2018). Hydro- and sediment dynamics in the Gironde estuary (France): sensitivity to seasonal variations in river inflow and sea level rise. *Continental Shelf Research*, 165:37–50.
- Van Maren, D. S., Winterwerp, J. C., and Vroom, J. (2015). Fine sediment transport into the hyperturbid lower Ems River: the role of channel deepening and sediment-induced drag reduction. *Ocean Dynamics*, 65:589–605.
- Wang, L. (2010). *Tide Driven Dynamics of Subaqueous Fluid Mud Layers in Turbidity Maximum Zones of German Estuaries*. PhD thesis, University of Bremen.
- Winterwerp, J. C., Vroom, J., Wang, Z. B., Krebs, M., Hendriks, E. C. M., Van Maren, D. S., Schrottke, K., Borgsmüller, C., and Schöl, A. (2017). SPM response to tide and river flow in the hyper-turbid Ems River. *Ocean Dynamics*, 67:559.
- Winterwerp, J. C. and Wang, Z. B. (2013). Man-induced regime shifts in small estuaries - I: theory. *Ocean Dynamics*, 63:1279–1292.

Winterwerp, J. C., Wang, Z. B., Van Brackel, A., Van Holland, G., and Kösters, F. (2013). Man-induced regime shifts in small estuaries - II: a comparison of rivers. *Ocean Dynamics*, 63:1293–1306.





# CHAPTER 6

Can the Scheldt River Estuary become hyperturbid?  
A model analysis of suspended sediment concentrations and  
transport in response to channel deepening

Dijkstra, Y. M., Schuttelaars, H. M., and Schramkowski, G. P. (*Submitted to Ocean Dynamics*). Can the Scheldt River Estuary become hyperturbid? A model analysis of suspended sediment concentrations and transport in response to channel deepening.

## Abstract

---

We investigate the hypothesis by Winterwerp and Wang (2013, OD 63:1279–1292) that channel deepening in the Scheldt River Estuary could lead to a large increase in suspended sediment concentrations, with subsequent severe consequences to primary production and navigation. To this end, we use an idealised model to investigate the long-term development of the sediment concentration under the uncertainty of future changes in model parameter values and channel deepening. The water motion is calibrated to recent conditions after which the sediment concentration is validated against long-term observations and is subsequently tested for a wide range of parameter settings and deepening scenarios. We also investigate the effect of anthropogenic dumping of dredged sediments in the estuary on the sediment concentration.

Deepening the channel, but keeping all other model parameters the same, we find lower long-term average sediment concentrations in most of the estuary. Thereby our results suggest that deepening in the Scheldt alone cannot lead to high sediment concentrations, and we reject the investigated hypothesis. Further study of uncertain model parameters reveals that an increase of the erosion parameter by an order of magnitude allows for the development of high concentrations of several 10s of g/l near the bed in narrow turbidity zones. It is unknown whether such an increase of the erosion parameter can happen in the future, which stresses the importance of further research into the factors that can lead to a change of this parameter.

---



## 6.1. INTRODUCTION

Suspended sediment dynamics is an important subject in the management of the Scheldt River Estuary, an estuary located in Belgium and Netherlands, see Fig. 6.1. Its importance is related to two factors. Firstly, primary production in the Scheldt estuary is to a large extent light limited due to suspended sediments (Kromkamp and Peene, 1995). Secondly, dredging of fine sediments poses a significant cost in the maintenance of the navigation channel to the port of Antwerp (IMDC et al., 2013b). These issues related to fine sediments have become increasingly important, as the long-term suspended sediment concentration has gradually increased by several 10s of mg/l over the last three decades in the Lower Sea Scheldt (km 55-95) and locally in the dry season in the Upper Sea Scheldt (> km 95) (Vandenbruwaene et al., 2016; Maris et al., 2017). At the same time, many anthropogenic changes to the estuary have been made, including extensive deepening of the channel for the mining of sand and improvement of navigability, the construction of locks and harbour basins and the development of intertidal area (see Van Braeckel et al. (2006) and Jeuken et al. (2007) for an overview). Moreover, sewage treatment has improved, thereby affecting the organic content of sediments and hence sediment properties (Maris and Meire, 2017).

It has been suggested by Winterwerp and Wang (2013) that deepening in the long-term may lead to the development of *hyperturbid conditions* in the Scheldt (see definition in Section 1.2.3). According to their hypothesis, deepening causes a deformation of the tide that leads to an increasing import of fine sediment. The imported sediment leads to a reduction of the hydraulic drag, which supposedly leads to a further deformation of the tide and more sediment import, hence leading to a dramatic increase of the sediment

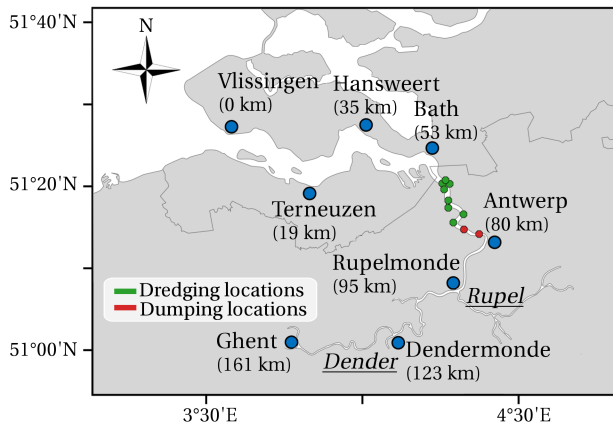


**Figure 6.1:** Map of the tidal part of the Scheldt River from Vlissingen to Ghent. The Scheldt River is separated into the Dutch Western Scheldt (< km 55) and the Belgian Sea Scheldt (> km 55). At the head of the estuary, the estuary is fed by water from the Upper Scheldt - Leie catchment. Two more tributaries are marked on the map in italics: the Dender and Rupel Rivers. Major locations where fine sediments are dredged and dumped in the Sea Scheldt are marked in green and red, respectively. Dredging and dumping also happens in the Western Scheldt but in smaller amounts, which are not considered in this study.

concentration. This hypothesis is mainly based on examples of the Ems (Germany) and Loire (France) Rivers, which have become hyperturbid following decades of substantial channel deepening. Despite regular and long-term monitoring of sediment concentrations in the Scheldt River since the 1990s, it remains unclear whether the observed long-term trends are part of a development towards hyperturbidity (Vandenbruwaene et al., 2016; Maris et al., 2017). Statistical analysis of trends in the observations is not only complicated by a high degree of natural variability but also by memory effects, by which the sediment concentration depends on both the hydrodynamic conditions of several months in the past (Brouwer et al., 2018) and recent sediment dredging and dumping. Sediments dredged in the port of Antwerp are dumped back into the channel of the estuary a few kilometres upstream at rates that far exceed fluvial sediment supply. Hence, variations in the observed sediment concentrations are strongly influenced by the spatial and temporal variability in anthropogenic sediment dredging and dumping (e.g. Depreiter et al., 2015). While such memory effects and the effects of dredging and dumping are included in models, only a few model projections have been made of the response of sediment concentrations to channel deepening (Van Kessel et al., 2008) and dumping strategy (Van Kessel and Vanlede, 2010; IMDC et al., 2013a). Some of the main challenges for such modelling studies are the long timescales at which the sediment concentration varies and large uncertainty in model parameters.

## 6

The goal of this study is to investigate if the Scheldt River can become hyperturbid as a response to channel deepening given the uncertainty in model parameters values. Moreover, we aim to gain insight into the processes and parameters that are most important to the sediment dynamics in the Scheldt. It should be stressed that we do not aim to explicitly describe variability on weekly, seasonal or yearly timescales in the past or future. Rather, we want to qualitatively capture the most important underlying physics, which allows us to extrapolate the modelled trends to uncertain future scenarios and the corresponding long-term average behaviour. To this end, we use the iFlow model (Chapter 2), which is a width-averaged, idealised process-based model. The model is used to directly compute the long-term equilibrium water motion and sediment concentration given prescribed geometry and forcing conditions, thus quickly showing the long-term response of the estuary to changing depth and model parameters. As the model is fast, it allows for extensive study of parameter sensitivity.

The set-up of the iFlow model used in this study is based on the model used in Chapter 4 to simulate the transition to hyperturbid conditions in the Ems after channel deepening. In addition, several processes thought to be essential for the sediment dynamics in the Scheldt River are added (Section 6.2). The model is calibrated against water levels for conditions of the year 2010 and modelled sediment concentrations are presented and compared to the long-term averaged observations (Section 6.3). Furthermore, the sensitivity of the results to the sediment settling velocity and erosion parameter is systematically analysed. Next, in Section 6.4, the model is applied to configurations with smaller and larger depths, investigating the response to past and possible future large-scale deepening. The physical processes explaining the results are analysed in Section 6.5. These processes are discussed in the context of the processes that act in the Ems estuary and in context of the model uncertainty in Section 6.6. This chapter ends with a summary of the main conclusions in Section 6.7.



## 6.2. MODEL AND METHODS

### 6.2.1. THE iFLOW MODEL

The model used in this study is the iFlow model (Chapter 2), a width-averaged idealised process-based model for water motion and sediment dynamics in estuaries and tidal rivers. Following the approach taken in Chapter 4, the model resolves subtidal,  $M_2$  and  $M_4$  water motion and sediment dynamics in a dynamic equilibrium state. This is done by solving approximations of the width-averaged continuity, momentum and sediment balance equations. The model also accounts for sediment-induced damping of turbulence, which represents the reduction in turbulent mixing due to vertical density stratification by sediment, and hindered settling, which represents a decreased sediment settling velocity due to particle-particle interactions when sediment concentrations are high. The model is forced by constant  $M_2$  and  $M_4$  tidal amplitudes and a subtidal depth-averaged sediment concentration at the mouth. Furthermore, constant river discharges are prescribed at the head of the estuary and at the confluences with the Dender and Rupel tributaries (see Fig. 6.1), and a discharge-dependent fluvial supply of sediments is prescribed at the discharge locations.

Depth and width profiles are represented in the model by smooth fits of the measured bathymetry, thereby ignoring the effect of small-scale bathymetric features on the estuary-scale dynamics. Additionally it is assumed that the water surface elevation is small compared to the subtidal depth. These assumptions allow for the use of scaling and perturbation methods, which lead to systems of mathematical equations that can be solved at low computational costs and allow for making a decomposition of the water motion and sediment transport into contributions by individual physical forcing mechanisms. The model is additionally solved in terms of tidal constituents in a dynamic equilibrium state, thereby preventing the need for time stepping routines. This leads to a further reduction in computational costs, as no spin-up time is required, and it leads to numerically accurate results as the model does not suffer from the accumulation of numerical errors over time.

The mathematical description of new model components related to input of fresh water and sediment from tributaries are discussed in Appendix 6.A, and an overview of the model for sediment-induced damping of turbulence and hindered settling is provided in Chapter 4. For a further detailed description of the basic model equations and solution methods we refer to Chapter 2.

The equations form a non-linear set of equations that is solved iteratively using the procedure summarised in Figure 6.2. The solution procedure consists of a combination of algebraic relations and numerical and analytical solution methods, where analytical methods are used for speed and accuracy whenever possible. The numerical computation of the water level and erodibility are done using a second-order finite difference method on an equidistant grid with 250 grid cells.

### 6.2.2. DESCRIPTION OF THE SCHELDT RIVER ESTUARY AND MODEL FORCING

The Scheldt River Estuary is modelled as a single channel from the mouth at Vlissingen to the tidal weir and locks at Ghent, 161 km upstream. Tidal propagation into the tributaries (see Fig. 6.1) is not explicitly taken into account. The width of the Scheldt in the

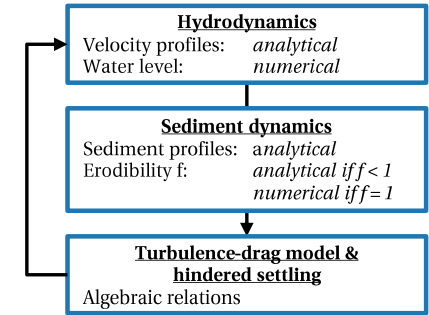


**Figure 6.2:** Summary of the model components (boxes) and the solution methods (in italics), indicating the iteration over the components by arrows.

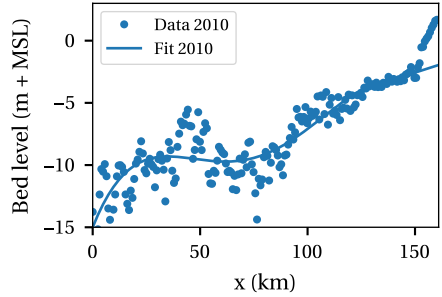


**Figure 6.3:** Bed level of the Scheldt in 2010 relative to mean sea level at Vlissingen ( $x = 0$ ). Dots represent the observed width-averaged bed level. The line is the smooth polynomial fit of the data used in the model.

	Discharge ( $\text{m}^3/\text{s}$ )	Upper Scheldt-Leie (km 161)	Dender (km 123)	Rupel (km 95)
Average	110	32%	10 %	58 %
Summer	56	27%	8 %	65 %
Winter	170	36%	11 %	53 %

**Table 6.1:** Discharge averaged over the year, summer (Jul-Sep) and winter (Jan-Mar) averaging over 1971 to 2017 and the percentage of river discharge per tributary. The contribution of the Rupel equals the sum of the contributions of its tributaries. Data from [www.waterinfo.be](http://www.waterinfo.be).

model is represented by the average of the width at the surface at high and low water and is fitted by a smooth function. The width-averaged depth of the Scheldt is derived by dividing the cross-sectional area by the width at high and low water, subsequently subtracting the average water level elevation at high and low water and then taking the average. The resulting depth is fitted using a smooth polynomial function, see Fig. 6.3. The procedure for deriving the depth is slightly different to that used by Brouwer et al. (2018) for the Scheldt and is used because, in contrast to the procedure of Brouwer et al. (2018), it can be repeated for the historical high and low water data used in Section 6.4.

The model is forced by an  $M_2$  and  $M_4$  tide at the mouth, representing year-averaged tidal conditions, obtained using a complex demodulation analysis (e.g. Jalón-Rojas et al., 2016) on the 10-minute resolution tidal elevation observations at Vlissingen for 2009. This yields an  $M_2$  amplitude of 1.81 m and an  $M_4$  amplitude of 0.16 m with a relative phase difference between the  $M_2$  and  $M_4$  tide of -4 degrees. Fresh water discharges into the Scheldt at three locations: at the upstream boundary from the Upper Scheldt - Leie system, at Dendermonde (km 123) from the Dender tributary and at Rupelmonde (km 95) from the Rupel tributary. The Rupel has several tributaries itself and its fresh water discharge equals the sum of the discharges of its tributaries. We use the average discharge for a year, summer (Jul-Sep) and winter (Jan-Mar) averaged over the years 1971-2017 (data from [www.waterinfo.be](http://www.waterinfo.be)), see Table 6.1.

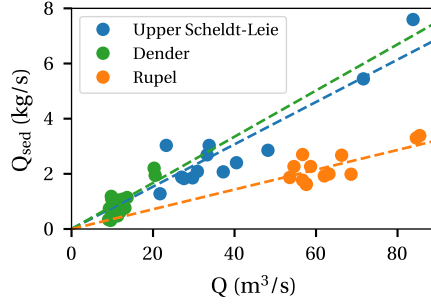


**Figure 6.4:** Estimated year-averaged fluvial sediment supply  $Q_{\text{sed}}$  for the three major tributaries as a function of the year-averaged discharge per tributary. Each dot represents a year between 2001 and 2015 (2012 and 2014 are missing). The dotted lines are linear least-squares fits through the data. Estimates of  $Q_{\text{sed}}$  are from Vanlierde et al. (2014), Vanlierde et al. (2016) and Vandenbruwaene et al. (2017).

Several methods can be used to estimate the fluvial sediment supply as a function of the river discharge. Vanlierde et al. (2016) present a simple regression model relating the instantaneous sediment concentration from 7-hourly measurements to the instantaneous river discharge for data of 2015. However, the number of data points and quality of the fit are low, so that this method is not reliable for estimating the long-term sediment supply. Therefore we choose to correlate the year-averaged estimated fluvial sediment supply and year-averaged river discharge of each tributary. The fluvial sediment supply is estimated using sediment concentration data obtained from weekly samples near the river bank between 2001 and 2015 (data from Vanlierde et al. (2014), Vanlierde et al. (2016) and Vandenbruwaene et al. (2017)), see Fig. 6.4. A linear fit is chosen over more conventional power-relations to prevent over-fitting of the small amount of data. The obtained relations for the fluvial sediment load (in kg/s) read

$$Q_{\text{sed, Upper Scheldt-Leie}} = 0.080 Q_{\text{Upper Scheldt-Leie}}, \quad (6.1)$$

$$Q_{\text{sed, Dender}} = 0.088 Q_{\text{Dender}}, \quad (6.2)$$

$$Q_{\text{sed, Rupel}} = 0.035 Q_{\text{Rupel}}. \quad (6.3)$$

A comparison of 7-hourly and weekly sediment measurements by Plancke et al. (2017) indicate that fits of Eqs. (6.1)-(6.3) likely underestimate the sediment supply per tributary by a factor 3 to 6 (3.5 for the entire estuary for 2016). However, as the 7-hourly data are only available for a few years, we base our fits on the weekly data. Sensitivity study showed that increasing the fluvial supply by a factor 3 to 6 does not notably change the results presented in this study.

At the seaward boundary, a depth- and tide-averaged sediment concentration  $c_{\text{sea}} = 0.06 \text{ kg/m}^3$  is prescribed, based on observations. The sediment settling velocity  $w_{s,0}$  is set to 2 mm/s based on the average settling velocity of the flocs, as measured during a one-day campaign in February 2005 near the port of Antwerp (IMDC et al., 2007). The erosion parameter  $M$  is calibrated in such a way that the model captures the order of magnitude of the maximum surface concentration observed in the estuary in 2010. The

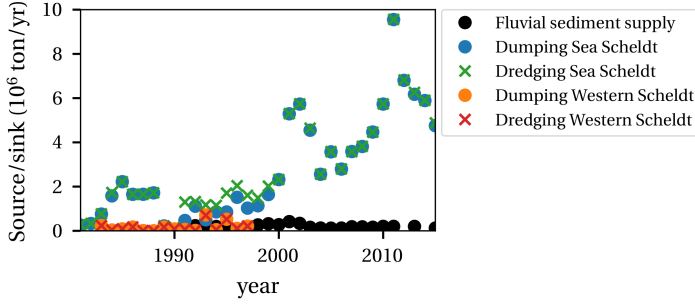


**Figure 6.5:** Reported dredging and dumping of fine sediments in the Western Scheldt (< km 55) and Sea Scheldt (> km 55) per year in Million ton/yr, compared to the estimated yearly fluvial sediment supply from all tributaries combined. Data on dredging and dumping are from IMDC et al. (2013b), Vandenbruwaene et al. (2016) and Barneveld et al. (2018).

sensitivity of the model results to  $w_{s,0}$  and  $M$  is investigated in Section 6.3.3. The default values of the model parameters are given in Table 6.2.

Salinity is represented in the model by a depth uniform and tide-averaged profile along the estuary, according to Talke et al. (2009)

$$s = \frac{s_{\text{sea}}}{2} \left( 1 - \tanh \left( \frac{x - x_c}{x_l} \right) \right), \quad (6.4)$$

where the model parameters are fitted surface salinity data gathered within the MWTL (Western Scheldt) and OMES (Sea Scheldt) programmes between 1982 and 2016. This yields  $s_{\text{sea}} = 31$  psu,  $x_l = 32$  km. The salt-intrusion length scale  $x_c$  is related to the discharge as  $x_c = \alpha \left( \frac{Q}{Q_{\text{average}}} \right)^\beta$ , where  $\alpha = 41$  km,  $\beta = -0.24$  and  $Q_{\text{average}} = 110 \text{ m}^3/\text{s}$ .

### 6.2.3. DREDGING AND DUMPING

Dredging of fine sediments predominantly takes place at eight sills, lock entrances and harbour basins located between km 60 and 71, see the green dots in Fig. 6.1 (IMDC et al., 2013b). All of the dredged fine sediments are dumped back into the navigation channel a few kilometres upstream at Punt van Melsele (km 73) and Plaat van Boomke / Oosterweel (km 78), see the red dots in Fig. 6.1. Exceptions are the years 1990-2000, when 300,000 ton dry fine sediment was removed from the estuary. Fig. 6.5 shows the amount of dredging and dumping in the Western Scheldt (< km 55) and Sea Scheldt (> km 55) in tons of dry sediment per year, compared to the estimated fluvial fine sediment supply from all tributaries (data from IMDC et al. (2013b), Vandenbruwaene et al. (2016) and Barneveld et al. (2018)). This shows that the sediment source due to dumping exceeds the fluvial supply by an order of magnitude.

As harbour basins, sills and shallow areas are not explicitly resolved by the model, sediment deposition is not fully resolved. Therefore we do not take dredging into account in the model, but we do consider dumping. Dumping of sediment is represented using continuous point sources at km 73 and 78 with rates of 60.5 and 98.5 kg/s, respec-

	Parameter		Value
Hydrodynamics	$A^0$	$M_2$ water level amplitude at $x=0$	1.81 m
	$A^1$	$M_4$ water level amplitude at $x=0$	0.16 m
	$\phi^1$	$M_4$ water level phase relative to $M_2$ tide at $x=0$	-4 deg
Sediment	$c_{\text{sea}}$	depth-averaged subtidal concentration at $x=0$	$0.06 \text{ kg/m}^3$
	$K_h$	Horizontal eddy diffusivity	$100 \text{ m}^2/\text{s}$
	$M$	Erosion parameter	$7 \cdot 10^{-4} \text{ s/m}$
	$w_{s,0}$	Clear-water settling velocity	$2 \text{ mm/s}$
	$c_{\text{gel}}$	Gelling concentration	$100 \text{ kg/m}^3$
Turbulence	$\sigma_\rho$	Prandtl-Schmidt number ( $=A_\nu/K_\nu$ for $Ri = 0$ )	1
	$u_{z,\text{min}}$	Velocity gradient for background turbulence production	$0.03 \text{ 1/s}$

**Table 6.2:** Default model parameters.

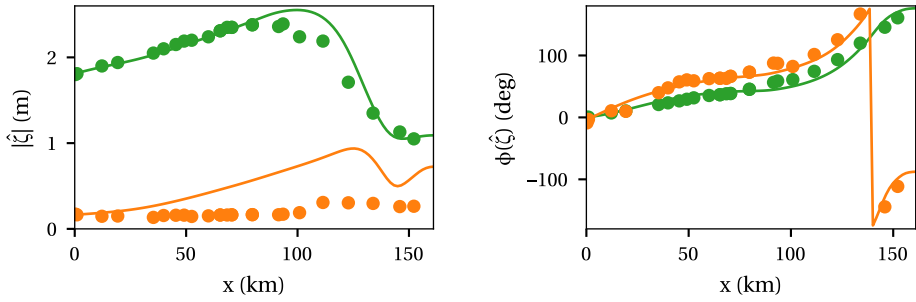
tively, corresponding to the average dumping rate in the Sea Scheldt between 2001 and 2015. Dumping of sediment in the Western Scheldt is neglected as the dumping volumes are relatively small, especially when considering the much larger volume of the Western Scheldt.

### 6.3. RESULTS AND SENSITIVITY OF THE 2010 CASE

#### 6.3.1. MODEL CALIBRATION

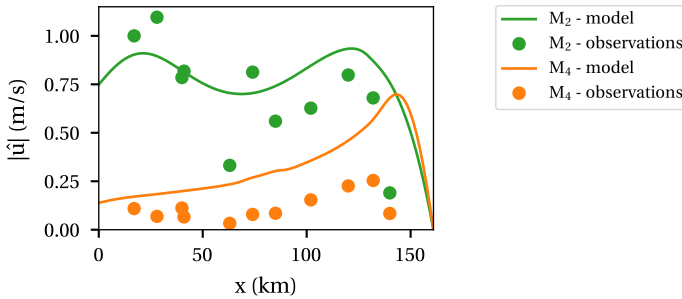
The  $M_2$  water level is calibrated to observations by varying the roughness parameter until a best fit to data is found; the optimal dimensionless roughness value is  $z_0^* = 5 \cdot 10^{-4}$ . The resulting  $M_2$  and  $M_4$  water level amplitude and phase and cross-sectionally averaged velocity amplitude are plotted in Fig. 6.6. The model results are compared to water level observations from 2009 and velocity observations from one 13-hour cross-section measurement in 2009 (data from Rijkswaterstaat, HIC and Flanders Hydraulics Research). The data are analysed using complex demodulation after which the average amplitude and phase over the year is used. The overall observed patterns for the  $M_2$  tidal amplitude are reproduced, but the  $M_4$  tidal amplitude is overestimated locally by more than a factor two. The tidal phases of both the  $M_2$  and  $M_4$  tide are reproduced well.

The modelled  $M_2$  tidal velocity shows two maxima near km 20 and km 120 and minima at the mouth, km 70 and at the landward boundary, where the tide vanishes. The same pattern is observed in the measurements and the overall magnitude of the modelled velocity corresponds to the measurements. The modelled  $M_4$  velocity increases up to km 140 before it vanishes at the landward boundary. While a maximum in the  $M_4$  velocity in the upstream part of the estuary is also found in the measurements, measured velocities are much lower than the modelled velocities, similar to what was found for the tidal elevation.



(a) Water level amplitude

(b) Water level phase



(c) Cross-sectionally averaged velocity amplitude

**Figure 6.6:** Water level amplitude (a) and phase (b) and cross-sectionally averaged velocity amplitude (c) for the  $M_2$  tide (green) and  $M_4$  tide (red). The model results are represented by the solid lines and compared to year-averaged observations from 2009 in dots.

### 6.3.2. SEDIMENT CONCENTRATION COMPARED TO DATA

In order to verify the performance of the model, we compare the modelled sediment concentration in the 2010 case using default parameter settings and the year-averaged discharge (Table 6.2) to long-term averages of sediment concentration observations. Observations of surface sediment concentrations were collected between 1990-2015 within the MWTL (Western Scheldt) and OMES (Sea Scheldt) programmes. The data was gathered bi-weekly to monthly, independent of the tidal conditions, by taking water samples (see Maris and Meire (2017) for details on the OMES programme). Observations of the depth-averaged sediment concentration were collected in the period 2001-2015 as part of the OMES programme and are based on pump samples at different depths with approximately equal coverage of the entire water column (Vandenbruwaene et al., 2016). Finally, we have included data from four permanent optical measurement stations at a depth roughly halfway the average water depth, hence roughly representing depth-averaged concentrations. Variations on time-scales smaller than one  $M_2$  tidal cycle have been filtered from the observations (see the caption of Fig. 6.7 for more information per station).

Modelled subtidal sediment concentrations for a year-averaged discharge ( $Q = 110 \text{ m}^3/\text{s}$ ) are plotted in Fig. 6.7. First we compare the observations and model results without dumping of sediment (Fig. 6.7a). At the water surface, the model reproduces the location of the ETM at km 115, with a concentration of around  $0.11 \text{ kg/m}^3$ , similar to the observations. A second ETM is found in the model around km 150 with a surface concentration of  $0.23 \text{ kg/m}^3$ . The measurements are not conclusive on whether the second ETM exists. The OMES surface data only shows a very narrow peak, which may be an artefact. On the other hand, the continuous turbidity measurements at Melle (sensor 1 m above the bed) show concentrations of around  $0.3\text{--}0.4 \text{ kg/m}^3$ , indicating elevated concentrations could be realistic. The depth-averaged concentration observations show an ETM around km 75 and 100, different to what is observed at the surface. These ETM are not captured by the model, which shows the same patterns as the surface concentration. When considering the model with dumping of sediment (Fig. 6.7b), the main difference is in the depth-averaged concentration. The model results now display an ETM at km 85, approximately corresponding to the observations on both location and order of magnitude of the sediment concentration. The location of the ETM does not correspond exactly to the dumping location, indicating that sediment concentrations are not just elevated because of the dumping of sediment but because sediment is trapped by the flow some distance upstream from the dumping location.

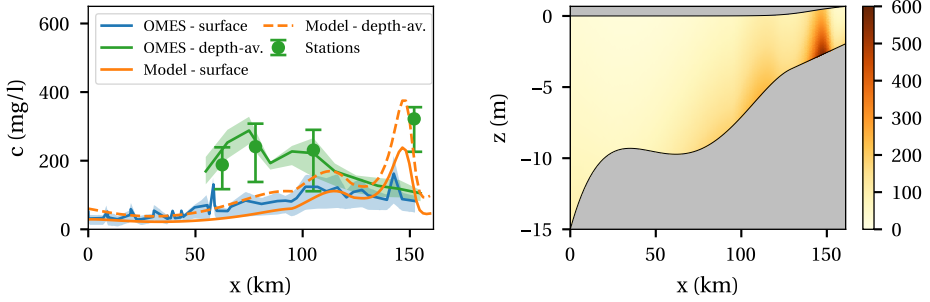
As the highest sediment concentrations typically occur during the relatively dry summer months, we also verify the model results using the average summer river discharge ( $Q = 56 \text{ m}^3/\text{s}$ ) to measurements taken in the summer (Jul-Sep), see Fig. 6.8. The modelled ETM at the surface moves a few km upstream to km 120 with a concentration of  $0.12 \text{ kg/m}^3$  without dumping (Fig. 6.8a) and  $0.18 \text{ kg/m}^3$  with dumping (Fig. 6.8b), corresponding to the large-scale trends observed in the measurements. The modelled surface ETM around 150 km decreases in magnitude to values that match OMES observations. Similar to the case with year-averaged discharge, the depth-averaged concentration observations are qualitatively reproduced in terms of the ETM location and magnitude only if dumping is included in the model. The depth-averaged ETM is located around km 100 with a concentration around  $0.27 \text{ kg/m}^3$ .

### 6.3.3. SENSITIVITY TO THE SETTLING VELOCITY AND EROSION PARAMETER

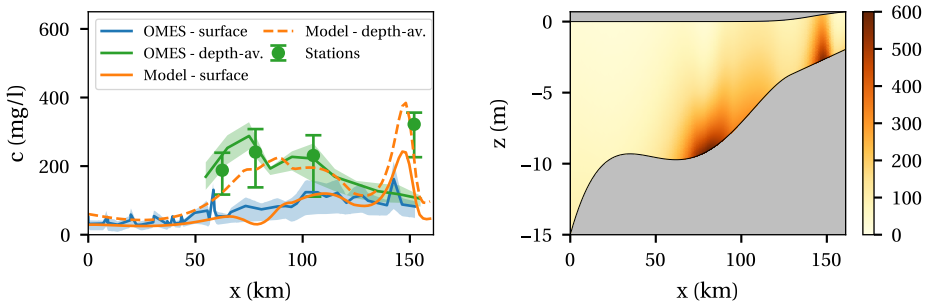
The characteristics of the sediment in the model are predominantly determined by the clear-water settling velocity  $w_{s,0}$  and erosion parameter  $M$ . Both parameters are highly uncertain and subject to natural variation. We therefore test the model sensitivity for settling velocities between  $0.5$  and  $4 \text{ mm/s}$  and erosion parameters between  $10^{-4}$  and  $10^{-1} \text{ s/m}$ , keeping all other settings the same. Model results including dumping of sediment for the average and summer discharge conditions are shown in Fig. 6.9. For both discharge conditions we find one ETM downstream of km 120 and one landward of km 130. Therefore the figure shows the maximum depth-averaged, subtidal sediment concentration seaward of km 125 and landward of km 125 for each combination of  $w_{s,0}$  and  $M$ .

For average discharge conditions in the ETM seaward of km 125 (Fig. 6.9a), the highest depth-averaged sediment concentrations are approximately  $2 \text{ g/l}$  and are found for  $M > 10^{-2} \text{ s/m}$  and  $w_{s,0}$  between  $2$  and  $3 \text{ mm/s}$ . The ETM landward of km 125 (Fig. 6.9b) shows





(a) Without dumping.

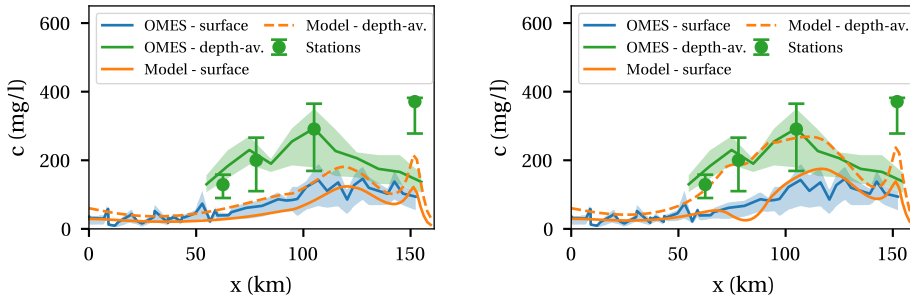


(b) With dumping.

**Figure 6.7:** Modelled subtidal sediment concentrations (mg/l) at the surface, depth-averaged and in an along-channel cross-section for a year-averaged discharge ( $Q = 110 \text{ m}^3/\text{s}$ ) with (a) and without (b) dumping of sediment. The modelled sediment concentration results are also plotted in the along-channel-vertical plane. The modelled sediment concentrations at the surface (orange solid line) are compared to the 1990-2015 average of surface MWT/OMES data (blue line: mean, blue band: 25-75 percentile). Depth-averaged modelled concentrations (orange dashed line) are compared to the 2010-2015 average of OMES data representative of the depth-averaged (green line: mean, green band: 25-75 percentile, data copied from Maris and Meire (2017)). The green dots and error bars represent the average and 25-75 percentile values of tide-filtered data from continuous optical stations at: Boei 84/Lillo Upper (km 63, Sep. 2005-2017, 3.75 m above the bed), Oosterweel Upper (km 78, 2001-2017, 4.5 m above the bed), Driegoten (km 105, 2009-May. 2016, 3 m below the surface) and Melle (km 152, 2010-2017, 1 m above the bed).

the highest depth-averaged concentrations up to  $9 \text{ g/l}$  for a combination of  $M > 10^{-2} \text{ s/m}$  and large  $w_{s,0}$ . High settling velocities correspond to large vertical gradients in the sediment concentration. As a result, the maximum concentration near the bed is  $22 \text{ g/l}$ , which is significantly larger than the depth-averaged concentration.

For summer discharge conditions, the ETM seaward of km 125 (Fig. 6.9c) shows the same behaviour for varying  $M$  and  $w_{s,0}$  as for average discharge conditions. However, depth-averaged concentrations are now up to approximately  $1 \text{ g/l}$  and therefore lower than for



(a) Without dumping.

(b) With dumping.

**Figure 6.8:** Modelled subtidal sediment concentrations at the surface and depth-averaged for summer discharge conditions ( $Q = 56 \text{ m}^3/\text{s}$ ) with (a) and without (b) dumping. Model results are compared to the average of observations obtained during the summer and winter months. See Fig. 6.7 for references to the observations.

average discharge conditions. The ETM landward of km 125 (Fig. 6.9d) shows a different behaviour for varying  $M$  and  $w_{s,0}$  within the tested range. The highest depth-averaged concentrations of approximately 11 g/l are found for the largest values of  $M$  and  $w_{s,0}$  around 1-1.5 mm/s. Near the bed, maximum concentrations of up to 40 g/l are found in the ETM landward of km 125.

While the ETM seaward of km 125 is strongly affected by dumping of sediment, high concentrations can also be attained in this ETM if dumping were excluded from the model (not shown). This confirms the earlier observation that this ETM corresponds to a sediment trapping location, not just a plume of dumped sediment. Without dumping, concentrations in the ETM seaward of km 125 would be similar as in Figs. 6.9a and 6.9c for  $w_{s,0}$  approximately  $> 3 \text{ mm/s}$ ; dumping strongly affects the concentration in this ETM for  $w_{s,0} < 3 \text{ mm/s}$ . The ETM landward of km 125 is not strongly affected by dumping for any combination of  $M$  and  $w_{s,0}$ .

To further illustrate the along-channel distribution of sediment for some of the cases with higher erosion parameter, Fig. 6.10 shows along-channel near-bed sediment concentrations for three situations, all with  $M = 0.1 \text{ s/m}$  and different  $Q$  and  $w_{s,0}$ , as marked by the coloured circles in Fig. 6.9. For all three plotted cases, the sediment concentration locally exceeds 10 g/l, concentrated around two ETM. Between these ETM concentrations are much lower with values around 100-200 mg/l. Even though concentrations are moderate in a large part of the estuary, we call these conditions hyperturbid, as the sediment concentrations are high over an along-channel distance of several tens of km and have a visible effect on the water motion (not shown). Thus, hyperturbid conditions can occur in our model of the Scheldt but only for values of  $M$  10-100 times the default value based on calibration.

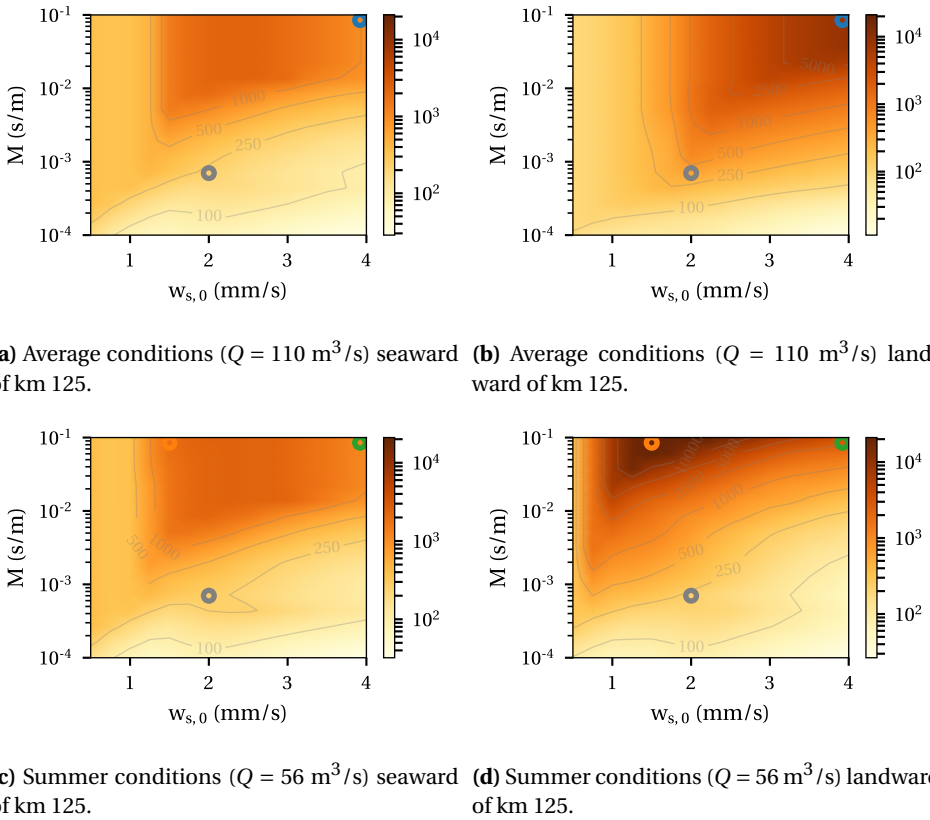


**Figure 6.9:** Maximum depth-averaged sediment concentration (indicated by the colours, in mg/l) in the area seaward and landward of km 125 for a range of values of the settling velocity  $w_{s,0}$  and erosion parameter  $M$  and for average and summer discharge conditions. The grey lines are iso-concentration lines. The grey circle indicates the default case (Table 6.2), the coloured circles correspond to along-channel concentration profiles plotted in Fig 6.10.

## 6.4. RESPONSE TO CHANNEL DEEPENING

### 6.4.1. WATER LEVEL AND SEDIMENT CONCENTRATION

Over the last decades, the Scheldt River Estuary has become deeper due to sand mining and channel deepening (also see Chapter 1). Measurements and smoothed approximations of the width-averaged depth in 1960 and 2010 are plotted in Fig. 6.11. Inspired by the along channel pattern of deepening in the past, we define depth profiles of the form

$$H_\alpha = (1 - \alpha)H_{1960} + \alpha H_{2010}, \quad (6.5)$$

where  $H_{1960}$ ,  $H_{2010}$  are the fitted depth profiles of 1960 and 2010 and  $\alpha$  is a bed-profile parameter. For  $\alpha = 0$ , we obtain the depth of 1960, for  $\alpha = 1$  we obtain the depth of 2010 and for  $\alpha > 1$  we obtain a depth larger than in 2010 by extrapolating the pattern of deepening between 1960 and 2010. We vary  $\alpha$  between 0 and 2, keeping all other parameters the same as in the default experiment (Table 6.2).

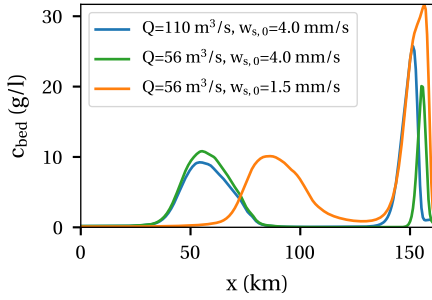


**Figure 6.10:** Modelled along-channel distribution of the subtidal sediment concentrations near the bed for three cases: (1)  $M = 0.1$  s/m,  $w_{s,0} = 4$  mm/s and average discharge, (2)  $M = 0.1$  s/m,  $w_{s,0} = 4$  mm/s and summer discharge and (3)  $M = 0.1$  s/m,  $w_{s,0} = 1.5$  mm/s and summer discharge.

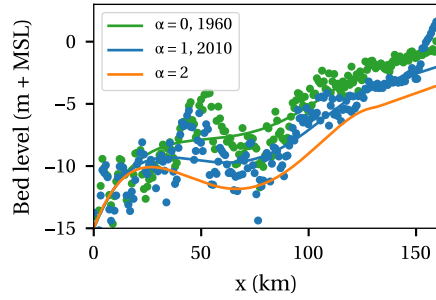
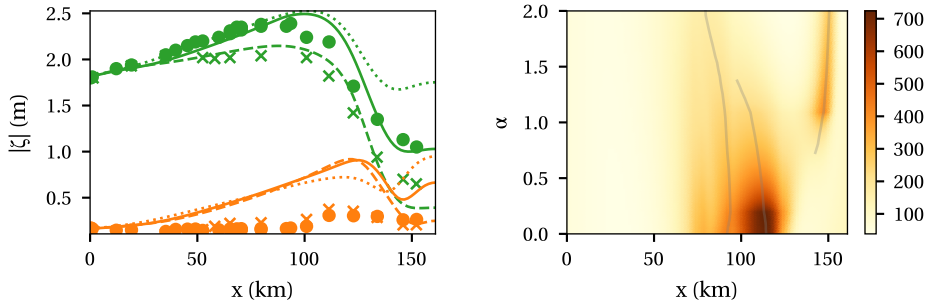


**Figure 6.11:** Width-averaged bed level (m + MSL) observed in 1960 and 2010 (dots) and smooth fits, together with smooth bed profiles for a deepening scenario with  $\alpha = 2$  (see Eq. (6.5)).

Model results show that channel deepening between 1960 and 2010 leads to an amplification of the  $M_2$  water level and a combination of amplification and damping of the  $M_4$  water level. To illustrate this, Fig. 6.12a shows the  $M_2$  and  $M_4$  water level amplitude for  $\alpha = 0, 1$  and  $2$ , together with observations of the tidal amplitude in 1960 and 2009. In order to compare the model result and measurements for 1960, the modelled water level for  $\alpha = 0$  is for a situation without sediment dumping, while dumping is taken into account for  $\alpha > 0$ . Although the modelled  $M_2$  tide is only calibrated for 2010 conditions, the  $M_2$  tide for  $\alpha = 0$  shows good correspondence with the 1960 observations. As  $\alpha$  increases, the  $M_2$  tidal amplitude increases for all tested values of  $\alpha$ . The  $M_4$  tidal amplitude is overestimated compared to the measurements in both 1960 and 2010 conditions. Between 1960 and 2010, the measurements show only very minor changes in  $M_4$  tidal amplitude, with amplification upstream from km 130 and reduction of the amplitude downstream from km 130. For  $\alpha$  increasing from 1 to 2, the model does capture a trend similar to what was observed between 1960 and 2010, with increasing  $M_4$  amplitude upstream from km 140 and decreasing amplitude elsewhere.

The maximum sediment concentrations become lower as a result of channel deepening. This is illustrated in Fig. 6.12b, which shows the depth-averaged sediment concentration as a function of  $x$  and the bed-profile parameter  $\alpha$  for year-averaged discharge. Sediment dumping is now taken into account and has its default value for all  $\alpha$ . For  $\alpha = 0$ , the figure shows two ETM around km 80 and 115. As  $\alpha$  increases (moving up along the vertical axis), the sediment concentrations in the ETM become lower. From approximately  $\alpha > 0.9$ , the ETM at km 115 starts to disappear and is replaced by an ETM at km 150. As  $\alpha$  increases further, the concentrations in this new ETM at km 150 also decrease. Repeating these model experiments without sediment dumping (not shown) yields similar results, however the ETM at km 80 is much weaker. Hence, regardless of sediment dumping, the effect of deepening alone leads to an upstream shift of the ETM from km 115 to km 150 and lower maximum sediment concentrations.



(a) Water level amplitude

(b) Subtidal depth-averaged sediment concentration (in mg/l).

**Figure 6.12:** a) Water level amplitude of the  $M_2$  (green) and  $M_4$  (red) tide for  $\alpha = 0$  (1960),  $\alpha = 1$  (2010) and  $\alpha = 2$  (dashed, solid, dotted, respectively), compared to observations from 1960 (crosses) and 2009 (dots). Results are for the average discharge case ( $Q = 110 \text{ m}^3/\text{s}$ ) with dumping for  $\alpha = 1, 2$  and without dumping for  $\alpha = 0$  in order to compare with 1960 observations. b) Subtidal depth-averaged sediment concentration as a function of  $x$  and bed-profile parameter  $\alpha$ , where increasing  $\alpha$  indicates increasing channel depth. Results are for the average discharge case ( $Q = 110 \text{ m}^3/\text{s}$ ) with dumping included for all  $\alpha$ . The grey contour lines indicate the location of the ETM.

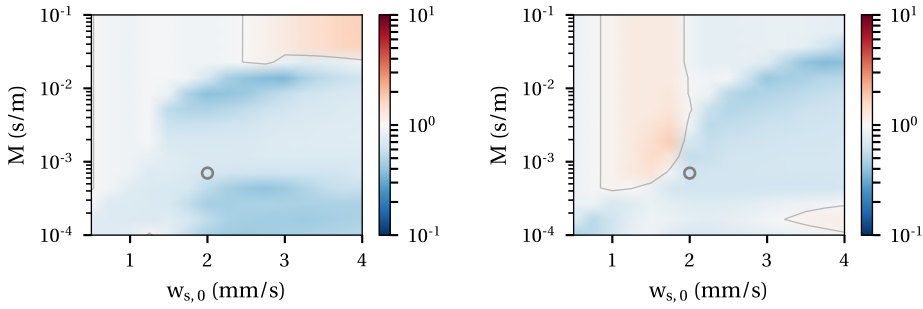
## 6

#### 6.4.2. SENSITIVITY TO THE SETTLING VELOCITY AND EROSION PARAMETER

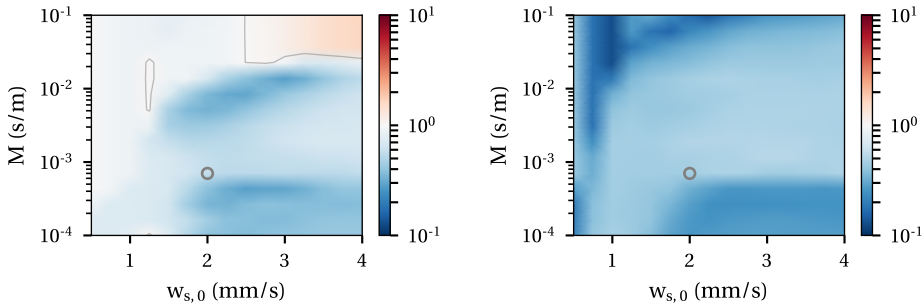
The effect of channel deepening for other values of the settling velocity  $w_{s,0}$  and erosion parameter  $M$  is generally consistent, i.e. showing decreasing concentrations with deepening. However, this is not true for all combinations of  $w_{s,0}$  and  $M$ , see Fig. 6.13. The figure shows the relative change of the maximum depth-averaged concentration for  $\alpha = 2$  compared to  $\alpha = 1$  (2010) for the ETM seaward and landward of km 125 for average and summer discharge cases. Red colours indicate an increase of the maximum concentration after deepening, while blue colours indicate a decrease. For both average ( $Q = 110 \text{ m}^3/\text{s}$ , Fig. 6.13a-6.13b) and summer ( $Q = 56 \text{ m}^3/\text{s}$ , Fig. 6.13c-6.13d) discharges, the concentrations predominantly decrease. Increasing concentrations with deepening are found for a combination of a high erosion parameter and high settling velocity in the ETM seaward of km 125. For these settings, the estuary is already highly turbid for 2010 depth conditions (see Section 6.3.3), so the increasing concentration with deepening does not signify a transition from low to high sediment concentrations. In the ETM landward of km 125, increasing concentrations are only found for the year-averaged discharge case for settling velocities between approximately 1 and 2 mm/s and  $M > 10^{-3} \text{ s/m}$ . The increase is, however, less than a factor two and also does not indicate a transition from low to high sediment concentrations.

#### 6.5. ANALYSIS

In order to gain a better understanding of and confidence in the presented results, we investigate the physical processes underlying the sediment dynamics in the model. Following the approach taken in Chapter 4, the model results before and after deepening



(a) Average conditions ( $Q = 110 \text{ m}^3/\text{s}$ ) seaward of km 125. (b) Average conditions ( $Q = 110 \text{ m}^3/\text{s}$ ) landward of km 125.



(c) Summer conditions ( $Q = 56 \text{ m}^3/\text{s}$ ) seaward of km 125. (d) Summer conditions ( $Q = 56 \text{ m}^3/\text{s}$ ) landward of km 125.

**Figure 6.13:** Ratio of the maximum depth-averaged concentration for  $\alpha = 2$  (deepened) divided by that for  $\alpha = 1$  (2010) in the areas seaward and landward of km 125 for average and summer discharge conditions, plotted for a range of values of  $w_{s,0}$  and  $M$ . Blue colours denote that the maximum concentration is lower for  $\alpha = 2$  than for  $\alpha = 1$ . Red colours denote that the maximum concentration is higher for  $\alpha = 2$  than for  $\alpha = 1$ . The contour line indicates no change between the scenarios. The circles indicate the default parameter settings (Table 6.2).

are analysed on the basis of two aspects:

1. along-channel suspended sediment transport; and
2. vertical resuspension

These aspects are quantitatively expressed in terms of the *transport capacity*, *erodibility* and *dimensionless erosion parameter*, which are introduced in Section 6.5.1. Next, in Section 6.5.2, we analyse the sediment dynamics in the 2010 case. This is used to explain the sensitivity to the erosion parameter in Section 6.5.3 and to deepening in Section 6.5.4.

### 6.5.1. TRANSPORT CAPACITY, ERODIBILITY AND DIMENSIONLESS EROSION PARAMETER

In order to analyse the vertical resuspension of sediment, we look closer at the formulation for erosion  $E$  in iFlow, which reads as

$$E = M|\tau_b|f. \quad (6.6)$$

Here,  $M$  is a prescribed erosion parameter,  $\tau_b$  is the bed shear stress and  $f$  is the tidally averaged erodibility. This erodibility indicates the tidally averaged amount of sediment on the bed. The erodibility is a number between 0 and 1, where 0 means that no sediment is available for erosion during the entire tidal cycle and 1 indicates that easily erodible sediment is available at the bed during the entire tidal cycle. A number between 0 and 1 indicates that sediment is available at the bed during some part of the tide. A formal mathematical definition is provided by Brouwer et al. (2018).

Using this erosion formulation, one can define a dimensionless erosion parameter  $\tilde{E}$  (see Chapter 3), which expresses the ability of the flow to resuspend sediment from the bed. For our model, it is mathematically expressed as

$$\tilde{E} = \frac{M|\tau_b|}{w_{s,0}c_{\text{gel}}}, \quad (6.7)$$

where the clear-water settling velocity  $w_{s,0}$  and gelling concentration  $c_{\text{gel}}$  are constants in our model. Hence, the along-channel variation of  $\tilde{E}$  expresses along-channel variations in the bed shear stress  $\tau_b$ .

In order to analyse changes in sediment dynamics, one could directly investigate the changes in the sediment transport. The disadvantage of this, is that the sediment transport is typically large near the ETM and small in areas with little sediment. Hence, when the ETM moves to a location where little sediment was available previously, this appears as a large change in the sediment transport. The changes in the sediment transport then simply reflect the changes in ETM location, not the changes in hydrodynamic forcing that caused the ETM to move. To circumvent this, we use the concept of transport capacity. A formal mathematical definition of the transport capacity is provided in Chapter 4. More intuitively, the transport capacity is defined as the sediment transport that would occur if a uniform layer of sediment were added on the bed everywhere in the estuary, given the modelled hydrodynamic conditions (flow velocity, turbulence field) and sediment parameters (effective settling velocity, erosion parameter). It therefore indicates the tidally averaged redistribution of a uniform layer of sediment on the bed. Trapping of sediment is indicated by a convergence of the transport capacity.

In iFlow, the transport capacity can be subdivided into various physical contributions. The most dominant contributions in the Scheldt River are the following (see also Chapter 2).

- The *external  $M_4$  tide* contribution is due to tidal asymmetry caused by the  $M_2$  tide and  $M_4$  tide entering the estuary at the mouth. The contribution to the  $M_4$  tide is generated outside the estuary on the shallow shelf and propagates through the estuary, causing asymmetry in the velocity and sediment resuspension during ebb and flood and therefore net sediment transport.

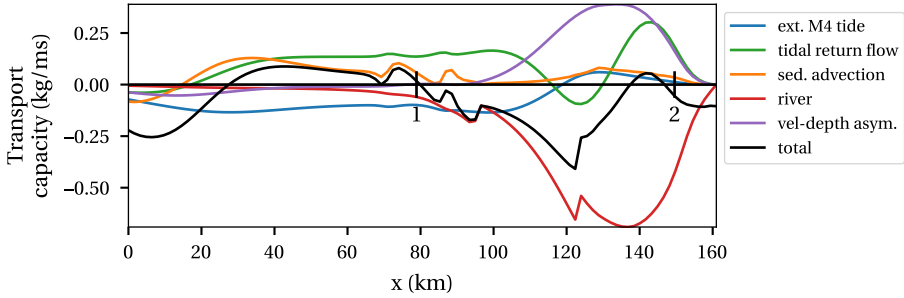


- The *tidal return flow* contribution is the transport capacity due to Stokes drift and the corresponding return flow. The Stokes drift is associated with sediment import. At least partly compensating this import, the return flow velocity contains a subtidal contribution which typically causes export of sediment. Additionally, the return flow velocity has an  $M_4$  contribution, which may cause import or export of sediment, depending on the phase-lag with the  $M_2$  tide.
- The *velocity-depth asymmetry* contribution is the transport capacity due to the asymmetry of the tide that is created because the depth is different during ebb and flood. This yields different velocity profiles during ebb and flood and hence asymmetric sediment resuspension and transport. Whether this effect is importing or exporting sediment, depends on the phase difference between the  $M_2$  velocity and surface elevation.
- The *sediment advection* contribution represents the transport due to spatial settling lag (see e.g. Van Straaten and Kuenen, 1957; De Swart and Zimmerman, 2009). This contribution tends to transport sediment towards along-channel minima in the tidal velocity amplitude.
- The *river* contribution consists of two parts: the river-induced flushing of tidally resuspended sediment and the transport due to the tidal asymmetry caused by the tide-river interaction. Both contributions cause an export of sediment

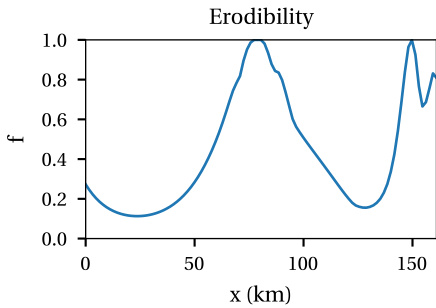
### 6.5.2. ANALYSIS OF THE 2010 CASE

Analysis of the sediment transport capacity provides more insight into the ETM near km 80 and 150. Fig. 6.14a shows the transport capacity for the 2010 case with average discharge ( $Q = 110 \text{ m}^3/\text{s}$ ) with sediment dumping and is almost the same for the case without dumping. The total transport capacity (black line) shows the ability of the flow to transport sediment upstream (positive) or downstream (negative). Sharp jumps occur in the transport capacity at km 95 and 123, due to the inflow of fresh water from tributaries. The ETM correspond to the two convergence zones near km 80 and 150, indicated by the numbers in the figure. The convergence near km 80 is a result of a clear upstream transport between km 25 and 80 and a clear downstream transport between km 80 and 140. The convergence near km 150 on the other hand results from only a small area of weak upstream transport near km 140 and downstream transport from the landward boundary. This trapping zone and the corresponding ETM are therefore not a very robust result; small changes to the parametrisation of the geometry near the landward end of the model domain can therefore potentially result in a disappearance of this trapping zone. While the ETM at km 150 is not a very robust model result, the measurements provide an ambiguous image of this ETM as well; the ETM at km 150 is not observed in the OMES observations, while it is observed by the continuous measurement station near Melle. Further research is needed to provide further understanding of the sediment concentration in this part of the estuary.

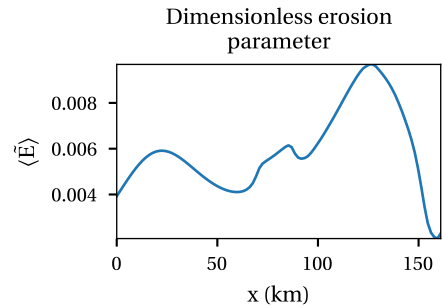
The reason why convergence of transport occurs, follows from the balance of dominant physical mechanisms, which are also shown in Fig. 6.14a. There are two dominant exporting (i.e. negative) contributions. The river discharge dominates the sediment export from the estuary for  $x > 80 \text{ km}$ . For  $x < 80 \text{ km}$ , sediment export is dominated by the sediment transport due to  $M_2$ - $M_4$  tidal asymmetry that is related to the externally forced



(a) Total transport capacity and decomposition of the transport capacity into its five most important contributions. The vertical markings and numbers denote trapping locations.



(b) Erodibility.



(c) Dimensionless erosion parameter.

**Figure 6.14:** Quantities used for the analysis of sediment transport and resuspension: the transport capacity, erodibility and dimensionless erosion parameter. These quantities are plotted for the case with average discharge ( $Q = 110 \text{ m}^3/\text{s}$ ) with dumping.

$M_4$  tide. Three contributions are important for import (i.e. positive): sediment advection (or spatial settling lag), tidal return flow and velocity-depth asymmetry. The latter two are associated with  $M_2$ - $M_4$  asymmetry of the tide. Hence, sediment transport due to  $M_2$ - $M_4$  tidal asymmetry is important, but not all contributions to this asymmetry lead to sediment import. The resulting combined transport by the  $M_2$ - $M_4$  asymmetry is a small import of sediment for  $x > 40 \text{ km}$ .

While the sediment transport capacity shows that the observed ETM near km 80 and 150 are results of sediment trapping, it cannot explain the ETM observed at the surface near km 115 (see Fig. 6.7b). This ETM is not directly related to a trapping zone but results from a large resuspension of sediment. This results from the combination of a sufficiently large availability of sediment, expressed by the erodibility (Fig. 6.14b) and a relatively large erosion, expressed by the tidally averaged dimensionless erosion parameter (Fig. 6.14c). The sediment available at the bed is suspended high up in the water column and is therefore observed as an ETM at the surface.

### 6.5.3. ANALYSIS OF THE SENSITIVITY TO THE EROSION PARAMETER

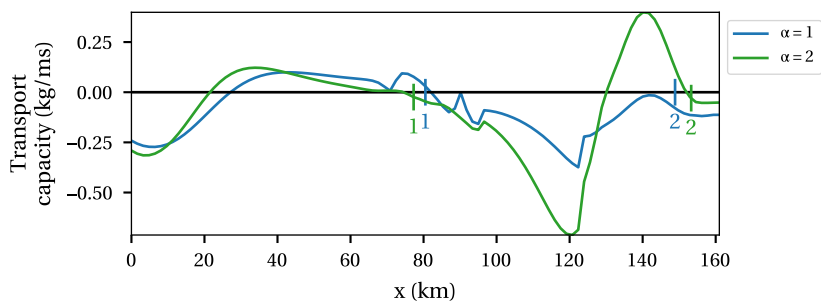
The erodibility helps to explain why the model results are sensitive to the erosion parameter, as was found in Fig. 6.9. Near the ETM at km 80 and 150, the erodibility (Fig. 6.14b) equals one. This means that sediment is always available on the bed at these locations. The maximum sediment concentration in these ETM is limited by the ability of the flow to resuspend sediment (i.e. erosion limited conditions). Hence, the sediment concentration at these locations increases when the erosion parameter is increased. Results indicate that erosion limited conditions prevail for average discharge conditions at these ETM locations for  $M$  up to  $10^{-2}$  s/m if the settling velocity exceeds 2 mm/s (not shown). This is over 10 times the erosion parameter used in this study. If dumping were not included in the model, less sediment would be available at the bed but erosion limited conditions still prevail for  $M$  up to  $10^{-3}$  s/m (for a settling velocity of 2 mm/s) to  $10^{-2}$  s/m (for a settling velocity of 4 mm/s). Therefore, regardless of dumping, the development of hyperturbid conditions in the Scheldt, within our model, is mainly controlled by the exchange of sediment between the water column and the bed, parametrised by the erosion parameter.

### 6.5.4. ANALYSIS OF THE RESPONSE TO DEEPENING

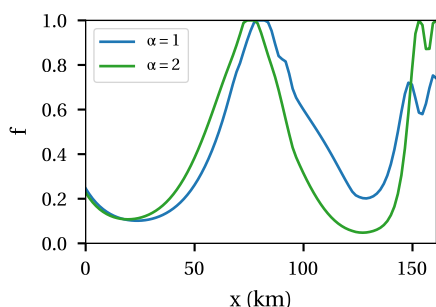
To analyse why deepening leads to lower sediment concentrations, the above analysis is repeated for the case  $\alpha = 2$  (i.e. deepening), and results are compared to the case  $\alpha = 1$  (i.e. 2010). The total sediment transport capacity (Fig. 6.15a) shows only minor changes due to deepening in the seaward half of the estuary. In addition, the locations of the trapping zones near km 80 and 150 (indicated by the numbers) change only little, moving slightly further apart. Only between the two trapping locations does the transport capacity change, leading to an increasing convergence of sediment near the trapping locations. Corresponding to this, the transport capacity diverges between the trapping zones, and less sediment is found between km 80 and 150.

The relatively minor changes in the transport capacity are caused by a mixed response of the underlying mechanisms to deepening (not shown). The sediment transport related to the external  $M_4$  tide becomes more exporting. Additionally, the sediment transport related to tidal return flow becomes less importing between km 0 and 80. The transport due to other mechanisms does not change much between km 0 and 80. Between the ETM at km 80 and 150, the increasing divergence is found in the tidal return flow, as well as the velocity-depth asymmetry and spatial settling lag.

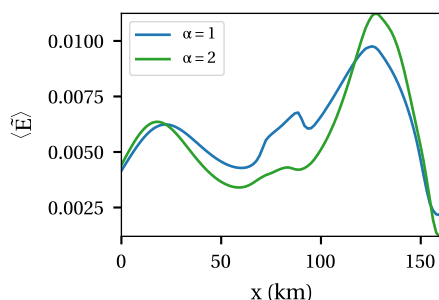
As the trapping locations do not change much due to deepening, the explanation for the lower maximum concentration follows from the erodibility and dimensionless erosion parameter. Near the ETM at km 115, increasing divergence of sediment transport capacity means that less sediment is available, which is expressed by a lower erodibility, see Fig. 6.15b. As a result, the sediment concentration in this ETM decreases with deepening. In the ETM near km 80 and 150, the erodibility remains equal to one, since the sediment transport still strongly converges in these areas. Therefore the maximum concentration in these ETM is restricted by the dimensionless erosion parameter. The dimensionless erosion parameter (Fig. 6.15c) decreases after deepening near km 80. This is related to a decrease in the bed shear stress, which is caused by a decrease in the  $M_2$  tidal velocity in response to deepening. This explains why the sediment concentra-



(a) Total transport capacity for the 2010 case ( $\alpha = 1$ ) and the case for  $\alpha = 2$ .



(b) Erodibility.



(c) Dimensionless erosion parameter.

**Figure 6.15:** Transport capacity, erodibility and dimensionless erosion parameter for the cases  $\alpha = 1$  (2010) and  $\alpha = 2$  for average discharge ( $Q = 110 \text{ m}^3/\text{s}$ ) with dumping.

tion becomes lower near km 80 after deepening. Near km 150, the trapping zone moves slightly upstream (see above), where the dimensionless erosion parameter is smaller. This explains the lower sediment concentrations in this ETM.

## 6.6. DISCUSSION

### 6.6.1. COMPARISON WITH THE EMS RIVER ESTUARY

The main motivation to study whether hyperturbid conditions can develop in the Scheldt as a consequence of deepening, is the development of hyperturbid conditions as a consequence of deepening in the Ems. However, we found that the effects of deepening in the Ems and Scheldt are different. These differences are explained below.

Using the same iFlow model as in this study, the observed transition to hyperturbid conditions in the Ems was qualitatively reproduced. This was done by calibrating the model to a situation representing 1965 (before hyperturbid conditions developed) and then changing the depth to conditions representing 2005 (after hyperturbid conditions developed). It was concluded that the sediment dynamics in the Ems is supply limited, i.e. the erodibility is smaller than 1, and sediment concentrations are restricted by the ability

of the estuary to import sediment. It was found that the most important physical mechanisms responsible for import in the Ems are the  $M_2$ - $M_4$  tidal asymmetries related to the externally generated  $M_4$  tide and tidal return flow. With deepening, both mechanisms become more importing. The additional import of sediment leads to sediment-induced stratification, which leads to damping of turbulence. This in turn leads to a further increase of sediment import due to the  $M_2$ - $M_4$  tidal asymmetry.

The sediment dynamics in the Scheldt behaves differently to the Ems in two aspects. Firstly, it is concluded in this study that the most intense ETM locations in the Scheldt are erosion limited. Hence, the maximum sediment concentration is not restricted by the ability of the estuary to import sediment but by the ability to resuspend sediment from the bed. With deepening, it is found that the bed shear stress decreases in the Scheldt in the ETM near km 80, explaining the lower sediment concentrations. A decrease in the bed shear stress with deepening is also found locally in the Ems but does not restrict the sediment concentration there. Secondly, deepening does not lead to an increasing import by all sediment transport mechanisms. On the contrary, the transport related to the externally generated  $M_4$  tide becomes more exporting, while transport related to the internally generated  $M_4$  tide become less importing in a large part of the estuary. As deepening does not lead to an increasing sediment concentration, a feedback between sediment-induced damping of turbulence and sediment import, as in the Ems, cannot develop in the Scheldt.

The underlying reasons why deepening lead to increasing sediment import in the Ems but not in the Scheldt follow from a complex interplay between the non-linear generation of the  $M_4$  tide and the phase difference between the  $M_2$  and  $M_4$  tide. Nevertheless, one of these reasons can be understood intuitively. At the mouth of the estuary (taking the mouth of the Ems River at Knock), the phase difference between the  $M_2$  and  $M_4$  tide is -4 degrees in the Scheldt and -172 degrees in the Ems. This is a difference of almost 180 degrees, explaining why the effects of the externally generated  $M_4$  tide on transport are almost completely opposite in the Scheldt and the Ems. Deepening leads to amplification of the externally generated  $M_4$  tide inside the estuary in both the Scheldt and Ems and hence to more export in the Scheldt and more import in the Ems.

### 6.6.2. EFFECT OF MODEL SIMPLIFICATIONS

As this model study is highly idealised, there are many physical processes that are not included and some processes that are not represented accurately. Nevertheless, as we have studied the sensitivity of the model to parameter variations and have investigated the most essential physical mechanisms in the model, it is possible to discuss the robustness of the results with respect to these model simplifications.

One of the main discrepancies between the model results and observations is the amplitude of the  $M_4$  water level and the velocity (e.g. Fig. 6.6), which are overestimated by more than a factor 2 in the upstream part of the estuary. The reason for this overestimation is unknown and could potentially be related to an oversimplification of the geometry or oversimplification of turbulence as a time-independent eddy viscosity. As the  $M_4$  tide is important for the sediment transport, this may have big consequences to the sediment transport. However, there are several arguments that support our conclusions

despite these discrepancies. Firstly, the phase difference between the  $M_2$  and  $M_4$  tide is captured accurately when compared to measurements. This means that the direction of the transport related to the  $M_4$  tide is captured correctly. Secondly, this study considered relative changes between cases with different degrees of deepening. Hence, the absolute values of the  $M_4$  amplitude are less important as long as relative changes are captured. Finally, while the  $M_4$  tide is important for the sediment transport, the main limitation to the maximum sediment concentration was found to be the bed shear stress. This is dominantly related to the  $M_2$  tidal velocity, which is captured correctly when compared to measurements. Hence, our conclusions seem robust to the errors in the modelled  $M_4$  tide, but further study is strongly recommended to verify what contributions to the  $M_4$  tide are missing in this model.

A process that is often considered to be important in the Scheldt is flocculation (e.g. Chen et al., 2005). Flocculation affects the settling velocity of sediment. In this study we have shown that the results are robust for large changes in the settling velocity in the entire estuary. Hence, large scale changes in the settling velocity due to changing flocculation properties do not affect our conclusions. The remaining uncertainty is related to spatial or temporal variations of the settling velocity, which are not taken into account.

As erosion is the most restricting process to the sediment concentration, and as it is found that higher sediment concentrations may occur in the Scheldt for larger values of the erosion parameter, the erosion formulation requires most direct attention of further research. The erosion formulation used in this study is based on Partheniades' formulation, which is also used in many state-of-the-art complex models. In this study, we have simplified this formulation by ignoring the critical shear stress and omitting tidal variations of the sediment availability at the bed. While these simplifications likely have important consequences for the quantitative results, they do not change the qualitative conclusions. The main source of uncertainty is the erosion parameter. It remains unknown whether the value of this parameter changes on the long timescale or as a response to deepening. It was identified in this study that hyperturbid conditions can occur in the Scheldt if the value of the erosion parameter is increased by one to two orders of magnitude. Further research is needed to investigate if this is possible.

Our conclusion are further supported by studies using complex models of the Scheldt. Using a depth-averaged Delft3D model, Van Kessel et al. (2008) investigated the effect of the second deepening campaign (1997-1998) and found that this deepening should lead to lower suspended sediment concentrations. Using a three-dimensional model, Vandenbruwaene and Stark (2018) show that the tide in the estuary became less flood dominant due to deepening since the 1930s, also suggesting less sediment import due to deepening.

## 6.7. CONCLUSION

We have investigated the hypothesis of Winterwerp and Wang (2013) that the Scheldt may become hyperturbid as a response to deepening. To this end, we have used the iFlow model to investigate the dynamic equilibrium sediment concentration in the Scheldt for a case representing conditions of 2010 and a range of cases with higher and lower bed levels, keeping all other parameters the same. In order to draw robust conclusions, all

cases have been tested for a range of values of uncertain parameters and the physics underlying the sediment dynamics has been investigated.

For the conditions representing 2010, the modelled sediment concentrations qualitatively reproduce observed long-term average ETM locations and sediment concentration magnitudes. From the analysis it is found that the most intense ETM locations in the Scheldt are erosion limited, i.e. the maximum sediment concentration is restricted by the ability of the flow to resuspend sediment from the bed, not by the availability of sediment. Hence, model results are sensitive to the quantities that control the amount of resuspension, which are mainly the bed shear stress and an erosion parameter.

Deepening of the estuary in the model generally leads to lower maximum sediment concentrations in the Scheldt. When investigating the sensitivity to varying parameter values, some parameter settings were identified where the maximum concentration increases with deepening but such increase is minor and does not lead to the development of hyperturbid conditions. The analysis shows that the flow velocity and hence the bed shear stress at the ETM locations generally decreases with deepening. This results in a reduction of resuspension, which in turn results in lower sediment concentrations. Furthermore, deepening does not lead to a clear trend of increasing sediment import in the Scheldt. Overall, deepening leads to less import in the most seaward part of the estuary and more convergence of sediment around the ETM.

Based on these results, we suggest to reject the hypothesis of Winterwerp and Wang (2013) that channel deepening alone may lead to development of hyperturbid conditions in the Scheldt. By combining the model results, sensitivity analysis and understanding of underlying processes, we argued that this is a robust conclusion, even though the model used is highly idealised. To further verify this conclusion, it is recommended to investigate some processes that are missing or inaccurately represented by the model. Firstly, this concerns the  $M_4$  tide, which is overestimated in the model. Secondly, this concerns the parametrisation for erosion. High sediment concentrations were found in the model of the Scheldt when the erosion parameter is increased by one or two orders of magnitude compared to its calibrated value and it remains unknown whether such an increase of the erosion parameter could occur.

## 6.A. NEW MODEL ADDITIONS RELATED TO TRIBUTARIES

The discharge of water into the estuary by tributaries is added to the model as depth-integrated point sources by adding source terms to the depth-averaged continuity equation, i.e.

$$B\zeta_t + \left( B \int_{-H}^{R+\zeta} u \right)_x = \sum_n S_{Q,n} \delta(x - x_n) \quad (6.8)$$

where  $B$  is the width,  $H$  is the depth below mean sea level (MSL)  $z = 0$ ,  $R$  is the reference level above MSL,  $\zeta$  is the surface elevation,  $u$  is the horizontal flow velocity and subscripts  $x$  and  $t$  indicate derivatives with respect to along-channel distance and time, respectively. The source terms  $S_{Q,n}$  represent the discharge of tributary  $n$  at location  $x_n$ ,  $\delta$  denotes the Dirac delta function, i.e. indicating a source at one point. These sources lead to an additional contribution to the first-order residual water motion (see Chapter 2) that can be analysed separately.

Sources of sediment enter into the The sediment concentration is computed using an equation for



mass conservation and an equilibrium condition, which requires that the cross-sectionally integrated sediment concentration does not vary on the subtidal timescale. This condition is equivalent to requiring

$$\left\langle B \int_{-H}^{R+\zeta} (uc - K_h c_x) dz \right\rangle_x = B(E - D) + S. \quad (6.9)$$

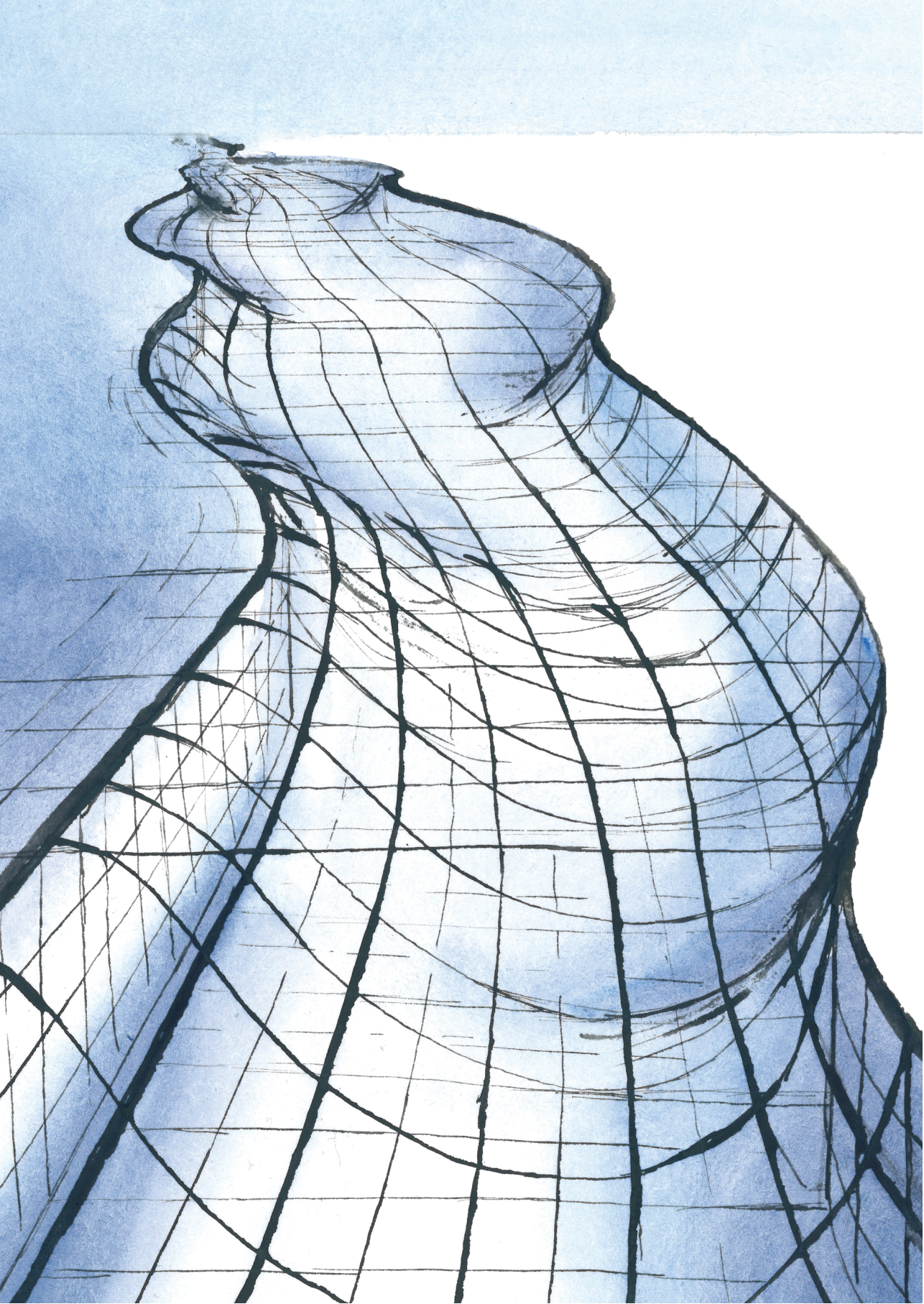
In this equation  $\langle \cdot \rangle$  denotes tidal averaging,  $c$  is the sediment concentration,  $K_h$  is the horizontal eddy diffusivity,  $E$  denotes erosion or resuspension from the bed and  $D$  denotes deposition. Fluvial sources of sediment, dredging and dumping are added to the model by adding a source or sink of sediment  $S$ , which consists of pulses that equal the rate of sediment added (positive) or extracted (negative) from the system at the confluences, dredging and dumping locations. The model computes itself how the sources and sinks are distributed over the water column and the bed in such a way that the model remains in dynamic equilibrium.

## REFERENCES

- Barneveld, H. J., Nicolai, R. P., Boudewijn, T. J., Van De Moortel, I., and Postma, R. (2018). Evaluatie Schelde-estuarium: de toestand van Veiligheid, Toegankelijkheid en Natuurlijkheid. Samenvatting van de T2015-rapportage. Technical Report PR3152.10, HKV, Bureau Waardenburg and Antea. In Dutch.
- Brouwer, R. L., Schramkowski, G. P., Dijkstra, Y. M., and Schuttelaars, H. M. (2018). Time evolution of estuarine turbidity maxima in well-mixed, tidally dominated estuaries: the role of availability- and erosion-limited conditions. *Journal of Physical Oceanography*, 48:1629–1650.
- Chen, M. S., Wartel, S., Eck, B. V., and Maldegem, D. V. (2005). Suspended matter in the Scheldt estuary. *Hydrobiologia*, 540:79–104.
- De Swart, H. and Zimmerman, J. (2009). Morphodynamics of tidal inlet systems. *Annual Review of Fluid Mechanics*, 41:203–229.
- Depreiter, D., Lanckriet, T., Van Holland, G., Vanlede, J., Beirinckx, K., and Maris, T. (2015). Mud disposal and suspended sediment concentration in the Lower Sea Scheldt - towards a hyperturbid system? In *E-proceedings of the 36th IAHR World Congress*.
- IMDC, Deltares, and Gens (2007). Uitbreiding studie denseitsstromingen in de Beneden Zeeschelde in het kader van LTV meetcampagne naar hooggeconcentreerde sliksuspensies. Deelrapport 3 : Valsnelheid slib - INSSEV. Technical report. In Dutch.
- IMDC, Deltares, Svasek Hydraulics, and Arcadis (2013a). Instandhouding vaarpassen Schelde Milieuvergunningen terugstorten baggerspecie. LTV - Veiligheid en Toegankelijkheid. Analyse stortvakken beneden-Zeeschelde. Basisrapport specifieke beheervragen B-23. Technical report. In Dutch. Available through <http://www.vnsc.eu>.
- IMDC, Deltares, Svasek Hydraulics, and Arcadis (2013b). Instandhouding Vaarpassen Schelde Milieuvergunningen terugstorten baggerspecie. LTV - Veiligheid en Toegankelijkheid Baggeren en storten. Achtergrondrapport A-31. Technical report. In Dutch. Available through <http://www.vnsc.eu>.
- Jalón-Rojas, I., Schmidt, S., Sottolichio, A., and Bertier, C. (2016). Tracking the turbidity maximum zone in the Loire Estuary (France) based on a long-term, high-resolution and high-frequency monitoring network. *Continental Shelf Research*, 117:1–11.
- Jeuken, C., Hordijk, D., Ides, S., Kuijper, C., Peeters, P., De Sonnevile, B., and Vanlede, J. (2007). Koploperproject LTV-O&M - Thema Veiligheid – deelproject 1. Inventarisatie historische ontwikkeling van de hoogwaterstanden in het Schelde estuarium. Technical Report Z4384, WL | Delft Hydraulics. In Dutch.
- Kromkamp, J. and Peene, J. (1995). Possibility of net phytoplankton primary production in the turbid Schelde Estuary (SW Netherlands). *Marine Ecology Progress Series*, 121:249–259.
- Maris, T., Cox, T., and Meire, P. (2017). Nota wijzigingen in oppervlakte SPM concentraties in de

- Boven-Zeeschelde. Technical Report 017-R205, University of Antwerp, Department of Ecosystem Management (ECOBE), Antwerp, Belgium. In Dutch.
- Maris, T. and Meire, P. (2017). Onderzoek naar de gevolgen van het Sigmaplan, baggeractiviteiten en havenuitbreiding in de Zeeschelde op het milieu. geïntegreerd eindverslag van het onderzoek verricht in 2016. Technical Report 017-R206, University of Antwerp, Department of Ecosystem Management (ECOBE), Antwerp, Belgium. In Dutch.
- Plancke, Y., Van De Moortel, I., Hertogs, R., Vereecken, H., Vos, G., Verdoodt, N., Meire, D., Deschamps, M., and Mostaert, F. (2017). Monitoring Effecten Ontwikkelingsschets (MONEOS) - Jaarboek monitoring 2016: Deelrapport 6 - Factual data rapportage van monitoring waterbeweging en fysische parameters in de Zeeschelde in 2016. Versie 4.0. Technical Report 12\_070\_6, Flanders Hydraulics Research. In Dutch.
- Talke, S. A., De Swart, H. E., and Schuttelaars, H. M. (2009). Feedback between residual circulations and sediment distribution in highly turbid estuaries: an analytical model. *Continental Shelf Research*, 29:119–135.
- Van Braeckel, A., Piesschaert, E., and Van den Bergh, E. (2006). Historische analyse van de Zeeschelde en haar getijgebonden zijrivieren. 19e eeuw tot heden. Technical Report INBO.R.2006.29, Instituut voor Natuur- en Bosonderzoek. In Dutch.
- Van Kessel, T. and Vanlede, J. (2010). Impact of harbour basins on mud dynamics Scheldt estuary in the framework of LTV. Technical Report 1200253-000, Deltares, Flanders Hydraulics.
- Van Kessel, T., Vanlede, J., Eleveld, M., and Van der Wal, D. (2008). Mud transport model for the Scheldt estuary in the framework of LTV. Technical report, Deltares, Flanders Hydraulics, IVM, NIOO.
- Van Straaten, L. M. J. U. and Kuenen, P. H. (1957). Accumulation of fine grained sediments in the Dutch Wadden Sea. *Netherlands Journal of Geosciences*, 19:329–354.
- Vandenbruwaene, W., Levy, Y., Plancke, Y., Vanlede, J., Verwaest, T., and Mostaert, F. (2017). Integraal plan Boven-Zeeschelde: Deelrapport 8. Sedimentbalans Zeeschelde, Rupel en Durme. Versie 4.0. Technical Report 13\_131\_8, Flanders Hydraulics, Antwerp, Belgium. In Dutch.
- Vandenbruwaene, W. and Stark, J. (2018). Kunnen simulaties helpen bij het verklaren van de relatie tussen getij en morfologie? Presentation at the Schelde Symposium 2018, available at <https://vnsc.eu/uploads/2018/11/rol-simulaties-bij-verklaren-relatie-tussen-getij-en-morfologie-wouter-vandenbruwaene.pdf>. In Dutch.
- Vandenbruwaene, W., Vanlede, J., Plancke, Y., Verwaest, T., and Mostaert, F. (2016). Slibbalans Zeeschelde: Deelrapport 4 - Historische evolutie SPM. Technical Report WL Rapporten 00\_-029\_4, Flanders Hydraulics Research and Antea, Antwerp, Belgium. In Dutch.
- Vanlierde, E., Ferket, B., Michielsen, S., Vereycken, K., Van Hoestenbergh, T., Levy, Y., Plancke, Y., Deschamps, M., Verwaest, T., and Mostaert, F. (2014). MONEOS - jaarboek monitoring WL 2013: Factual data rapportage van monitoring hydrodynamiek en fysische parameters zoals gemeten door WL in het Zeescheldebekken in 2013. Technical report, Flanders Hydraulics Research, Antwerp, Belgium. In Dutch.
- Vanlierde, E., Ferket, B., Pauwaert, Z., Michielsen, S., Van De Moortel, I., Levy, Y., Plancke, Y., Meire, D., Deschamps, M., Verwaest, T., and Mostaert, F. (2016). MONEOS - jaarboek monitoring WL 2015. Factual data rapportage van monitoring hydrodynamiek en fysische parameters zoals gemeten door WL in het Zeescheldebekken in 2015. Versie 3.0. Technical Report 12\_070, Flanders Hydraulics Research. In Dutch.
- Winterwerp, J. C. and Wang, Z. B. (2013). Man-induced regime shifts in small estuaries - I: theory. *Ocean Dynamics*, 63:1279–1292.







# CHAPTER 7

Important processes and challenges in modelling  
the transition to a hyperturbid state

A discussion using Delft3D in an idealised setting



## Abstract

---

Some of the essential processes that drive the transition from low to high sediment concentrations, observed in some estuaries, are qualitatively understood using idealised models. However, to simulate such a transition in more detail, it is important to transfer this understanding to more complex models and test the effect of the more complex parametrisations included in such models. In this study we compare results of the idealised iFlow model and a complex Delft3D model with an idealised geometry and idealised forcing conditions, applied to the Ems River Estuary before and after the observed transition to hyperturbid conditions. Differences between the model results are systematically investigated and attributed to differences in parametrisations between the two models.

In the case before the transition and given suitable parameter choices, iFlow and Delft3D results match closely. However, hyperturbid conditions could not be reproduced using Delft3D for the Ems case. These cases point out three important results that were not found using iFlow due to a different implementation of processes and form important challenges to further research. Firstly, we identified a value of the erosion parameter for which the suspended sediment concentration is maximised. Hence, a higher erosion parameter does not simply lead to higher sediment concentrations, making the results quite sensitive to the choice of the erosion parameter. Secondly, it was found that sediment-induced damping of turbulence can strongly suppress the bed shear stress and therefore reduce resuspension from the bed. Finally, spurious oscillations with unknown origin were found in Delft3D when high sediment concentrations are attained. Therefore those simulations that resulted in high sediment concentrations could not be trusted.

---



## 7.1. INTRODUCTION

The physics of suspended sediment transport in estuaries is complex, as it relates to many processes of which the relative importance differs from one estuary to the next. In order to understand and predict sediment transport, many different models exist, ranging from exploratory or idealised to complex (Murray, 2003). Much of the knowledge of individual sediment transport processes comes from idealised modelling studies, which focus on one or a few processes in isolation and study their dependencies on e.g. geometry, tidal propagation and salt intrusion, see Burchard et al. (2018) or Chapter 1 for a review. However, in order to describe or predict sediment dynamics and transport in estuaries for engineering and management purposes, complex models are often required. Such models include many sediment transport processes in complex geometries and under constantly varying flow conditions. It is difficult to link the influence of elementary transport processes identified in idealised models to the results of such complex models. As a result, idealised and complex models are usually only compared on the basis of primary quantities, such as the water level, velocity and sediment concentration (Schuttelaars et al., 2013). This is a serious problem whenever complex models fail to describe observed phenomena, because it means that we lack systematic tools to understand which process descriptions need to be improved and what parameter values need to be changed to get better descriptions of the phenomena under investigation.

A particular application where this problem is at the heart of the scientific discussion is the regime shift from low to very high sediment concentrations observed in, e.g., the Ems River (Winterwerp et al., 2013; Van Maren et al., 2015). From the idealised model study using the iFlow model (Chapter 4) the regime shift observed in the Ems is qualitatively understood. Using a state-of-the-art model, Van Maren et al. (2015) reproduced some features of the low and high sediment concentration regimes observed in the Ems but could not reproduce the shift between these states without recalibrating the model.

In order to transfer the qualitative understanding of regime shifts to high sediment concentrations from idealised to more realistic models, it is necessary to make a systematic analysis of the differences between the iFlow model and more complex models and their effect on the trapping of sediment. In view of this, the goals of this study are defined as:

1. to assess the role and importance of differences between different types of models concerning regime shifts to high sediment concentrations, and
2. to assess the validity of the iFlow results and the corresponding understanding of processes and parameter sensitivity in the context of a more complex model.

To these ends we make a comparison of the results of the idealised width-averaged iFlow model of Chapter 4 and a Delft3D model. The Delft3D model is applied to a simplified width-averaged geometry and simplified hydrodynamic forcing. Simulations are continued until a dynamic equilibrium is attained. The results are analysed in terms of subtidal and tidal components. By using these simplifications and analysis methods in Delft3D, it is possible to compare the results from this model with results from iFlow in terms of primary quantities and identify differences between the models and their importance on the sediment dynamics. The models are applied specifically to the Ems River for cases representing a situation of 1965, with low sediment concentrations, and 2005, with high sediment concentrations (see Chapter 4). These specific results are then generalised to

conclusions that hold in general for fine sediment modelling in estuaries and to general challenges in modelling transitions to hyperturbid conditions in estuaries.

This chapter is organised as follows: Section 7.2 introduces the Delft3D model and points out our specific model choices and corrections to the model necessary to make it comparable to iFlow. Next, in Section 7.3, we present results for the 1965 case, explicitly comparing iFlow and Delft3D results and connecting the observed differences to differences in the model description. The results of the 2005 case are discussed in Section 7.4. In this section, focus is shifted from the inter-model comparison to the essential processes and challenges in modelling a transition to a hyperturbid situation. Finally, the results are generalised in Section 7.5.

## 7.2. MODEL DESCRIPTION

Delft3D is a numerical three-dimensional model for environmental flows. Below in Section 7.2.1 we give a short general introduction to the equations and processes used for solving the water motion, salinity and suspended sediment concentration and to the numerical grid. For further details we refer to the Delft3D manual (Deltares, 2014). In Section 7.2.2 we discuss several aspects that are important for setting up the Delft3D model for comparison with the iFlow model, highlighting the modelling choices, several corrections to the code and the remaining differences with the iFlow model used in Chapter 4. These differences are summarised in Section 7.2.3. Finally, we discuss the specific set-up for the Ems case in Section 7.2.4.

### 7.2.1. GENERAL DESCRIPTION OF DELFT3D

In Delft3D, the water motion is computed using the non-linear three-dimensional hydrostatic continuity and momentum equations with Boussinesq approximation. At open boundaries of the domain, a temporally varying water level or velocity profile may be prescribed. At the bed, a quadratic friction law is imposed as a function of a prescribed roughness parameter. At the moving surface, the flow satisfies kinematic boundary conditions with an imposed shear stress.

Suspended sediments may be modelled using one or several classes of sediment that represent different types of sediment with different properties. The sediment concentration in each class is computed using a three-dimensional advection-diffusion equation. This equation includes settling of sediment with a settling velocity which may depend on the salinity (parametrising the effect of salinity on flocculation) and includes hindered settling. A no-flux boundary is prescribed at the surface, while erosion and deposition fluxes are allowed at the bottom boundary. Deposition equals the settling flux at the bottom boundary if the shear stress is below the critical shear stress for deposition. Erosion is modelled using an empirical erosion law (see Section 7.2.2 for more details) and depends on the amount of sediment available on the bed. The amount of sediment on the bed is computed using a bed-evolution equation (i.e. Exner equation) for each sediment class. In the standard bed module of Delft3D, the sediment on the bed in each class is assumed to be one layer with a uniform and prescribed density and erosion properties. Alternative bed modules that account for multiple layers or bed stratigraphy exist and are discussed in the manual (Deltares, 2014). One can choose whether to account for morphological coupling between the thickness of the sediment layer on the bed and the



water depth.

For each suspended sediment class, time-varying vertical profiles should be prescribed at open boundaries. These boundary conditions can optionally include a Thatcher-Harleman time lag, which prescribes the boundary condition during inflow as a smooth transition between the concentration at the boundary during outflow and the prescribed boundary conditions. The Delft3D manual states that these open boundary conditions are only used for computing an advective flux. Hence, the equation across the boundary is hyperbolic and only requires a boundary condition when the flow is directed inward, while the boundary condition is ignored during outward directed flow. However, this is incorrect: diffusive fluxes are computed over open boundaries in Delft3D at all times<sup>1</sup>.

The effect of turbulence is parametrised by an eddy viscosity and eddy diffusivity and is computed using the  $k - \varepsilon$  model with buoyancy effects to account for turbulence damping due to vertical density gradients (see Uittenbogaard et al. (1992) and Dijkstra et al. (2016) for specific implementation details). Besides vertical exchange processes, the model implements horizontal advection of  $k$  and  $\varepsilon$  with the Reynolds-averaged flow. The Prandtl-Schmidt number, relating the eddy viscosity and eddy diffusivity, equals fixed numbers of 1.0 for sediment and 0.7 for salinity. The bed and surface boundaries are Dirichlet conditions for  $k$  and  $\varepsilon$  following the law-of-the-wall. Delft3D furthermore allows for prescribing a minimum background eddy viscosity and eddy diffusivity<sup>2</sup>.

Delft3D uses a staggered grid in the horizontal direction, see e.g. Fig. 7.1. Along-channel velocities, shear stresses and turbulence quantities are computed on cell interfaces (-), and depths, water levels, salinities and sediment concentrations are computed in cell centres (+) of the active grid. The active grid is defined as the set of complete grid cells inside the model domain. The exact size of this model domain depends on the hydrodynamic boundary conditions. If the water level is prescribed at an open boundary, the edge of the computational domain is located on the cell centres outside of the active grid (see blue dotted line on the left side in Fig. 7.1). If instead a velocity profile is prescribed, the boundary is located on the cell edge at the boundary of the active grid. As a consequence, the size of the model domain changes when the boundary condition type is changed on the same grid. Boundary conditions for salinity and sediment concentration are prescribed in cell centres half a cell outside of the active grid regardless of the hydrodynamic boundary conditions (in  $x$ -direction marked by the circles in Fig. 7.1).

The numerical implementation of the water motion, turbulence, salinity and sediment concentration are (semi-)implicit in time and, for our application, impose no time step restrictions. Only the bed evolution equation is solved explicitly in time and results in a previously unidentified time step restriction, which we derive in the next section. The mutual interactions between the water motion, turbulence, salinity and sediment concentration are also implemented explicitly. To our knowledge there are no studies proving whether such a system of explicitly coupled mutually interacting components is un-

<sup>1</sup>Note that the model output does not include the diffusive flux over left and lower boundaries and is inconsistent with the actual model computations.

<sup>2</sup>Delft3D does not apply the minimum eddy diffusivity for sediment concentration computations. The source code has been changed to add this.

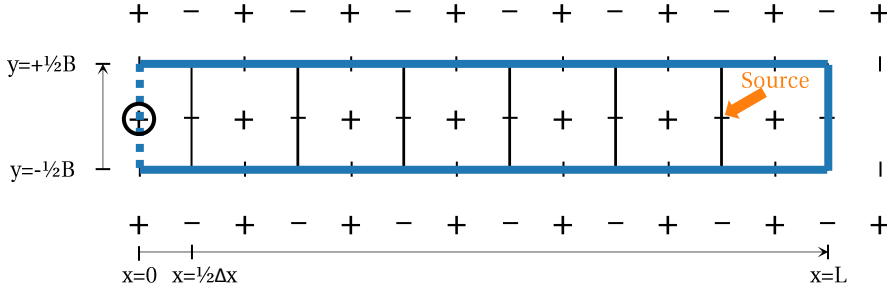


**Figure 7.1:** Sketch of the horizontal grid of Delft3D in width-averaged mode. Cell centres are indicated by + and interfaces are indicated by - and |. The blue dotted line shows the location of the open boundary, which extends beyond the active grid due to the location of the boundary condition. The blue solid line denotes closed boundaries. The black boxes indicate active grid cells; all other points are ghost cells. The black circle denotes the location of the salinity and sediment boundary condition. The orange arrow denotes the source term used to prescribe the fresh water discharge.

conditionally stable. Vertical advection of momentum, salinity and sediment is implemented using a central discretisation scheme, which can result in spurious oscillations if the Péclet-number exceeds 2, which can occur with strong stratification (see the manual Deltares (2014)). For this study, we have changed this scheme to a first-order upwind scheme to prevent such oscillations.

### 7.2.2. MODEL CHOICES AND CONSIDERATIONS FOR COMPARISON TO IFlow

In order to set-up the Delft3D model in such a way that results can be compared to results from iFlow, we use the model in a width-averaged mode. This is done by using only one computational cell in the lateral direction (see the grid of Fig. 7.1). The model depth and width are described by smooth profiles varying in the along-channel direction. At the seaward boundary, the water level is forced to vary according to an  $S_2$  and  $S_4$  tide. These tidal constituents are chosen over the  $M_2$  and  $M_4$  tidal constituents, because the analysis on them is easier as an integer number of time steps fits in one tidal period. At the landward boundary, we simulate the effects of a tidal weir. One could argue whether to model this as an open or a closed boundary in Delft3D. A weir should support advective fluxes from upstream but not diffusive fluxes across it. Diffusive fluxes are always computed over open boundaries in Delft3D (see Section 7.2.1) and Delft3D only allows for prescribing the advective flux across the boundary. Therefore, the only correct way is to model a weir as a closed boundary. The advective inflow of water from upstream is imposed by adding a source term in the computational cell closest to the boundary.

For hydrodynamics, the bed roughness is prescribed using a Chézy parameter  $C$ . This is equivalent to prescribing a dimensionless roughness height  $z_0^* = z_0/H$  such as in iFlow, because there is a direct relation between  $z_0^*$  and  $C$  that does not involve any other estuary-specific parameters. This relation is given by  $z_0^* = (e^{1+\kappa C/\sqrt{g}} - e)$ , where  $\kappa$  is the Von Kármán constant and  $g$  is the acceleration of gravity (Deltares, 2014).

Salinity is not resolved in our model schematisation. This is done because the only salinity-related process resolved in iFlow is gravitational circulation, which is not very important to the sediment transport in the Ems (see Chapter 4). Including salinity in Delft3D leads to other processes as well, including SIPS. The importance of these processes is not investigated in this chapter and hence salinity is not included.

For the sediment concentration we prescribe depth and time uniform values at the open boundary and do not use Thatcher-Harleman lags. This is done because it is virtually impossible to define a vertical and temporal structure of the sediment concentration at the boundary which is consistent with the interior solution. The resulting mismatch between the boundary condition and interior solution leads to the formation of a boundary layer with a typical length scale of a few kilometres, which may not be regarded as a physically correct solution. The physically relevant boundary condition felt by the model is the solution found on the inside of the boundary layer and therefore differs from the prescribed boundary condition. This is different to iFlow, where the temporal and vertical structure at the boundary is computed by the model itself and no boundary layers are formed. If the prescribed boundary concentration in iFlow is too large to be in equilibrium with the bottom pool at the boundary, this indicates that the boundary condition cannot match the internal dynamics and it is adjusted to the maximum sediment concentration that can be in equilibrium with the bottom pool.

For sediment, we furthermore assume one sediment class with a constant clear water settling velocity. Hindered settling is taken into account using the formulation of Richardson and Zaki (1954), which reads as

$$w_s = w_{s,0} \left( 1 - \frac{c}{c_{\text{gel}}} \right)^5. \quad (7.1)$$

Here  $w_{s,0}$  is the clear water settling velocity,  $c_{\text{gel}}$  is the gelling concentration and  $c$  is the instantaneous local sediment concentration. A similar formulation for hindered settling was used in iFlow but then using the tidally averaged near-bed concentration instead of  $c$ . Erosion at the bed  $E$  is computed using the standard bed module in Delft3D, which uses Partheniades' formulation and is a function of the amount of available sediment:

$$E = \overline{M} \frac{\max(\tau - \tau_c, 0)}{\tau_c} f^*, \quad (7.2)$$

where  $\overline{M}$  is an erosion parameter (in  $\text{kg}/(\text{m}^2\text{s})$ ),  $\tau$  is the bed shear stress and  $\tau_c$  is the critical shear stress for erosion. Furthermore the instantaneous erodibility  $f^*$  is a measure of the amount of sediment on the bed (following the notation and terminology of Brouwer et al. (2018)). In Delft3D,  $f^*$  is computed as

$$f^* = \min \left( \frac{S_{\text{bed}}}{\rho_{\text{bed}} d_{\text{thresh}}}, 1 \right), \quad (7.3)$$

where  $S_{\text{bed}}$  is the dry sediment mass on the bed (in  $\text{kg}/\text{m}^2$ ),  $\rho_{\text{bed}}$  is a prescribed bed density and  $d_{\text{thresh}}$  is a threshold thickness. Physically, the threshold thickness of sediment represents that a thin layer of sediment is not equally spread over the bed but concentrated in smaller pools and therefore not as easily eroded as a thicker and uniformly

spread sediment pool. Compared to iFlow, the erosion formulation contains two differences. Firstly, the critical shear stress for erosion is not included in iFlow but cannot be set to zero in Delft3D, as it appears in the denominator in Eq. (7.2). Therefore we set  $\tau_c$  to a small value so that its effect can be neglected. The erosion parameter  $M$  used in iFlow is then approximately equal to

$$M = \overline{M} / \tau_c. \quad (7.4)$$

Secondly, Delft3D accounts for a time-varying erodibility  $f^*$ , while a tidally averaged erodibility  $f$  is used in iFlow. The instantaneous erosion in iFlow is therefore related to the tidally averaged amount of sediment on the bed. Morphological coupling in Delft3D is switched off, so that both models do not account for morphological changes.

Related to erosion in the standard Delft3D bed module, we have identified a time-step restriction that, to our knowledge, is not mentioned in the manual nor in other literature. The restriction is related to the bed evolution equation, which computes the amount of sediment on the bed as a function of the erosion and deposition. This equation is solved explicitly in time. Hence, when the erosion during a time step exceeds the amount of sediment available for erosion, the amount of sediment on the bed becomes negative. This is corrected in Delft3D by re-setting the amount of sediment to zero, thus artificially creating sediment and violating mass conservation. It is possible to derive a restriction on the time step  $\Delta t$  to prevent such a violation of mass conservation (see Appendix 7.A for the derivation):

$$\Delta t \leq \frac{\rho_{\text{bed}} d_{\text{thresh}}}{\overline{M}} \frac{\tau_c}{\max_{x,y,t}(\tau) - \tau_c}. \quad (7.5)$$

This time step restriction depends on prescribed model parameters and the maximum bed shear occurring in the model domain, which may be estimated a priori. The time step restriction is a conservative estimate. Larger time steps may be allowed, but this cannot be guaranteed a priori.

The turbulence models in Delft3D (i.e. the  $k - \varepsilon$  model) and iFlow both contain a similar dependence on the along-channel depth-averaged velocity, depth and both depend on sediment-induced damping of turbulence. However, the turbulence models are different in many respects, as the Delft3D model computes vertical and temporal variations of the eddy viscosity and eddy diffusivity and the formulation for sediment-induced turbulence damping is different between the models. Notably, iFlow includes a sediment-induced reduction of the bed shear stress due to stratification near the bed. Such effect is not included in Delft3D, although it could be implemented to modify the assumed log-layer near the bed. We have changed the Delft3D turbulence model in one aspect by adding a source of background turbulence production in the buoyancy frequency. This is necessary, because we use Delft3D in width-averaged mode and therefore lack a source of turbulence production originating from lateral flows. Moreover, as the along-channel flow velocity represents width-averaged velocities, which are typically lower than the thalweg velocity, the turbulence production in the model is lower than what is actually produced in the main channel. This under-prediction of turbulence production may lead to strong stratification at relatively low density differences. To prevent such strong

stratification we add a background shear production term  $u_{z,\min}^2$  to the buoyancy frequency  $N$  used in the turbulence model, according to

$$N^2 = -\frac{g}{\rho} \rho_z \frac{u_z^2}{u_z^2 + u_{z,\min}^2}, \quad (7.6)$$

where  $g$  is the acceleration of gravity,  $\rho$  is density and  $u$  is the along-channel velocity and subscripts  $z$  denote derivatives in vertical direction. This is a similar use of  $u_{z,\min}$  as in Chapter 4 for iFlow, but the values of  $u_{z,\min}$  cannot be compared between the two models.

In several model experiments for this study it has been found that spurious oscillations of the sediment concentration, velocity, eddy viscosity and settling velocity may occur in the along-channel direction. These oscillations occur on a length scale similar to the horizontal grid cell size and at a timescale which seems irregular and unrelated to any forcing. An example of these spurious oscillations is presented in Section 7.4.4. We attempt to suppress the instability at least to some extent by including an along-channel smoothing of the turbulence quantities  $k$  and  $\varepsilon$  and settling velocity  $w_s$ . This is a first attempt, which should be improved when more is known about the origin of the oscillations. The smoothing procedure is based on a weighed moving average with a window of 15 grid points. For any quantity  $q_i$  on grid point  $i$ , this is done according to

$$q_i = \frac{24}{80} q_i + \sum_{n=1}^7 \frac{8-n}{80} (q_{i+n} + q_{i-n}). \quad (7.7)$$

Near the boundary, this filter is corrected, so that points outside of the model domain are not used. Eq. (7.7) additionally helps to prevent localised strong stratification at relatively low density differences, adding to the effect of Eq. (7.6).

The model is initialised using zero water level, velocity and sediment concentration and no sediment on the bed initially. The simulation continues until a dynamic equilibrium condition is attained, measured by requiring a near-zero change in the water motion and sediment concentration in the entire estuary at equal tidal phase. As we do not consider morphological coupling, the amount of sediment on the bed may keep growing in dynamic equilibrium (see the definition of the concentration equilibrium in Section 1.4.2).

### 7.2.3. SUMMARY OF DIFFERENCES BETWEEN DELFT3D AND iFLOW

When using the above configuration, only a few, yet important, differences exist between the Delft3D and iFlow. Focussing on differences in model description, not numerical implementation, the differences are summarised below.

1. **The turbulence model.** Contrary to the turbulence model in iFlow, the  $k - \varepsilon$  turbulence model in Delft3D resolves:
  - (a) time-variations of the eddy viscosity and eddy diffusivity;
  - (b) vertical profile of the eddy viscosity and eddy diffusivity. Most notably the local effect of sharp density gradients on turbulence; and
  - (c) a different degree of sediment-induced turbulence damping.

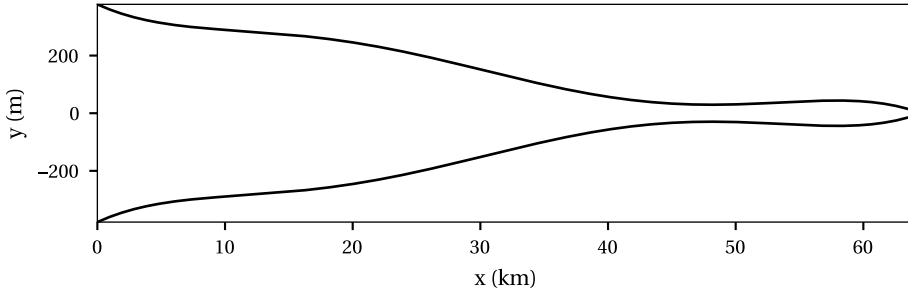
2. **Turbulence damping in the bed friction parametrisation.** iFlow includes a reduction of the bed shear stress for hydrodynamics as a result of near-bed stratification, which is not implemented in Delft3D.
3. **Open boundary conditions.** It is not possible to prescribe a boundary condition in Delft3D that is consistent with the interior solution, leading to the formation of a non-physical boundary layer near the open boundary. In iFlow, this problem does not exist.
4. **Time variable erodibility.** The amount of sediment on the bed, denoted by the erodibility  $f^*$  (Eq. (7.3)) is allowed to vary every time step in Delft3D, while iFlow uses a weighed tidally averaged erodibility  $f$  (Brouwer et al., 2018), thus assuming that erosion only depends on the amount of sediment on the bed on a subtidal basis.
5. **Hindered settling.** While both models are based on the formulation of Richardson and Zaki (1954), iFlow bases its hindered settling only on the near-bed subtidal sediment concentration, while Delft3D uses the local instantaneous sediment concentration.
6. **Approximation.** The iFlow model approximates the solution for the water motion and sediment concentration by computing a limited number of orders in the perturbation expansion and a limited number of tidal components (see Chapter 2). Delft3D also approximates the solutions of the water motion and sediment concentration but does this by linearising the equations per time step. As the time step is much smaller than a tidal cycle, this yields a better approximation of the non-linear equations.

#### 7.2.4. EMS CASE CONFIGURATION

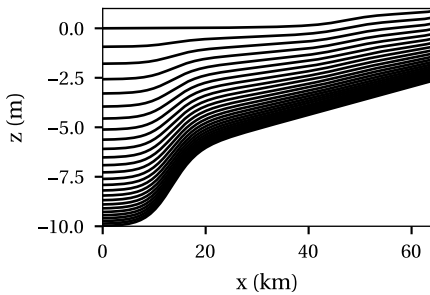
The Ems case in Delft3D is configured to resemble the set-up used in Chapter 4 as much as possible. The model is configured for two cases, representing the years 1965 and 2005, which differ only in the depth profile and a small change in the tidal forcing at the seaward boundary. The depth and width profiles are identical to those prescribed in Chapter 4 and are shown in Fig. 7.2. Values of the model parameters for both cases are summarised in Table 7.1.

The numerical grid consists of 200 equidistant cells in the along-channel direction and 25 cells in vertical directions, exponentially refined towards the bed with an exponent 1.09 (see Fig. 7.2). As a result, the top and bottom cells cover 9.3% and 1.2% of the water column, respectively. The time step is equal to 1 minute unless the time step restriction of Eq. (7.5) requires a smaller time step. The total simulation time is between 9 and 18 months, depending on the time required to reach dynamic equilibrium conditions.

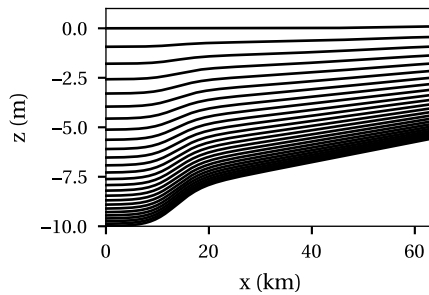
The model is calibrated through the Chézy roughness parameter  $C$  and erosion parameter  $\bar{M}$ . The roughness parameter is set to give the best fit between the modelled  $S_2$  water level amplitude and observed  $M_2$  water level amplitude for average discharge conditions in 1965, resulting in  $C=38 \text{ m}^{1/2}/\text{s}$ . The roughness parameter is not changed for simulations of the 2005 case. The default value of the erosion parameter is chosen such that the best correspondence is found between the subtidal surface sediment concentrations in Delft3D and iFlow for average discharge conditions in 1965. This is done so that the



(a) Width profile used in both the 1965 and 2005 case.



(b) Depth and layer distribution for the 1965 case.



(c) Depth and layer distribution for the 2005 case.

**Figure 7.2:** Width and depth profiles used representing the Ems in 1965 and 2005.

results of iFlow and Delft3D can easily be compared. The effect of choosing different values of the erosion parameters will be discussed extensively.

### 7.3. RESULTS 1965 CASE AND COMPARISON WITH iFLOW

Using this calibrated model, results obtained with the Delft3D model are compared to results obtained using iFlow for the 1965 case. First we present the differences in water motion and sediment concentration and qualitatively attribute the observed differences between the results of the two models to the differences in process formulation listed in Section 7.2.3. Next we analyse two of these differences in detail: time-varying turbulence and erodibility.

#### 7.3.1. DEFAULT CASE

Figure 7.3 shows results of the 1965 case from Delft3D (solid lines) and iFlow (dotted lines). Water level amplitudes and phases (Fig. 7.3a-7.3b) of the  $M_2/S_2$  (green) and  $M_4/S_4$  (orange) tides show a good correspondence between the models up to roughly km 45. Upstream from km 45 the  $S_2$  tide shows more damping, yet faster tidal propagation (i.e. smaller phase difference) than the  $M_2$  tide in iFlow. The  $S_4$  tide is more amplified in Delft3D and moves faster compared to the  $M_4$  tide in iFlow. These differences



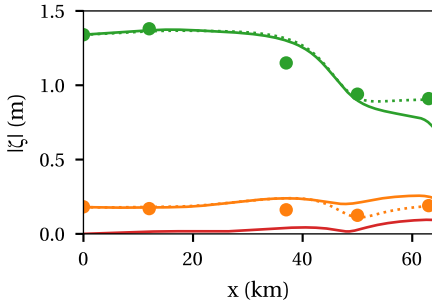
Symbol	Description	Value	
		1965	2005
$A_{S_2}$	$S_2$ water level amplitude at $x = 0$	1.34 m	1.4 m
$A_{S_4}$	$S_4$ water level amplitude at $x = 0$	0.18 m	0.21 m
$\phi_{S_4}$	Relative phase difference between the $S_2$ and $S_4$ water level at $x = 0$	-178 deg	-171 deg
$Q$	River discharge	80 m <sup>3</sup> /s	40 m <sup>3</sup> /s
$A_{v,\min}$	Minimum eddy viscosity	10 <sup>-4</sup> m <sup>2</sup> /s	
$K_{v,\min}$	Minimum eddy diffusivity	10 <sup>-4</sup> m <sup>2</sup> /s	
$A_h$	Horizontal eddy viscosity	1 m <sup>2</sup> /s	
$K_h$	Horizontal eddy diffusivity	100 m <sup>2</sup> /s	
$c_{\text{sea}}$	Cross-sectionally uniform sediment concentration at $x = 0$	0.1 kg/m <sup>3</sup>	
$w_{s,0}$	Clear-water settling velocity	1 mm/s	
$c_{\text{gel}}$	Gelling concentration	100 kg/m <sup>3</sup>	
$\bar{M}$	Erosion parameter (Eq. (7.2))	10 <sup>-4</sup> kg/(m <sup>2</sup> s)	
$\tau_c$	Critical shear stress for erosion (Eq. (7.2))	10 <sup>-2</sup> Pa	
$\rho_{\text{bed}}$	Density of sediment on the bed (Eq. (7.3))	500 kg/m <sup>3</sup>	
$d_{\text{thresh}}$	Threshold thickness for erosion (Eq. (7.3))	0.05 m	
$C$	Chézy roughness coefficient	38 m <sup>1/2</sup> /s	

**Table 7.1:** Default settings for the model parameters in Delft3D.

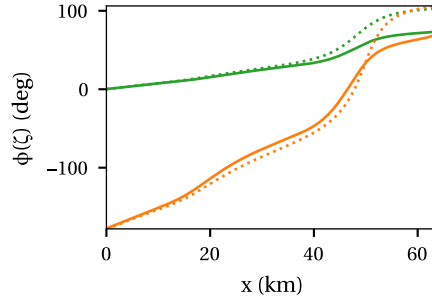
are likely caused by non-linear interactions, such as tide-river interaction and interaction between the tidal velocity and the varying surface level, which are less accurately resolved in iFlow than in Delft3D (point 6 in Section 7.2.3). In iFlow it is assumed that the surface elevation  $\zeta$  is small compared to the depth and the river-induced velocity  $u_{\text{riv}}$  is much smaller than the  $S_2$  tidal velocity amplitude  $U$ . In this area,  $\varepsilon = \zeta/H > 0.25$  and  $u_{\text{riv}}/U > 0.5$ , such that these assumptions do not strictly hold. The Delft3D result also includes higher-frequency overtides, including the  $S_6$  tide. From the figure it follows that this tidal component (red line) is much smaller than the  $S_2$  and  $S_4$  tide in most of the estuary, so that it may be neglected in the analysis of the most important physical processes.

The along-channel depth-averaged velocity amplitude and phase (Fig. 7.3c-7.3d) depend on the same equations and assumptions as the water level, yet the differences are visible in slightly different locations. The  $S_2/M_2$  amplitude in both models corresponds closely in the entire model domain, while the  $S_4/M_4$  amplitude deviate upstream from km 30. The velocity phases show a similar pattern as the water level phases, with Delft3D results showing a faster propagation of the tidal wave.

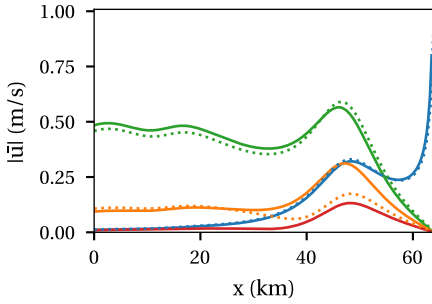
As the eddy viscosity (Fig. 7.3e) in iFlow is depth uniform and constant over the tide, we only plot the subtidal contribution from iFlow and compare this to the depth-averaged, tidally varying eddy viscosity from Delft3D. The overall patterns along the estuary are similar between the subtidal components in both models, due to their similar dependence on velocity and depth and because they both account for sediment-induced tur-



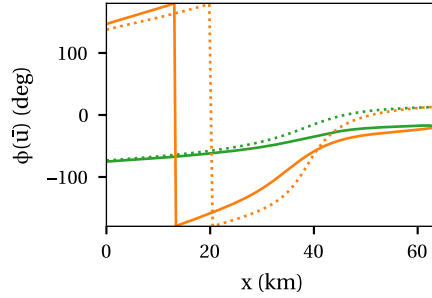
(a) Water level amplitude



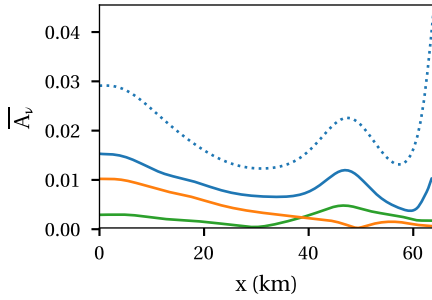
(b) Water level phase



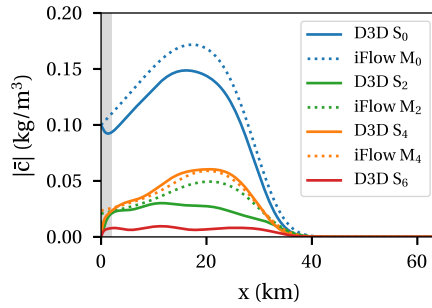
(c) Along-channel depth-averaged velocity amplitude



(d) Along-channel depth-averaged velocity phase

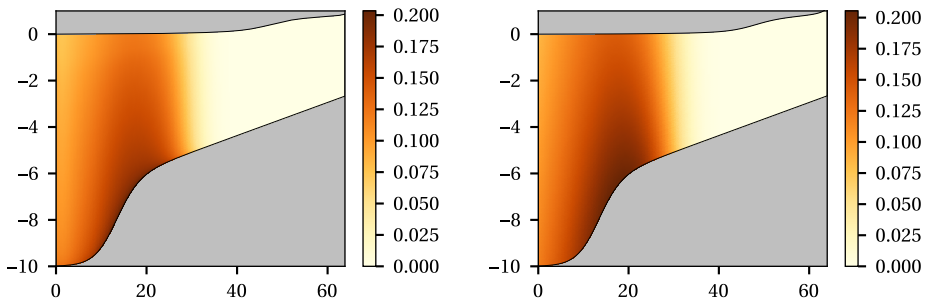


(e) Depth-averaged eddy viscosity amplitude



(f) Depth-averaged sediment concentration amplitude. The grey band denotes the diffusive boundary layer in Delft3D.

**Figure 7.3:** Water motion, eddy viscosity and sediment concentration in Delft3D (solid lines) and iFlow (dotted lines) in the 1965 case.



(a) Subtidal sediment concentration ( $\text{kg/m}^3$ ) in Delft3D. (b) Subtidal sediment concentration ( $\text{kg/m}^3$ ) in iFlow.

**Figure 7.4:** Subtidal sediment concentration in the 1965 case in Delft3D (a) and iFlow (b).

bulence damping. However, the magnitude of the depth-averaged eddy viscosity is clearly different. As the water motion in Delft3D and iFlow are comparable, the eddy viscosity in both models must result in a similar amount of energy dissipation. This means that the vertical and temporal structure of the eddy viscosity in Delft3D is important in determining the total dissipation and that the models cannot be compared directly on the level of the eddy viscosity.

The subtidal sediment concentration (Fig. 7.3f) has been calibrated such that the maximum subtidal concentrations in the Delft3D and iFlow results are similar. Not calibrated are the ETM location, shape and magnitude of the tidally varying components. The ETM location and shape as well as the  $S_4/M_4$  concentration signal are remarkably similar in both models. The  $S_2/M_2$  component is smaller in Delft3D than in iFlow. The  $M_6$  sediment concentration amplitude in Delft3D is again significantly smaller than the other tidal constituents. To also compare the vertical structure of the sediment concentration, Fig. 7.4 shows the subtidal sediment concentration in an along-channel-vertical section of the model. While the overall distribution of the sediment concentration is similar between the models, iFlow shows a more uniformly mixed water column.

The model differences listed in Section 7.2.3 can all potentially result in differences in the sediment distribution between the models. However, for this case where we find moderate sediment concentrations mostly in the deeper part of the estuary, it can be argued that several of these differences are negligible. Firstly, sediment induced turbulence damping (item 1c and 2 in Section 7.2.3) is not very important as sediment concentrations are moderate. Secondly, hindered settling (item 5) is only important at much higher concentrations. Finally, the differences in the approximation of the water motion (item 6) do not result in a very different distribution of sediment, since almost all sediment is located between km 0 and 40, where the water motion is highly similar between the models. More important is the vertical structure of turbulence (item 1b), which is partly responsible for the difference in vertical structure of the sediment concentration shown in Fig. 7.4. As a result, the vertical distribution of sediment in iFlow

follows what one could call a Schmidt profile (Toorman, 2000), while it follows a Rouse profile in Delft3D. Also important is the mismatch between open boundary conditions and interior dynamics in Delft3D (item 3). This results in a boundary layer between km 0 and 2 marked by the grey band in Fig. 7.3f. The actual boundary condition near km 2 has slightly lower subtidal concentrations than iFlow and these differences persist throughout the model domain. The remaining differences are related to the sediment transport due to temporal variability of the eddy viscosity and eddy diffusivity (item 1a) and temporal variability of the erodibility (item 4). In the next sections we illustrate the importance of these processes.

### 7.3.2. SEDIMENT TRANSPORT DUE TO TIME-VARYING EDDY DIFFUSIVITY

It is not possible to unambiguously compute the individual physical processes that contribute to sediment transport in Delft3D. Therefore, to gain insight into which sediment transport processes are dominant in Delft3D in the 1965 Ems case, we assume that the transport processes resolved by iFlow are representative for the transport processes in Delft3D. This assumption seems reasonable, since the water motion and sediment concentration in the two models compare reasonably well. Fig. 7.5 shows these sediment transport contributions. The main mechanisms responsible for sediment import are related to the tidal asymmetry generated by the externally imposed  $M_4$  tide and the internally generated  $M_4$  tide due to the tidal return flow contribution (see Chapter 4 for details). Also important is spatial settling lag, which is generally importing sediment. These contributions, together with the exporting contribution due to river-induced asymmetry form the tidal pumping sediment transport contribution.

Two potentially important sediment transport contributions that are not explicitly resolved by iFlow but are included in Delft3D, are those related to the time-varying eddy viscosity and time-varying eddy diffusivity. It is difficult to compute the transport contribution due to the time-varying eddy viscosity, as this requires reconstruction of the contribution of the time-varying eddy viscosity to both the velocity and surface elevation. Such elaborate reconstruction is beyond the scope of this study. The effect of the time-varying eddy diffusivity can be reconstructed more easily. Evaluating this effect requires reconstruction of the sediment concentration for constant and varying eddy diffusivity, given the computed water motion and settling velocity, see Appendix 7.B for details. This transport contribution is plotted in Fig. 7.5 (black line), together with a reconstruction of the river-induced export due to the interaction between the subtidal velocity and subtidal sediment concentration (green solid line). The latter is for comparison between iFlow and Delft3D and shows that this contribution is slightly smaller than the corresponding contribution in iFlow (green dashed line). This is due to the difference in subtidal sediment concentration between the two models (cf. Fig. 7.3f). The observations that the river-induced export in both models compares well, indicates that the overall pattern and magnitude of the reconstructed contribution of time-varying eddy diffusivity can be compared to the transport mechanisms in iFlow, although it may be slightly underestimated. The transport due to time-varying eddy diffusivity is a small positive contribution with a magnitude comparable to that of the transport due to gravitational circulation in iFlow.

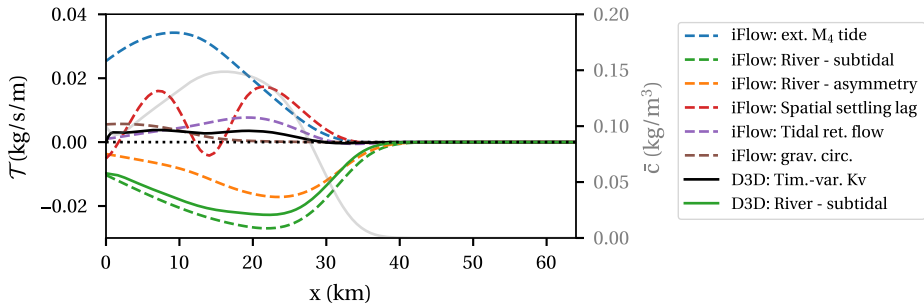


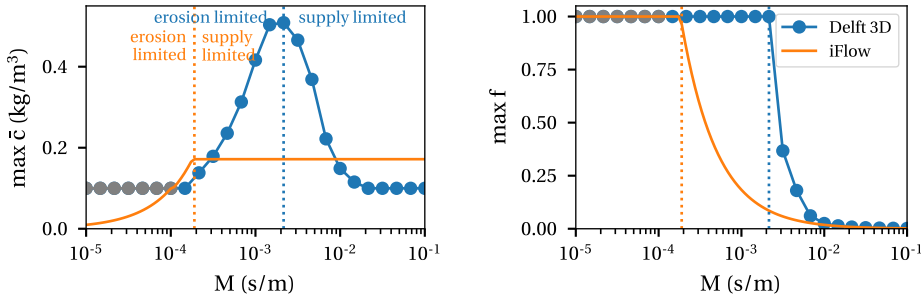
**Figure 7.5:** Sediment transport contributions per metre width in the 1965 case. Contributions derived from iFlow are plotted with dashed lines. Contributions estimated from Delft3D output are plotted with solid lines. The river-induced transport due to subtidal interaction is plotted for both iFlow and Delft3D for comparison. This allows for the comparison between the transport due to the temporally variable eddy diffusivity and the transport contributions derived from iFlow. The grey line shows the depth-averaged subtidal sediment concentration from Delft3D for reference.

### 7.3.3. SENSITIVITY TO THE EROSION PARAMETER AND IMPORTANCE OF ERODIBILITY

To investigate the effect of the different parametrisation of the erodibility in iFlow and Delft3D, we investigate the sensitivity of the model results to the erosion parameter  $M$ . Fig. 7.6a shows the maximum subtidal depth-averaged concentration obtained using Delft3D and iFlow for the 1965 case for varying erosion parameter. We separate this figure into two parts: an erosion limited domain where concentrations increase with increasing  $M$  (for iFlow  $M < 1.5 \cdot 10^{-4}$  s/m and for Delft3D  $M < 2 \cdot 10^{-3}$  s/m) and a supply limited range where concentrations are constant or decreasing with  $M$  (for iFlow  $M > 1.5 \cdot 10^{-4}$  s/m and for Delft3D  $M > 2 \cdot 10^{-3}$  s/m).

In the erosion limited domain, the maximum concentration is limited by the capacity of the flow to resuspend sediment from the bed (e.g. Brouwer et al., 2018). This is characterised by an erodibility  $f^*$  equal to its maximum value of 1 during the entire tidal cycle. Since erosion scales as  $M \max(\tau - \tau_c, 0) f^*$  (see Eq. (7.2)) and assuming  $\tau$  does not change much when  $M$  changes, the erosion and therefore the maximum subtidal sediment increases linearly with  $M$ . This corresponds to the behaviour of both models in Fig. 7.6a in their respective erosion limited domains. The exception are the grey points, where the maximum concentration equals the prescribed concentration at the open boundary in Delft3D, which is no longer consistent with the internal dynamics; a problem that is corrected in iFlow (see Section 7.2.2). The erosion limited domain extends to larger erosion parameters and higher sediment concentrations in Delft3D than in iFlow, showing that iFlow underpredicts the sediment import compared to Delft3D. The exact mechanisms that are underpredicted or missing in iFlow have not been identified.

In the supply limited range, the maximum concentration is limited by the ability of the flow to import sediment into the estuary. In other words, at each location there is a moment during the tidal cycle where no easily erodible sediment is available at the bed. The maximum concentration in the supply limited range in Delft3D decreases with increas-



(a) Maximum subtidal depth-averaged sediment concentration. (b) Maximum weighed subtidal erodibility  $f$ .

**Figure 7.6:** Response of the maximum subtidal depth-averaged sediment concentration and erodibility to the erosion parameter  $M = \frac{\bar{M}}{\tau_c}$  in the 1965 case. Results from Delft3D are plotted in blue, results from iFlow are plotted in red. The results plotted in grey are Delft3D results where the seaward boundary condition cannot attain equilibrium with the bed. The figure can be separated into an erosion limited and a supply limited range, with different response of the models to variations in  $M$ .

ing  $M$ . The maximum concentration in iFlow on the other hand remains constant with varying  $M$ . To explain the differences we give an intuitive explanation of the role of  $M$  in both models here and provide a more formal mathematical argument in Appendix 7.C.

For the explanation we assume that, to leading order, sediment is conserved locally in the water column and the bed. Sediment can therefore be exchanged between the water column and the bed but is not advected from elsewhere (consistent with the scaling in Chapter 2). Then, in Delft3D, the result of increasing  $M$  in the supply limited range is that sediment is resuspended more easily, so that all the available sediment is suspended in the water column for longer. Therefore, the variation of the sediment concentration over the tidal cycle decreases relative to the average sediment concentration. This in turn means a decrease of the sediment transport due to the correlation between the tidally varying sediment concentration and velocity, i.e. tidal pumping. As tidal pumping is the dominant sediment importing mechanism, the sediment import decreases with increasing  $M$ , leading to lower sediment concentrations.

In iFlow, the conservation of sediment in the water column and bed is only obeyed on a tidally averaged timescale and is violated on the intratidal timescale. This is because iFlow only computes the subtidal erodibility  $f$  instead of the instantaneous erodibility  $f^*$  (see Section 7.2.2). Therefore, increasing  $M$  has no effect on the tidal variation of the sediment concentration relative to the average sediment concentration. In fact, the product  $Mf$ , which determines the suspended sediment concentration, remains constant so that the sediment concentration is independent of  $M$ .

As a consequence of the increasing and decreasing concentrations in the erosion and

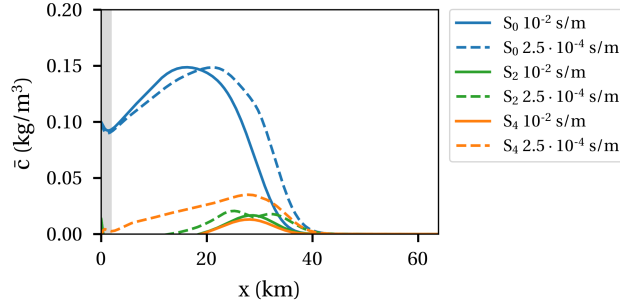


**Figure 7.7:** Depth-averaged sediment concentration in the 1965 case from Delft3D with two different values of the erosion parameter in the erosion limited domain (dashed) and supply limited domain (solid). The values are chosen such that the subtidal maximum depth-averaged concentration is the same between the two simulations.

supply limited ranges in Delft3D, two ways of attaining similar maximum sediment concentrations are found. This is demonstrated for  $M = 2.5 \cdot 10^{-4}$  s/m and  $M = 10^{-2}$  s/m in Fig. 7.7. As models are often calibrated based on limited observations, both values of  $M$  could be chosen as the best calibration parameters to fit a set of observations. However, these different values of  $M$  represent a very different sediment dynamics. This is an important observation, given the fact that  $M$  (i.e. describing both  $\bar{M}$  and  $\tau_c$ ) is often regarded as a calibration parameter which can attain values with different orders of magnitude.

#### 7.4. RESULTS 2005 CASE

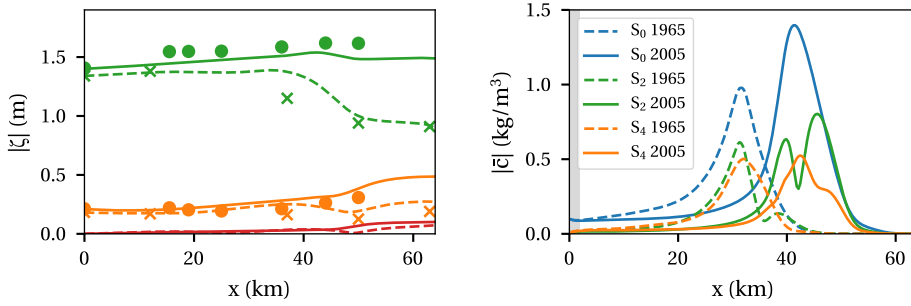
The 2005 case only differs from the 1965 case in the bed level and a small change in the tidal forcing. The other parameters, including calibration parameters are the same as in 1965. Instead of directly comparing the results from the Delft3D and iFlow models, Delft3D results for the 2005 case are compared instead to Delft3D 1965 results. This shows the response of the model to channel deepening. The comparison between Delft3D and iFlow is made more qualitatively. In iFlow, high sediment concentrations were found for the 2005 case for river discharges below  $70 \text{ m}^3/\text{s}$ . Therefore we focus on the average summer discharge case, where the discharge is  $40 \text{ m}^3/\text{s}$ .

In this section we first investigate the results for default parameters (see Table 7.1). Next we investigate the two processes that are most restrictive to the sediment concentration: the erosion parametrisation and sediment-induced turbulence damping. Finally, we briefly discuss several model results that did not converge.

##### 7.4.1. DEFAULT CASE

Fig. 7.8 shows a comparison of the tidal water level amplitude (Fig. 7.8a) and depth-averaged sediment concentration (Fig. 7.8b) between the 1965 and 2005 cases in Delft3D for default parameters with summer-averaged discharge ( $Q = 40 \text{ m}^3/\text{s}$ ). While the  $S_2$  water level amplitude in 2005 is significantly amplified compared to 1965, the amplification is somewhat weaker than indicated by observations. The  $S_4$  water level is also amplified





(a) Water level amplitude. Dots indicate 2005 observations, crosses indicate 1965 observations. (b) Depth-averaged sediment concentration. The grey area indicates the boundary layer.

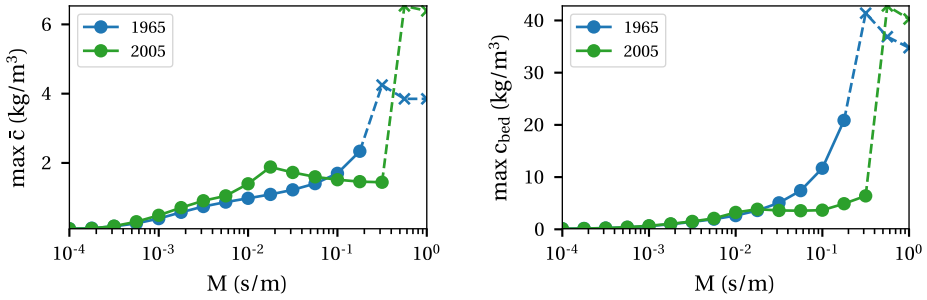
**Figure 7.8:** Water level amplitude and depth-averaged sediment concentration in the 2005 default case (solid lines) and 1965 case (dashed lines) with summer-averaged discharge ( $Q = 40 \text{ m}^3/\text{s}$ ).

and corresponds reasonably well to measurements. The  $S_6$  water level is also amplified but remains small compared to the  $S_2$  and  $S_4$  amplitude. The maximum depth-averaged sediment concentration is approximately a factor 1.5 larger in 2005 than in 1965, in an ETM that is located approximately 10 km further upstream. Clearly, the regime shift to hyperturbid conditions is not reproduced.

#### 7.4.2. SENSITIVITY TO THE EROSION PARAMETER AND ANALYSIS

To investigate if hyperturbid conditions can be attained by varying the erosion parameter, we test the sensitivity of the dynamic equilibrium to this parameter. Fig. 7.9 shows the maximum depth-averaged (Fig. 7.9a) and near-bed (Fig. 7.9b) sediment concentration in the 1965 (blue) and 2005 (green) cases as function of  $M$ . Points marked by crosses indicate results that have not converged to equilibrium and are discussed in Section 7.4.4. Focussing on converged results, maximum concentrations in 1965 increase up to  $20 \text{ kg/m}^3$ . Concentrations in 2005 are higher than in 1965 up to a value  $M = 10^{-1} \text{ s/m}$  (depth-averaged concentration) or  $M = 2 \cdot 10^{-2} \text{ s/m}$  (near-bed concentration) but remain lower than in 1965 for larger  $M$ . Resulting maximum near-bed concentrations in 2005 remain below  $6 \text{ kg/m}^3$ . Results of the erodibility (not shown) show that  $f = 1$  locally in all cases, indicating erosion limited conditions. Corresponding to the behaviour in the erosion limited regime in Section 7.3, sediment concentrations increase with increasing  $M$  for the 1965 case and for the 2005 case up to  $M = 10^{-2} \text{ s/m}$  (Fig. 7.9a). However, for larger  $M$  in 2005, the maximum near-bed concentration decreases slightly before increasing again, while the depth-averaged concentration gradually decreases.

These results can be explained from the change in along-channel sediment distribution with  $M$ , shown by the distribution of the tidally averaged erodibility  $f$  (Fig. 7.10a-7.10b). In 1965, the trapping zone remains roughly in the same position when varying  $M$ . Hence, as  $M$  increases, and as the system remains erosion limited, the sediment concentration increases. In 2005 we find only one trapping zone for  $M = 10^{-2} \text{ s/m}$  (cf. Fig. 7.8b) but two



(a) Maximum depth-averaged concentration. (b) Maximum near-bed concentration.

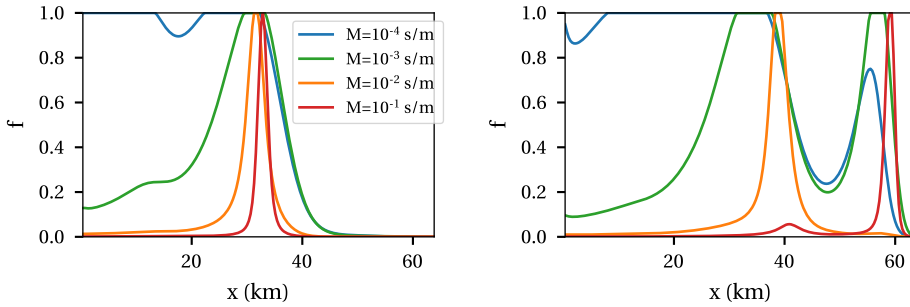
**Figure 7.9:** Sensitivity of the depth-averaged (a) and near-bed (b) sediment concentration to the erosion parameter  $M$  for the 2005 and 1965 case with summer-averaged discharge ( $Q = 40 \text{ m}^3/\text{s}$ ). Results are plotted as maximum concentration versus  $M$ , with 1965 in blue and 2005 in green. Several results are marked by dashed lines and crosses, indicating that these results have not converged.

trapping zones for the other plotted results. The first trapping zone is erosion limited for  $M \leq 10^{-2} \text{ s/m}$  and therefore sediment concentrations in the ETM increase with increasing  $M$ . However, when  $M > 10^{-2} \text{ s/m}$ , the dynamics becomes supply limited ( $f < 1$ ) and sediment concentrations in the ETM decrease with increasing  $M$ . As the highest sediment concentrations are found in this ETM, the maximum sediment concentration decreases with  $M$  when  $M > 10^{-2} \text{ s/m}$ . The second trapping zone on the other hand is erosion limited for small and large  $M$ . When  $M > 10^{-1} \text{ s/m}$ , the sediment concentration near the bed in the second ETM exceeds that in the first ETM, so that the maximum near-bed concentration again increases with  $M$  (see Fig. 7.9b).

To gain insight into the mechanisms that restrict further increasing maximum concentrations in 2005, we look at the limiting mechanism to the sediment concentration. As all simulations for the 2005 case are erosion limited, this restricting mechanism is local resuspension (Chapter 4), which is quantified using the tidally averaged dimensionless erosion parameter  $\langle \tilde{E} \rangle$  (see Chapter 3). For the Delft3D model, this parameter is defined as

$$\langle \tilde{E} \rangle = \left\langle \frac{M \max(\tau - \tau_c, 0)}{\tau_c w_{s,0} c_{gel}} \right\rangle. \quad (7.8)$$

In Chapter 3 it was derived that the maximum sediment concentration can be restricted by local resuspension if  $\langle \tilde{E} \rangle$  is smaller than a threshold value. In Delft3D, the threshold value is approximately equal to 0.067, but the exact value cannot be determined a priori (see Chapter 3). The dimensionless erosion parameter is plotted for the 2005 case for various values of  $M$  in Fig. 7.11a, together with the approximate threshold value of 0.067. The value of  $\langle \tilde{E} \rangle$  increases almost linearly with increasing  $M$ , due to the dependency between  $\langle \tilde{E} \rangle$  and  $M$  (see Eq. (7.8)). However, near km 40 and 60,  $\langle \tilde{E} \rangle$  increases more slowly. As a result,  $\langle \tilde{E} \rangle$  locally remains significantly below the threshold even for  $M$  as



(a) 1965.

(b) 2005.

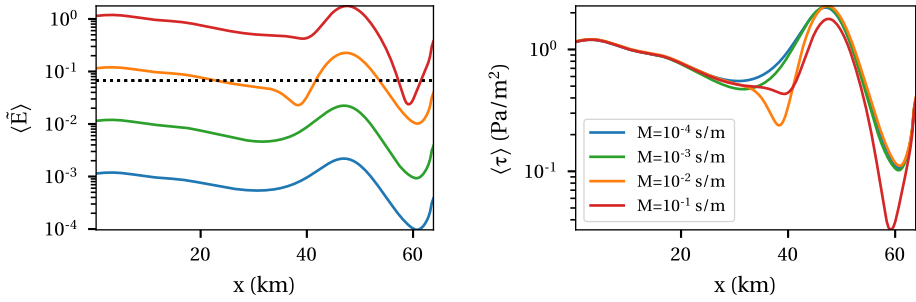
**Figure 7.10:** Tidally averaged erodibility  $f$  for various  $M$  (stable results) in 1965 (a) and 2005 (b).

high as 0.1 s/m. While for  $M = 0.1$  s/m  $\langle \tilde{E} \rangle$  is above the threshold in most of the estuary, there is a small area where  $\langle \tilde{E} \rangle$  is below the threshold. In this area, the bed acts as a strong sediment sink, leading to a relatively low suspended sediment concentration. The reason why  $\langle \tilde{E} \rangle$  remains relatively small near km 40 and 60 is a reduction of the bed shear stress, see Fig. 7.11b. The reduction of the bed shear stress with increasing  $M$  shown by the figure is caused by sediment-induced damping of turbulence and is most pronounced in the ETM near km 40 and 60.

#### 7.4.3. IMPORTANCE OF SEDIMENT-INDUCED TURBULENCE DAMPING

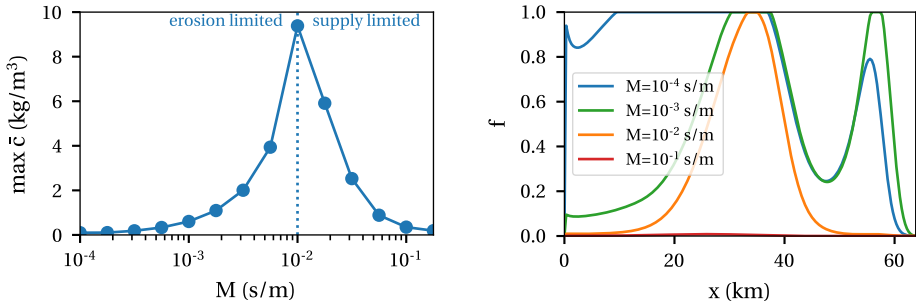
To further understand the role of sediment-induced damping of turbulence on the 2005 results, Fig. 7.12 shows results of the 2005 case with summer average discharge ( $Q = 40$  m<sup>3</sup>/s) without sediment-induced turbulence damping. Fig. 7.12a shows that maximum depth-averaged sediment concentrations increase with increasing  $M$  up to  $M = 10^{-2}$  s/m and a depth-averaged maximum concentration of approximately 9 kg/m<sup>3</sup> in an erosion limited situation. For larger  $M$ , the situation becomes supply limited and concentrations rapidly decrease with increasing  $M$ . This is because of the reduction of tidal pumping discussed in Section 7.3. Fig. 7.12b shows along-channel profiles of the tidally averaged erodibility, indicating that two trapping zones exist for small erosion parameters, but that the second trapping zone disappears for larger  $M$ . As a result, the highest depth-averaged sediment concentrations up to 9 kg/m<sup>3</sup> are found in a single ETM.

Comparing these results to the results with sediment-induced turbulence damping (Fig. 7.9), the transition from erosion to supply limited conditions occurs for smaller  $M$  and the second ETM is absent. This indicates that sediment-induced turbulence damping is important for generating sediment import into the estuary. We have thus found two opposing effects of sediment-induced turbulence damping: on the one hand it leads to a reduction in bed shear stress, hence reducing the ability of the estuary to resuspend sediment from the bed, while on the other hand it increases sediment import.



(a)  $\langle \tilde{E} \rangle$  and the estimated threshold value. (b) Bed shear stress.

**Figure 7.11:** Sensitivity of the tidally averaged dimensionless erosion parameter  $\langle \tilde{E} \rangle$  (Eq. (7.8)) and bed shear stress to the erosion parameter  $M$  in the 2005 case. Plotted with  $\langle \tilde{E} \rangle$  is also the estimated threshold value of 0.067 (black dotted line), above which local resuspension cannot restrict the suspended sediment concentration.

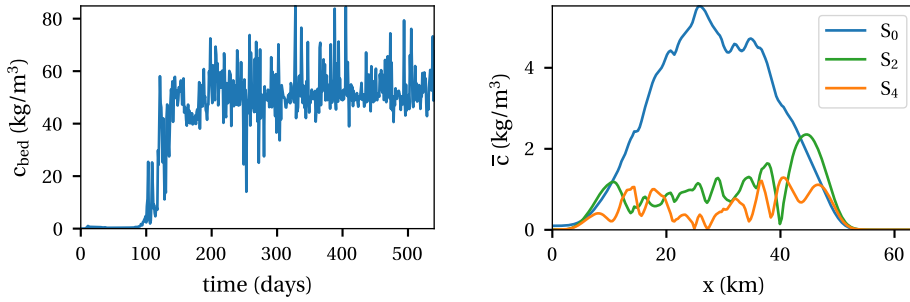


(a) Maximum depth-averaged concentration. (b) Tidally averaged erodibility  $f$ .

**Figure 7.12:** Sensitivity of the depth-averaged sediment concentration to the erosion parameter  $M$  for the 2005 case without sediment-induced turbulence damping. Results are plotted as maximum concentration versus  $M$  and as along-channel profiles of the tidally averaged erodibility for various  $M$ .

#### 7.4.4. UNCONVERGED RESULTS

Several results with high erosion parameters, marked in Fig. 7.9 by crosses, do not converge. Fig. 7.13 demonstrates the characteristics of one such simulation for the 2005 case with  $M = 1$  s/m. Fig. 7.13a shows the near-bed sediment concentration at  $x = 35$  km at a fixed moment in every tidal cycle some time after HW slack. In dynamic equilibrium, this signal should converge to a constant value. Instead, the figure shows oscillations with fluctuating amplitude and period. Hence, we argue that these oscillations do not indicate cyclic behaviour but are spurious. Apart from a lack of convergence, the simulation shows oscillations in the along-channel sediment concentration, see Fig. 7.13b.



(a) Near-bed sediment concentration at  $x = 35$  km recorded at a fixed moment after slack tide. (b) Depth-averaged sediment concentration.

**Figure 7.13:** Two characteristics of an unconverged model result in the 2005 case with  $M = 1$  s/m. (a) shows that the simulation does not converge to a dynamic equilibrium. (b) shows spurious oscillations in the along-channel depth-averaged sediment concentration profile.

These oscillations are also thought to be spurious. The reason for the oscillations is unknown; they could originate from an instability in the equations or from the numerical implementation.

## 7.5. DISCUSSION AND CONCLUSIONS

In this study, we have made a first exploration of the question whether the knowledge of regime shifts from low to high sediment concentrations may be transferred from the idealised iFlow modelling studies in this thesis to a more complex model. To this end, we have systematically investigated the differences between results of iFlow and a Delft3D model in a similar geometry and with similar forcing conditions, applied to the Ems case in 1965 and 2005. The 1965 case is characterised by moderate sediment concentrations located mostly in the deeper part of the estuary. For this case, given that the value of the erosion parameter is properly chosen, good correspondence may be found between the iFlow and Delft3D result. The 2005 case is characterised by higher sediment concentrations located closer to the upstream boundary, where the estuary is relatively shallow. Some characteristics of the results correspond between the iFlow and Delft3D models: both models show two trapping zones located in the upstream half of the estuary for low river discharges. However, using Delft3D we have not been able to reproduce the high sediment concentrations of much more than  $10 \text{ kg/m}^3$  observed in reality and found with iFlow.

This study points to three important results in modelling the transition from low to high sediment concentrations, which appeared in Delft3D but were not observed or much less pronounced in iFlow. Firstly, when the bed erodibility  $f^*$  is allowed to change continuously in time, an ‘optimum’ value of the erosion parameter  $M$  exists for which the suspended sediment concentration is maximised. This implies that similar concentrations may be found for  $M$  on either side of the optimum, which makes the choice of  $M$  ambivalent. Moreover, it means that the calibration of the erosion parameter is essential

for reproducing high sediment concentrations in models. For  $M$  smaller than the optimum, the estuary is erosion limited. This means that not all of the imported sediment can be kept in suspension. Some sediment is deposited on the bed resulting in a subtidally growing bottom pool. For  $M$  larger than the optimum, the estuary is supply limited. An additional requirement for hyperturbidity is that the tidally averaged dimensionless erosion parameter  $\langle \tilde{E} \rangle$ , which scales linearly with  $M$ , is above a threshold value (see also Chapter 3). Combining the above criteria, modelling hyperturbidity requires that  $M$  is sufficiently high so that most of the imported sediment is kept in suspension, i.e.  $\langle \tilde{E} \rangle$  is above the threshold. However, if tidal pumping is important to the sediment import,  $M$  should be sufficiently small so that tidal pumping is not diminished.

Secondly, it was found that sediment-induced turbulence damping plays a similarly ambiguous role in the modelling of the Ems estuary. On the one hand, sediment-induced turbulence damping locally leads to a reduced bed shear stress, which reduces the ability of the flow to keep sediment in suspension (i.e. it reduces  $\langle \tilde{E} \rangle$ ). This is not only true for the Ems but holds in general. On the other hand, sediment-induced turbulence damping is essential to generate the sediment import required to reproduce the transition to hyperturbidity in the Ems. This effect is not expected to be true in general but likely holds for a larger class of estuaries.

Finally, the parametrisations and their numerical implementation chosen in Delft3D, and likely in many other complex models, pose several challenges of their own. Explicit temporal coupling between the water column and bed was shown to impose a time-step restriction, which may become severe for large erosion parameters and bed shear stresses. Furthermore, vertical sediment concentration profiles may locally collapse, showing much stronger stratification in one or a few computational cells, resulting in sharp along-channel gradients. This effect was suppressed in this study by implementing background turbulence and along-channel smoothing of the eddy viscosity and eddy diffusivity. Finally, we found that Delft3D results do not converge for some settings that lead to high sediment concentrations, so that no trustworthy results with high sediment concentrations could be obtained.

Each of these three results leads to a challenge in modelling a regime shift to high sediment concentrations in complex models in general. These challenges are related to (1) improving understanding of erosion from the bed and the value of the erosion parameter in a changing regime, (2) improving understanding of the role of sediment-induced turbulence damping on friction and erosion near the bed and (3) stabilising model results in situations with high sediment concentrations. Apart from these challenges, it is important to extend these results to other domains and more complex three-dimensional domains to investigate if the results found in this chapter apply more widely.

## REFERENCES

- Brouwer, R. L., Schramkowski, G. P., Dijkstra, Y. M., and Schuttelaars, H. M. (2018). Time evolution of estuarine turbidity maxima in well-mixed, tidally dominated estuaries: the role of availability- and erosion-limited conditions. *Journal of Physical Oceanography*, 48:1629–1650.
- Burchard, H., Schuttelaars, H. M., and Ralston, D. K. (2018). Sediment trapping in estuaries. *Annual review of Marine Science*, 10:14.1–14.25.

- Deltares (2014). *Delft 3D user manual*. Version 3.15.34158.
- Dijkstra, Y. M., Uittenbogaard, R. E., Van Kester, J. A. T. M., and Pietrzak, J. D. (2016). Improving the numerical accuracy of the  $k-\epsilon$  model by a transformation to the  $k-\tau$  model. *Ocean Modelling*, 104:129–142.
- Murray, A. B. (2003). *Prediction in Geomorphology*, chapter Contrasting the Goals, Strategies, and Predictions Associated with Simplified Numerical Models and Detailed Simulations, pages 151–165. American Geophysical Union, Washington, D. C.
- Richardson, J. F. and Zaki, W. N. (1954). The sedimentation of a suspension of uniform spheres under conditions of viscous flow. *Chemical Engineering Science*, 8:65–78.
- Schuttelaars, H. M., de Jonge, V. N., and Chernetsky, A. S. (2013). Improving the predictive power when modelling physical effects of human interventions in estuarine systems. *Ocean and Coastal Management*, 79:70–82.
- Toorman, E. A. (2000). Sediment-laden turbulent flow: a review of theories and models. Technical Report HYD/ET/00/COSINUS1, Hydraulics laboratory, KU Leuven, Belgium.
- Uittenbogaard, R. E., Van Kester, J. A. T. M., and Stelling, G. S. (1992). Implementation of three turbulence models in 3D-TRISULA for rectangular grids. Technical Report Z81, WL | Delft Hydraulics, Delft, Netherlands.
- Van Maren, D. S., Winterwerp, J. C., and Vroom, J. (2015). Fine sediment transport into the hyper-turbid lower Ems River: the role of channel deepening and sediment-induced drag reduction. *Ocean Dynamics*, 65:589–605.
- Winterwerp, J. C., Wang, Z. B., Van Brackel, A., Van Holland, G., and Kösters, F. (2013). Man-induced regime shifts in small estuaries - II: a comparison of rivers. *Ocean Dynamics*, 63:1293–1306.

## 7.A. TIME STEP RESTRICTION DUE TO EROSION

Delft3D imposes a time-step restriction that, to our knowledge, has not been identified before. The restriction is related to the sediment mass balance on the bed

$$S_{\text{bed},t} = D - E, \quad (7.9)$$

where  $S_{\text{bed}}$  is the amount of sediment (in kg dry material per  $\text{m}^2$ ),  $D$  is deposition and  $E$  is erosion. Rewriting this expression using time stepping and dividing by  $S_{\text{bed}}$  at the current time level, we obtain

$$\frac{S_{\text{bed}}^{n+1} - S_{\text{bed}}^n}{S_{\text{bed}}^n} = \Delta t \frac{D - E}{S_{\text{bed}}^n}, \quad (7.10)$$

where  $n$  indicates the time level. This expression simplifies to

$$\frac{S_{\text{bed}}^{n+1}}{S_{\text{bed}}^n} = \Delta t \frac{D - E}{S_{\text{bed}}^n} + 1 \geq 0. \quad (7.11)$$

This expression is larger than or equal to zero, because  $S_{\text{bed}}$  is non-negative. To obtain a conservative estimate for the restriction imposed by this inequality, deposition is ignored. Next, we combine Eqs. (7.2)-(7.3) for erosion to

$$E = \overline{M} \frac{\max(\tau - \tau_c, 0)}{\tau_c} \frac{S_{\text{bed}}^n}{\rho_{\text{bed}} d_{\text{thresh}}}. \quad (7.12)$$

In Delft3D, this expression depends on the amount of sediment on the bed  $S_{\text{bed}}$  at the current time level (i.e. explicit). Combining Eq. (7.12) and Eq. (7.11) for  $D = 0$ , we obtain the time step restriction

$$\Delta t \leq \frac{\rho_{\text{bed}} d_{\text{thresh}}}{\overline{M}} \frac{\tau_c}{\max_{x,y,t}(\tau) - \tau_c}. \quad (7.13)$$



The maximum time step depends on prescribed parameters and on the maximum occurring bed shear stress, which may be estimated a priori. Note that such time step criterion would not exist if the erosion were treated implicitly in time.

## 7.B. RECONSTRUCTING TRANSPORT BY TEMPORALLY VARYING EDDY DIFFUSIVITY

Temporal variations of the eddy diffusivity affect the sediment concentration only, not the water motion. Therefore, the advective sediment transport contribution due to time variations of the eddy diffusivity can be reconstructed from Delft3D model output, by computing the sediment concentration if the eddy viscosity were constant  $c_{\langle K_v \rangle}$  and comparing it to the sediment concentration  $c_{D3D}$  from Delft3D. Since we will not use the exact same numerical scheme for reconstructing  $c_{\langle K_v \rangle}$  as Delft3D uses to compute  $c_{D3D}$ , our reconstruction is not precise enough to compare directly to  $c_{D3D}$ . Therefore, we reconstruct not only  $c_{\langle K_v \rangle}$  but also the concentration assuming the full eddy diffusivity signal  $c$ . It is verified that  $c$  is a good approximation of  $c_{D3D}$ . The tidally averaged advective transport per metre width due to time-varying eddy diffusivity  $T_{\text{tvd}}$  is given by

$$T_{\text{tvd}} = \left\langle \int_{-H}^{\zeta} u (c - c_{\langle K_v \rangle}) dz \right\rangle,$$

where  $\langle \cdot \rangle$  denotes tidal averaging,  $u$  is the along-channel velocity,  $\zeta$  is the surface elevation,  $H$  is the bed level and  $K_v$  is the eddy diffusivity.

We will assume that the sediment concentration follows mainly from vertical processes, so that it suffices to use a water column model with an imposed correction due to horizontal processes. The imposed horizontal sediment concentration gradient  $c_{D3D, x}$  is taken from the Delft3D output and written as  $c_{D3D, x} = \varsigma$ . The resulting sediment balance is written in  $\sigma$ -coordinates and reads

$$c_t - \frac{1}{H + \zeta} \left( (w_s - w)c + \frac{K_v}{H + \zeta} c_\sigma \right)_\sigma = -u\varsigma + (K_h \varsigma)_x, \quad (7.14)$$

subject to

$$\begin{aligned} \frac{K_v}{H + \zeta} c_\sigma &= 0 & \text{at } \sigma = 0, \\ \frac{K_v}{H + \zeta} c_\sigma &= -E & \text{at } \sigma = -1. \end{aligned}$$

This equation is solved numerically using a finite volume approach on a staggered grid as in Delft3D. Using the tidally averaged  $K_v$  from Delft3D as input to the equation yields  $c_{\langle K_v \rangle}$  and using the complete  $K_v$  signal from Delft3D as input yields  $c$ , allowing computation of  $T_{\text{tvd}}$ .

## 7.C. THE ROLE OF THE EROSION PARAMETER IN THE SUPPLY LIMITED DOMAIN

In Section 7.3.3 we investigated the role of the erosion parameter  $M$  on the the sediment concentration assuming supply limited conditions. In Delft3D, increasing  $M$  leads to lower sediment concentrations due to a decrease in tidal pumping. In this section we will show this using a mathematical argument. First it is shown that an increasing erosion parameter leads to reduced tidal pumping in a water column, next this argument is extended to more dimensions. Finally, it is shown why this argument does not hold for iFlow.

Let us assume a water column anywhere in the estuary at location  $x_i$  where the sediment is only exchanged between the water column and the bed and not advected from elsewhere and assume

that the subtidal depth-integrated sediment concentration  $\langle H\bar{c} \rangle$  is a prescribed constant. This concentration is directly related to resuspension and can be expressed as

$$\langle H\bar{c} \rangle \sim M f(\langle S_{\text{bed}} \rangle), \quad (7.15)$$

where  $f(S_{\text{bed}})$  is the weighed time average of the erodibility  $f^*$  (see Brouwer et al. (2018) for details), which is a monotonically increasing function of  $S_{\text{bed}}$  in supply limited conditions. As  $H\bar{c}$  is kept constant, an increasing  $M$  therefore means that  $\langle S_{\text{bed}} \rangle$  decreases.

As we have assumed a local balance in the water column, it is required that the amount of sediment on the bed  $S_{\text{bed}}$  plus the amount of sediment suspended in the water column  $H\bar{c}$  is constant over time. Therefore the amount of sediment on the bed and in the water column at any moment is equal to its time-average, i.e.

$$H\bar{c} + S_{\text{bed}} = \langle H\bar{c} \rangle + \langle S_{\text{bed}} \rangle. \quad (7.16)$$

In supply limited conditions, there is an instance of time at which  $S_{\text{bed}} = 0$  and the total amount of sediment suspended in the water column is at its maximum  $H\bar{c}_{\text{max}}$ . Rewriting the above expression for this instance of time yields

$$H\bar{c}_{\text{max}} - \langle H\bar{c} \rangle = \langle S_{\text{bed}} \rangle. \quad (7.17)$$

As a result, as  $\langle S_{\text{bed}} \rangle$  decreases with increasing  $M$ , the temporal variation of the sediment concentration  $H\bar{c}_{\text{max}} - \langle H\bar{c} \rangle$  decreases as well. If the water motion does not depend on the sediment concentration and it is assumed that the relative phase difference between the sediment concentration and velocity changes only little, the correlation between the tidally varying water motion and sediment concentrations becomes smaller.

The sediment transport by the interaction of the river discharge and subtidal sediment concentration changes little with changing  $M$ , as it was assumed that the depth-integrated sediment concentration is constant. The only change in this river-induced transport can therefore be due to changes in the vertical structure of the sediment concentration. Hence, it is expected that tidal pumping reduces in magnitude relative to the subtidal river-induced sediment transport.

This argument for the water column may be extended to two dimensions (along-channel-vertical), because the two-dimensional sediment dynamics, to leading order, obeys the vertical exchange model (see Scaling in Chapter 2). In two dimensions, we choose the location of our water column  $x_i$  just outside of the boundary layer close to the seaward boundary, where  $\langle \bar{c} \rangle$  is fixed by the boundary condition. In the Ems model, the relative reduction of tidal pumping means a reduction of the sediment import. The only way to find a new equilibrium between sediment import and export is to reduce the diffusive sediment transport. This is established by reducing the subtidal along-channel concentration gradient  $\langle \bar{c} \rangle_x$ , meaning that the concentration just upstream from  $x_i$  decreases. This reasoning can be repeated for  $x_i$  moving upstream through the estuary, showing that the sediment concentration must decrease if the main sediment balance is between import by tidal pumping and export by the river-induced flow.

In the iFlow model, the sediment transport and sediment concentration are insensitive to the value of  $M$  in the supply limited zone. To explain this, let us again focus on a water column and assume that  $\langle H\bar{c} \rangle$  is constant. Eq. (7.15), relating  $\langle H\bar{c} \rangle$  to  $Mf$  is still valid in iFlow. However, Eq. (7.16) does not hold in iFlow, because the model only accounts for the tidally averaged erodibility  $f$  instead of  $f^*$ . Hence, it assumes that the amount of sediment at the bed at any time equals the time average  $\langle S_{\text{bed}} \rangle$  and Eq. (7.16) reduces to  $H\bar{c} = \langle H\bar{c} \rangle$ , which is obviously not true. The meaning of this is that iFlow does not obey mass conservation in the water column and bed on an intratidal time scale

but is mass conserving on a subtidal time scale. Instead of intratidal mass conservation, iFlow extends Eq. (7.15) to the instantaneous sediment concentration, i.e.

$$H\bar{c} \sim Mf.$$

Therefore

$$\frac{Hc_{\max} - \langle H\bar{c} \rangle}{\langle H\bar{c} \rangle} \sim \frac{Mf}{Mf} \sim \text{constant}$$

and the value of  $M$  has no influence on tidal pumping or any other sediment transport contribution in supply limited conditions.

# CHAPTER 8

Conclusions



## 8.1. DISCUSSION OF THE RESEARCH QUESTIONS

Five research questions were posed in Chapter 1. The answers to these research questions will be discussed below. Next, in Section 8.2, the general conclusions are summarised in answer to the two overarching goals of this thesis. Finally, several opportunities for further research have been identified throughout this study and are presented in Section 8.3.

### 21 What are the essential processes describing the sediment dynamics in the Ems River before reaching a hyperturbid state and in the Scheldt River in the 2010 state?

The processes driving the sediment dynamics have been analysed with respect to two aspects:

1. (Along-channel) sediment transport and trapping
2. (Vertical) sediment resuspension

Concerning each of these aspects, the advances in the model description and the results obtained in application to the Ems and Scheldt are discussed below.

**SEDIMENT TRANSPORT** To investigate the sediment transport, the width-averaged idealised iFlow model was developed (**Chapter 2**). Building further on a method first demonstrated for estuarine sediment dynamics by Chernetsky et al. (2010), this model can be used to make an explicit decomposition of many contributions to the along-channel sediment transport in estuaries. Compared to the work of Chernetsky et al. (2010), the model has been extended by many features, including more general geometries, several additional non-linear processes and the ability to compute the total amount of sediment in the estuary instead of only the redistribution of sediment.

In the Ems in the low concentration regime (i.e. 1965 case, **Chapter 4**) the sediment transport balance is governed by tidal pumping and river-induced sediment export. The main contributions to tidal pumping are related to the externally generated  $M_4$  tide (i.e. generated on the coastal shelf), internally generated  $M_4$  tide (i.e. generated inside the estuary due to non-linear interaction between velocity and surface elevation) and, to a lesser extent, spatial settling lag. These contributions are predominantly responsible for an import of sediment. Classical processes such as gravitational circulation (see **Chapter 4**) and asymmetric mixing (see **Chapter 7**) are also importing sediment, but the transport by these contributions is much smaller than that by tidal pumping. The balance of all sediment transport processes leads to sediment trapping in one zone near or downstream of Terborg (km 26).

In the Scheldt in the 2010 situation (**Chapter 6**), it is also found that the sediment transport follows from a balance between tidal pumping and river-induced export. However, the tidal pumping contribution by the externally generated  $M_4$  tide leads to export of sediment in most of the estuary. This is different than in the Ems, because the relative phase difference between the  $M_2$  and  $M_4$  tide on the adjacent shelf is almost 180 degrees different between the Ems and Scheldt. As the transport contributions related to the internally generated  $M_4$  tide and spatial settling lag predominantly contribute to sediment import, tidal pumping in total is still responsible for sediment import in most of the estuary. The balance of all sediment transport processes generate two trapping

zones: one near Antwerp (km 80) and the other near Melle (km 150). Additional to natural processes, dumping of dredged sediments is important to the sediment dynamics in the Scheldt. The sediment dumped especially leads to higher sediment concentrations near the Antwerp trapping zone.

**SEDIMENT RESUSPENSION** The ability of the flow to resuspend sediment from the bed was derived to be related to a tidally averaged dimensionless erosion parameter  $\langle \tilde{E} \rangle$ , which depends on the erosion parameter, bed shear stress, critical shear stress for erosion, settling velocity and gelling concentration (Eq. (3.11) in **Chapter 3**).

For the Ems Estuary model (**Chapter 4**), a sufficiently high erosion parameter was chosen, such that resuspension is not restricting the maximum concentration. Instead, sediment transport restricts the maximum concentration (i.e. supply limited). Observed sediment dynamics could be qualitatively reproduced with these settings. In the Scheldt, calibration of the model to observed maximum sediment concentrations (**Chapter 6** and Brouwer et al. (2018)) led to a choice of the erosion parameter such that resuspension is locally limiting at the Melle ETM and the sediment dumping area close to Antwerp during average or low discharge conditions (i.e. erosion limited). As a result, some of the imported or dumped sediment deposits on the bed, forming a growing mud pool.

## 22 What are the essential additional processes and changes to processes that explain the shift to a hyperturbid regime in the Ems?

To better understand the regime shift to high sediment concentrations in the Ems, the iFlow model was used with several highly non-linear processes representing the effect of sediment stratification on turbulence and hindered settling (**Chapter 4**). The model was calibrated for a case representing 1965 (before the regime shift) and then deepened to 2005 conditions (after the observed regime shift), but the model is not recalibrated. Assuming 2005 conditions and a river discharge below  $70 \text{ m}^3/\text{s}$  (approximately 60% of the time), two ETM were found in the upstream part of the estuary, with concentrations up to  $30 \text{ kg/m}^3$  near the bed, thereby capturing the main qualitative characteristics of the regime shift.

On a process level, the regime shift was explained in terms of changes to the along-channel sediment transport. Deepening mainly leads to amplification of the  $M_4$  velocity amplitude and a change in the relative phase difference between the  $M_2$  and  $M_4$  velocity. These changes lead to an increased import of sediment, related to the externally generated  $M_4$  tide, as well as the internally generated  $M_4$  tide. The increased sediment import and hence increased sediment concentration lead to a suppression of turbulence. The suppression of turbulence in turn allows for further amplification of the  $M_4$  velocity amplitude and change in  $M_2$ - $M_4$  phase difference, in such a way that sediment import is further increased. This feedback between the  $M_4$  tide and sediment-induced damping of turbulence is the main process explaining the regime shift in our model. This process is particularly effective at importing sediment, because the  $M_4$  tide is close to resonance in the 2005 situation. This means that the amplification of the tidal velocity is close to its maximum given the amount of friction. In further detail, suppression of turbulence is expressed as a reduction of the eddy viscosity, eddy diffusivity and bed friction experienced by the water motion, which are all found to be important. Winterwerp and



Wang (2013) hypothesised that a feedback between tidal water level amplitude or tidal asymmetry and reduction of friction explains the regime shift in the Ems. The feedback discussed above confirms the overall idea of this hypothesis.

Vertical resuspension is not limiting in the iFlow model of the Ems. This was achieved by choosing the value of the erosion parameter sufficiently high, such that the dimensionless erosion parameter  $\langle \tilde{E} \rangle$  is above its threshold value (see 21 and **Chapter 3**) in those parts of the estuary where sediment is trapped. The threshold value exists because of the process of hindered settling. Hence, the process of hindered settling is important to the regime shift in the Ems indirectly, by allowing the flow to keep a large amount of sediment in suspension.

### **23 What is the timescale of the regime shift in the Ems and what does this imply with respect to the essential processes responsible for this regime shift?**

By computing dynamic equilibrium conditions in the iFlow Ems model for a range of depth profiles interpolating between the 1965 and 2005 depth, two distinct regimes were identified (**Chapter 5**). The first regime is characterised by low-moderate sediment concentrations in a narrow ETM. The identified feedback mechanism between tidal asymmetry and sediment-induced turbulence damping (see 22) is not important. In the second, hyperturbid regime, sediment concentrations are high, up to  $30 \text{ kg/m}^3$  in two ETM, together covering the upper half of the estuary. The identified feedback mechanism is important here and can additionally be observed by an amplification of the  $M_2$  water level.

Comparing observed and modelled tidal ranges, it was found that the observations are close to the first regime until approximately 1989 and close to the second regime since approximately 1995. A gradual transition between the two regimes was observed in the intermediate years. Hence the timescale of the regime shift is estimated to be of the order of several years. On the one hand this timescale is significantly shorter than the earlier hypothesised timescale of decades (Winterwerp and Wang, 2013). On the other hand the timescale is much longer than a seasonal timescale. This implies that the sediment import necessary for the regime shift did not occur during one dry season. However, it also means that sediment imported during a dry season is not flushed out of the estuary during one wet season. As this study focussed on dynamic equilibrium conditions, this seasonal behaviour is not fully understood yet.

### **24 Can the Scheldt undergo a regime shift to hyperturbid conditions due to the same processes that are responsible for the regime shift in the Ems?**

The Scheldt model in iFlow was tested for a range of depth profiles representative of depth profiles attained between 1960 (relatively shallow) and 2010 (deeper) and scenarios of further deepening (**Chapter 6**). It was found that deepening, without changing any other parameters, leads to slightly lower suspended sediment concentrations for the default parameter settings. For some other values for the erosion parameter or settling velocity, a slight increase in concentration was observed. A regime shift to hyperturbid conditions as a consequence of deepening similar to what was found in the Ems, was therefore not found in the Scheldt.

These results were explained through an analysis of the most important physical processes. Firstly, in our model, the maximum sediment concentration in the Scheldt is restricted by local resuspension instead of along-channel sediment transport. As the bed shear stress decreases due to deepening in the Scheldt, resuspension becomes weaker, leading to generally lower concentrations. Secondly, even if the along-channel sediment transport were limiting the maximum sediment concentration, the feedback process identified in the Ems is absent in the Scheldt. This is because deepening does not clearly lead to stronger sediment import due to tidal pumping. On the one hand, deepening leads to an increased sediment export due to the externally generated  $M_4$  tide. On the other hand, deepening leads to a mixed response of the sediment transport due to the internally generated  $M_4$  tide, with less import in some areas and more import in other areas. This only results in either a weak increase or decrease of the sediment concentration, depending on the exact parameter choices. Based on these results, it is suggested to reject the hypothesis of Winterwerp et al. (2013), which states that the Scheldt may become hyperturbid due to a similar feedback process as in the Ems.

### **25 To what extent is the description of the regime shift using only a set of essential processes sufficiently representative of the physics described in state-of-the-art models?**

By comparing results of iFlow and a Delft3D model with idealised geometry and forcing conditions (**Chapter 7**), a better understanding was obtained of the effect of some of the assumptions made in the iFlow model. Two results in particular stand out. Firstly, due to the more realistic modelling of the water-bed exchange in Delft3D, sediment import due to tidal pumping decreases if the erosion parameter becomes large. Hence, when simulating high sediment concentrations, one cannot choose an arbitrarily large value of the erosion parameter in Delft3D, as one can in iFlow. Instead, one has to find a value sufficiently high to reproduce the necessary high resuspension rate, while not overly suppressing sediment import due to tidal pumping. Secondly, sediment-induced damping of turbulence strongly reduced the bed friction in the Delft3D experiments, hence reducing the ability of the model to resuspend sediment from the bed. This was also visible in iFlow but was less pronounced. These two findings narrow down the parameter space in which the transition from low to high sediment concentrations may be found. Hence, the iFlow model used in this thesis provides a good tool for exploration of this parameter space, but the results require further verification and specification of the parameter space using a more complex model.

Apart from these two processes, comparison of the iFlow model results with observations pointed to several other important processes that are better implemented in state-of-the-art models, such as Delft3D. These processes are mostly related to hyperturbid conditions. While the iFlow model captures some of the qualitative characteristics of the estuary-scale ETM, it does not seem to capture the essential dynamics within the ETM in hyperturbid conditions. Specifically, the model does not capture strong vertical stratification or temporal variations in mixing and stratification sufficiently well to even qualitatively reproduce observed tidally varying behaviour of a highly turbid water column (Becker et al., 2018). Hence, the conclusions of this thesis are restricted to the low-moderate concentration regime and transition to hyperturbid conditions, but the results are not suitable for studying more detailed sediment dynamics in the hypertur-

bid regime.

Additionally, by taking width-averages in iFlow, the model underestimates shear stresses and turbulence production in the main channel and hence underestimates resuspension. In the shallow parts of the estuary by the side of the channels, the model overestimates the shear stresses and turbulence production and hence the sediment deposition. Further investigation is required to identify to what extent such three-dimensional behaviour is important to the overall sediment balance and sediment concentration compared to the width-averaged behaviour.

## 8.2. GENERAL CONCLUSION

Further summarising the results of this thesis, the general conclusion is formulated in answer to the goals of this thesis, which are:

1. to identify and better understand the essential processes driving a shift of the regime to hyperturbid conditions, by studying observed characteristics exemplified by the Ems River, and
2. to determine whether these processes are generically able to drive a regime shift to hyperturbidity in other estuaries, demonstrated by taking the Scheldt River as an example.

In this thesis, the observed regime shift from low to high sediment concentrations in the Ems was qualitatively reproduced using an idealised model. The modelled regime shift is directly related to deepening of the channel, which amplifies sediment import through a feedback mechanism between the  $M_2$ - $M_4$  tidal asymmetry and sediment-induced damping of turbulence. All of the imported sediment can be kept in suspension (i.e. supply limited conditions), provided the process of hindered settling is included in the model, and provided that suitable choices are made for the erosion parameter. As a result of this feedback, two distinct regimes representing low sediment concentrations and hyperturbid conditions were distinguished within the context of the model.

Using the Scheldt River Estuary as an example, it was demonstrated that the feedback process identified in the Ems does not generically lead to a shift to hyperturbid conditions. In the Scheldt, deepening of the estuary leads to a competition between additional sediment import and export related to several contributions to the  $M_2$ - $M_4$  tidal asymmetry. Hence, deepening is found to result in either a slight increase or decrease of the sediment import within the large range of parameter uncertainty. Moreover, it was found that sediment resuspension from the bed restricts the maximum sediment concentration to moderate levels (i.e. erosion limited conditions). Deepening in the Scheldt leads to a small decrease of the bed shear stress in the ETM, hence leading to a small decrease of the maximum sediment concentration in these ETM.

Concluding, the feedback process that is responsible for the transition to hyperturbid conditions in the Ems can theoretically also cause such a regime shift in other estuaries but does not occur in every estuary. In order to find out whether a regime shift can occur in another estuary, a careful analysis of the sediment transport processes in that estuary is required.

### 8.3. OPPORTUNITIES FOR FUTURE RESEARCH

Results in this thesis point to several opportunities for further research that would further contribute to the goals of this thesis or slightly broaden the research scope. I distinguish between research opportunities using and extending iFlow and general research opportunities using other methods.

#### 8.3.1. FUTURE DEVELOPMENT AND USE OF IFLOW

**APPLICATION TO OTHER ESTUARIES** To further use and extend the theoretical framework developed in this thesis, the model can be applied to other estuaries. The Loire River Estuary underwent a regime shift to hyperturbid conditions. By investigating this regime shift, it can be found if this happened due to the same processes as in the Ems or if other processes are responsible. Furthermore, the Weser and Elber River Estuaries are explicitly named by Winterwerp et al. (2013) as estuaries where a regime shift to hyperturbid conditions may occur. This hypothesis needs to be further investigated.

**THREE-DIMENSIONAL MODEL** Kumar et al. (2017) developed a three-dimensional idealised model for sediment dynamics in estuaries using perturbation techniques, thereby making it the equivalent to iFlow in three dimensions. Using this model, the experiments in this thesis can be repeated with a more realistic geometry. However, this requires extension of this model by the processes identified as important in this thesis, i.e. non-linear erodibility, sediment-induced damping of turbulence and hindered settling. These tests can be used to describe the different dynamics in the main channel and on the flanks of the estuary and the importance of these differences to the estuary-scale results. Moreover, such tests would yield better knowledge about the importance of using a more realistic geometry.

**SEASONAL DYNAMICS** The finding that the regime shift in the Ems likely happened on the timescale of a few years, implies that sediment import or flushing of the estuary cannot occur during a single dry or wet season. To further understand this behaviour, it is necessary to investigate the dynamics on a seasonal timescale, rather than a investigating dynamic equilibrium. iFlow has already been extended to investigate dynamic behaviour on such timescales by Brouwer et al. (2018) but still needs to be applied to the regime shift in the Ems. When investigating dynamic behaviour on subtidal timescales it is important to account for time-dependent forcing conditions, including river discharge variations, the spring-neap cycle and consolidation.

**STRATIFICATION** Resolving the sediment-induced stratification is important in order to better capture the dynamics of a hyperturbid estuary. Stratification includes at least three aspects: (1) capturing the vertical profile of the eddy viscosity and eddy diffusivity representative for a state anywhere between well-mixed to strongly stratified; (2) capturing temporal variations of the eddy viscosity and eddy diffusivity and (3) modelling the local and temporal variations in hindered settling.

**TIDALLY VARYING ERODIBILITY** Allowing variations of the erodibility of the bed on a tidal timescale, instead of keeping it constant, was found to result in a different sensitivity of the model to the erosion parameter (Chapter 7). As one of the main strengths of iFlow is the possibility to perform sensitivity studies, it is important that such processes

are included in the model.

**TIDALLY VARYING EDDY VISCOSITY/DIFFUSIVITY** While tidal variations of the eddy viscosity and eddy diffusivity were only found to yield a small transport contribution in the 1965 Ems case (Chapter 7), these processes are thought to be important to sediment transport in the Ems in its hyperturbid state (Becker et al., 2018). Therefore it is useful to include these processes in the model when modelling hyperturbid conditions.

**FLOCCULATION** The settling velocity of sediment is known to vary in time and space due to flocculation, depending on factors including the sediment concentration, salinity and biological activity due to flocculation. Resolving flocculation results in a temporally and spatially varying settling velocity. As sediment with different settling velocities tend to be trapped in different locations, it is speculated that the inclusion of flocculation in the model leads to a wider spreading of sediment throughout the estuary, which may further reinforce a hyperturbid state. Furthermore, due to the dependence of flocculation on biological activity, a model that resolves flocculation can give insight into the response of the sediment concentration to changing water quality, which may be relevant in the Scheldt (Barneveld et al., 2018).

**REGIME SHIFT IN PHYTOPLANKTON DYNAMICS** One of the main reasons why a regime shift to hyperturbidity is a practically relevant research subject, is the consequences it has for the functioning of the estuary as an ecosystem. However, drastic changes in the ecosystem can potentially already occur at much more moderate changes in the suspended sediment concentration. Growth of phytoplankton is strongly inhibited by sediment-induced light limitation when the sediment concentration is of the order of 100 mg/l (e.g. Cloern, 1987). However, if and what changes in the sediment concentrations can lead to a regime shift in phytoplankton dynamics is unknown. A first step extending iFlow to include phytoplankton-nutrient dynamics has already been made by Dijkstra et al. (Submitted to *Estuaries and Coasts*)

**BIFURCATION ANALYSIS TOOLBOX** In Chapter 5 two sets of stable dynamic equilibria were identified. Theoretically, these sets should be connected by a branch of unstable equilibria. Identifying this branch of unstable equilibria provides a stronger mathematical foundation to the results and provides more information about the domain of attraction and response of the system to perturbations. To find the exact bifurcation point and the set of unstable equilibria, a toolbox for parameter continuation and analysis of bifurcations needs to be added to iFlow. Such a toolbox is also of great value in identifying possible other bifurcations in estuarine dynamics, a subject that is best approached using idealised models because of the need for accuracy and computational speed.

### 8.3.2. RESEARCH OPPORTUNITIES IN GENERAL OR USING OTHER MODELS

**PARAMETRISATION OF RESUSPENSION** resuspension of sediment from the bed is identified as one of the main processes determining sediment dynamics in general and the transition to hyperturbidity specifically. However, even in state-of-the-art models, resuspension is usually parametrised using one or two parameters with uncertain values, viz. the erosion parameter and critical shear stress for erosion. Little is known about changes to these parameters with changing bed composition (e.g. from sandy to muddy)

or changing sediment characteristics (e.g. floc size).

Another factor affecting resuspension is the bed shear stress, which depends on the bed friction. While experimental research has been done assessing the effect of near-bed sediment-induced stratification on both the skin friction (Gust, 1976) and form drag, this effect is not generally included in state-of-the-art models and the consequences of these effects on estuarine-scale sediment dynamics are not well understood.

**ROLE OF SALINITY** This study focusses on well-mixed estuaries and does not focus strongly on the role of salinity on sediment transport. However, if the theory developed in this thesis is to be applied to more strongly stratified estuaries, the salinity needs to be considered in more detail. In such estuaries, the importance of salinity-related sediment transport may possibly lead to a different feedback process that allows a transition to hyperturbid conditions than the feedback identified in this thesis.

In addition, even in well-mixed estuaries, salinity-induced gravitational circulation and strain-induced periodic stratification (SIPS) are considered to be potentially important mechanisms keeping sediment in the estuary. The gravitational circulation was found not to be very important in width-averaged sense (Chapter 4) but becomes more important in three dimensions (Wei et al., 2018). The effects of this on the large-scale sediment dynamics need further investigation. The effect of SIPS on sediment transport has not been investigated in this study.

**UNDERSTAND AND RESOLVE MODEL INSTABILITY** In Chapter 7 spurious oscillations in several Delft3D simulations were identified. These oscillations occur in certain cases with large sediment concentrations and may be either due to an instability in the model equations or an inaccuracy in the numerical solution method. In order to proceed study into hyperturbid conditions in estuaries, this instability needs to be better understood and resolved.

## REFERENCES

- Barneveld, H. J., Nicolai, R. P., Van Veen, M., Van Haaster, S., Boudewijn, T. J., De Jong, J. W., Van Ditteren, K., Van de Haterd, R. J. W., Middenveld, P. P., Michielsen, S., Van de Moortel, I., Velez, C., and De Wilde, E. (2018). Analyse rapport T2015 - rapportage Schelde estuarium. Technical Report PR3152.10, Antea, Bureau Waardenburg, HKV. In Dutch.
- Becker, M., Maushake, C., and Winter, C. (2018). Observations of mud-induced periodic stratification in a hyperturbid estuary. *Geophysical Research Letters*, 45:5461–5469.
- Brouwer, R. L., Schramkowski, G. P., Dijkstra, Y. M., and Schuttelaars, H. M. (2018). Time evolution of estuarine turbidity maxima in well-mixed, tidally dominated estuaries: the role of availability- and erosion-limited conditions. *Journal of Physical Oceanography*, 48:1629–1650.
- Chernetsky, A. S., Schuttelaars, H. M., and Talke, S. A. (2010). The effect of tidal asymmetry and temporal settling lag on sediment trapping in tidal estuaries. *Ocean Dynamics*, 60:1219–1241.
- Cloern, J. E. (1987). Turbidity as a control on phytoplankton biomass and productivity in estuaries. *Continental Shelf Research*, 7:1367–1381.
- Dijkstra, Y. M., Chant, R. J., and Reinfeldt, J. R. (Submitted to *Estuaries and Coasts*). Factors controlling seasonal phytoplankton dynamics in the Delaware River Estuary: an idealized model study.
- Gust, G. (1976). Observations on turbulent-drag reduction in a dilute suspension of clay in sea-

- water. *Journal of Fluid Mechanics*, 75:29–47.
- Kumar, M., Schuttelaars, H. M., and Roos, P. C. (2017). Three-dimensional semi-idealized model for estuarine turbidity maxima in tidally dominated estuaries. *Ocean Modelling*, 113:1–21.
- Wei, X., Kumar, M., and Schuttelaars, H. M. (2018). Three-dimensional sediment dynamics in well-mixed estuaries: Importance of the internally generated overtide, spatial settling lag, and gravitational circulation. *Journal of Geophysical Research: Oceans*, 123:1062–1090.
- Winterwerp, J. C. and Wang, Z. B. (2013). Man-induced regime shifts in small estuaries - I: theory. *Ocean Dynamics*, 63:1279–1292.
- Winterwerp, J. C., Wang, Z. B., Van Brackel, A., Van Holland, G., and Kösters, F. (2013). Man-induced regime shifts in small estuaries - II: a comparison of rivers. *Ocean Dynamics*, 63:1293–1306.





# Model availability and acknowledgement for data

## MODEL AVAILABILITY

Three models have been used in this thesis. Below ownership, licence of use and the versions of these codes are outlined.

**iFlow** The iFlow model used in this study is available under open source GNU Lesser General Public License v3 (LGPL)<sup>1</sup>. The code is available on GitHub via doi 10.5281/zenodo.822394. The version number of the code is updated per publication, see the table below. Included with iFlow are extensive manuals explaining the model structure, equations and solution method (related to version 2.4 at moment of publication), a getting started tutorial and basic input files corresponding to various publications using iFlow.

Version	Description	Chapter	Publication
2.4	Starting version	-	Dijkstra et al (2017, GMD 10:2697-2713)
2.5	Erodibility and long timescale integration	Chapter 2	Brouwer et al (2018, JPO 48:1629–1650)
2.6	Sediment-induced turbulence damping and hindered settling	Chapters 4 & 7	Dijkstra et al (2019, JGR 124:1–17)
2.6.2		Chapter 5	Dijkstra et al (Accepted to GRL)
2.7	Fluvial sediment source, water and sediment sources and sinks	Chapter 6	Dijkstra et al (Submitted to OD)

**WATER COLUMN MODEL** The water column model used in Chapter 3 is owned by Deltares and is not publicly available at moment of publication of this thesis. I thank Rob Uittenbogaard and Han Winterwerp for sharing the code.

**DELFT3D** The Delft3D model is open source software available under open source GNU General Public License v3 (GPL)<sup>2</sup> The code is available via <https://oss.deltares.nl/>. In Chapter 7 we have adapted version 5.09.00.

---

<sup>1</sup>Free for commercial and non-commercial use. Any changes to the existing code need to be published under the same license. Any additions to the code that do not require changes to the existing code may be kept under any license.

<sup>2</sup>Free for commercial and non-commercial use. Any changes to the code or programmes using the code must be published under the same licence.

**ACKNOWLEDGEMENTS FOR USED DATA AND OTHER INFORMATION**

All the observational data used in this thesis was collected and is owned by others. Where appropriate I have cited the publications that presented the data in the text.

**EMS** I thank the WSA Emden for giving access to the 2005 depth data and historical observations of the tidal range. I also thank Julia Benndorf (BAW) for sharing her insight into the available data and providing the publication with observations of sediment concentrations from 1949. I finally like to thank Erik Ensing and Huib de Swart for giving insight into their unpublished work on the Ems that provided inspiration for this study.

**SCHELDT** I sincerely thank Yves Plancke (Flanders Hydraulics Research) and Wouter Vandenbruwaene (Flanders Hydraulics Research, HIC) for providing insight into available data and studies on the Scheldt. I thank Rijkswaterstaat for providing data on water levels, velocities, salinities and sediment concentrations in the Western Scheldt. I thank HIC for providing the water level observations and data from the continuous sediment concentration measurement stations in the Sea Scheldt and Flanders Hydraulics Research (MONEOS programme) for the velocity measurements. I further thank the Flemish Waterway for permission to use the OMES dataset. Finally I thank Thijs van Kessel (Deltares) for sharing earlier studies done in context of the LTV project on mud modelling.

# Acknowledgements

My PhD would not have been possible and would have definitely not been such a nice experience for me without the help of others. Below I would like to express my gratitude to some who have contributed greatly to my PhD and my life during the past four years.

This PhD project started for me with Han Winterwerp. While me and Han did not know each other in person at the time, one of the first things Han did after introducing himself, was to offer me a PhD position. I agreed to work on this project with Henk Schuttelaars as my main advisor. Soon, I discovered one of the main challenges in science: acquiring funding. What followed was a chaotic process with great effort put in by Han and Henk to create this position for me. Han and Henk, I am very grateful for all the work you have done to achieve this.

Henk, after working together on my Master's thesis, I knew I wanted to work together again for my PhD. I think you are a great researcher with a great vision on the long-term goals of your work and a fearless approach to using and developing different methods than anyone else. I admire your patience and your sincere happiness with even the smallest sign of progress in my work. This uplifting enthusiasm, especially at times when I felt bad about work, really pulled me through the last four years. I hope that we will still work together for a long time, so I can learn more from your ways of planning research, teaching and supervising students. I also hope to get back to doing mathematics together, instead of only discussing the revisions of draft number 253 of the next paper.

I would also like to thank George Schramkowski. I have sometimes called you my 'mathematical conscience', as your precision and aspiration to find explicit analytical solutions or proofs to mathematical problems has often helped me to think more carefully about my results and methods. I would also like to thank you for your efforts in promoting iFlow and my work at Flanders Hydraulics Research. I very much enjoyed working with you over the past four years and even liked the odd complains about strange administrative procedures. I hope to continue our work together in the future.

Ronald Brouwer, I very much liked to work together with you. It was a real pleasure to develop a new code together and I enjoyed our iFlow development weeks. I especially liked the fact that we could so much reinforce each other's enthusiasm for this model, making plans more ambitious every time we worked on it. The fact that we developed this together furthermore really sped-up the process, not to mention the endless list of bugs you found in my code.

Furthermore I would like to thank my colleagues at the university. Especially, Kees Lemmens for trusting me and helping me in the teaching of the PDE lab course; Corine for our frequent talks about pretty much anything and for the research suggestion that unknowingly meant a breakthrough in my work; Xiaoyan, Tugce, Bijan and Mohit for being

such unconditionally nice colleagues and introducing me to so many different cultures and foods; Lisa for our lunch meetings that we should have started years earlier; and to my other officemates including Tjebbe, Kaihua, Isabel, Jie, Feng, Jianbing, Mahya and Henrique for making our office such a nice working place.

I am grateful to my colleagues at Deltares' department of Ecosystems and Sediment Dynamics for accepting me as a member of the department, despite the fact that was mostly working alone on my own project. I felt very welcome and it has been a great inspiration for me to work at Deltares as well as at the university. Especially, I would like to thank Zheng Bing Wang for his interest in the project and faith in me as a researcher; Marcel Taal for having the confidence that my rather scientific work would eventually be useful in practice (which I hope it is in the end); Miguel de Lucas for the perseverance while working on our idealised Delft3D project and trying to learn things from me that I only learned the day before and only half understood; Ankie Bruens for inspiration on how to connect my work to the practice of Deltares; and Bas, Thijs and Han for all the small suggestions and attentive remarks and for staying awake during my few overly long presentations.

During my PhD, I spent three months in the USA. I would very much like to thank Bob Chant for the great hospitality, the time to discuss work and help in finding me a room to stay and bike to get around. I would also very much like to thank you and your wife for inviting me to Thanksgiving dinner; it felt very special to me to experience this tradition with you and your family. I would like to thank John Reinfelder for helping me to get started in the field of ecology. Your ability to translate ecological science to me as non-ecologist was invaluable to my work. I am indebted to Carl Friedrichs for welcoming me at VIMS and carefully filling my schedule with so many meetings and lunches that I had almost met everyone at VIMS within the course of a week and never got bored. I also would like to thank Rocky Geyer for welcoming me at WHOI and giving me the intellectually toughest week I have had during my entire PhD. I was much inspired by our discussions and the great difficulty that was hidden in the seemingly easy project that you gave me. Finally, I would like to thank my housemates in Highland Park: Schuyler, Emily, Liza, Lucy and Abigail, and the Rutgers tango community for welcoming me and making my stay such a nice experience.

In my personal life, I have always been blessed with the support and unconditional love of my family. Papa en Mama, bedankt voor al jullie steun, liefde en vertrouwen. Het is geweldig hoe jullie mij hebben geholpen, vooral tijdens de momenten dat er ineens veel te veel moest gebeuren in veel te korte tijd. Aron, bedankt dat je altijd voor me klaar staat. Ik ben er erg trots op dat een echte 'Aron Dijkstra' de cover van mijn proefschrift siert en ik kijk er naar uit om samen met jou dit proefschrift te verdedigen. Nathalie, bedankt voor je enthousiasme. Jij en Aron vormen een sterk stel en zijn fantastisch om als familie te hebben. Opa en Oma, ik weet hoeveel jullie er naar uitgekeken hebben om bij mijn verdediging te zijn. Ik ben daarom erg blij dat ik jullie dit proefschrift kan overhandigen en dat jullie er bij kunnen zijn. Voor jullie wil ik er graag een extra mooie dag van maken.

Tenslotte wil ik mijn dank betuigen aan mijn vrouw, Yaroslava. Yasya, onze ontmoeting op die grijze dag in Hamburg is absoluut het beste wat me tijdens deze promotietijd is

overkomen. Je hebt me zoveel nieuwe dingen laten zien en me begeleid naar een hele nieuwe fase in mijn leven. Ik denk niet dat ik ooit iemand heb ontmoet die in zoveel aspecten op mij lijkt, zo eigenzinnig is en me zo veranderd heeft. Ik ben gigantisch trots op je enorme doorzettingsvermogen in de afgelopen jaren, die zeker niet altijd makkelijk voor je zijn geweest. Bedankt dat je ondanks alles nog steeds wilde luisteren naar mijn geklaag en dat je me zoveel ruimte hebt gegeven om mezelf te zijn. Ik kijk er erg naar uit om samen met jou binnenkort de volgende nieuwe fase in ons leven in te gaan.

Yoei Dijkstra  
Delft, March 2019





# Curriculum Vitæ

Yoei Dijkstra was born on September 26, 1990 in Sneek, Netherlands. Between 2002 and 2008 he attended CSG Bogerman in Sneek for his secondary education at Gymnasium level, majoring in science & engineering (Dutch: profiel natuur & techniek). In March 2012, he received two Bachelor of Science degrees with distinction in Civil Engineering and in Applied Mathematics from the University of Twente, Enschede, Netherlands. After this, he moved to Delft University of Technology, where, in November 2014, he received two Master of Science degrees with distinction in Civil Engineering, specialisation Environmental Fluid Mechanics, and in Applied Mathematics, specialisation Computational Science and Engineering. He graduated through a 14-month research internship at research institute Deltares, where he wrote his Master's theses on the numerical accuracy of the  $k - \epsilon$  turbulence model and on the development of a new theoretical framework explaining exchange flows created by eddy-viscosity shear covariance (ESCO).

Yoei started his PhD at the Department of Applied Mathematics at Delft University of Technology and Deltares in April 2015, working on improving understanding of regime shifts from low to high sediment concentrations in estuaries. Besides research, he supervised one Master student, assisted in the teaching of several Bachelor and Master courses on partial differential equations and was a member of the faculty and university PhD council. From September to November 2017, he was a visiting scientist at the Department of Marine and Coastal Sciences of Rutgers University, New Brunswick, NJ, USA. Here he worked on improving insight into the link between suspended sediment and phytoplankton dynamic in estuaries.

From January 2019, Yoei works as a post-doctoral researcher at the Department of Applied Mathematics at Delft University of Technology on a project that aims to improve understanding of salt intrusion in estuaries.



# List of Publications

## PEER REVIEWED - IN THIS THESIS

1. **Dijkstra, Y. M.**, Schuttelaars, H. M. and Schramkowski, G. P. (Manuscript submitted to Ocean Dynamics). Can the Scheldt River Estuary become hyperturbid? A model analysis of suspended sediment concentrations and transport in response to channel deepening.
2. **Dijkstra, Y. M.**, Schuttelaars, H. M. and Schramkowski, G. P. (Manuscript accepted to Geophysical Research Letters). A regime shift from low to high sediment concentrations in a tide-dominated estuary.
3. **Dijkstra, Y. M.**, Schuttelaars, H. M., Schramkowski, G. P., and Brouwer, R. L. (2019). Modeling the transition to high sediment concentrations as a response to channel deepening in the Ems River Estuary. *Journal of Geophysical Research: Oceans*, 124:1-17.
4. **Dijkstra, Y. M.**, Schuttelaars, H. M., and Winterwerp, J. C. (2018). The hyperturbid state of the water column in estuaries and rivers: the importance of hindered settling. *Ocean Dynamics*, 68: 377-389.
5. **Dijkstra, Y. M.**, Brouwer, R. L., Schuttelaars, H. M. and Schramkowski, G. P. (2017). The iFlow Modelling Framework v2.4. A modular idealized process-based model for flow and transport in estuaries. *Geoscientific Model Development*, 10:2691-2713.

## PEER REVIEWED - NOT IN THIS THESIS

6. **Dijkstra, Y. M.**, Chant, R. J., Reinfeldt, J. R. (Manuscript submitted to Estuaries & Coasts). Factors controlling seasonal phytoplankton dynamics in the Delaware River Estuary: an idealized model study.
7. Brouwer, R. L., Schramkowski, G. P., **Dijkstra, Y. M.** and Schuttelaars, H. M. (2018). Time evolution of estuarine turbidity maxima in well-mixed, tidally dominated estuaries: the role of availability- and erosion-limited conditions. *Journal of Physical Oceanography*, 48: 1629-1650.
8. **Dijkstra, Y. M.**, Schuttelaars, H. M. and Burchard, H. (2017). Generation of exchange flows in estuaries by tidal and gravitational eddy viscosity - shear covariance (ESCO). *Journal of Geophysical Research: Oceans*, 122:4217-4237.
9. **Dijkstra, Y. M.**, Uittenbogaard, R. E., Van Kester, J. A. Th. M. and Pietrzak, J. D. (2016). Improving the numerical accuracy of the  $k-\epsilon$  model by a transformation to the  $k-\tau$  model. *Ocean Modelling*, 104:129-142.
10. Kranenburg, W. M. , Van der Kaaij, T., van den Boogaard, H., Uittenbogaard, R. E. and **Dijkstra, Y. M.** (2016). Unraveling salt fluxes: A tool to determine flux components and dispersion rates from 3D models Sustainable Hydraulics in the Era of Global Change - *Proceedings of the 4th European Congress of the International Association of Hydroenvironment engineering and Research, IAHR 2016*: 1010-1017.



